

FROM ALGORITHMS TO ASTROPHYSICS: MACHINE LEARNING IN GRAVITATIONAL WAVE ASTRONOMY

NIKOLAOS STERGIOULAS

DEPARTMENT OF PHYSICS

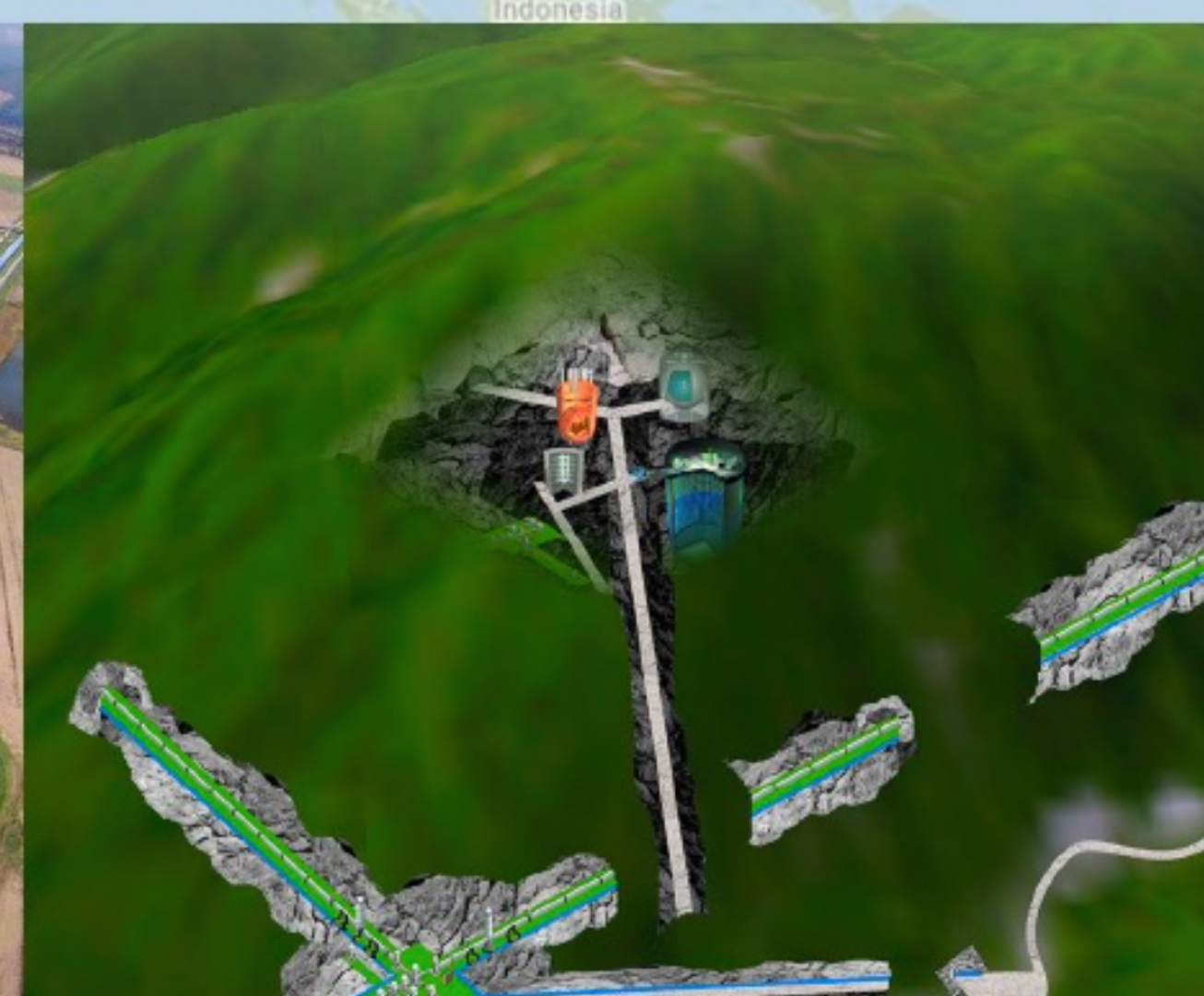
ARISTOTLE UNIVERSITY OF THESSALONIKI



21st Conference of HSRGC, Corfu, September 4, 2025

PART A. BINARY BLACK HOLE MERGERS

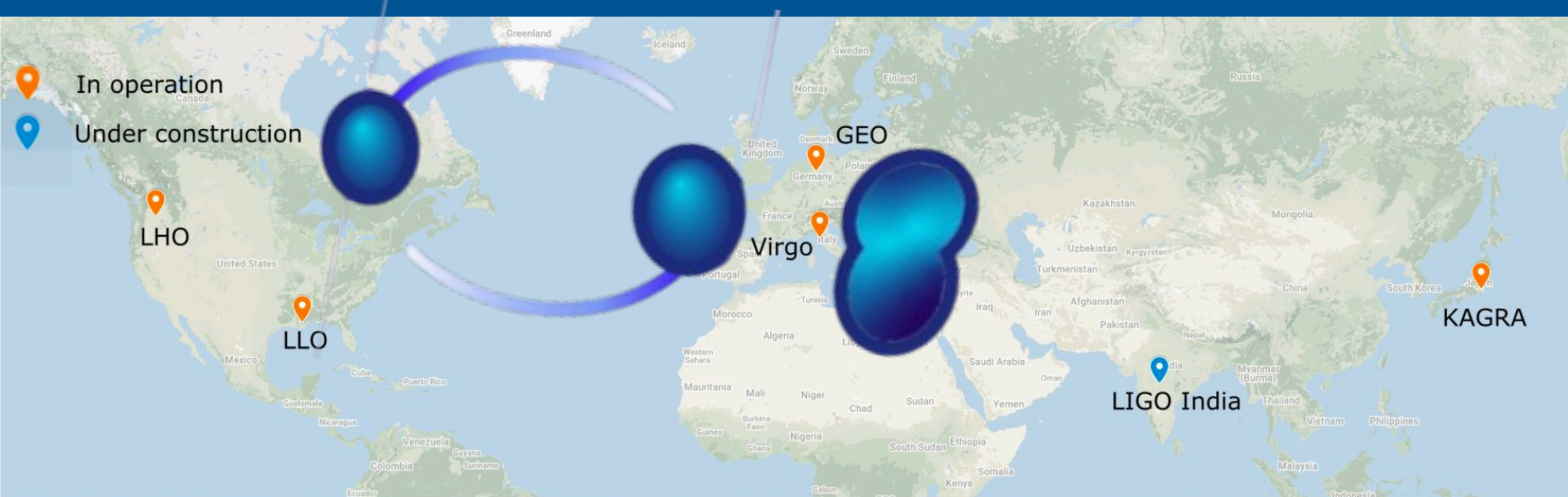
INTERNATIONAL GRAVITATIONAL-WAVE OBSERVATORY NETWORK (IGWN)



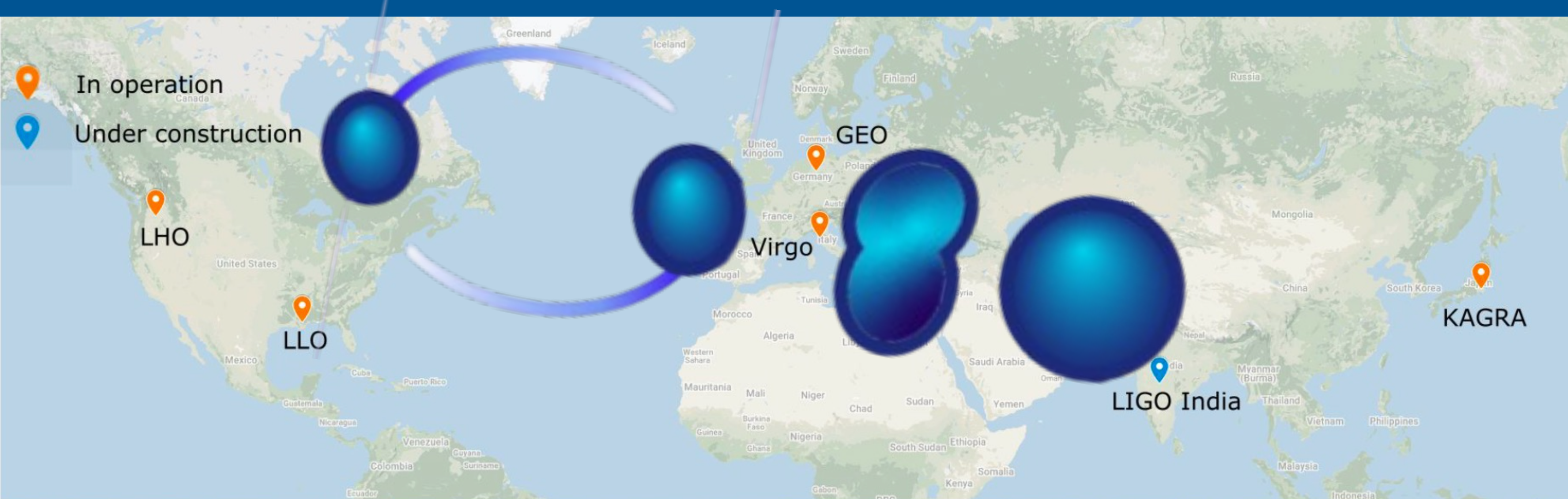
INTERNATIONAL GRAVITATIONAL-WAVE OBSERVATORY NETWORK (IGWN)



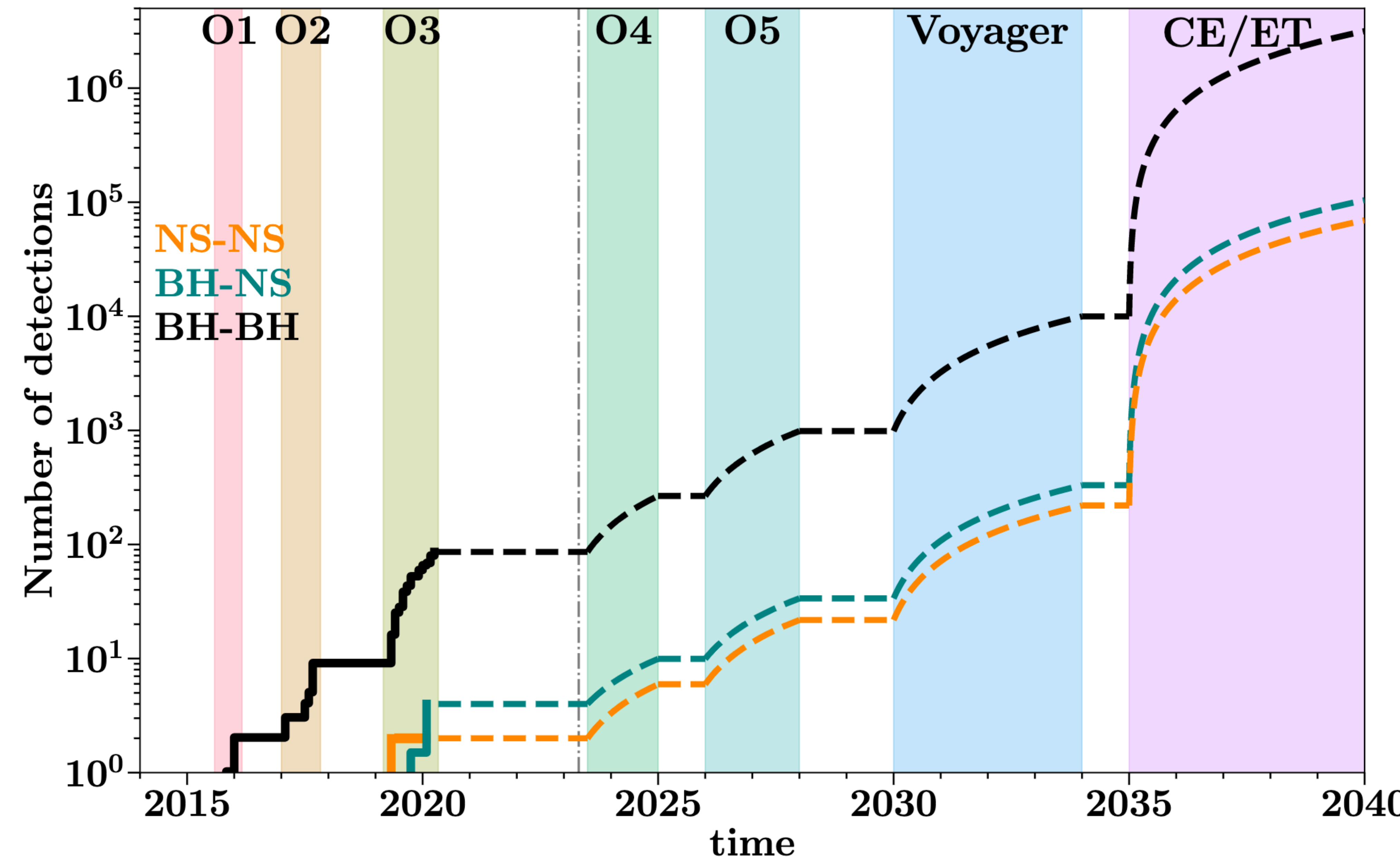
INTERNATIONAL GRAVITATIONAL-WAVE OBSERVATORY NETWORK (IGWN)



INTERNATIONAL GRAVITATIONAL-WAVE OBSERVATORY NETWORK (IGWN)

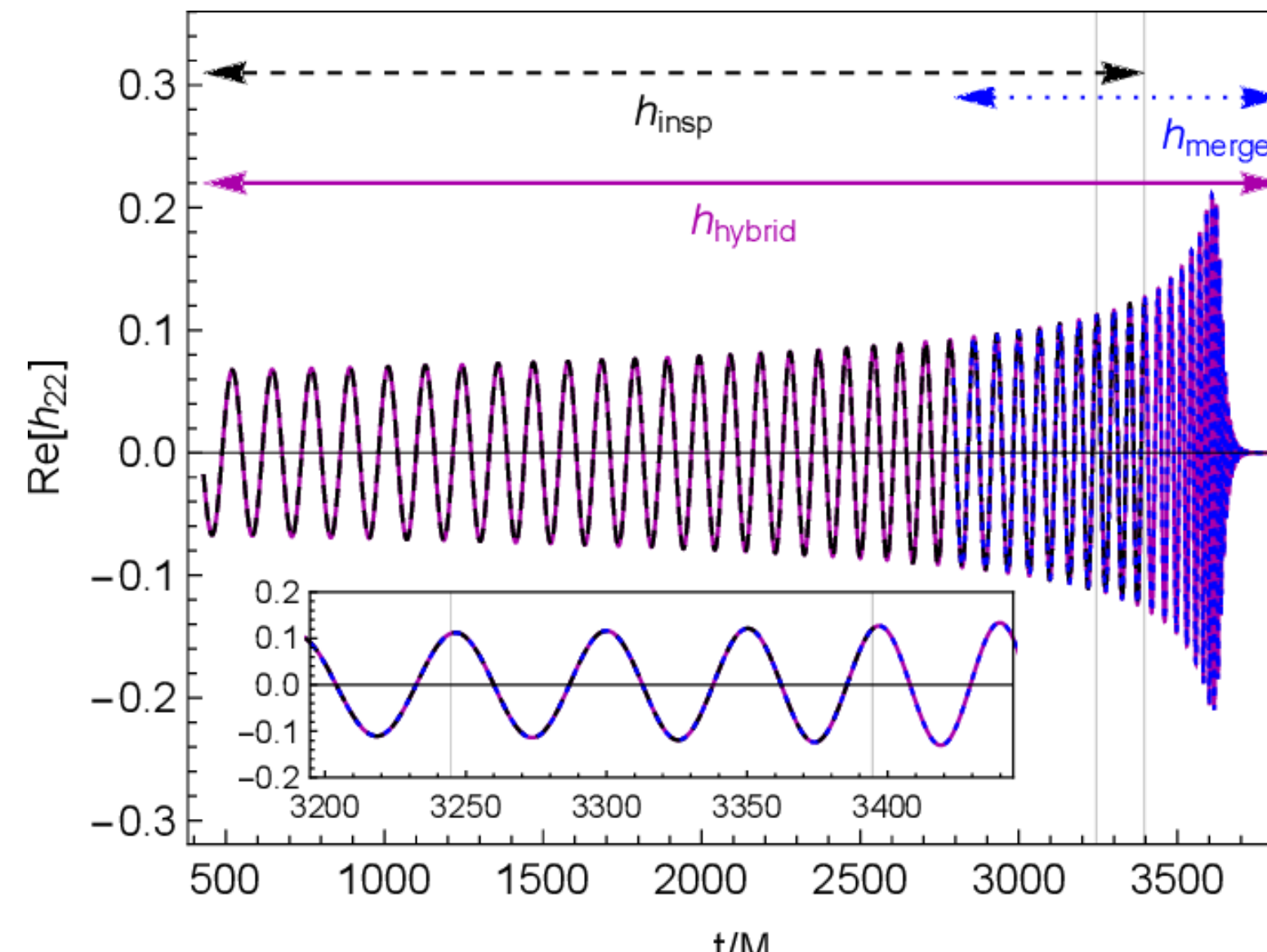


EXPECTED NUMBER OF DETECTIONS

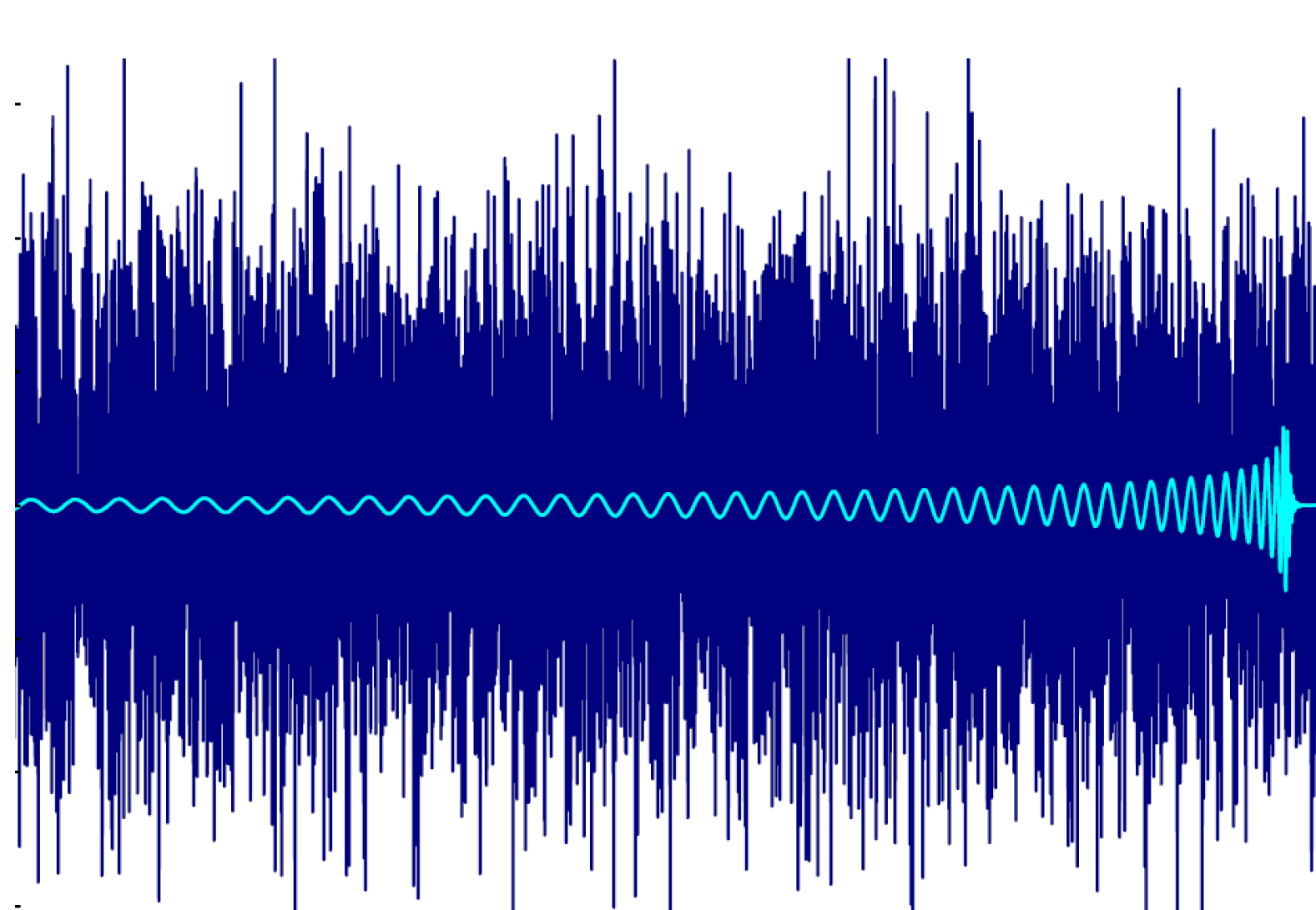


MACHINE LEARNING IN GRAVITATIONAL WAVE ASTRONOMY

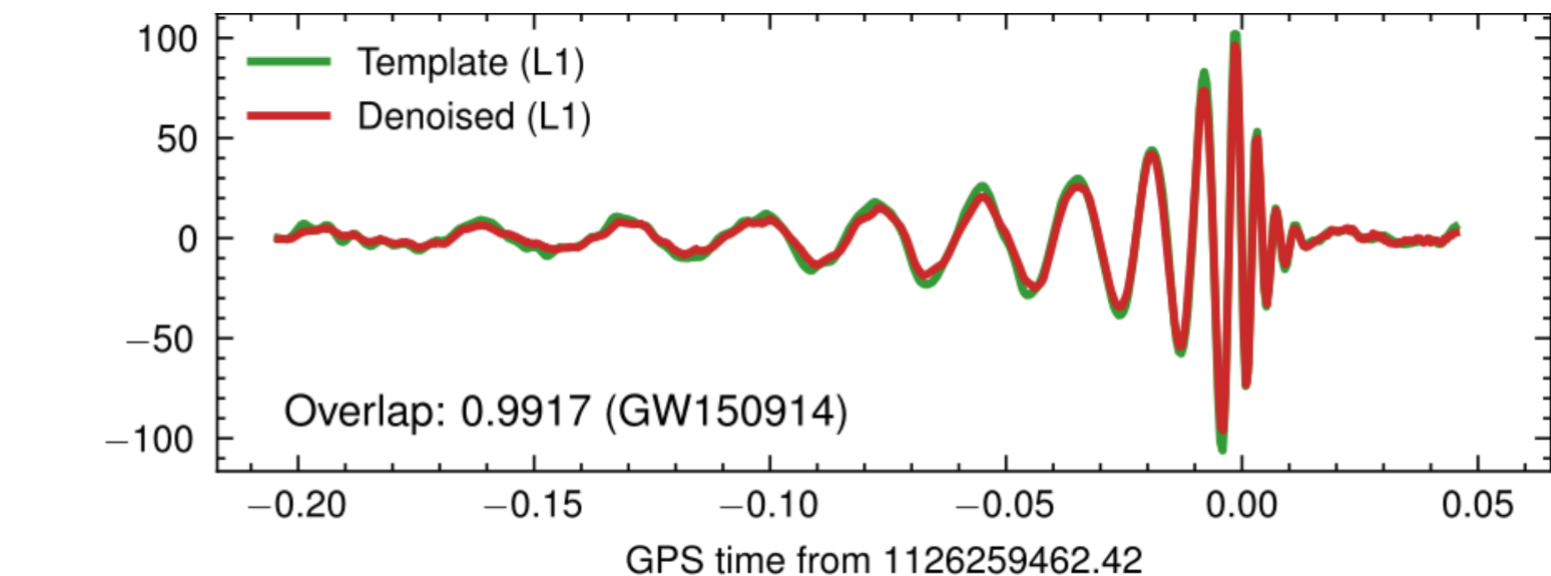
Waveform Modeling



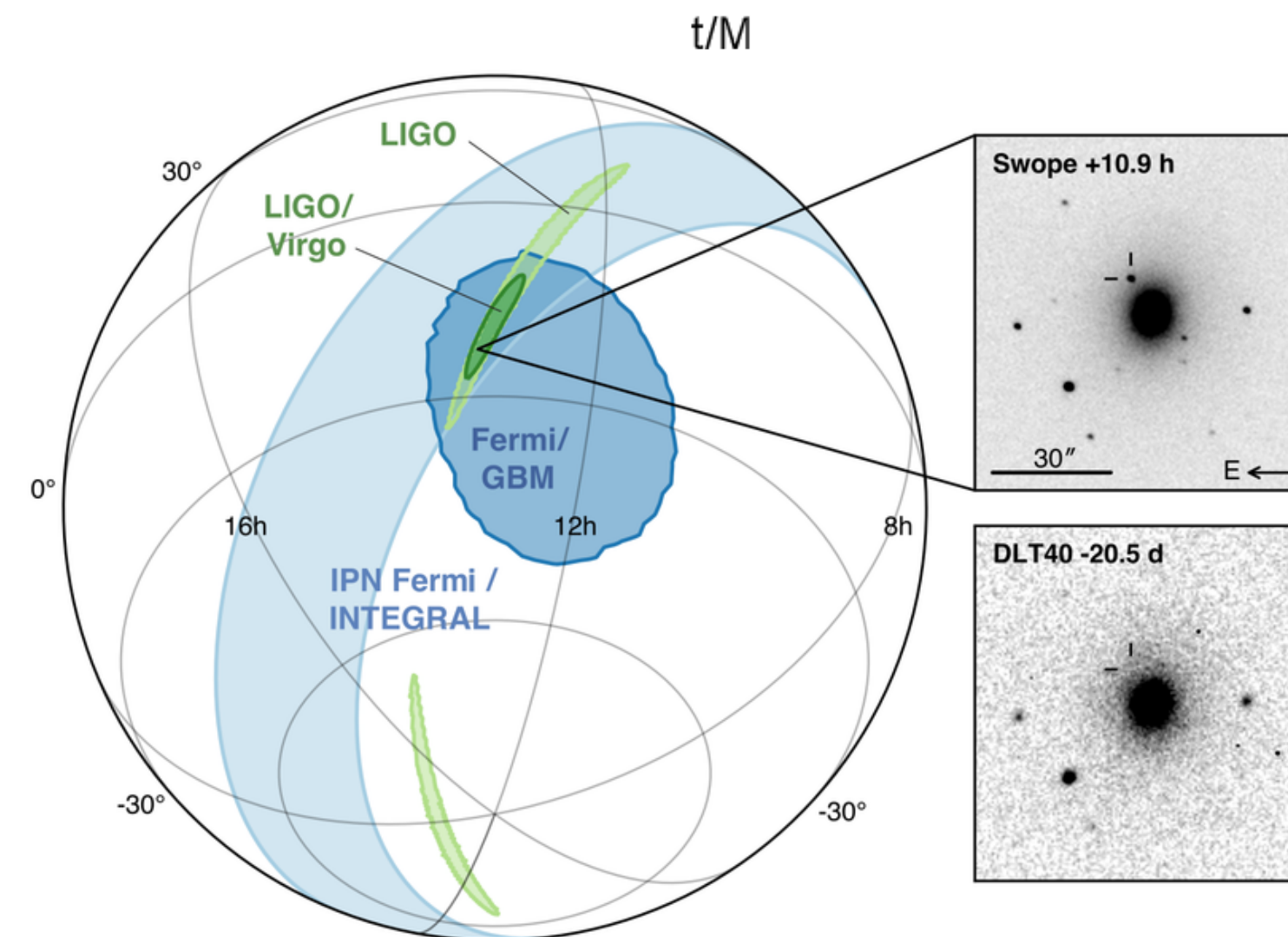
Detection



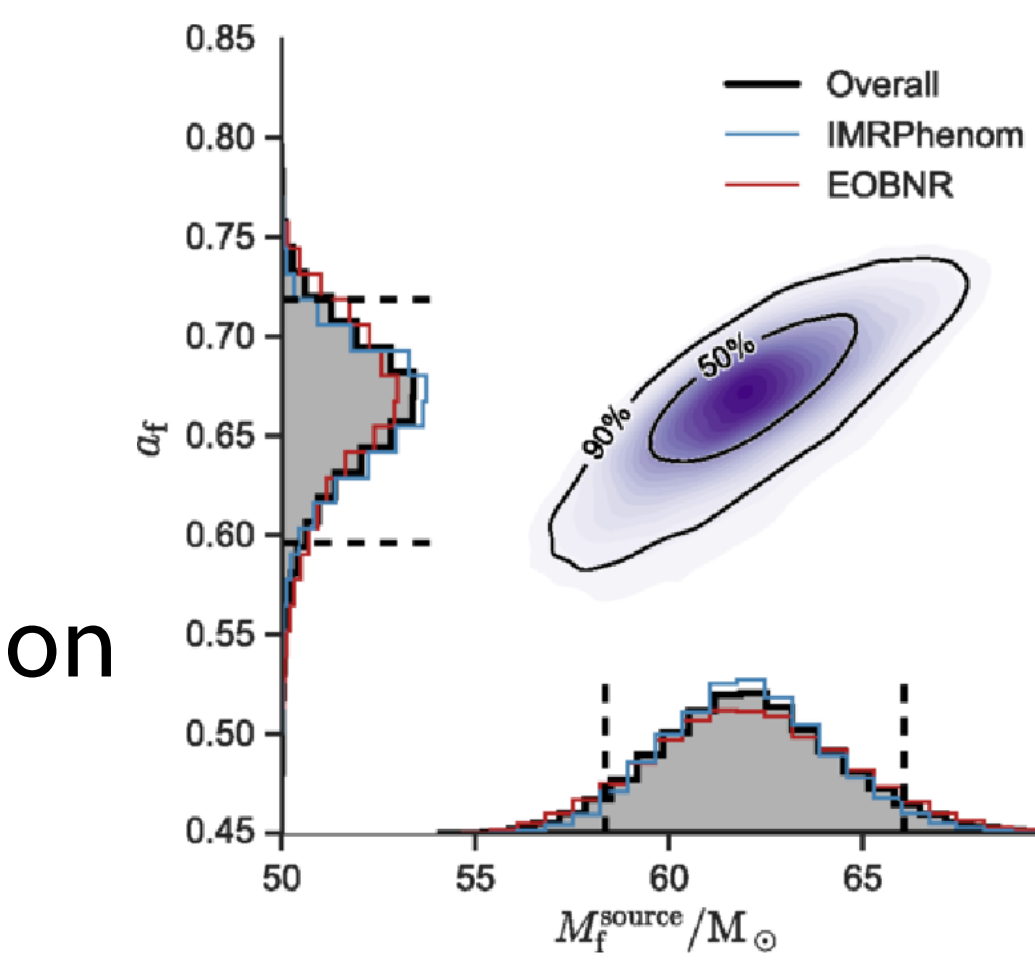
Denoising



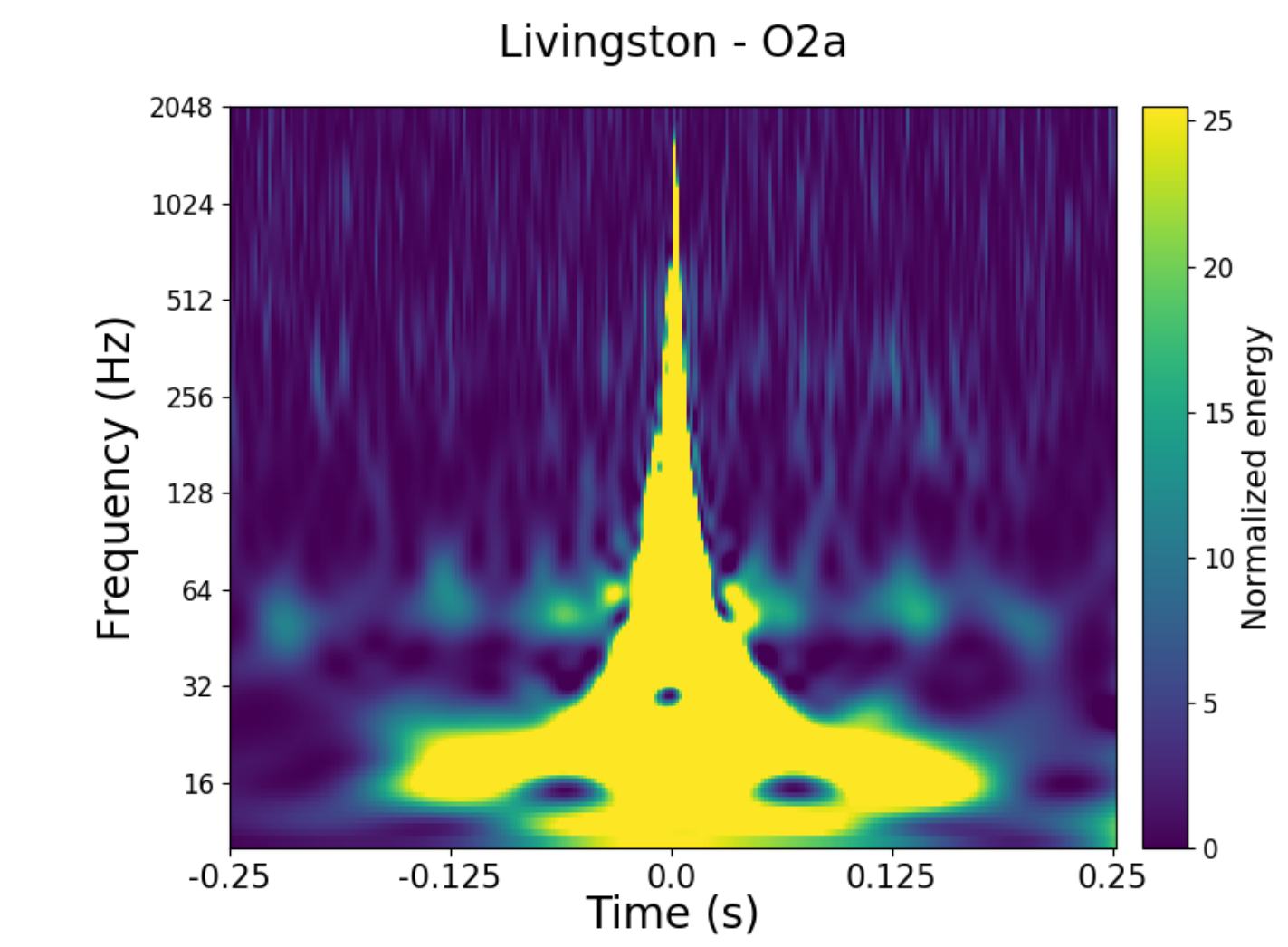
Glitch Classification



Parameter Estimation

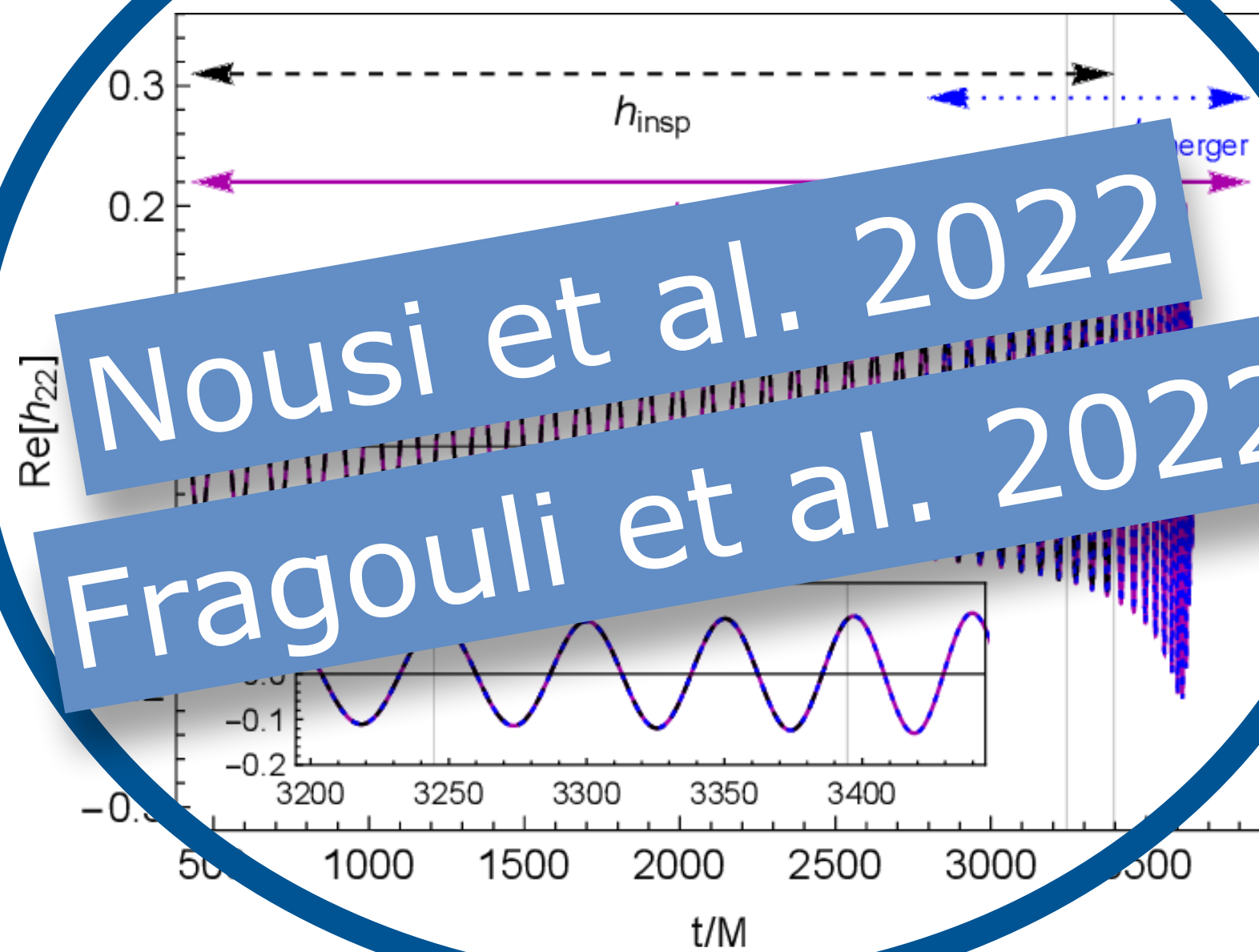


Sky Localization

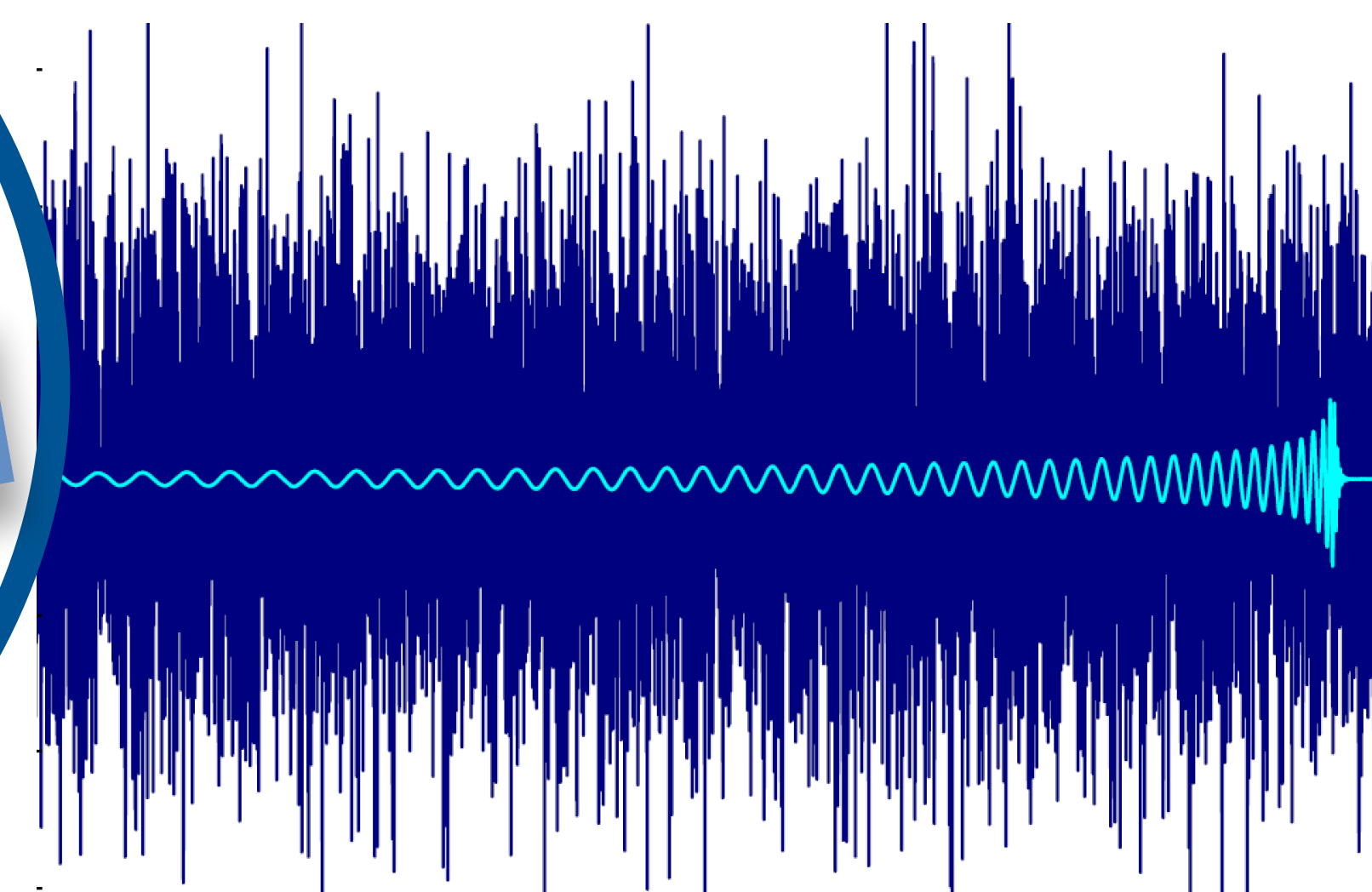


MACHINE LEARNING IN GRAVITATIONAL WAVE ASTRONOMY

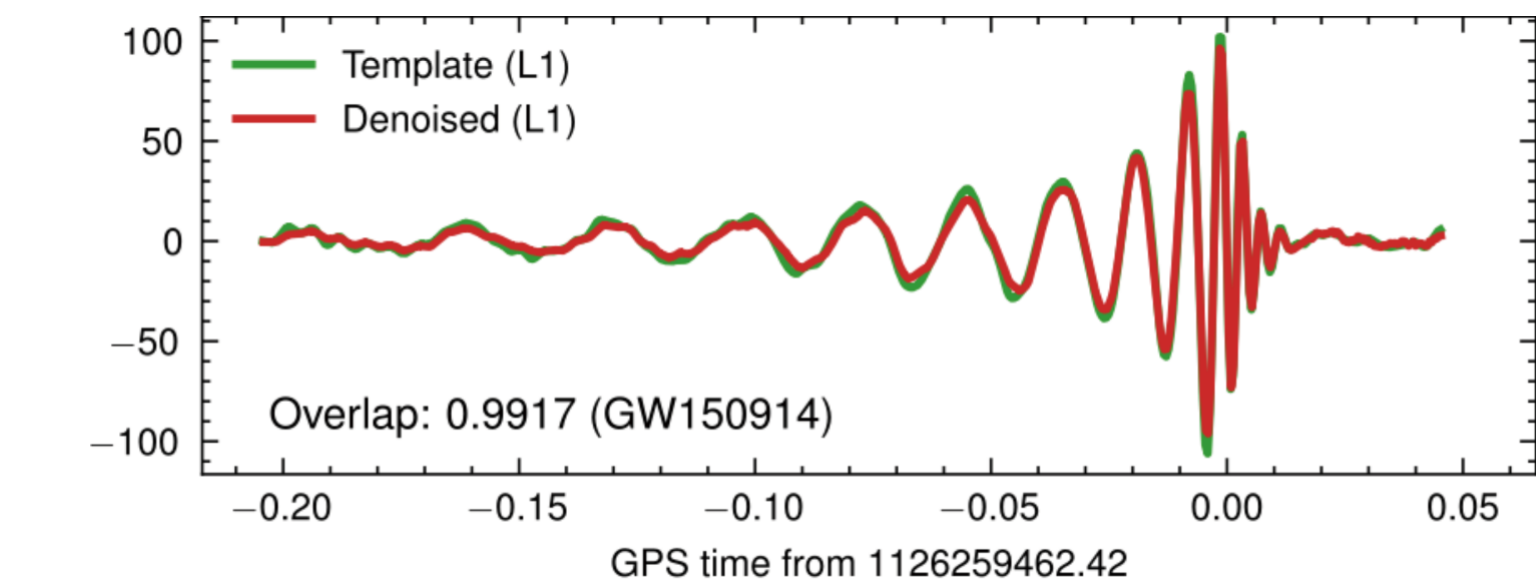
Waveform Modeling



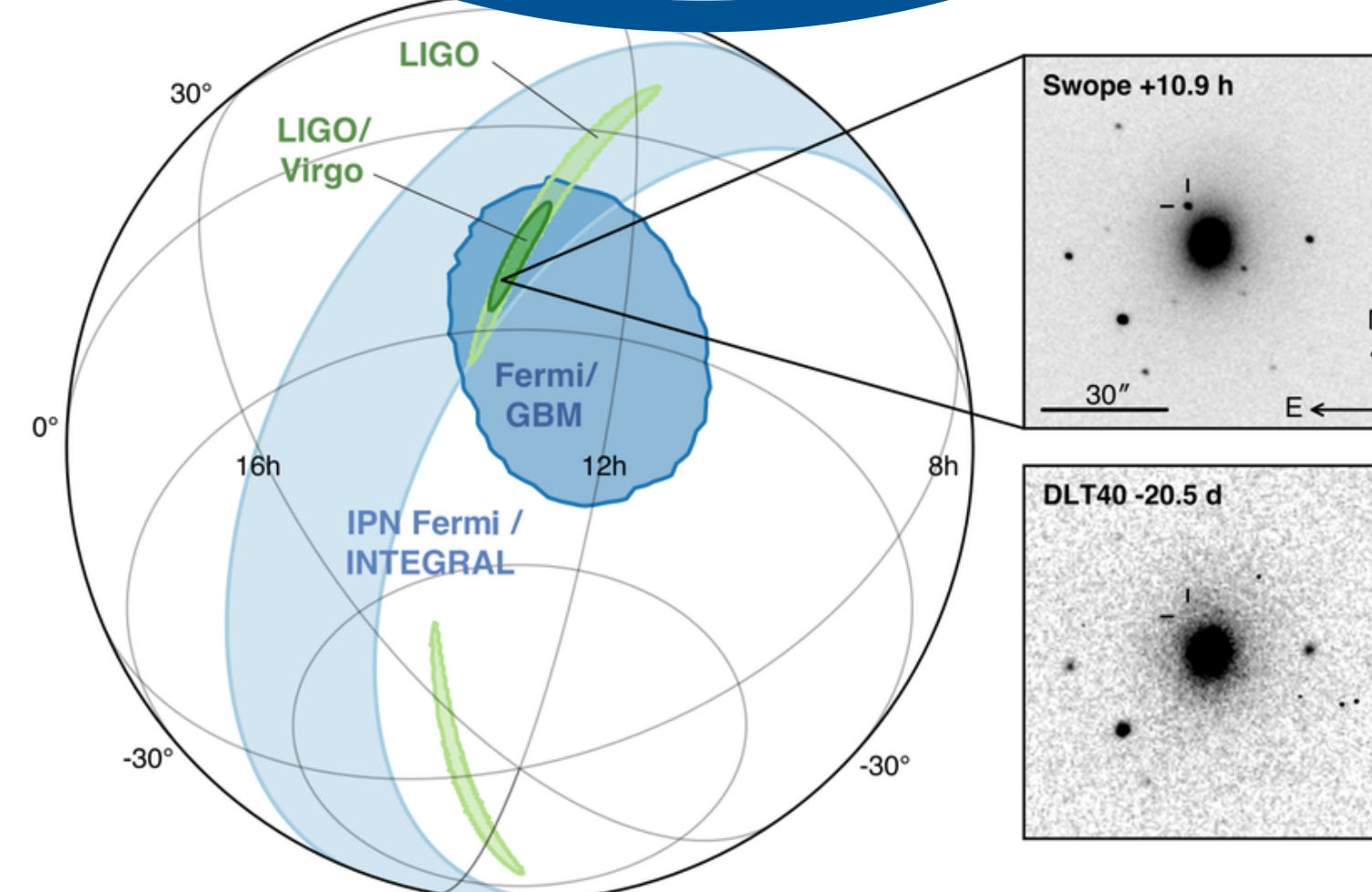
Detection



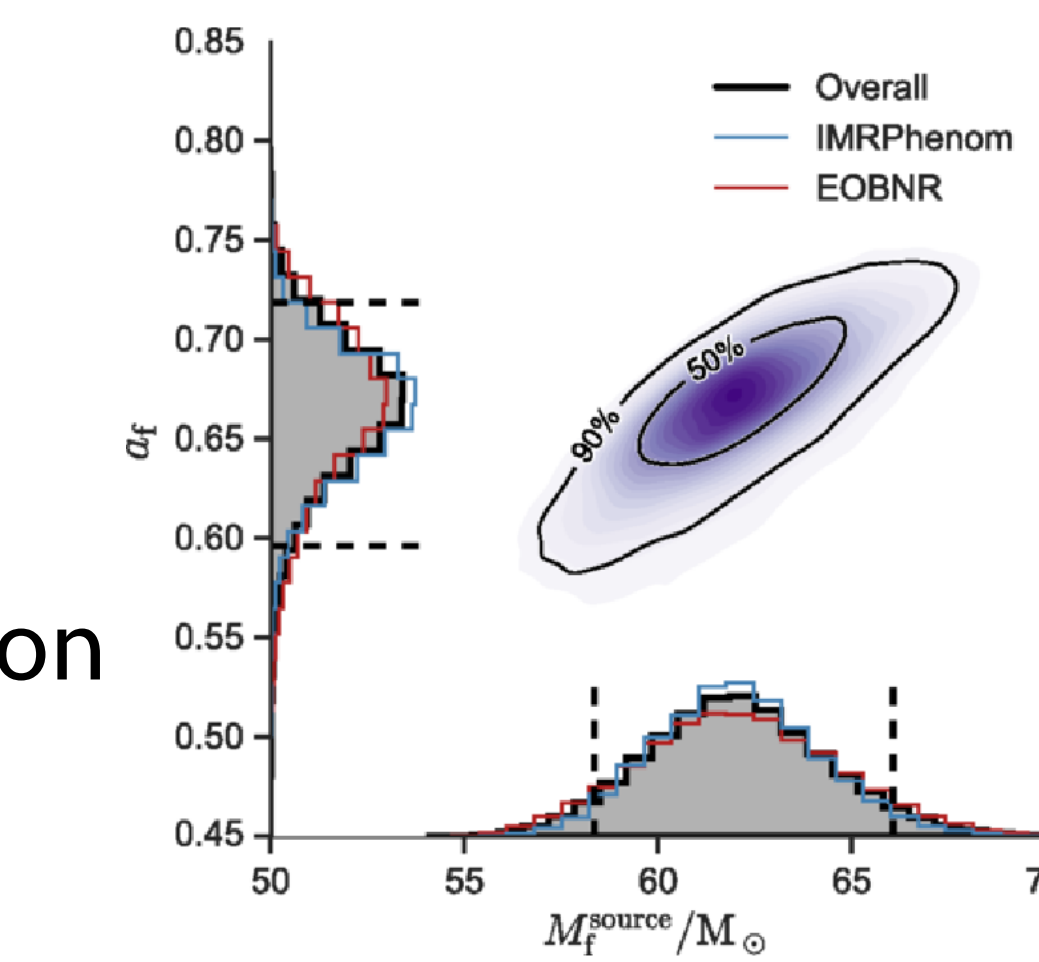
Denoising



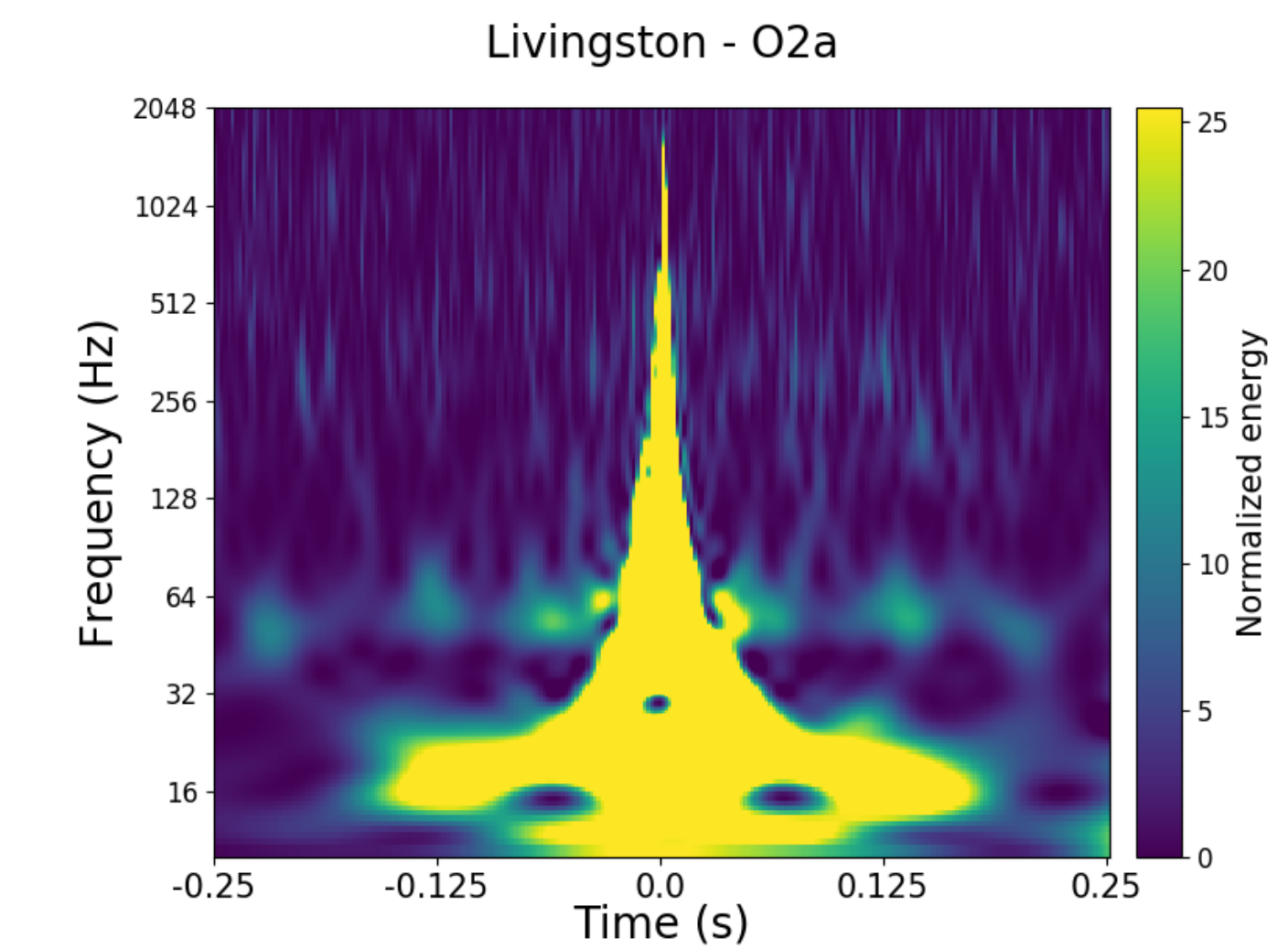
Glitch Classification



Parameter Estimation

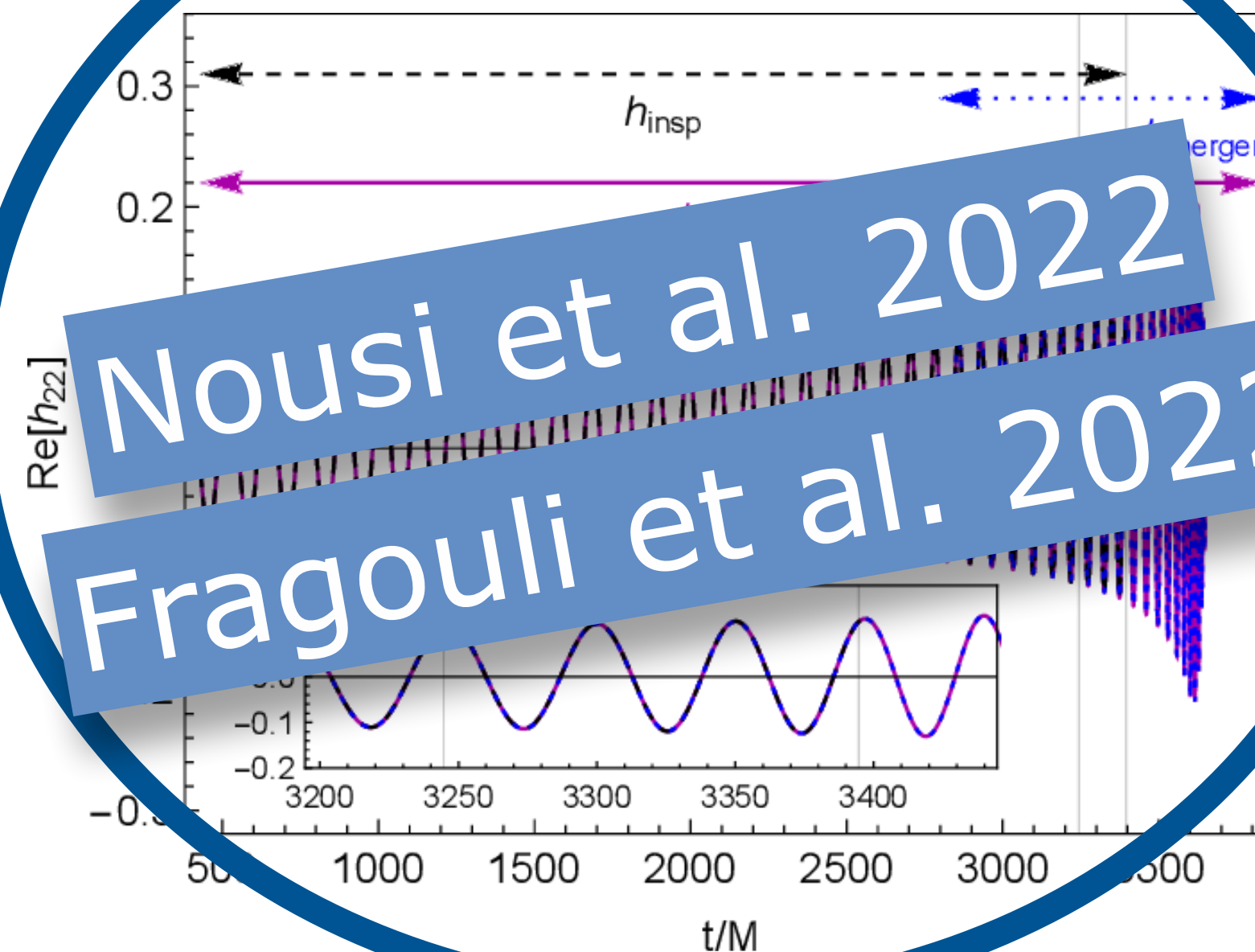


Sky Localization



MACHINE LEARNING IN GRAVITATIONAL WAVE ASTRONOMY

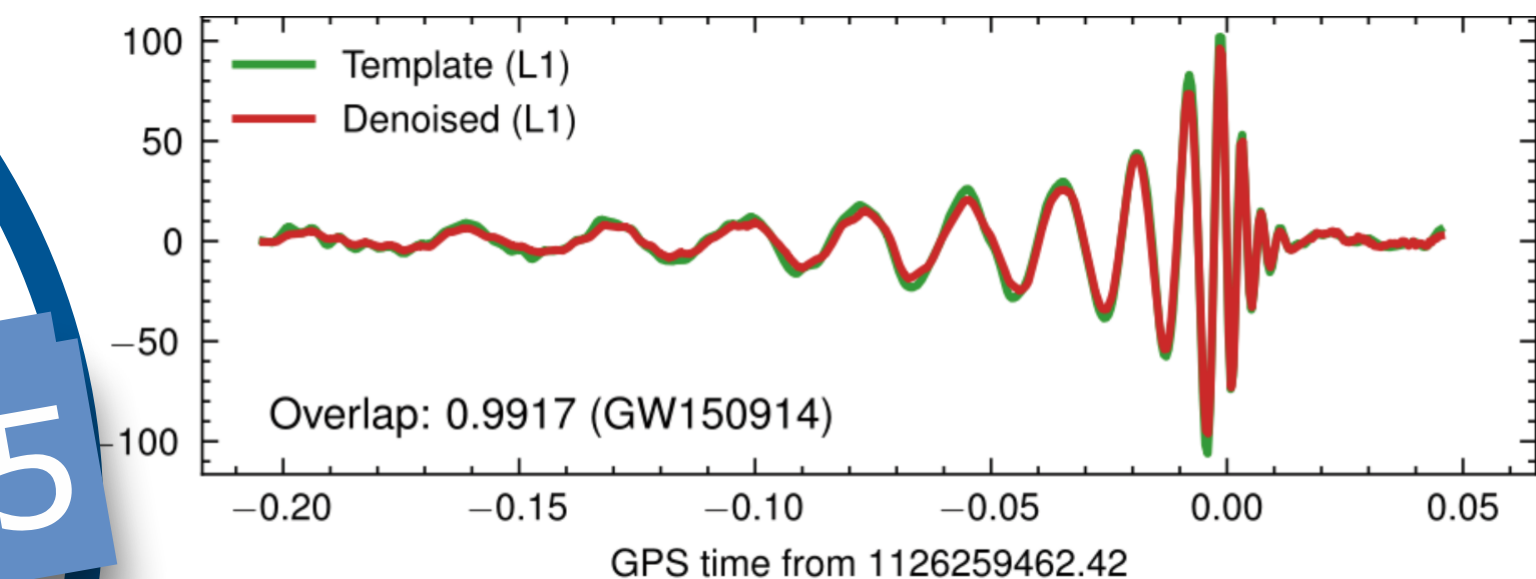
Waveform Modeling



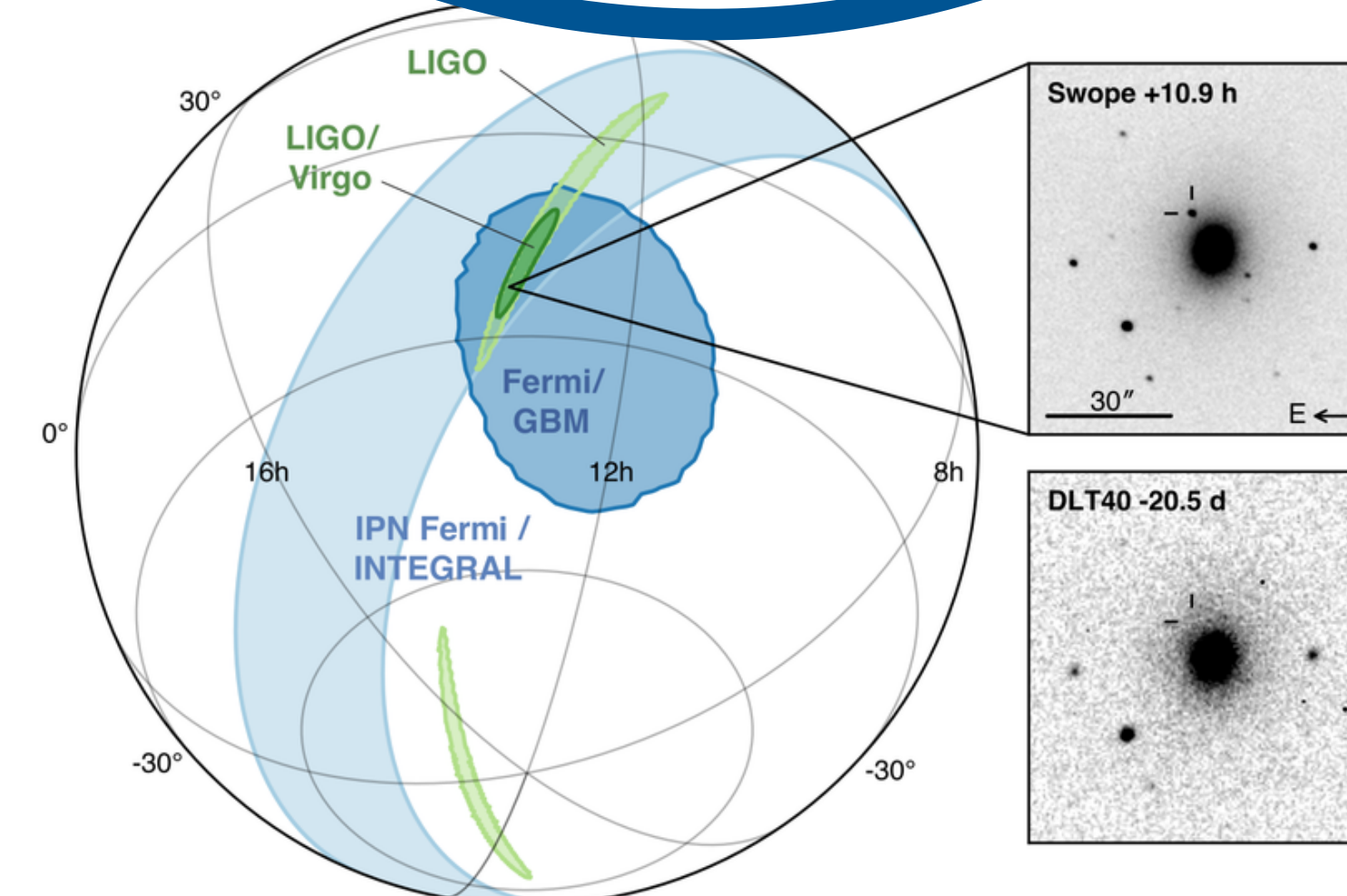
Detection



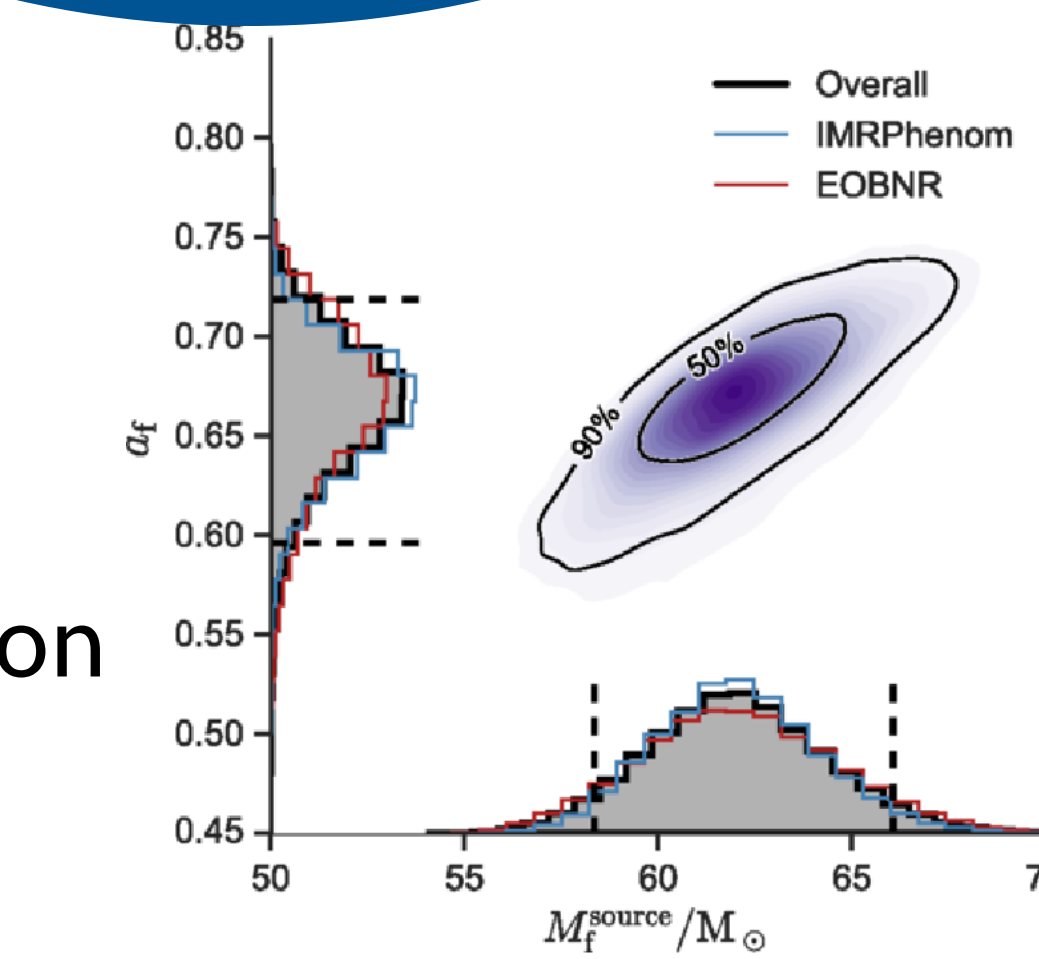
Denoising



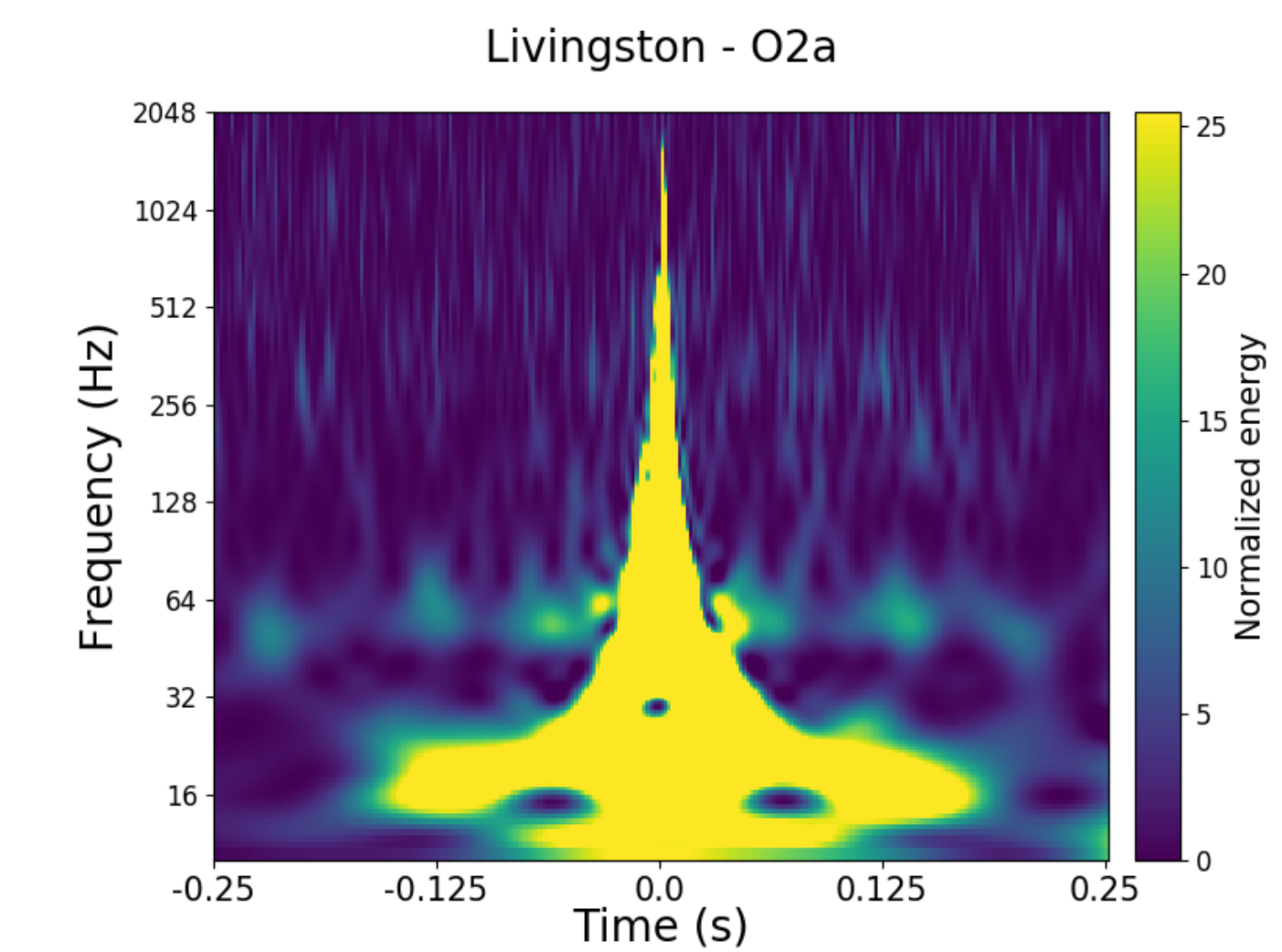
Glitch Classification



Parameter Estimation

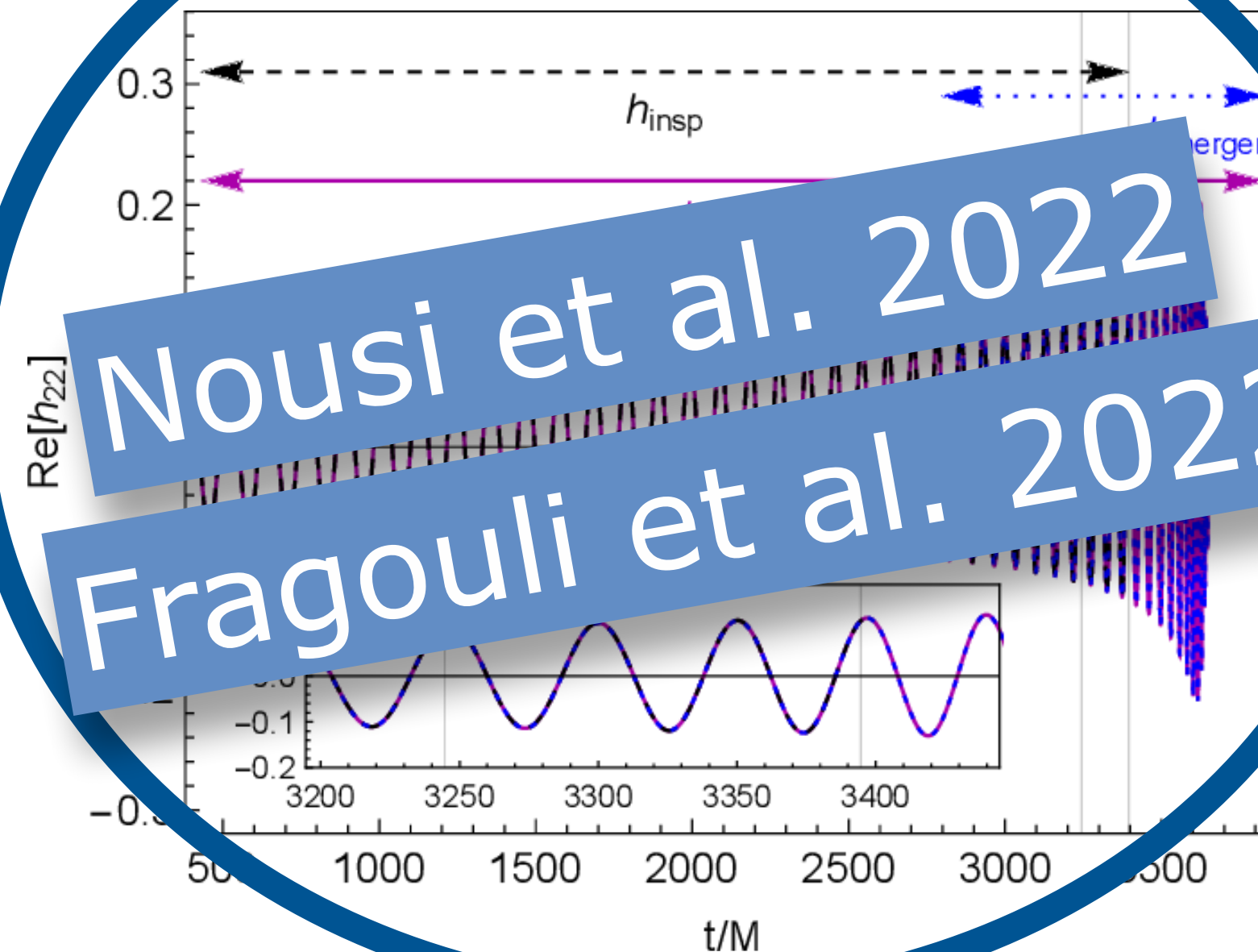


Sky Localization



MACHINE LEARNING IN GRAVITATIONAL WAVE ASTRONOMY

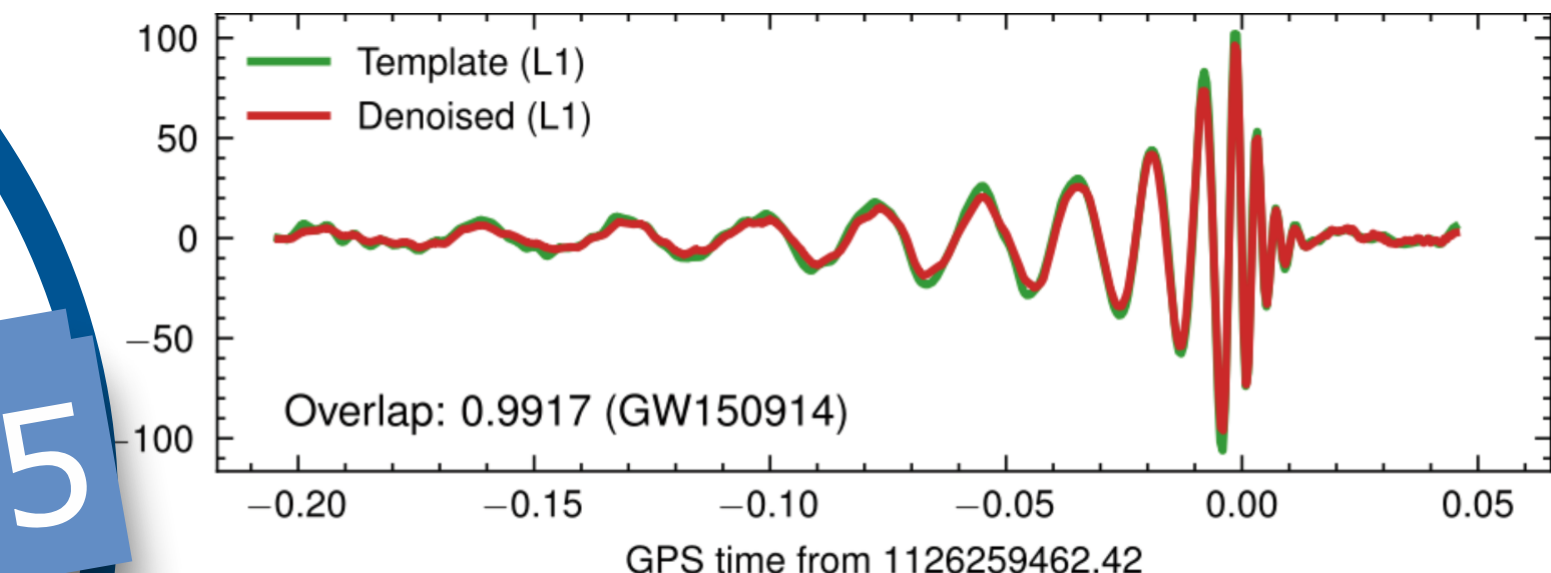
Waveform Modeling



Detection



Denoising

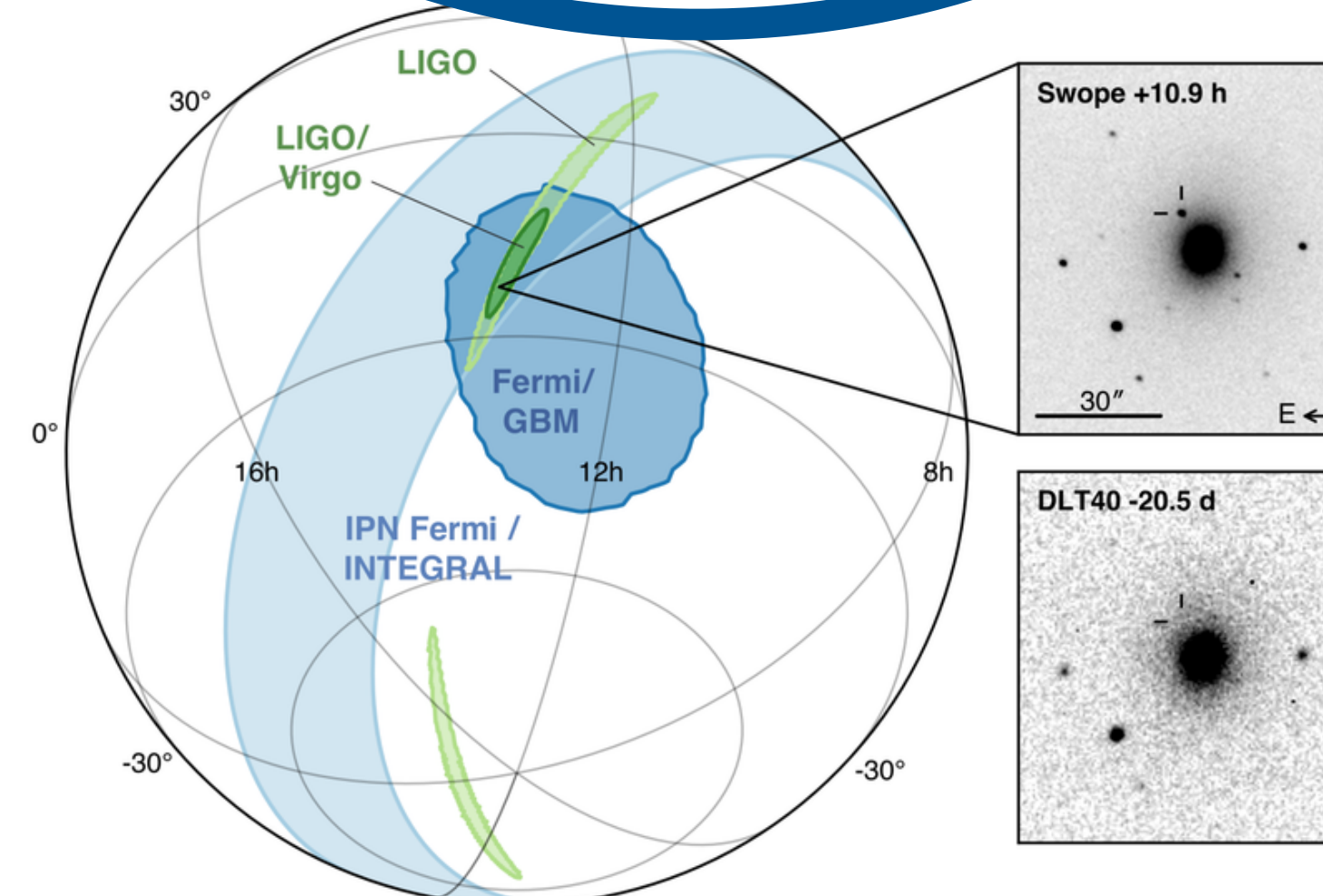


Glitch
Classification

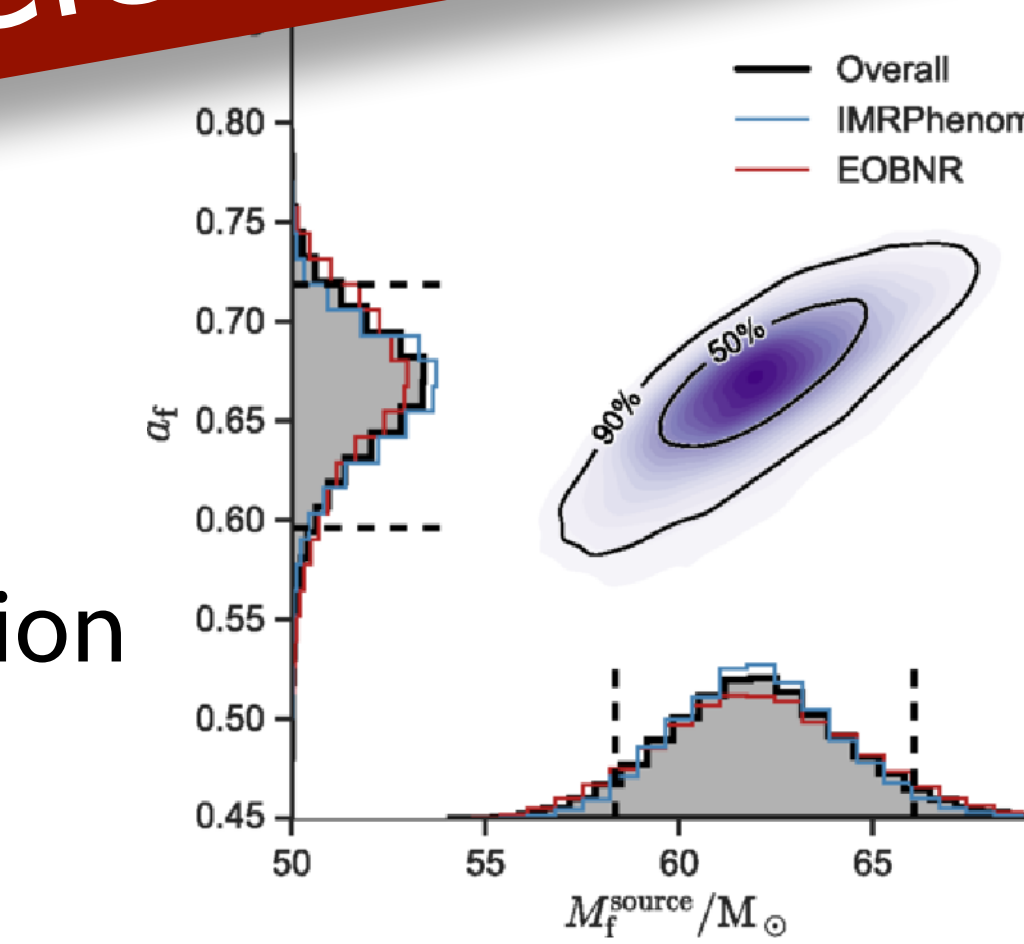
Nousi et al. 2023

Koloniari et al. 2025

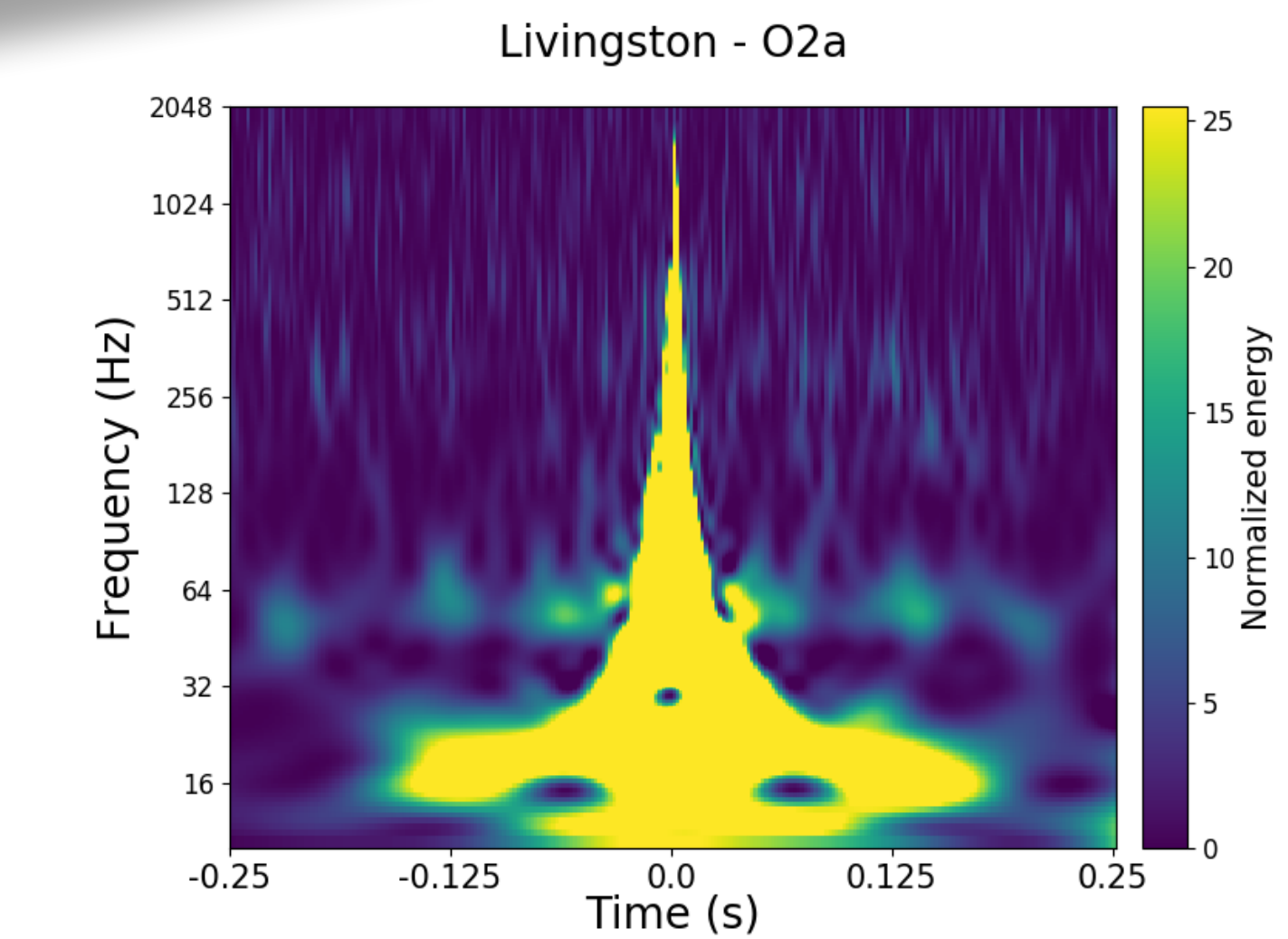
See also A. Koloniari and O. Zelenka talks



Parameter
Estimation

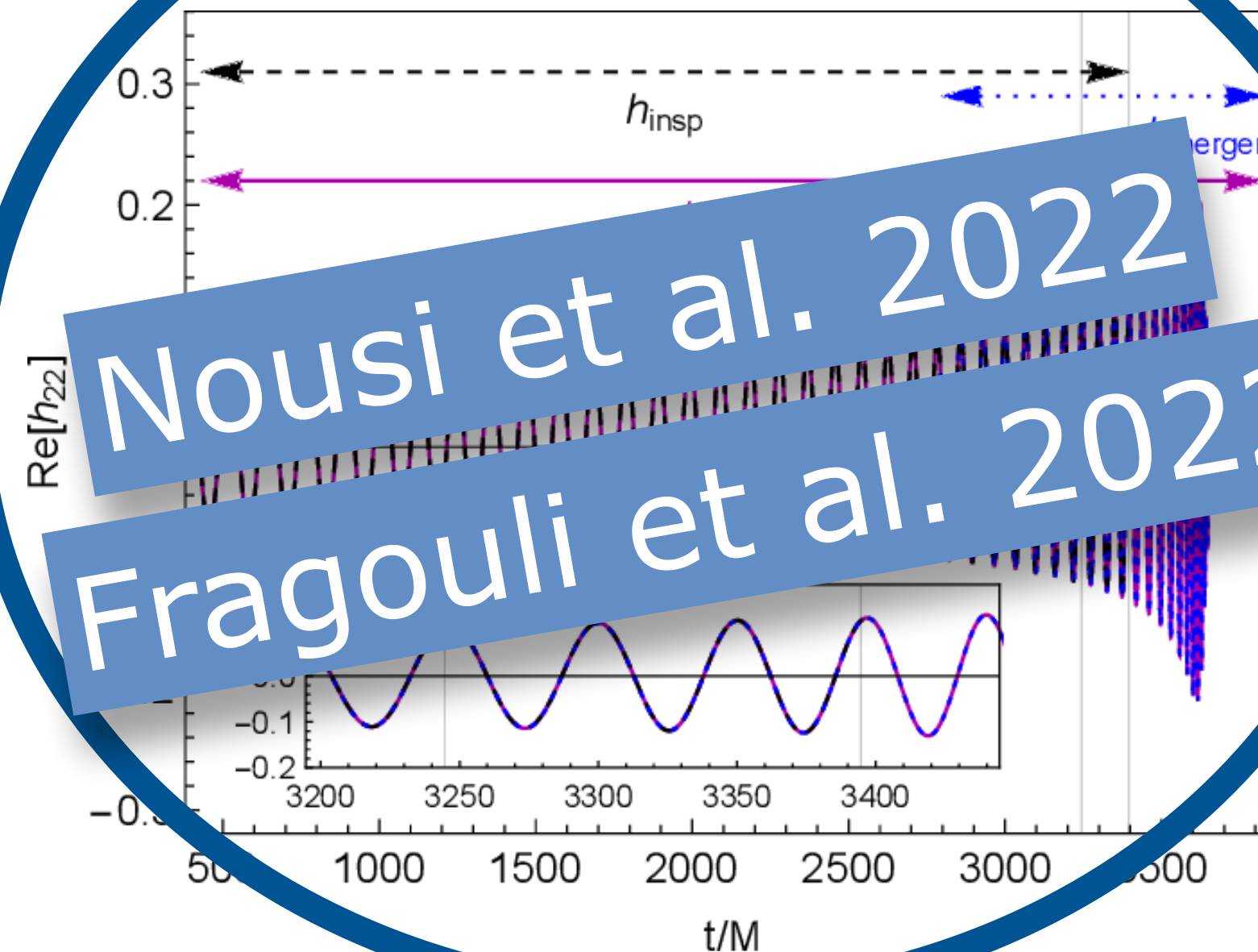


Sky Localization



MACHINE LEARNING IN GRAVITATIONAL WAVE ASTRONOMY

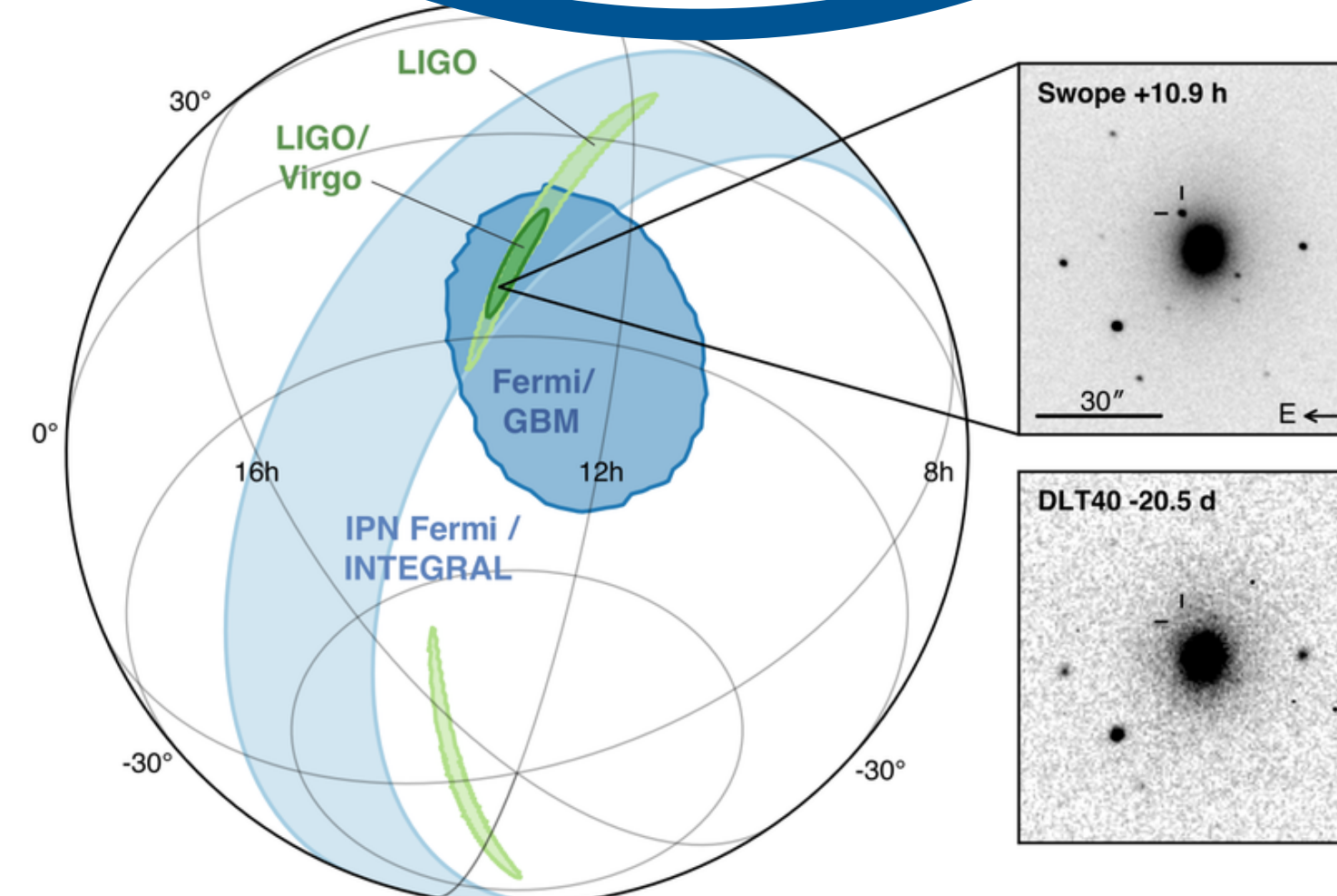
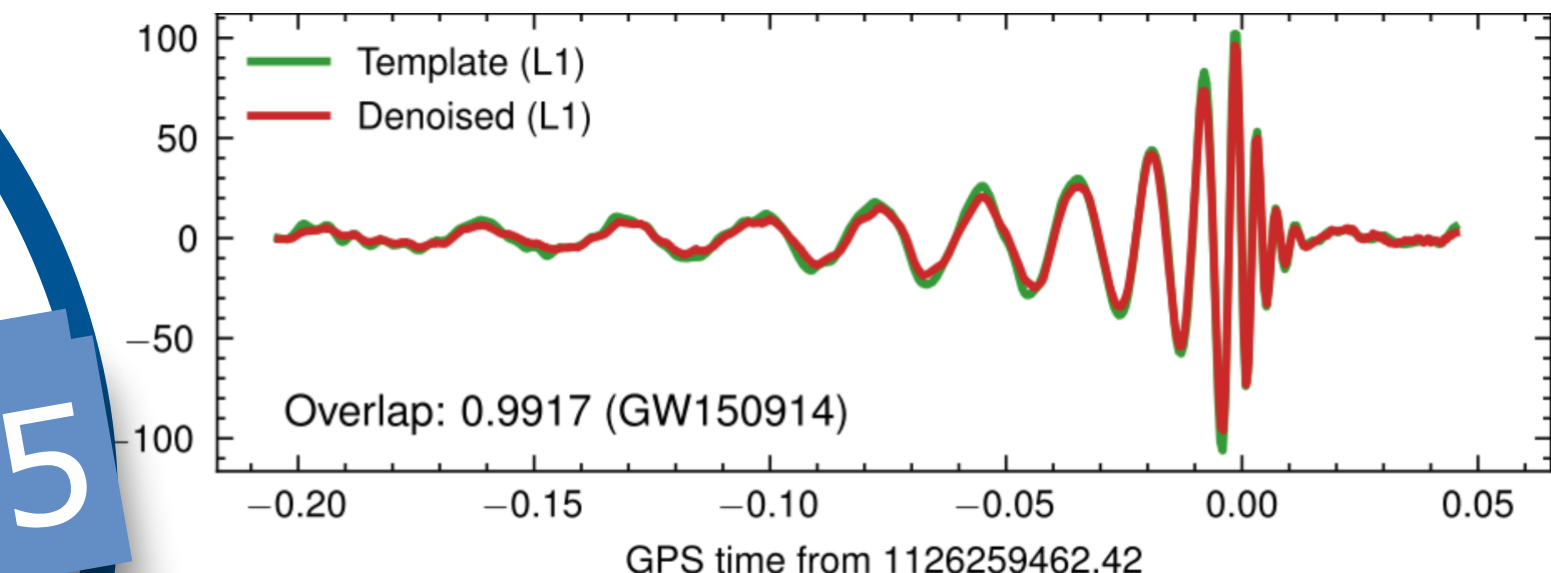
Waveform Modeling



Detection

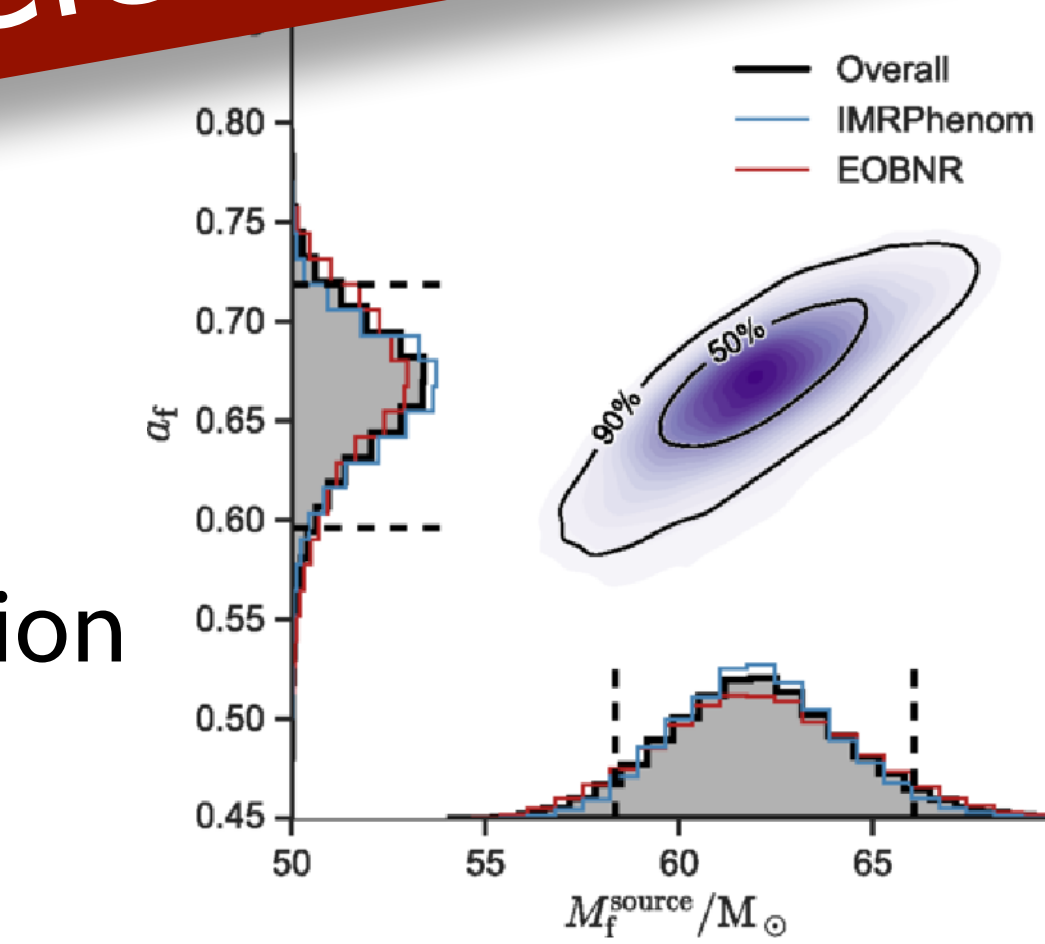


Denoising

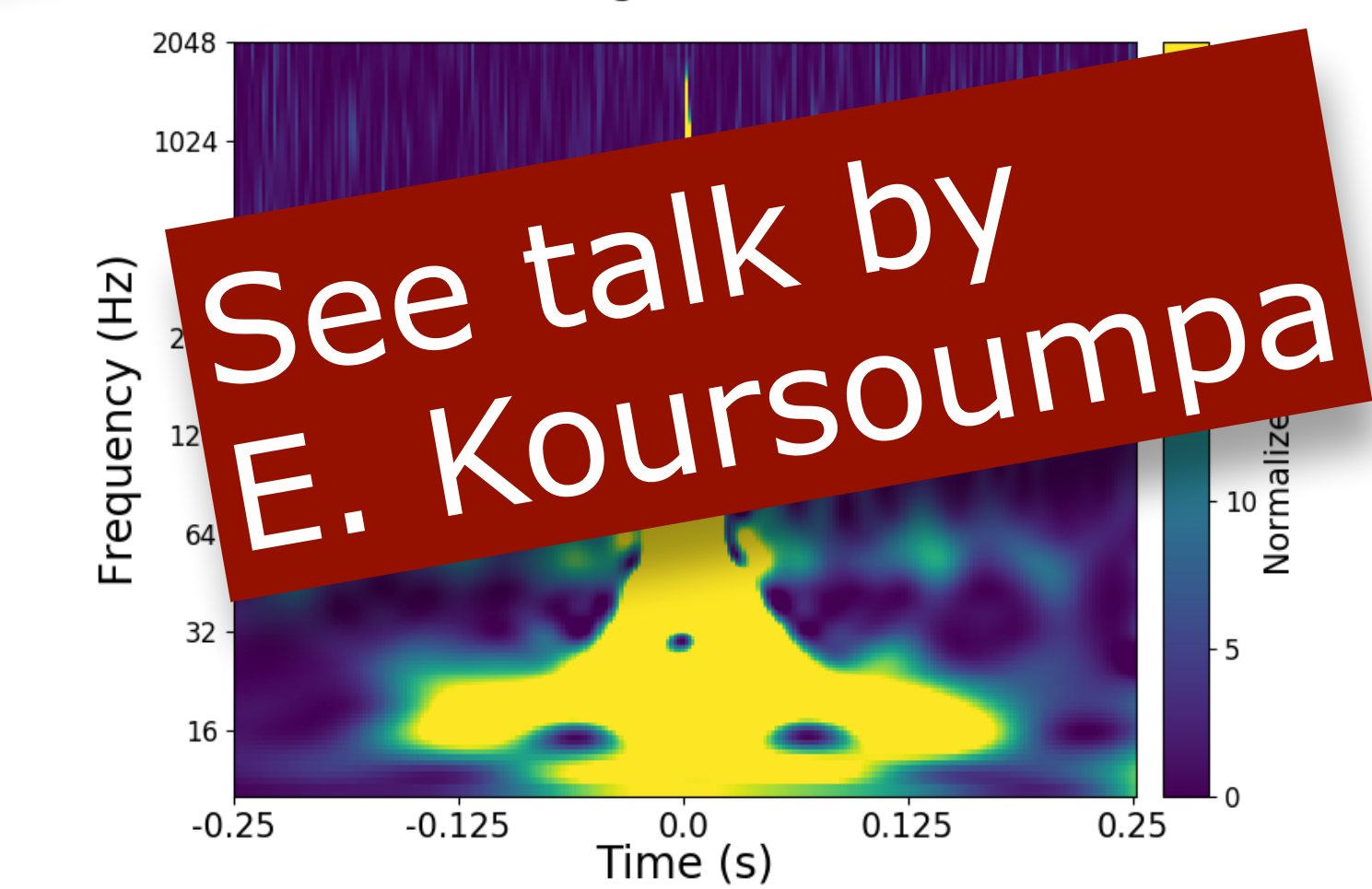


Parameter Estimation

Sky Localization

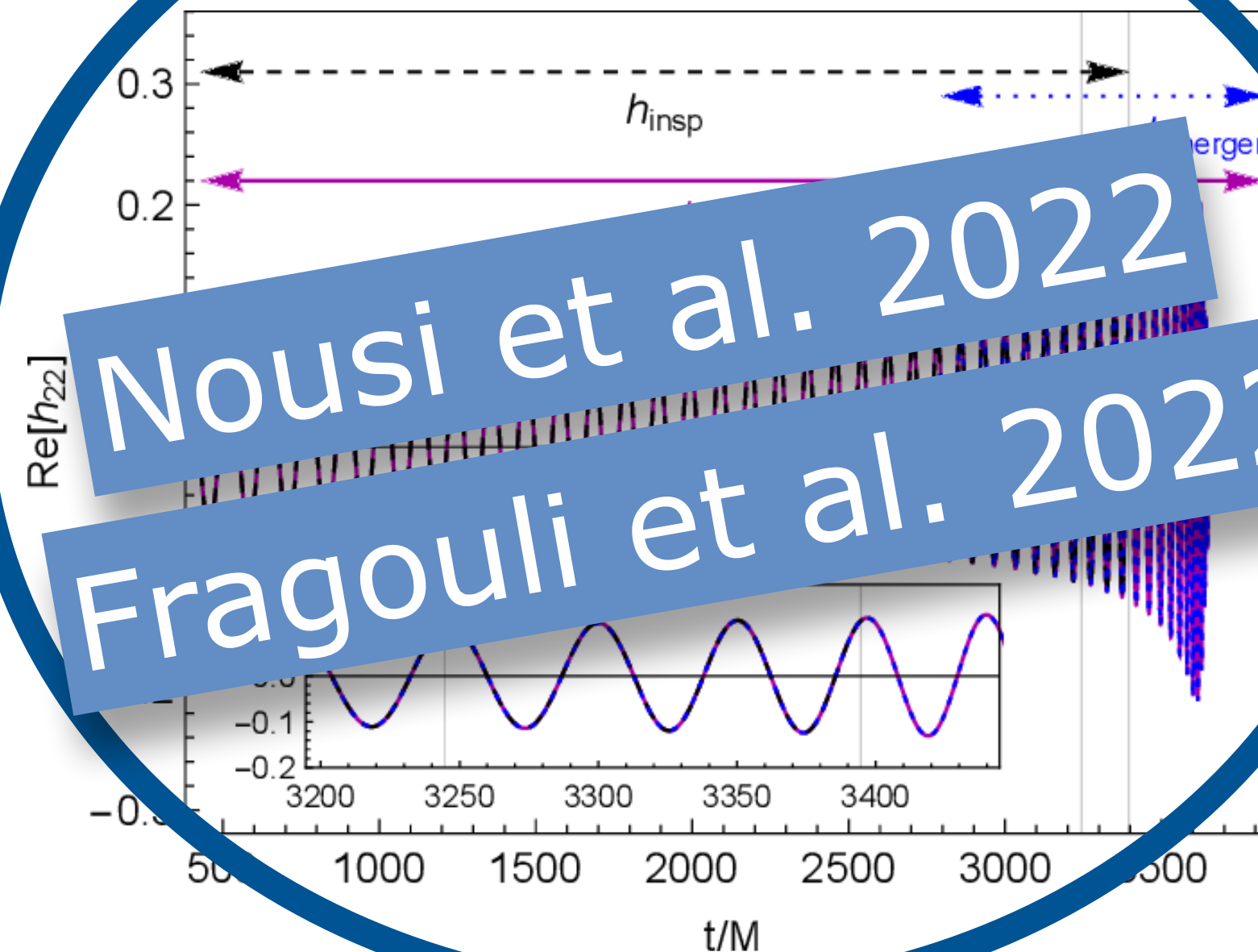


Livingston - O2a



MACHINE LEARNING IN GRAVITATIONAL WAVE ASTRONOMY

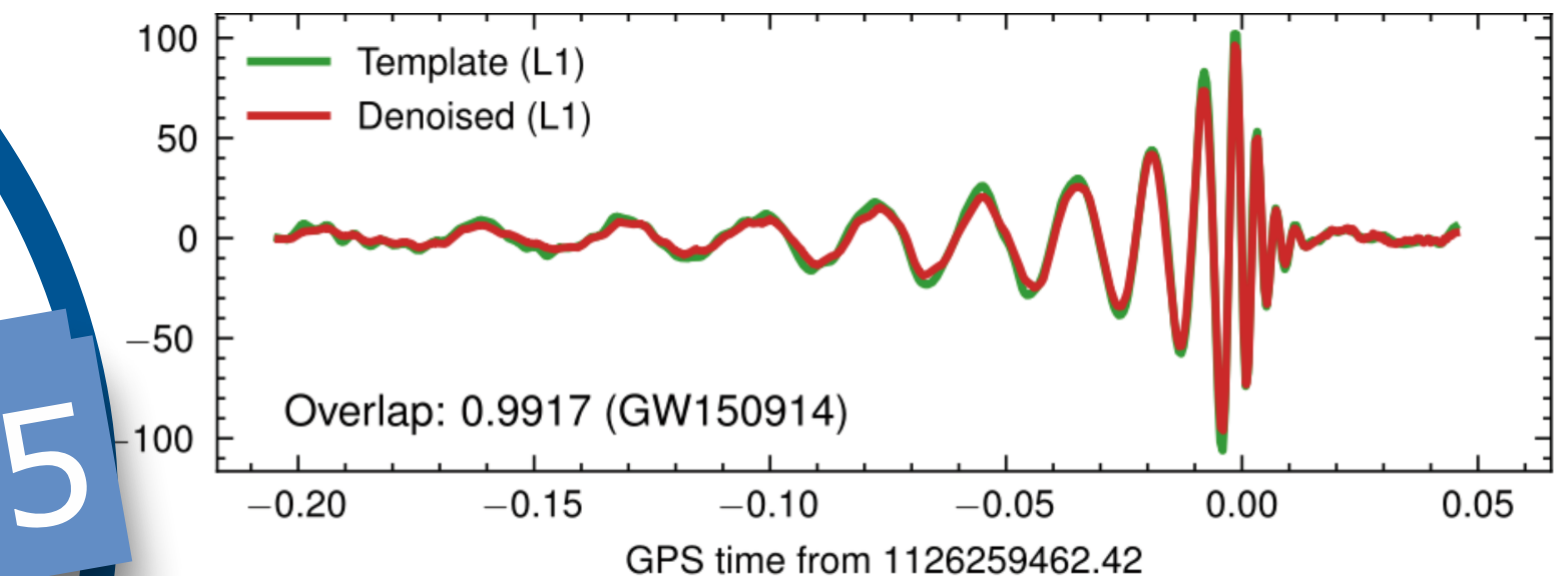
Waveform Modeling



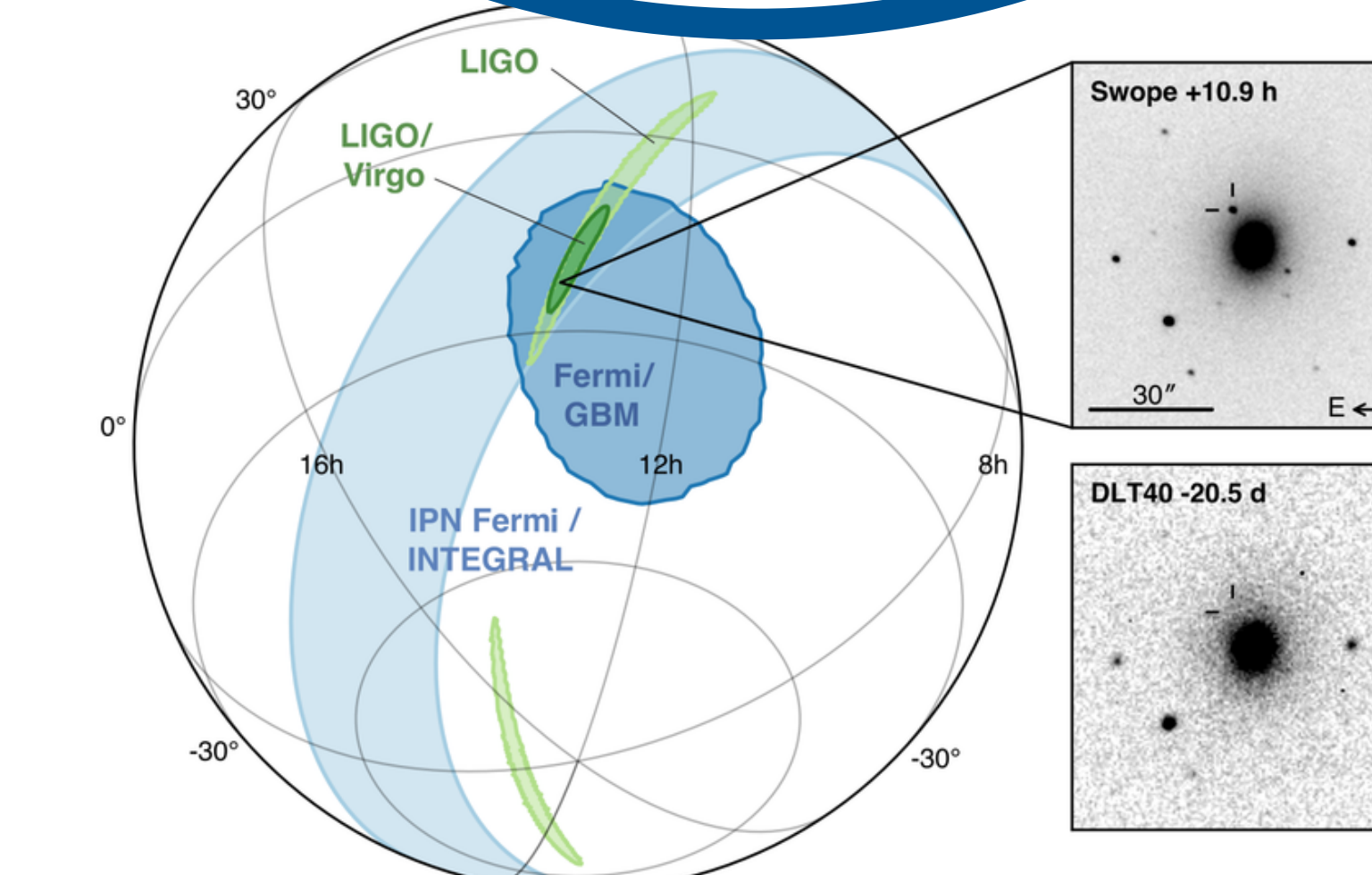
Detection



Denoising



Glitch
Classification

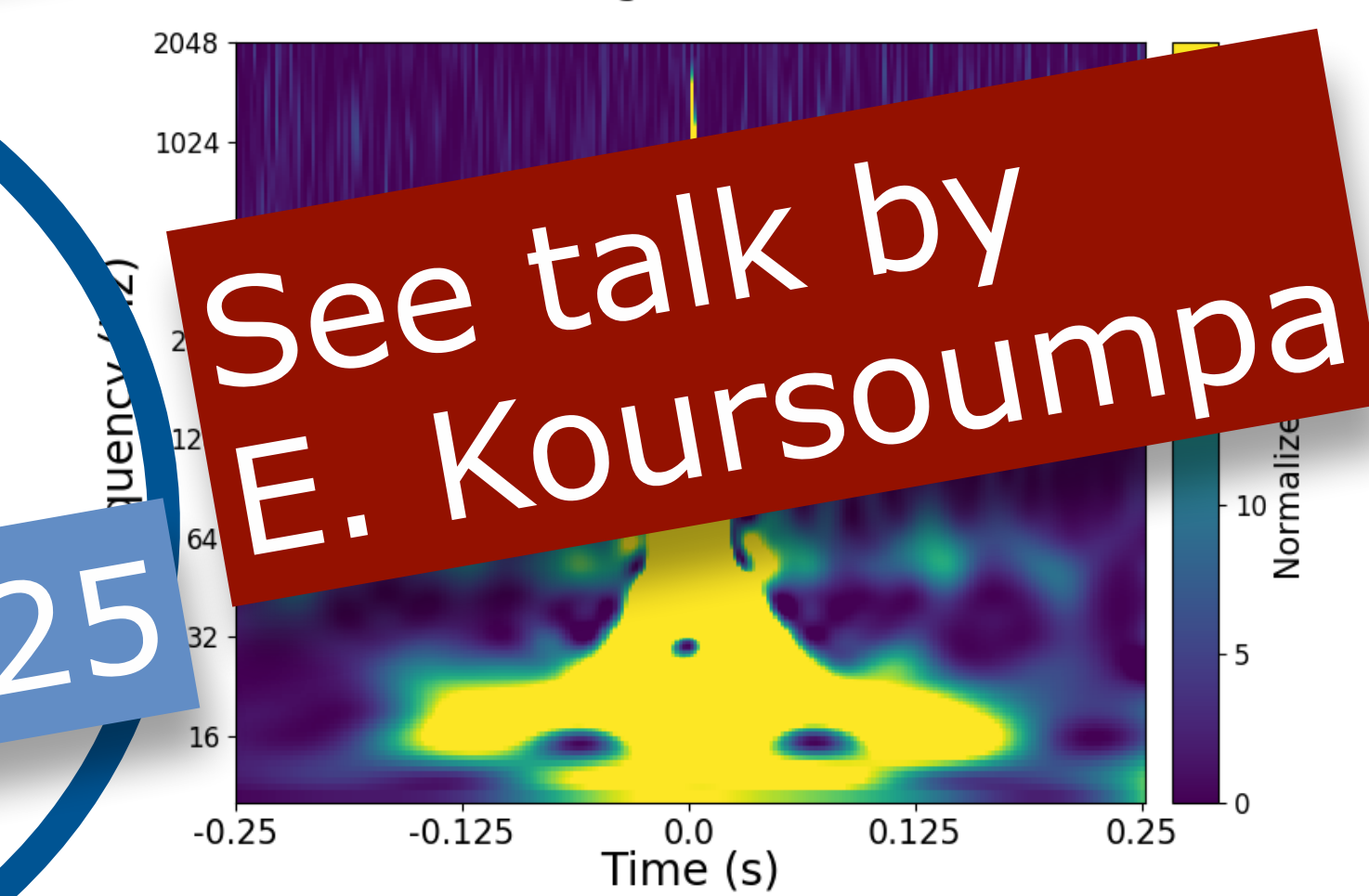


Parameter
Estimation

Sky Localization



Livingston - O2a



Vretinaris et al. 2025

GRAVITATIONAL WAVE DETECTION

PHYSICAL REVIEW D 108, 024022 (2023)



Deep residual networks for gravitational wave detection

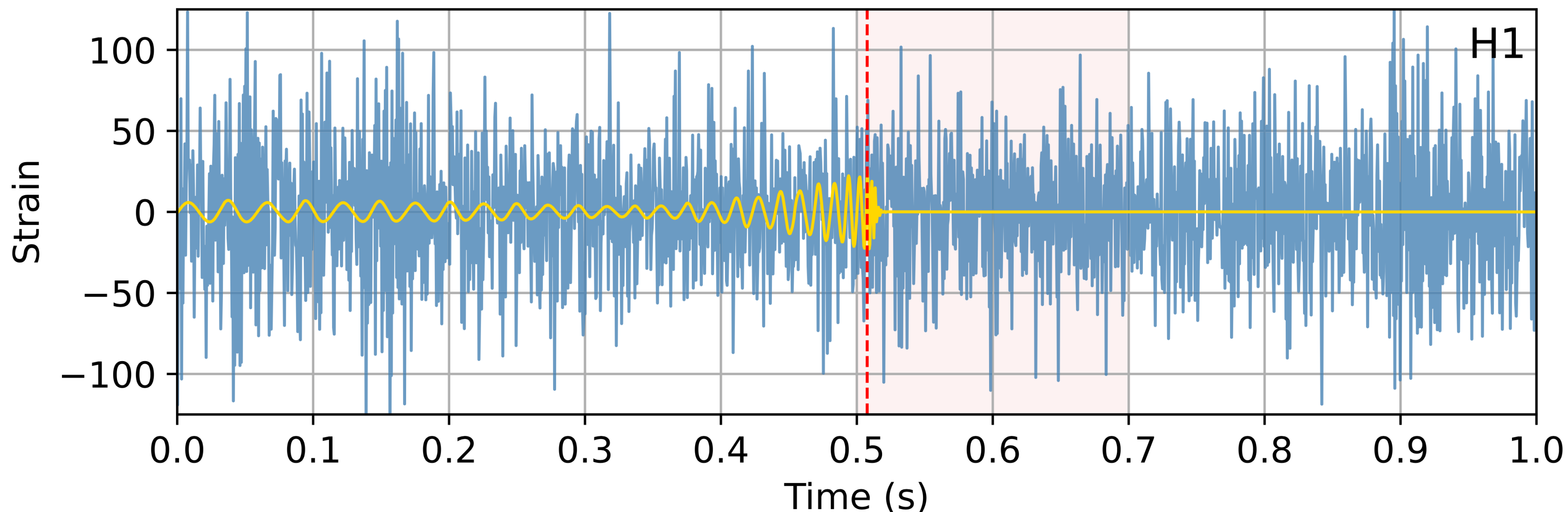
Paraskevi Nousi^{ID},¹ Alexandra E. Koloniari,² Nikolaos Passalis,¹ Panagiotis Iosif^{ID},²
Nikolaos Stergioulas^{ID},² and Anastasios Tefas¹

¹*Department of Informatics, Aristotle University of Thessaloniki, 54124 Thessaloniki, Greece*

²*Department of Physics, Aristotle University of Thessaloniki, 54124 Thessaloniki, Greece*



(Received 17 December 2022; accepted 14 June 2023; published 11 July 2023)



Architecture:

- 54-layer Resnet-1D
- Deep Adaptive Input Normalization
- SNR-based Curriculum Learning
- 30x faster than PyCBC (using a single GPU card)



Architecture:

- 54-layer Resnet-1D
- Deep Adaptive Input Normalization
- SNR-based Curriculum Learning
- 30x faster than PyCBC (using a single GPU card)



Training: 1-second segments @2kHz of BBH injections with **IMRPhenomXPHM** in real O3 noise from L1 and H1

Mass range:

$$7M_{\odot} \leq M \leq 50M_{\odot}$$

Architecture:

- 54-layer Resnet-1D
- Deep Adaptive Input Normalization
- SNR-based Curriculum Learning
- 30x faster than PyCBC (using a single GPU card)



Training: 1-second segments @2kHz of BBH injections with **IMRPhenomXPHM** in real O3 noise from L1 and H1

Mass range:

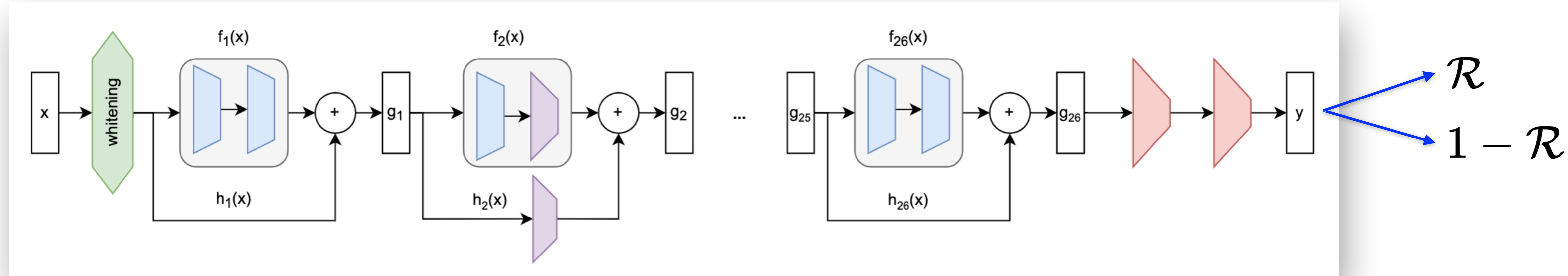
$$7M_{\odot} \leq M \leq 50M_{\odot}$$

Leading algorithm (Virgo-AUTH) in the **1st ML GW search challenge** in the most demanding dataset.

<https://github.com/gwastro/ml-mock-data-challenge-1>

NETWORK ARCHITECTURE OF ARES-GW

1-D ResNet-54 (27 residual blocks with 2 convolutional layers each and skip connections)!

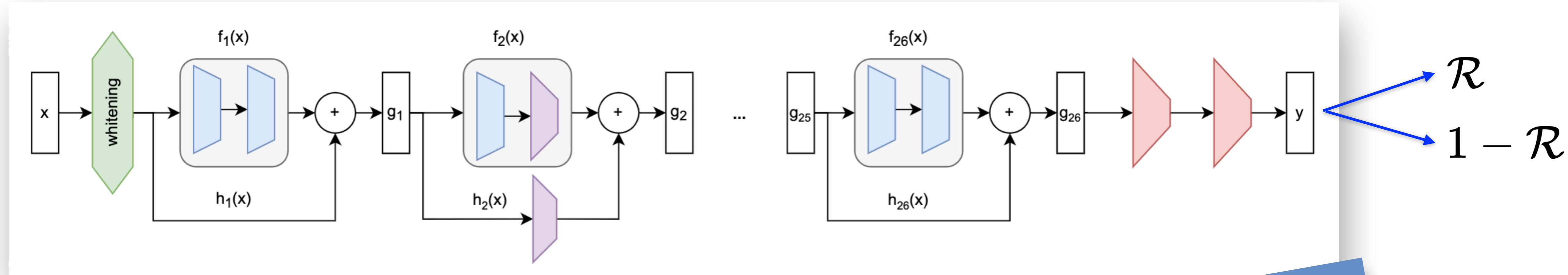


- Residual blocks with skip connections: $g(\mathbf{x}) = f(\mathbf{x}) + h(\mathbf{x})$
- $h(\mathbf{x}) = \mathbf{x}$ or a strided convolutional layer
- After each convolutional layer: batch normalization + ReLU activation
- Mini-batch size of 400 segments
- Adam optimizer for back propagation
- Objective function = regularized binary cross entropy

Residual blocks	Filters	Strided	Input D
4	8		2×2048
1	16	✓	8×2048
2	16		16×1024
1	32	✓	16×1024
2	32		32×512
1	64	✓	32×512
2	64		64×256
1	64	✓	64×256
2	64		64×128
1	64	✓	64×128
2	64		64×64
5	32		64×64
3	16		32×64

NETWORK ARCHITECTURE OF ARES-GW

1-D ResNet-54 (27 residual blocks with 2 convolutional layers each and skip connections)!



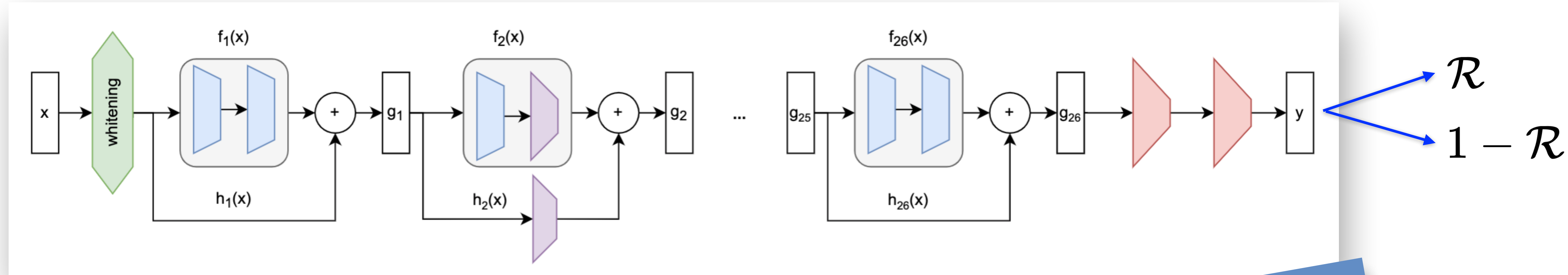
- Residual blocks with skip connections: $g(\mathbf{x}) = \mathbf{x}$
- $h(\mathbf{x}) = \mathbf{x}$ or a strided convolutional layer
- After each convolutional layer: batch norm
ReLU activation
- Mini-batch size of 400 segments
- Adam optimizer for back propagation
- Objective function = regularized binary cross entropy

Gradient problem solved!
-> much deeper networks

	Input D	
10	2×2048	✓
16	8×2048	
32	16×1024	
64	16×1024	
32	32×512	
64	32×512	✓
64	64×256	
64	64×256	✓
64	64×128	
64	64×128	✓
64	64×64	
32	64×64	
16	32×64	

NETWORK ARCHITECTURE OF ARES-GW

1-D ResNet-54 (27 residual blocks with 2 convolutional layers each and skip connections)!



- Residual blocks with skip connections: $g_i(\mathbf{x}) + \mathbf{x}$
- $h_i(\mathbf{x}) = \mathbf{x}$ or a strided convolutional layer
- After each convolutional layer: batch norm + ReLU activation
- Mini-batch size of 400 segments
- Adam optimizer for back propagation
- Objective function = regularized binary cross-entropy

Gradient problem solved!
-> much deeper networks

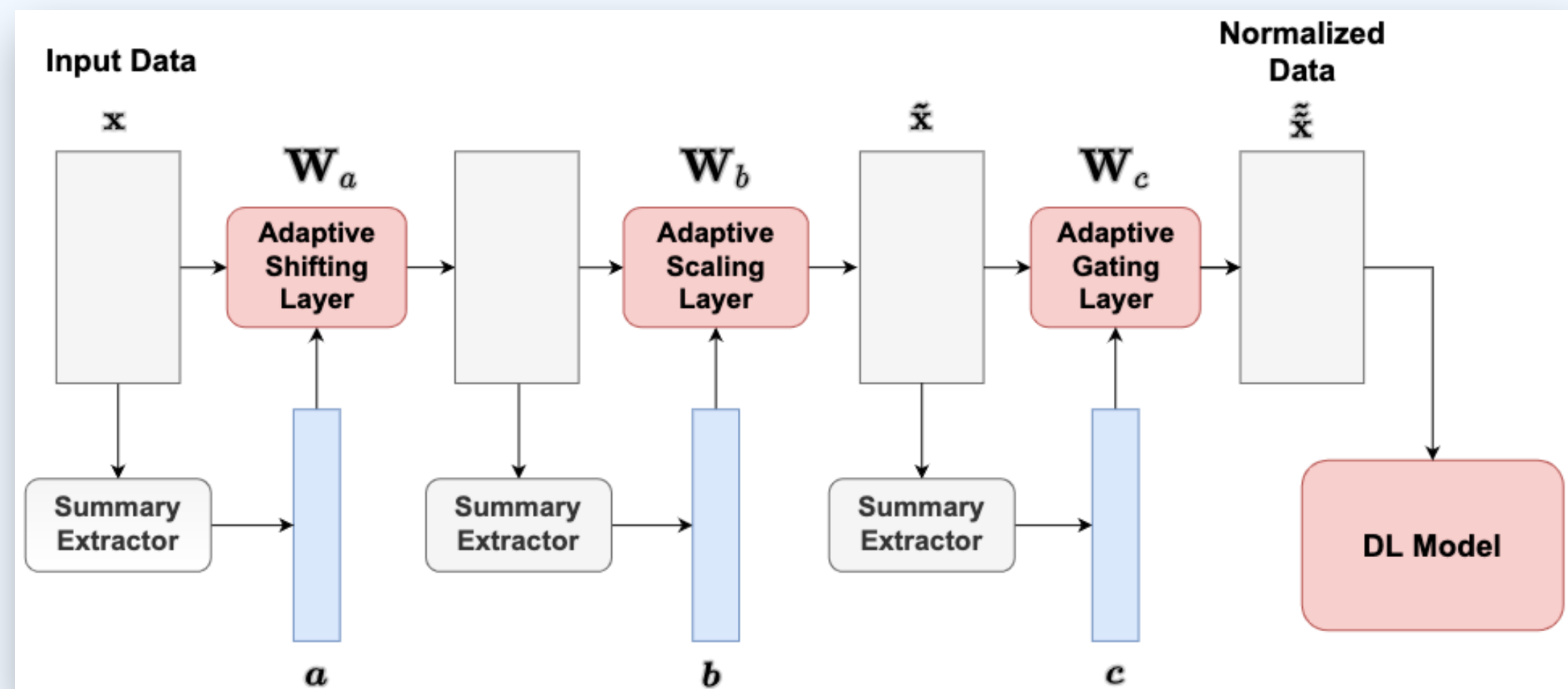
1-D ResNet-54 now used by most
ML GW detection codes

Input D	64 × 256
2 × 2048	✓
8 × 2048	
10	
16	
32	
1	
2	
5	64
3	64
7	64
6	64
4	64
8	64
9	64
11	64
12	64
13	64
14	64
15	64
17	64
18	64
19	64
20	64
21	64
22	64
23	64
24	64
25	64
26	64
27	64
28	64
29	64
30	64
31	64
33	64
34	64
35	64
36	64
37	64
38	64
39	64
40	64
41	64
42	64
43	64
44	64
45	64
46	64
47	64
48	64
49	64
50	64
51	64
52	64
53	64
54	64
55	64
56	64
57	64
58	64
59	64
60	64
61	64
62	64
63	64
64	64
65	64
66	64
67	64
68	64
69	64
70	64
71	64
72	64
73	64
74	64
75	64
76	64
77	64
78	64
79	64
80	64
81	64
82	64
83	64
84	64
85	64
86	64
87	64
88	64
89	64
90	64
91	64
92	64
93	64
94	64
95	64
96	64
97	64
98	64
99	64
100	64
101	64
102	64
103	64
104	64
105	64
106	64
107	64
108	64
109	64
110	64
111	64
112	64
113	64
114	64
115	64
116	64
117	64
118	64
119	64
120	64
121	64
122	64
123	64
124	64
125	64
126	64
127	64
128	64
129	64
130	64
131	64
132	64
133	64
134	64
135	64
136	64
137	64
138	64
139	64
140	64
141	64
142	64
143	64
144	64
145	64
146	64
147	64
148	64
149	64
150	64
151	64
152	64
153	64
154	64
155	64
156	64
157	64
158	64
159	64
160	64
161	64
162	64
163	64
164	64
165	64
166	64
167	64
168	64
169	64
170	64
171	64
172	64
173	64
174	64
175	64
176	64
177	64
178	64
179	64
180	64
181	64
182	64
183	64
184	64
185	64
186	64
187	64
188	64
189	64
190	64
191	64
192	64
193	64
194	64
195	64
196	64
197	64
198	64
199	64
200	64
201	64
202	64
203	64
204	64
205	64
206	64
207	64
208	64
209	64
210	64
211	64
212	64
213	64
214	64
215	64
216	64
217	64
218	64
219	64
220	64
221	64
222	64
223	64
224	64
225	64
226	64
227	64
228	64
229	64
230	64
231	64
232	64
233	64
234	64
235	64
236	64
237	64
238	64
239	64
240	64
241	64
242	64
243	64
244	64
245	64
246	64
247	64
248	64
249	64
250	64
251	64
252	64
253	64
254	64
255	64
256	64
257	64
258	64
259	64
260	64
261	64
262	64
263	64
264	64
265	64
266	64
267	64
268	64
269	64
270	64
271	64
272	64
273	64
274	64
275	64
276	64
277	64
278	64
279	64
280	64
281	64
282	64
283	64
284	64
285	64
286	64
287	64
288	64
289	64
290	64
291	64
292	64
293	64
294	64
295	64
296	64
297	64
298	64
299	64
300	64
301	64
302	64
303	64
304	64
305	64
306	64
307	64
308	64
309	64
310	64
311	64
312	64
313	64
314	64
315	64
316	64
317	64
318	64
319	64
320	64
321	64
322	64
323	64
324	64
325	64
326	64
327	64
328	64
329	64
330	64
331	64
332	64
333	64
334	64
335	64
336	64
337	64
338	64
339	64
340	64
341	64
342	64
343	64
344	64
345	64
346	64
347	64
348	64
349	64
350	64
351	64
352	64
353	64
354	64
355	64
356	64
357	64
358	64
359	64
360	64
361	64
362	64
363	64
364	64
365	64</

ADAPTIVE INPUT NORMALIZATION

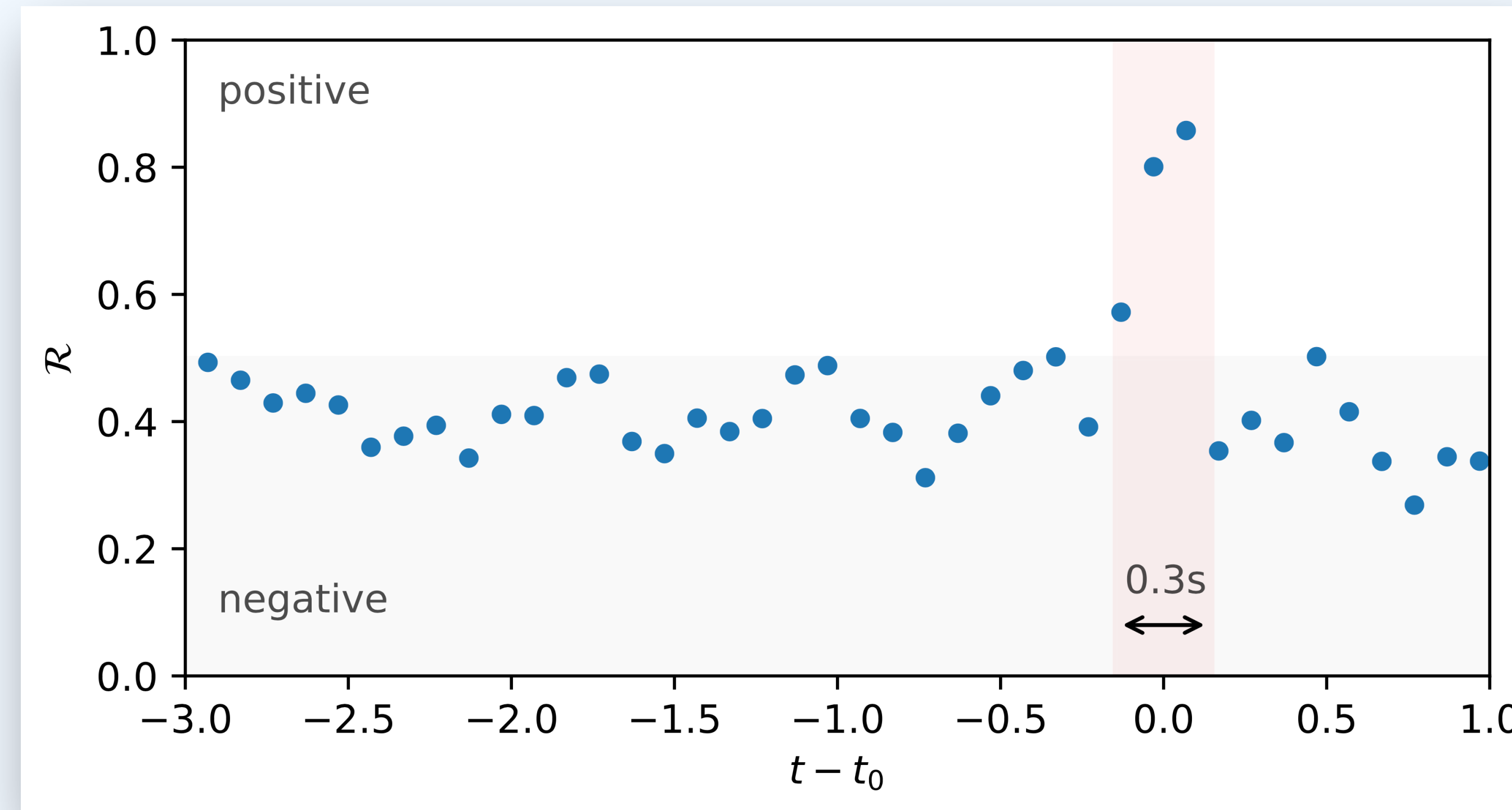
Deep Adaptive Input Normalization (DAIN) (Passalis et al. 2019)

Is applied during training - weights \mathbf{W}_a , \mathbf{W}_b , \mathbf{W}_c are learnable and adapt to input data!



RANKING STATISTIC

Neural Network Ranking Statistic R is reported every 0.1 s of input data



Logarithmic Ranking Statistic

$$\mathcal{R}_s = -\log_{10}(1 - \mathcal{R} + 10^{-16})$$

ARESGW ON GITHUB

<https://github.com/vivinousi/gw-detection-deep-learning>

vivinousi / gw-detection-deep-learning Public

Code Issues Pull requests Actions Projects Security Insights

master 1 Branch Tags Go to file Code

vivinousi	readme update	dde2791 · 2 years ago	8 Commits
doc	readme update	2 years ago	
modules	training code initial commit	2 years ago	
trained_models	training code initial commit	2 years ago	
utils	training code initial commit	2 years ago	
LICENSE	Initial commit	2 years ago	
README.md	readme update	2 years ago	
run_on_test.sh	training code initial commit	2 years ago	
test.py	training code initial commit	2 years ago	
test_challenge_model.py	training code initial commit	2 years ago	
train.py	readme update	2 years ago	

About

Gravitational wave detection in real noise timeseries using deep residual neural networks

Readme Apache-2.0 license Activity 22 stars 7 watching 2 forks Report repository

Releases No releases published

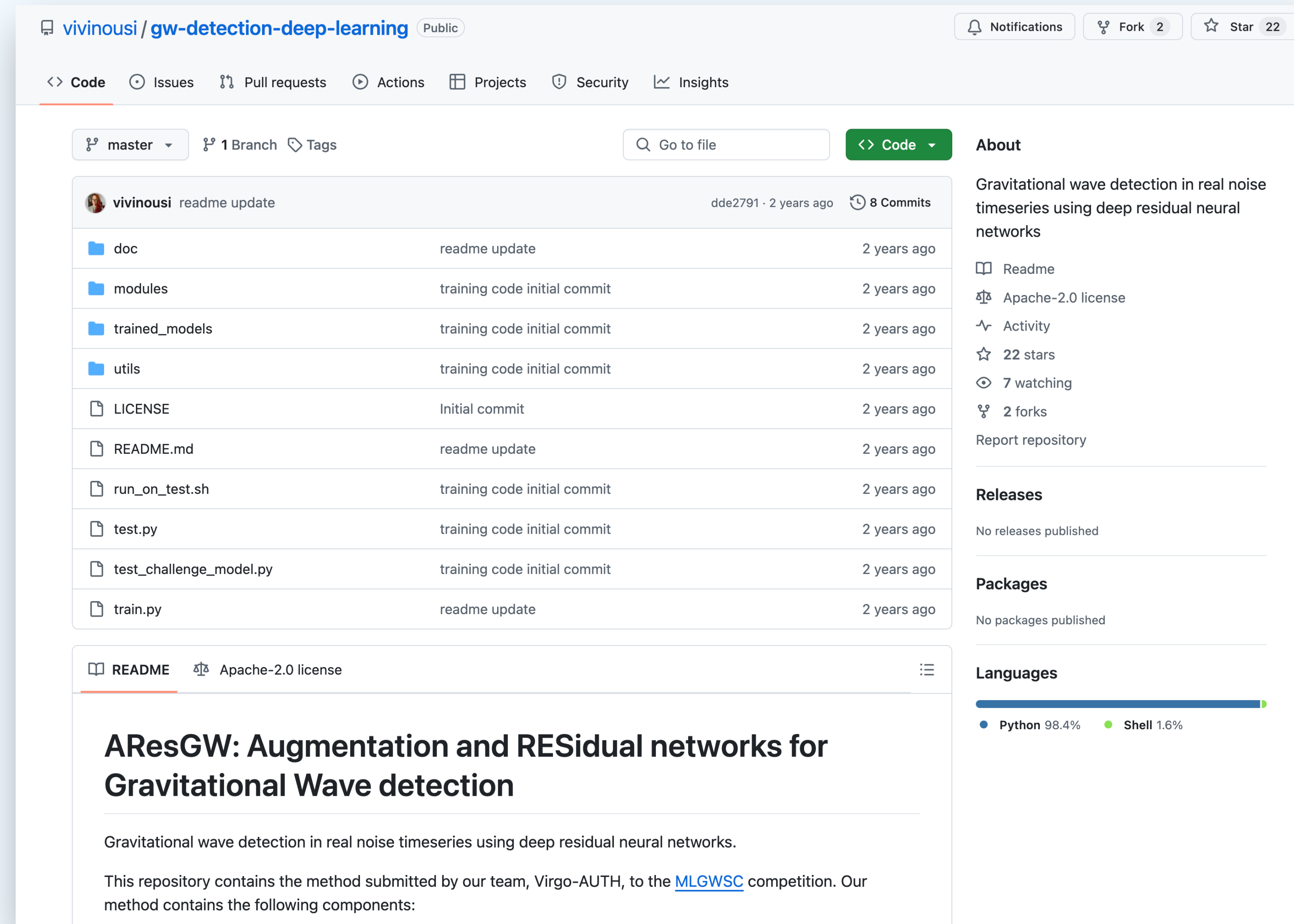
Packages No packages published

Languages Python 98.4% Shell 1.6%

AResGW: Augmentation and RESidual networks for Gravitational Wave detection

Gravitational wave detection in real noise timeseries using deep residual neural networks.

This repository contains the method submitted by our team, Virgo-AUTH, to the [MLGWSC](#) competition. Our method contains the following components:



PAPER

New gravitational wave discoveries enabled by machine learning

Alexandra E Koloniari^{1,*} , Evdokia C Koursoumpa¹ , Paraskevi Nousi² , Paraskevas Lampropoulos¹ , Nikolaos Passalis³ , Anastasios Tefas⁴  and Nikolaos Stergioulas¹ 

¹ Department of Physics, Aristotle University of Thessaloniki, 54124 Thessaloniki, Greece

² Swiss Data Science Center, ETH, Zürich, Switzerland

³ Department of Chemical Engineering, Faculty of Engineering, Aristotle University of Thessaloniki, 54124 Thessaloniki, Greece

⁴ Department of Informatics, Aristotle University of Thessaloniki, 54124 Thessaloniki, Greece

* Author to whom any correspondence should be addressed.

E-mail: akolonia@auth.gr



OPEN ACCESS

RECEIVED

20 September 2024

REVISED

16 January 2025

ACCEPTED FOR PUBLICATION

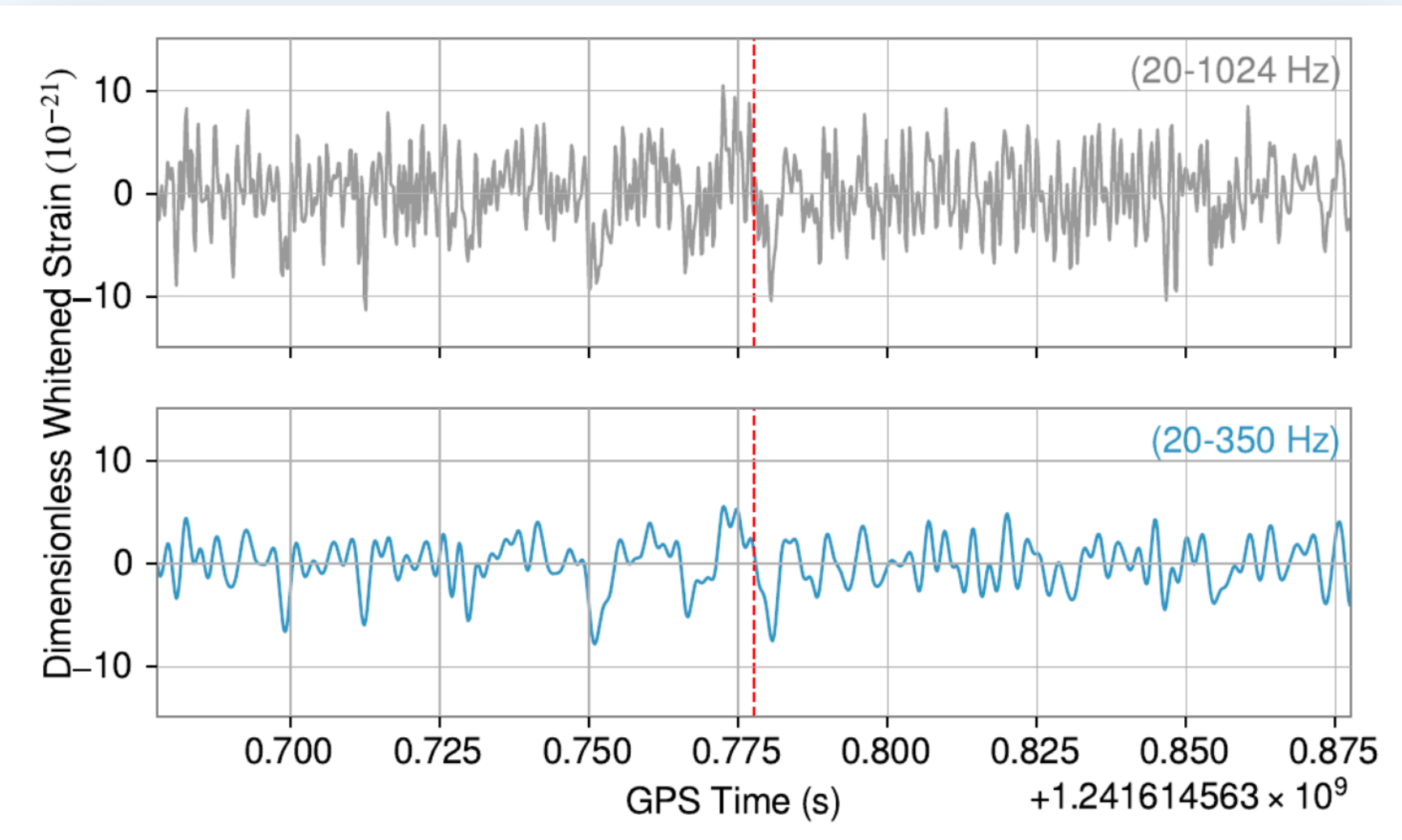
13 February 2025

PUBLISHED

27 February 2025

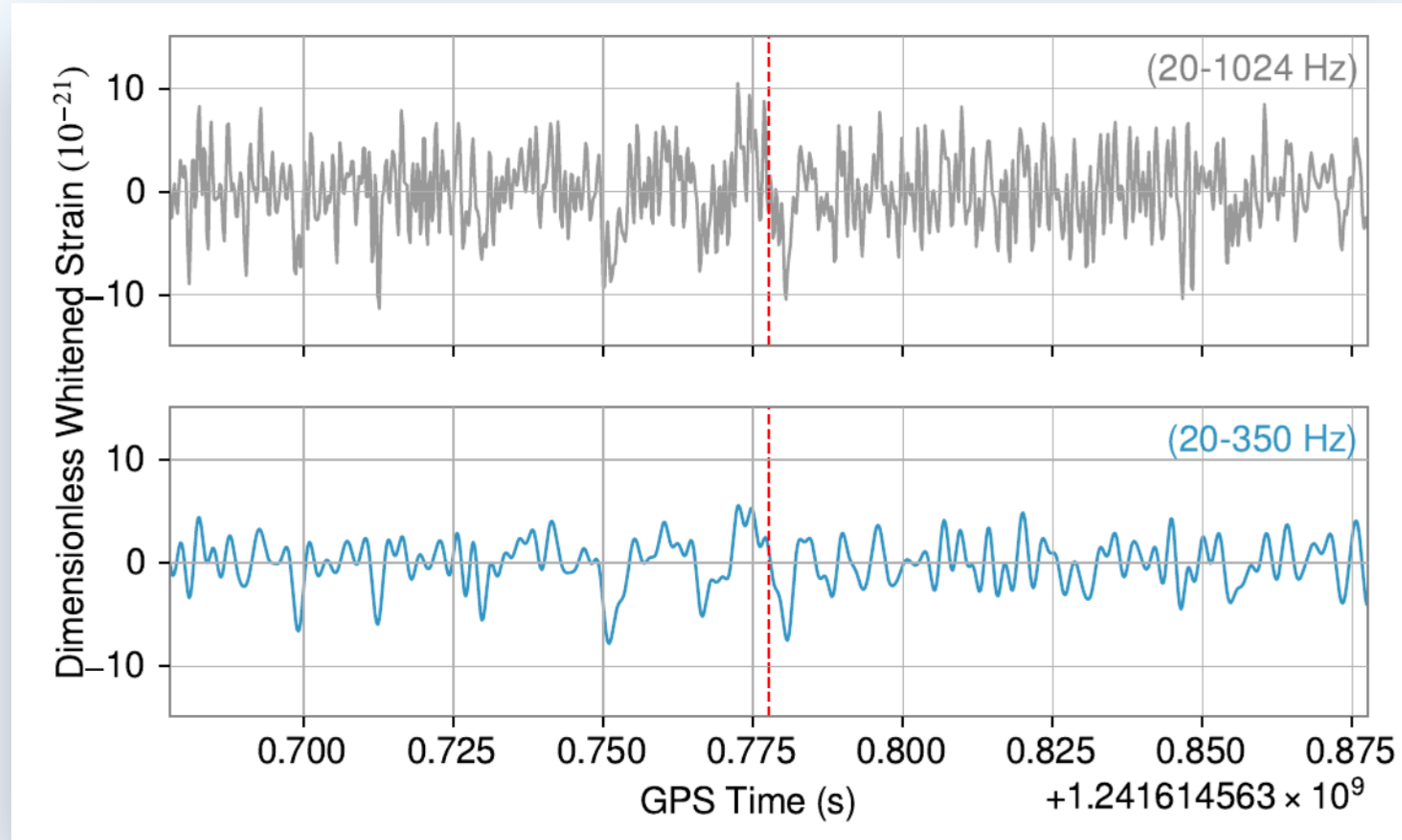
MAIN ENHANCEMENTS:

1) Training on low-pass filtered data

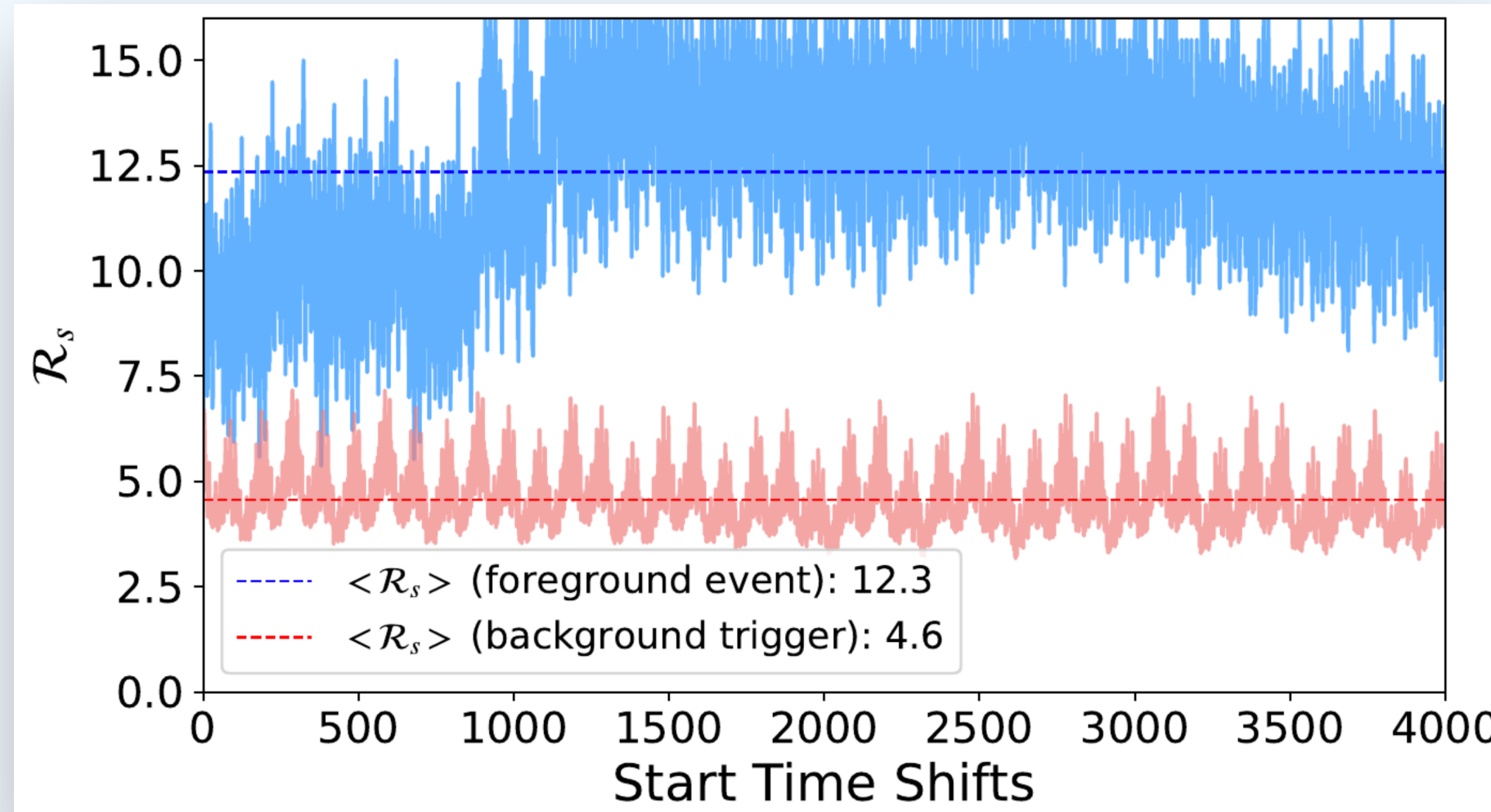


MAIN ENHANCEMENTS:

1) Training on low-pass filtered data

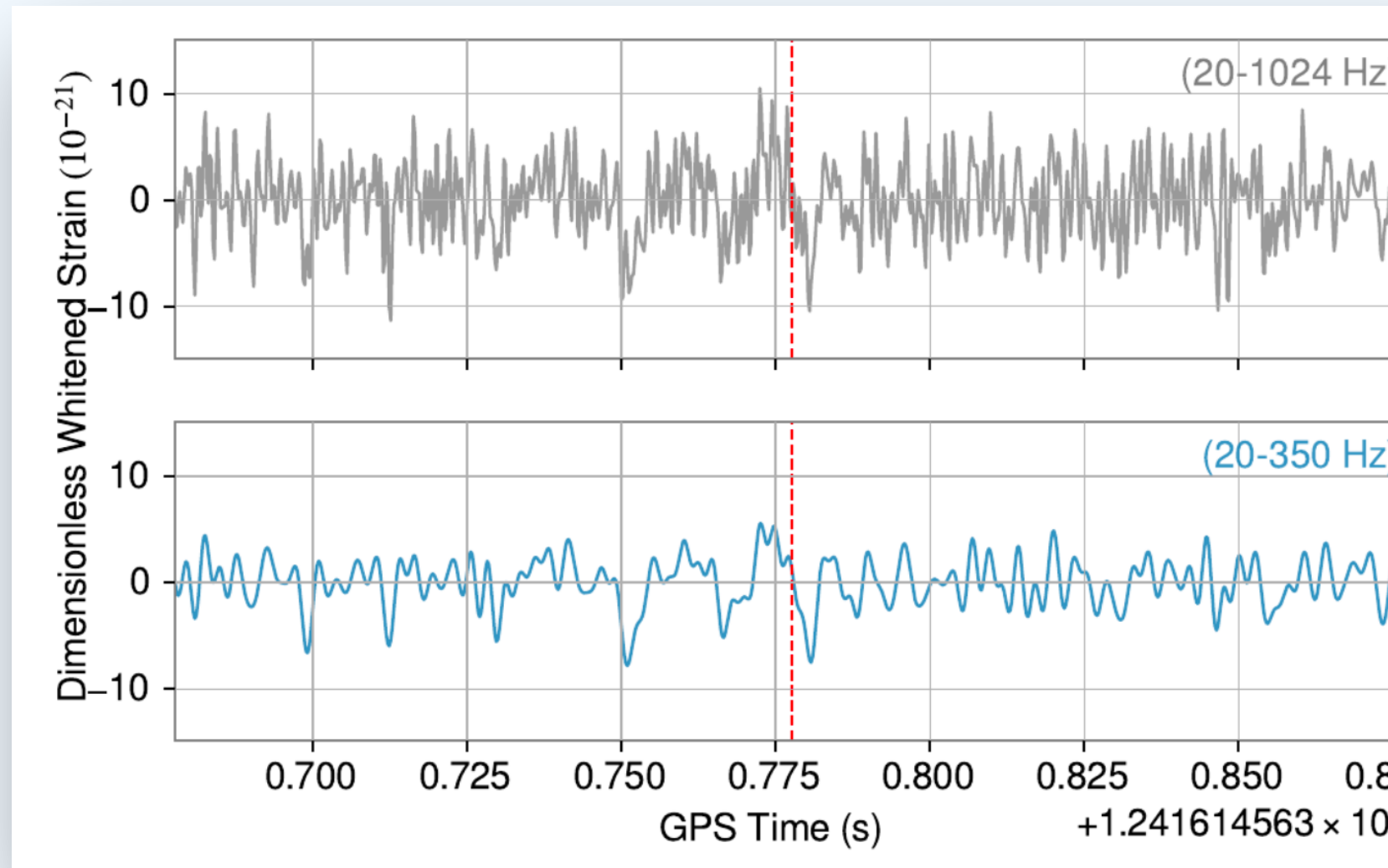


2) Ensemble-averaged ranking statistic

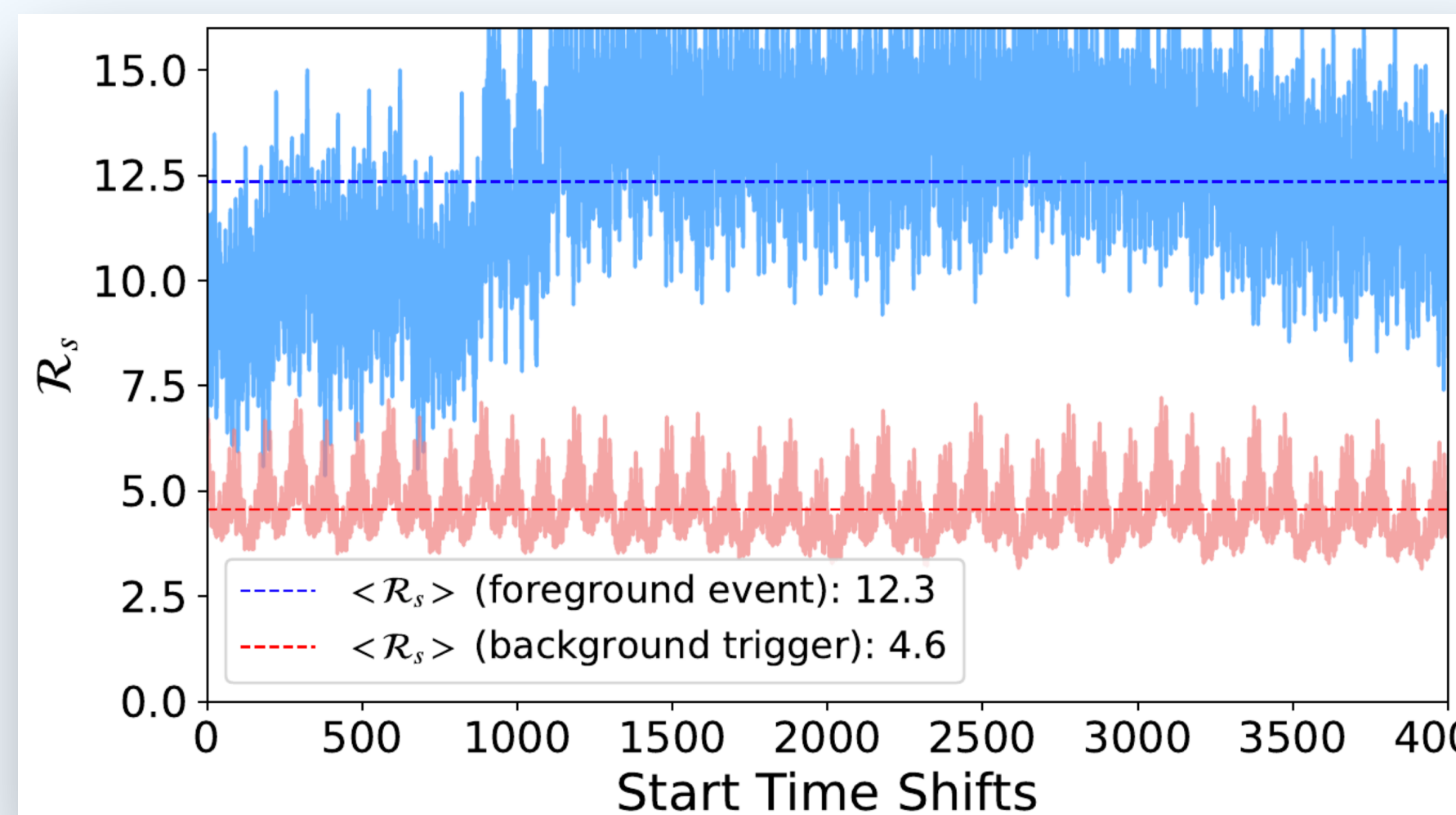


MAIN ENHANCEMENTS:

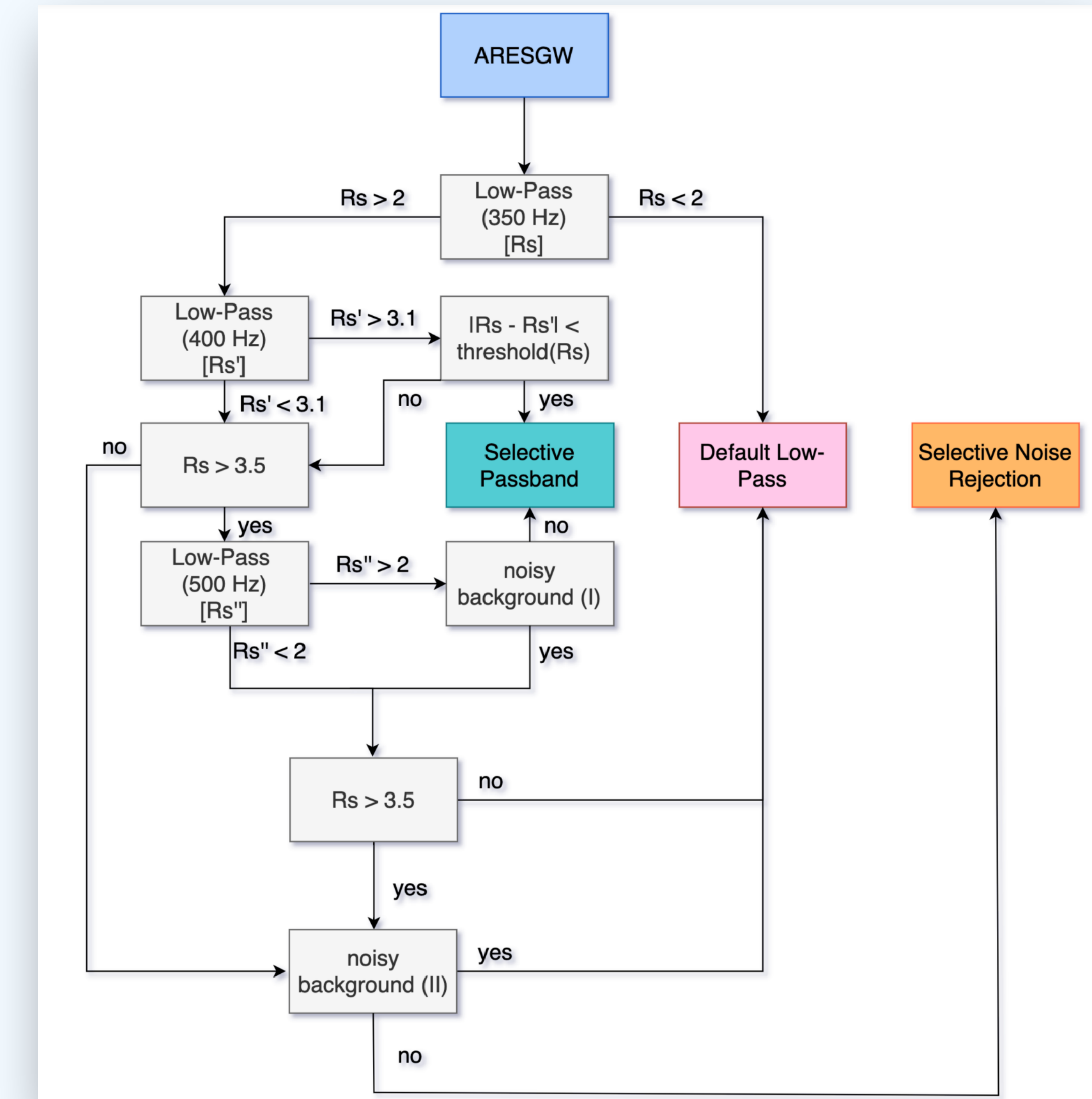
1) Training on low-pass filtered data



2) Ensemble-averaged ranking statistic



3) Application of noise filters to reduce background FAR.



ASTROPHYSICAL PROBABILITY

p_astro is calculated as

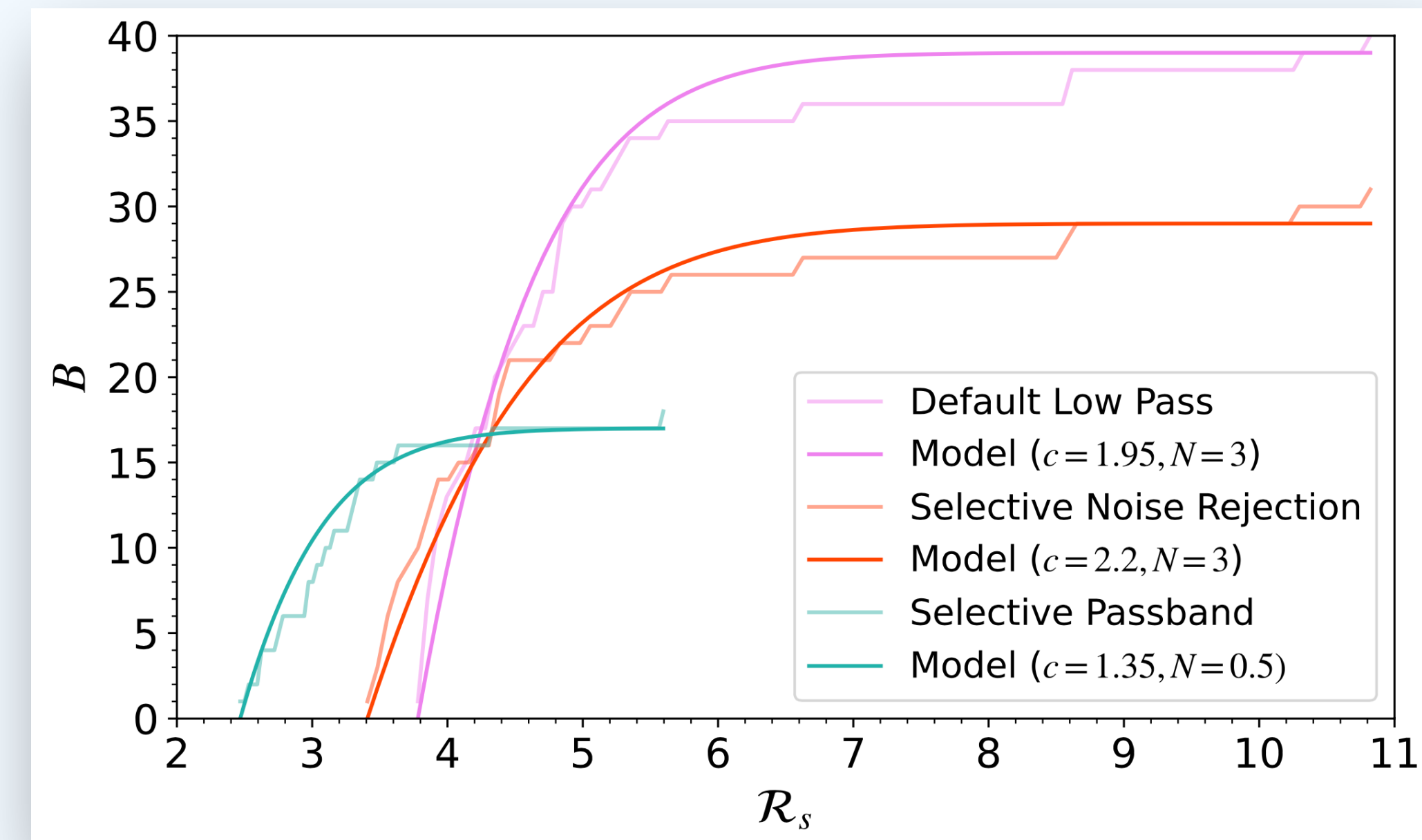
$$p_{\text{astro}} = \frac{f(\mathcal{R}_s)}{b(\mathcal{R}_s) + f(\mathcal{R}_s)}$$

where the **background** and **foreground** differential rates are

The cumulative distribution of the **O3 background** is modeled **analytically** as

$$b(\mathcal{R}_s) = \frac{dB}{d\mathcal{R}_s} \quad f(\mathcal{R}_s) = \frac{dF}{d\mathcal{R}_s}$$

$$\hat{B}(x) = \frac{\left(1 + \operatorname{erf}\left(\frac{x}{\sqrt{2}}\right)\right)^N - \left(1 + \operatorname{erf}\left(\frac{x_{\min}}{\sqrt{2}}\right)\right)^N}{2^N - \left(1 + \operatorname{erf}\left(\frac{x_{\min}}{\sqrt{2}}\right)\right)^N}$$

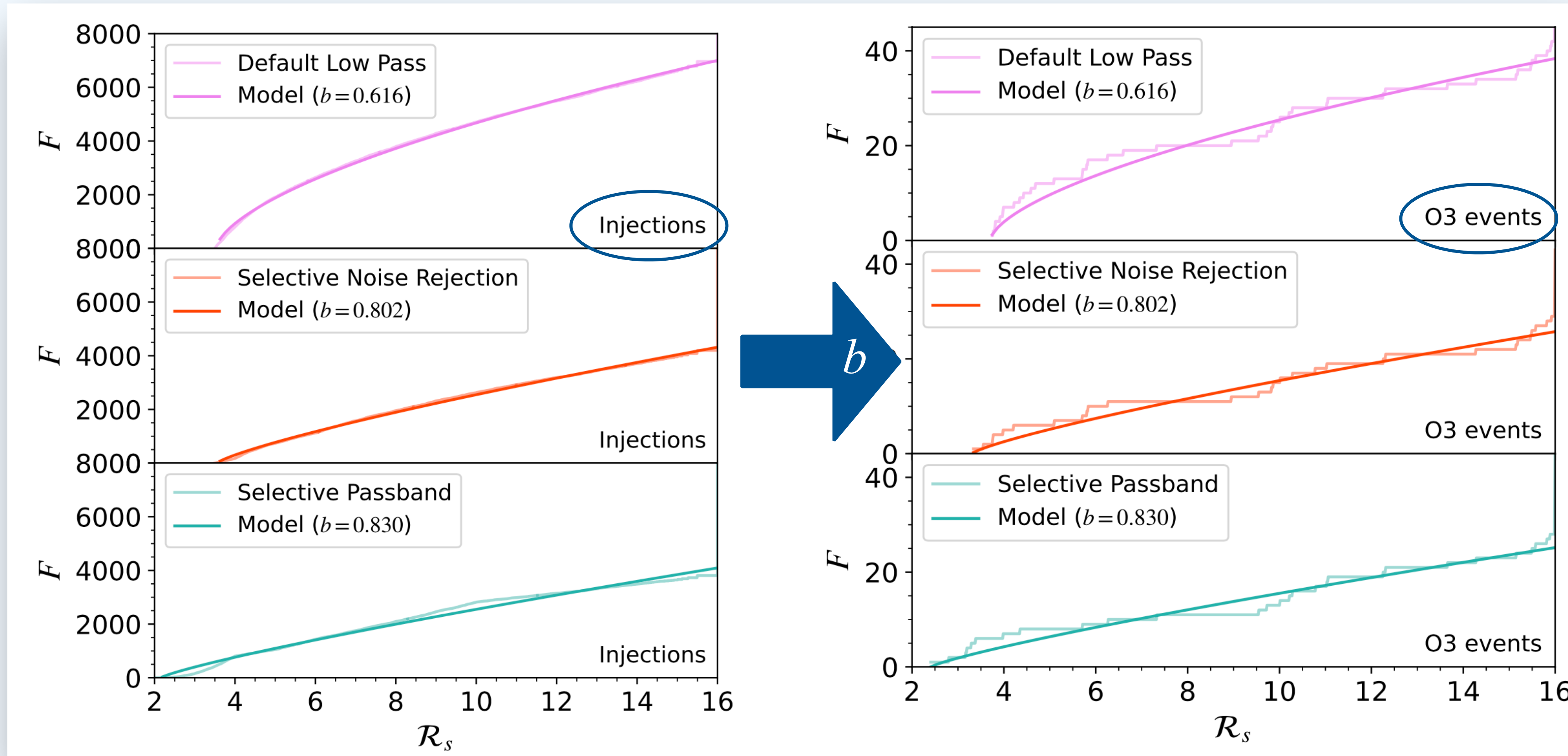


ASTROPHYSICAL PROBABILITY

Analytic model of cumulative **foreground** distribution:

$$F(x) = a(x - x_{\min})^b$$

Coefficient **b** determined through injections in O3 noise:



NEW GW DETECTIONS WITH AresGW IN O3 DATA

AresGW detects **42 out of 51** known O3 events (*most sensitive pipeline in this mass range*)

We found **8 new gravitational wave candidates** with $p_{\text{astro}} > 50\%$ (3 $p_{\text{astro}} > 99\%$).

TABLE VII: New candidate events identified by AresGW.

#	Event Name	GPS Time (s)	p_{astro}	FAR (1/yr)	$\langle \mathcal{R}_s \rangle$	Time delay (s)	χ_L^2	χ_H^2	Class
1	GW190511_125545	1241614563.77	1.00	0.27	9.54	0.0027	1.16	1.46	Selective Passband
2	GW190614_134749	1244555287.93	0.99	4.6	5.80	0.0012	0.65	0.80	Selective Passband
3	GW190607_083827	1243931925.99	0.99	6.5	8.95	0.0056	0.90	0.48	Selective Noise Rejection
4	GW190904_104631	1251629209.01	0.72	14	4.35	0.0002	0.38	0.71	Selective Passband
5	GW190523_085933	1242637191.44	0.68	20	6.60	0.0054	0.75	1.39	Selective Noise Rejection
6	GW200208_211609	1265231787.68	0.55	18	4.0	0.0063	0.69	0.98	Selective Passband
7	GW190705_164632	1246380410.88	0.51	49	5.82	0.0103	1.05	0.98	Default Low-Pass*
8	GW190426_082124	1240302101.93	0.50	20	3.91	0.0007	1.48	0.53	Selective Passband

NEW GW DETECTIONS WITH AresGW IN O3 DATA

AresGW detects **42 out of 51** known O3 events (*most sensitive pipeline in this mass range*)

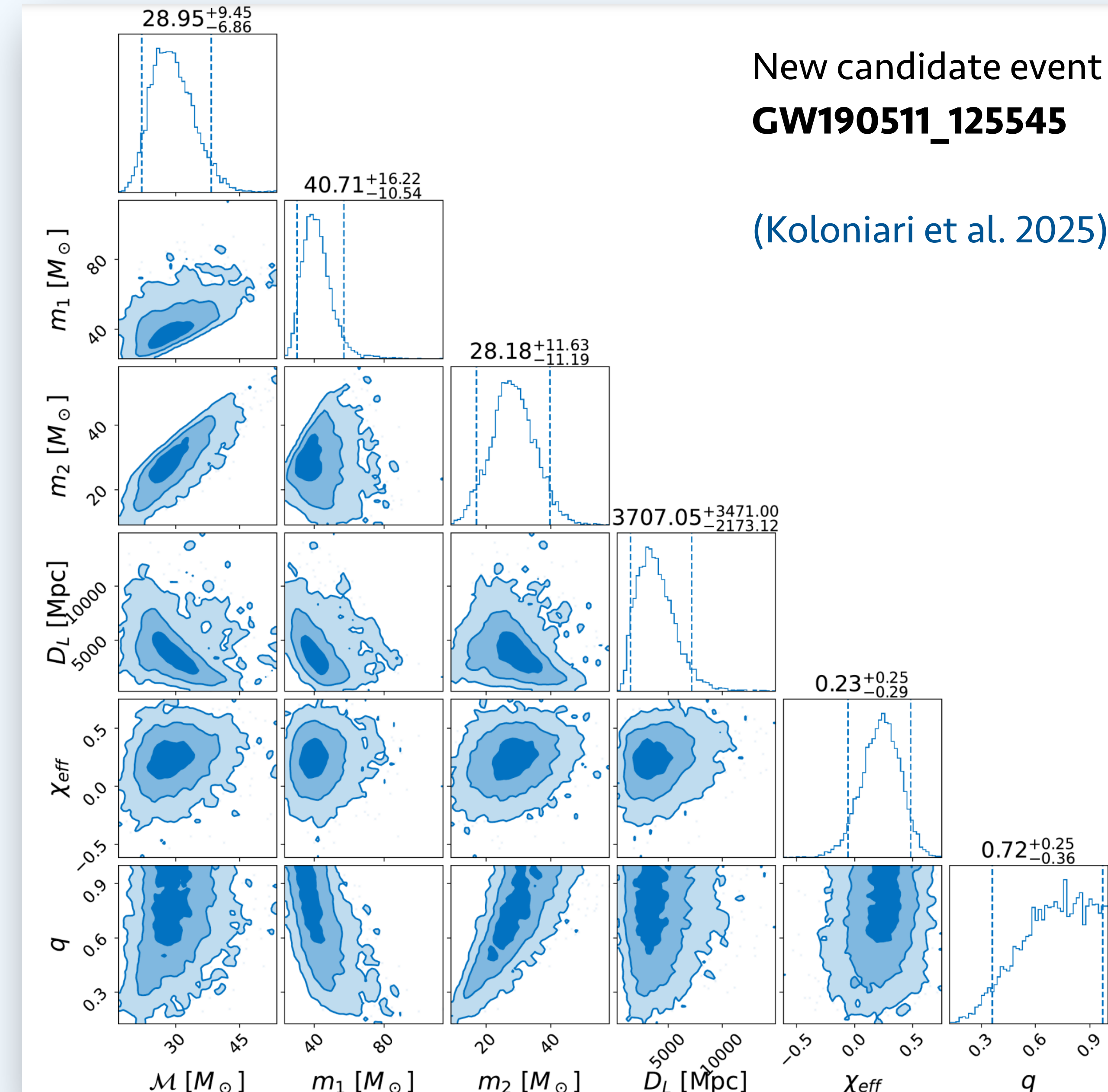
We found **8 new gravitational wave candidates** with $p_{\text{astro}} > 50\%$ (3 $p_{\text{astro}} > 99\%$).

TABLE VII: New candidate events identified by AresGW.

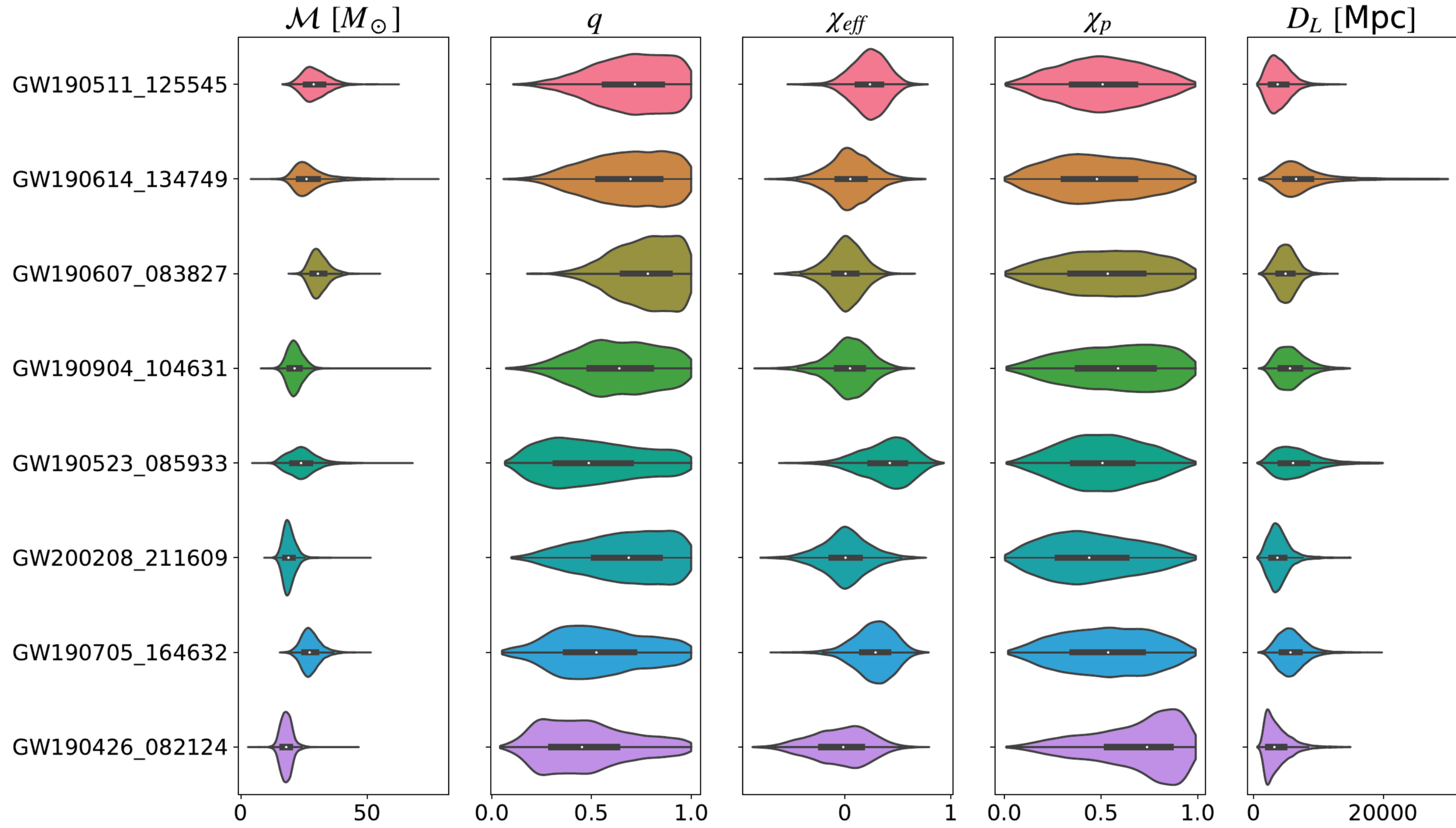
#	Event Name	GPS Time (s)	p_{astro}	FAR (1/yr)	$\langle \mathcal{R}_s \rangle$	Time delay	χ^2	S	Class
1	GW190511_125545	1241614563.77	1.00	1.00	0.55	0.0056	0.90	0.80	Selective Passband
2	GW190614_134749	1242637191.44	0.68	20	6.60	0.0054	0.75	1.39	Selective Noise Rejection
3	GW190607_083441	1242637191.44	0.72	14	4.35	0.0002	0.38	0.71	Selective Passband
4	GW190904_104231	1241614563.77	0.68	20	6.60	0.0054	0.75	1.39	Selective Noise Rejection
5	GW200208_211609	1265231787.68	0.55	18	4.0	0.0063	0.69	0.98	Selective Passband
7	GW190705_164632	1246380410.88	0.51	49	5.82	0.0103	1.05	0.98	Default Low-Pass*
8	GW190426_082124	1240302101.93	0.50	20	3.91	0.0007	1.48	0.53	Selective Passband

First GW events identified
using a machine-learning algorithm

PARAMETER ESTIMATION USING BILBY



PARAMETER ESTIMATION USING BILBY



RECONSTRUCTED WAVEFORMS FOR NEW EVENTS

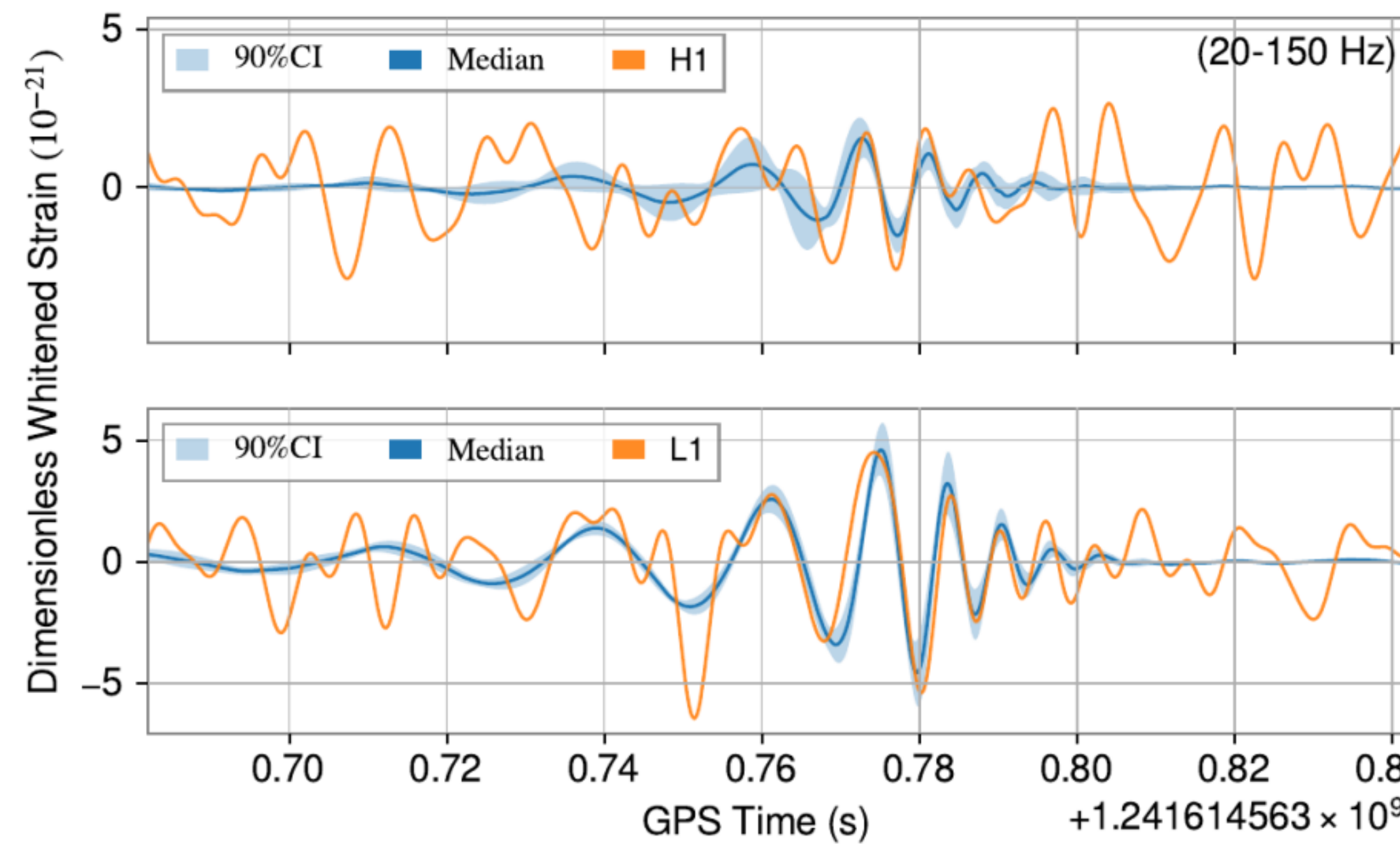


FIG. 35: Whitened, bandpassed strain data and reconstructed waveform for the new event GW190511_125545 identified by AresGW.

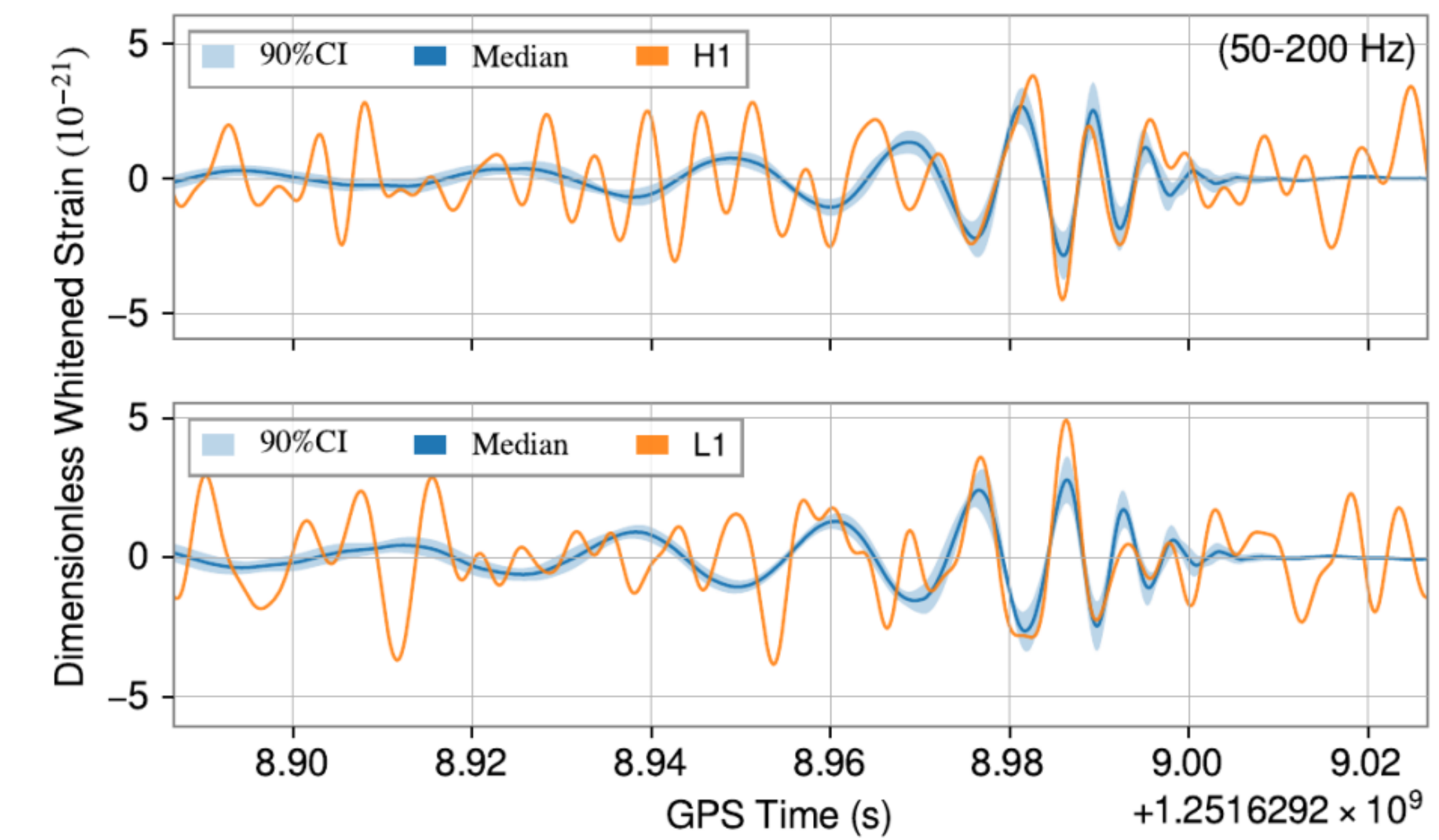
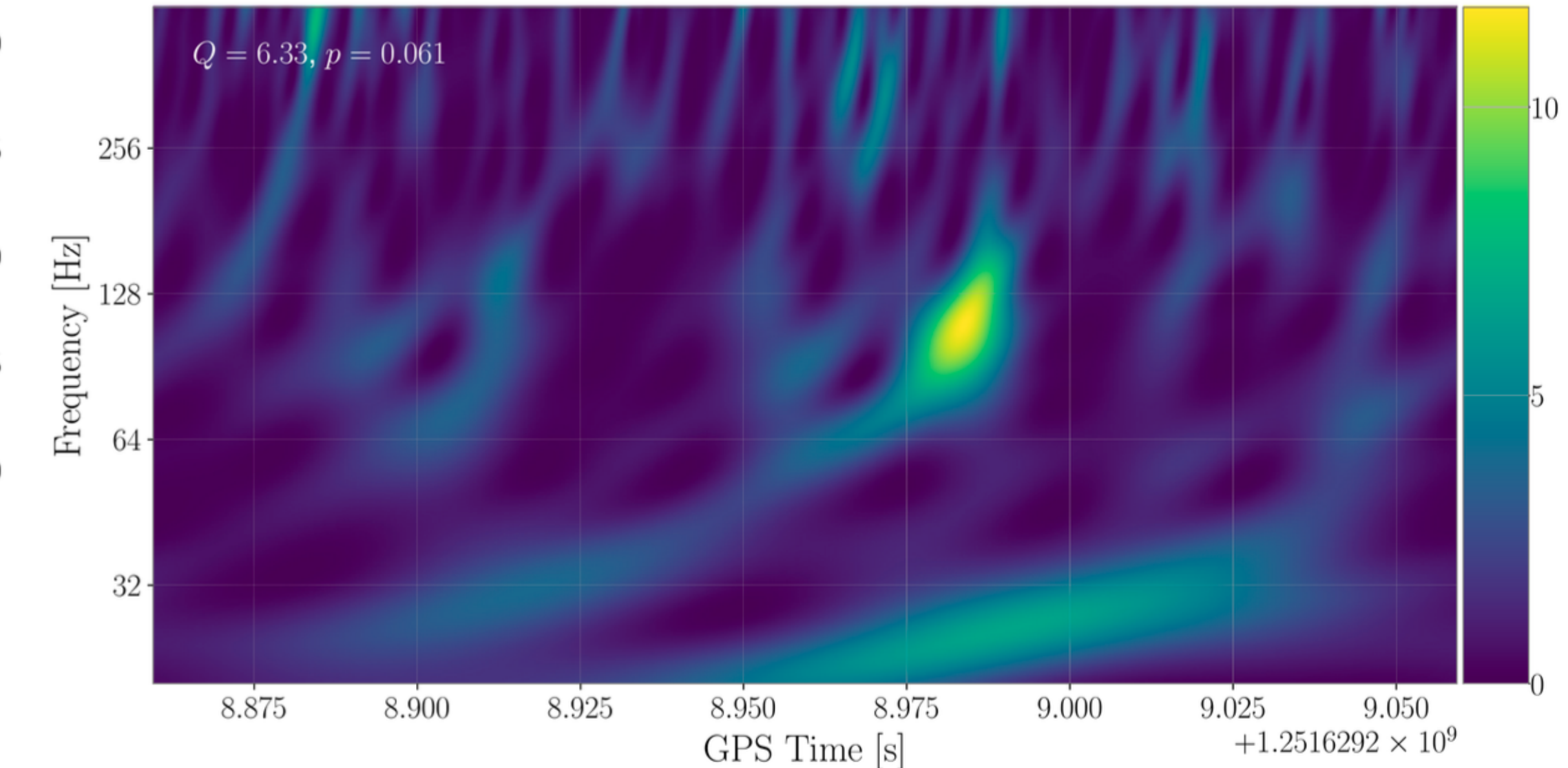
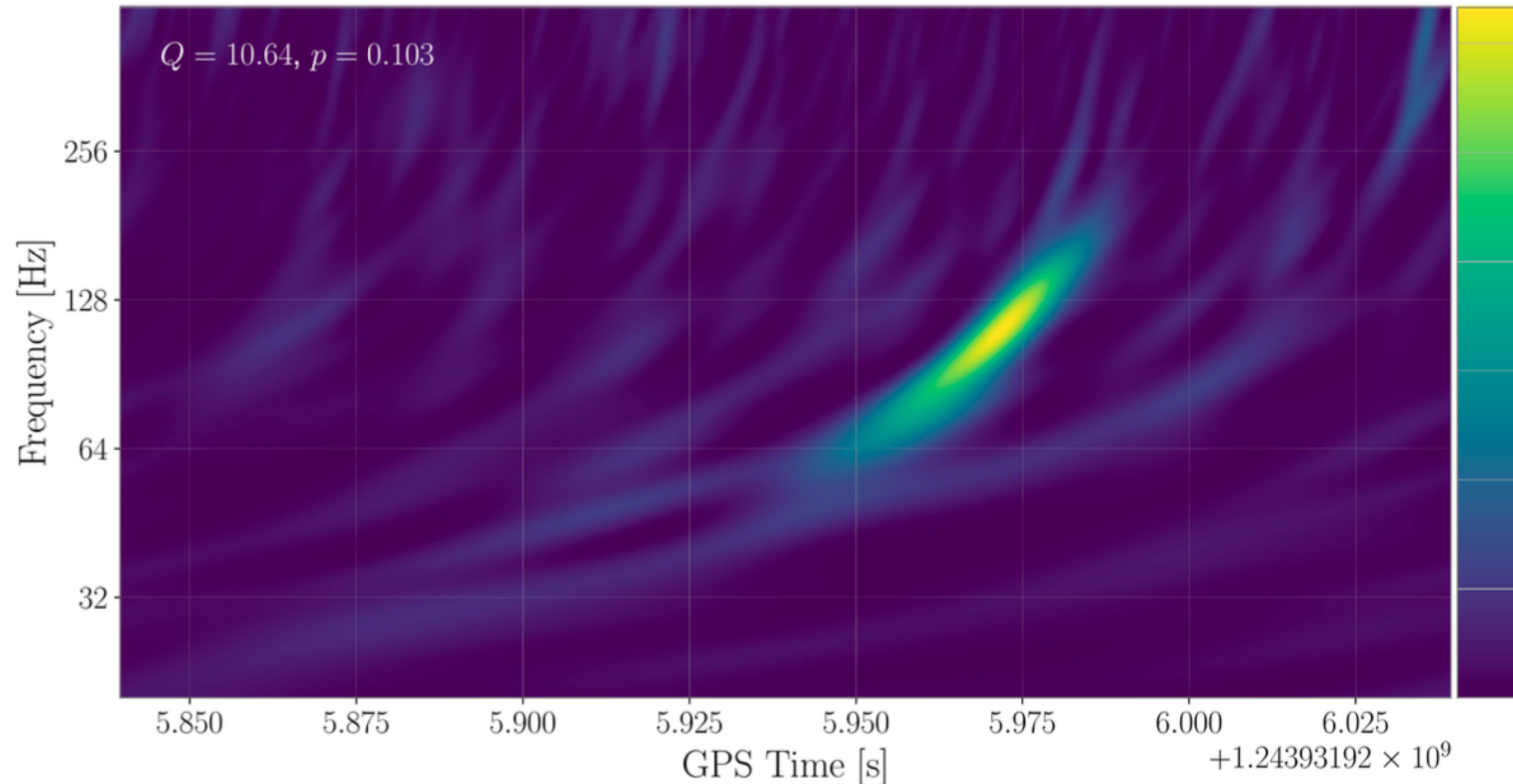
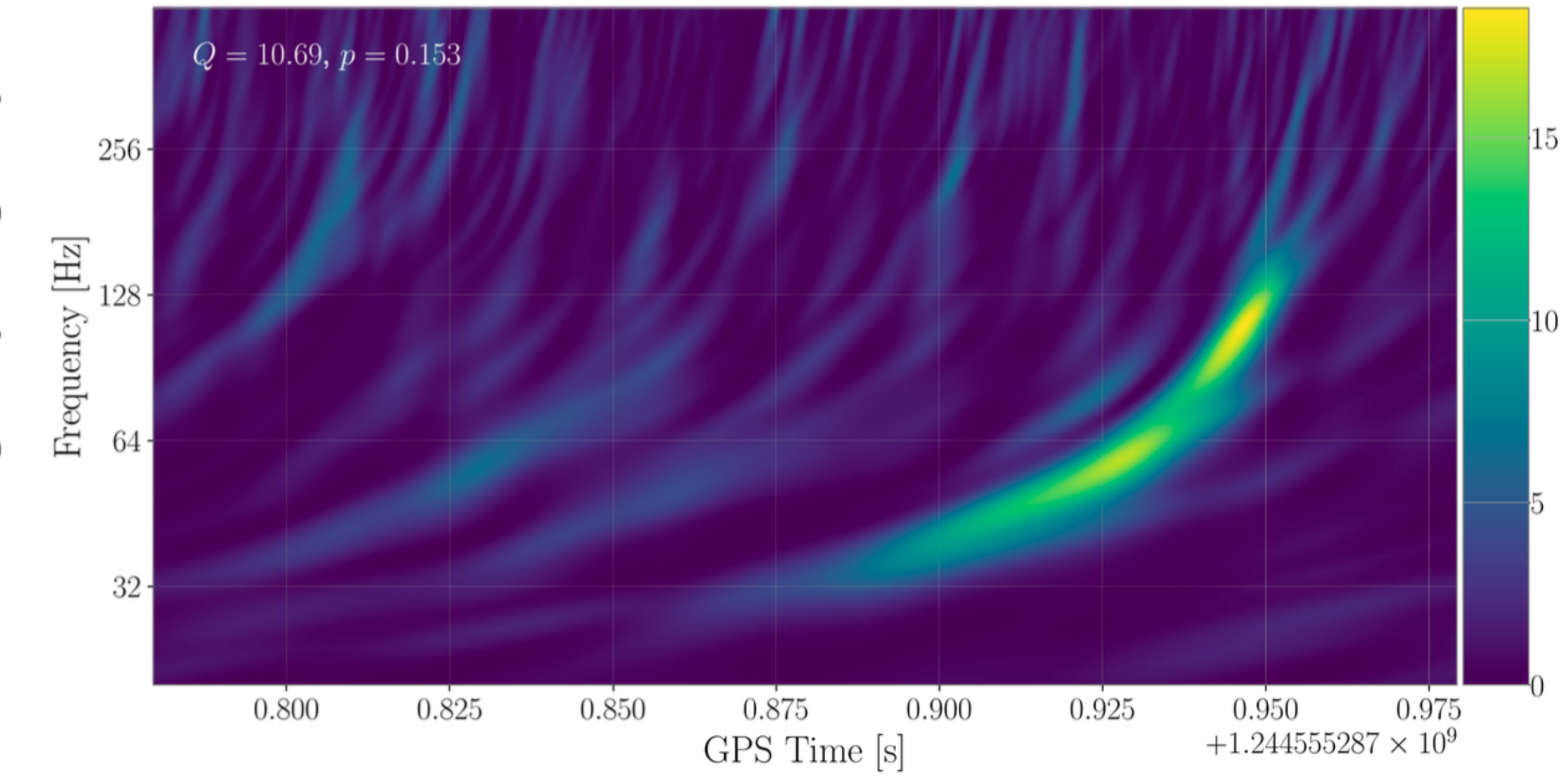
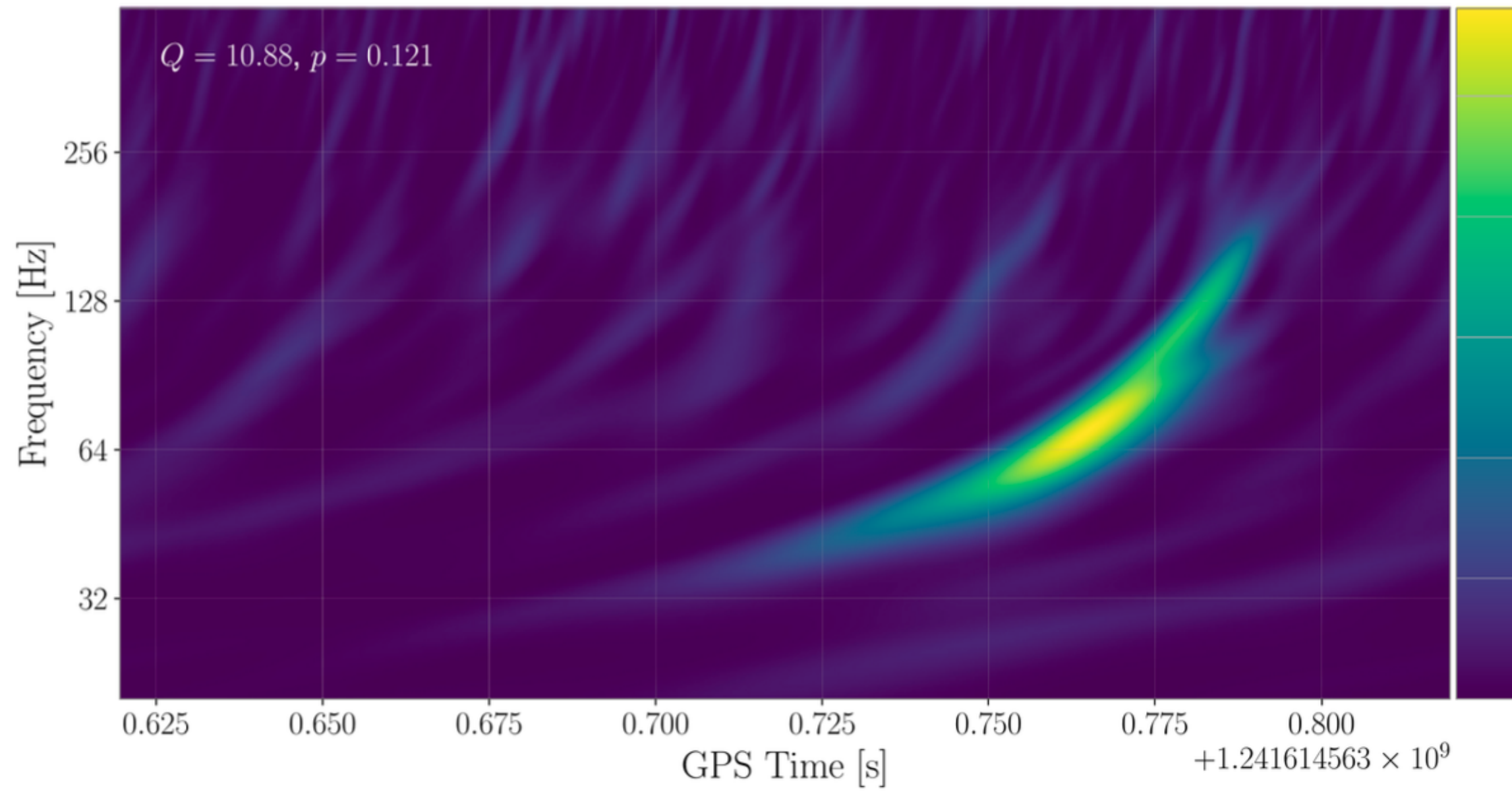
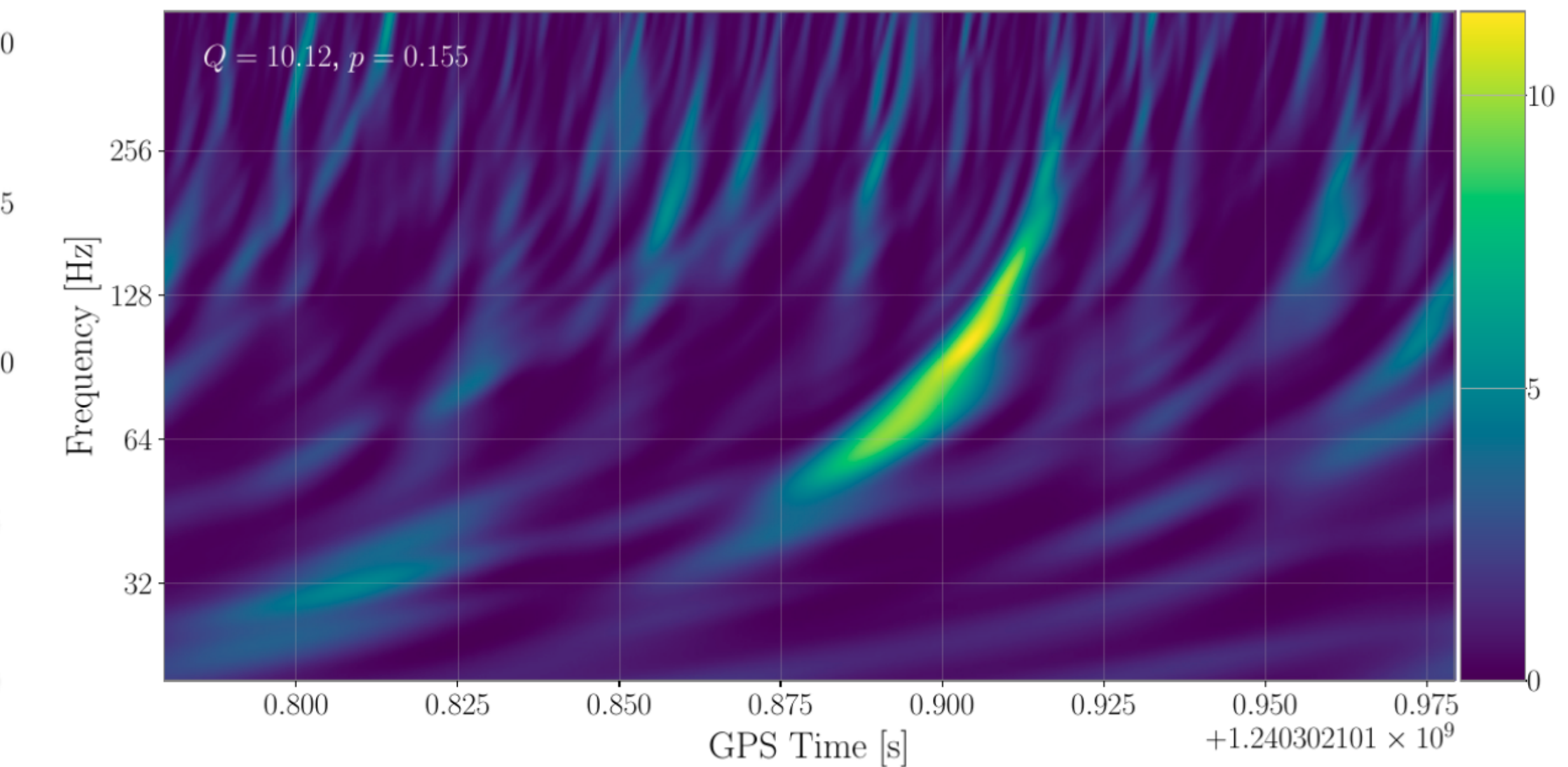
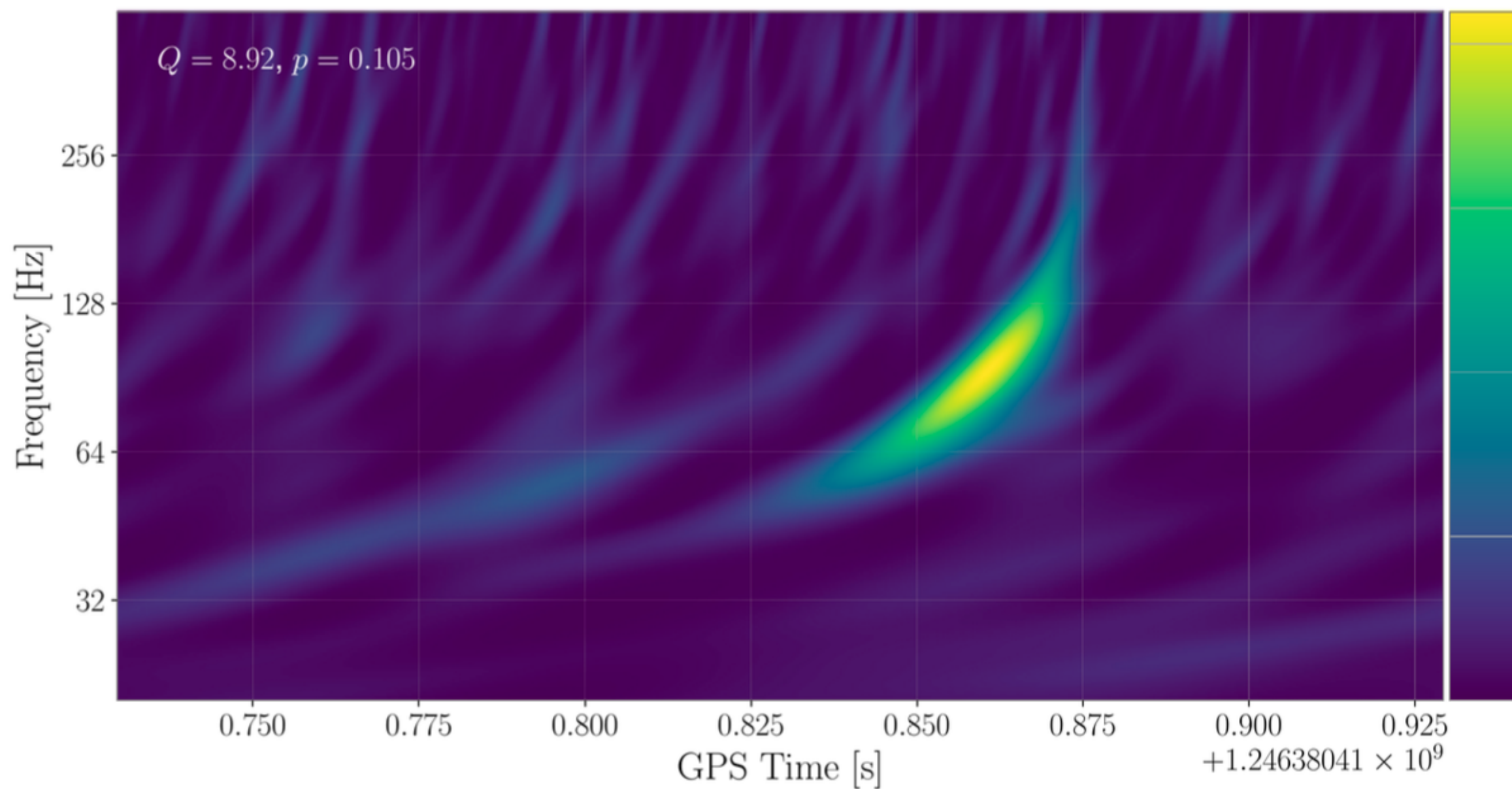
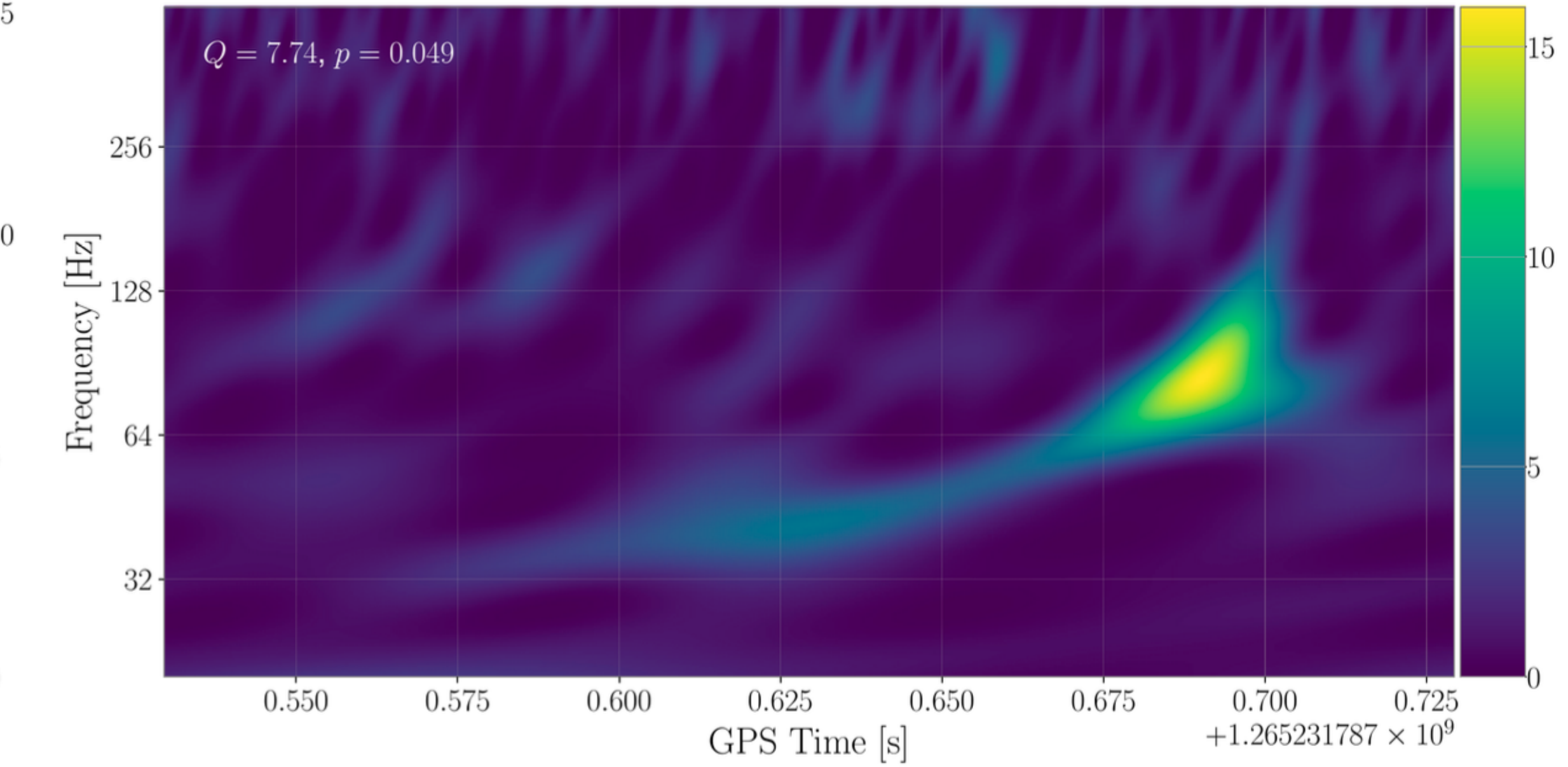
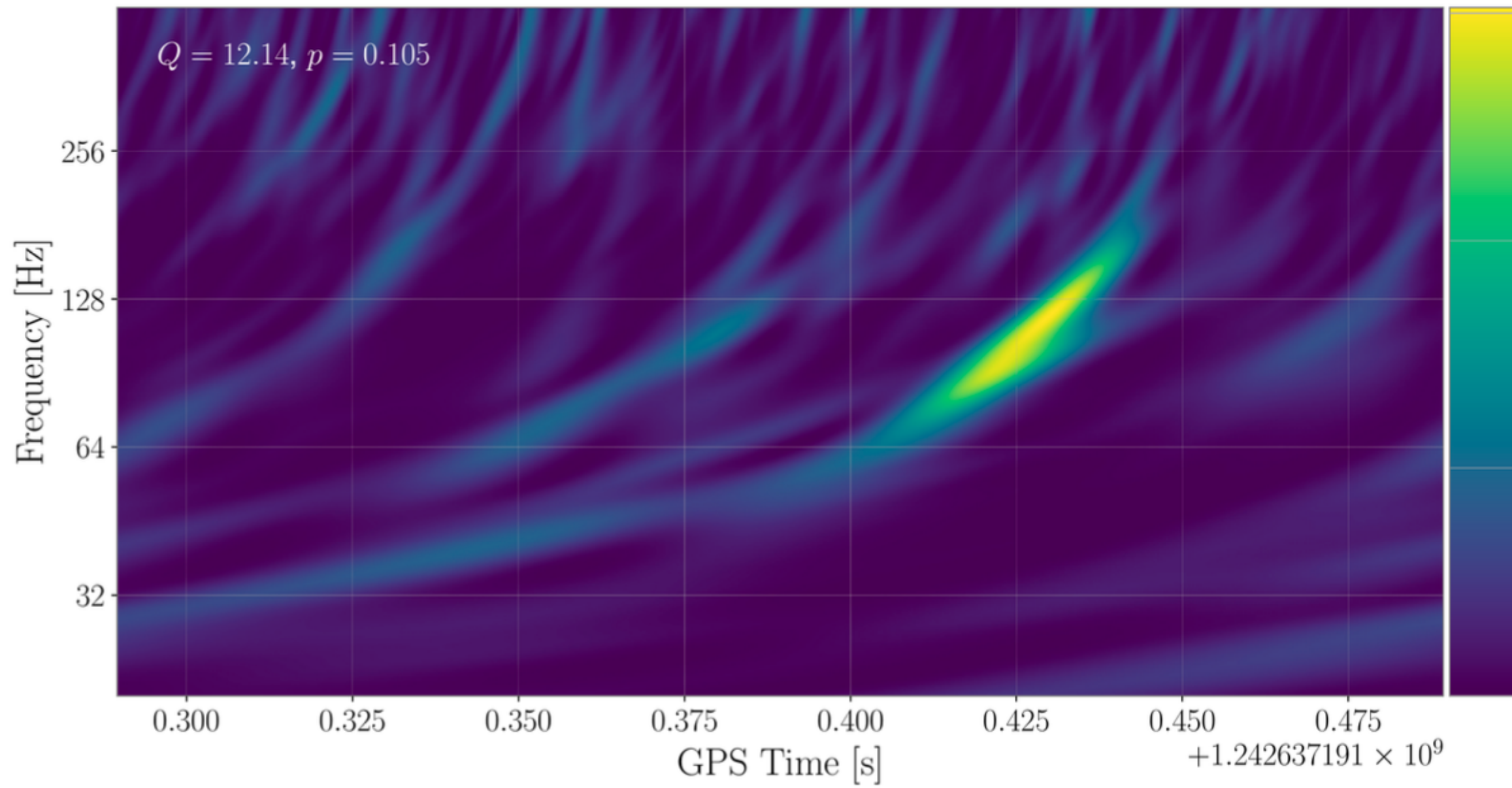


FIG. 38: Same as Fig. 35, but for the new event GW190904_104631.

ARESGW NEW CANDIDATE EVENTS



ARESGW NEW CANDIDATE EVENTS



PART B.
BINARY NEUTRON STAR POST-MERGER PHASE

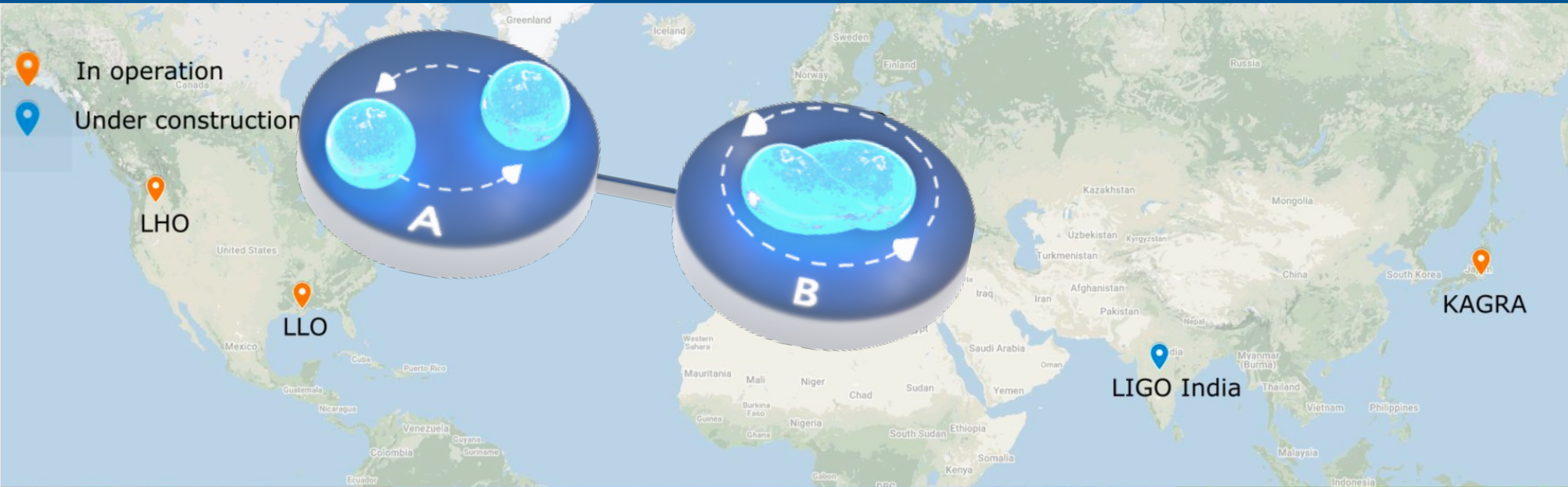
INTERNATIONAL GRAVITATIONAL-WAVE OBSERVATORY NETWORK (IGWN)



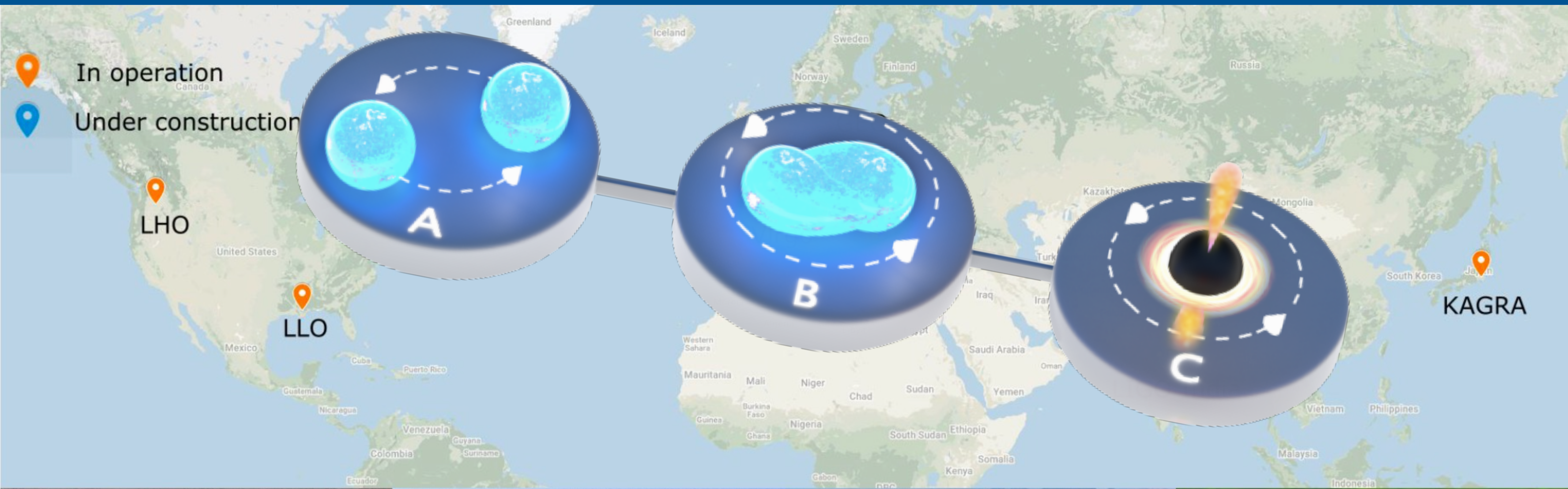
INTERNATIONAL GRAVITATIONAL-WAVE OBSERVATORY NETWORK (IGWN)



INTERNATIONAL GRAVITATIONAL-WAVE OBSERVATORY NETWORK (IGWN)



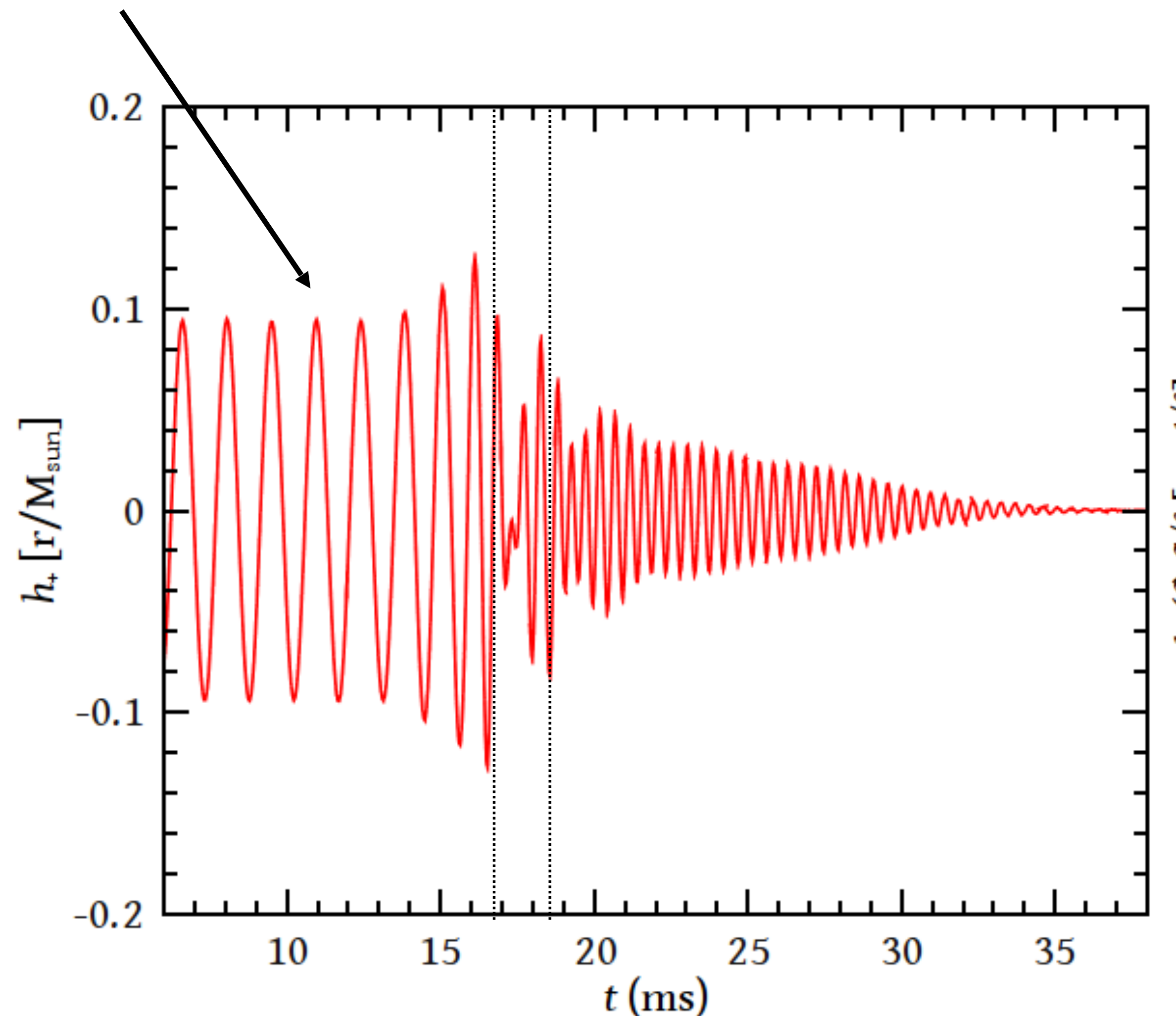
INTERNATIONAL GRAVITATIONAL-WAVE OBSERVATORY NETWORK (IGWN)



POST-MERGER PHASE IN BNS MERGERS

Time domain: three distinct phases of the GW signal:

inspiral, *merger* and *post-merger oscillations*.

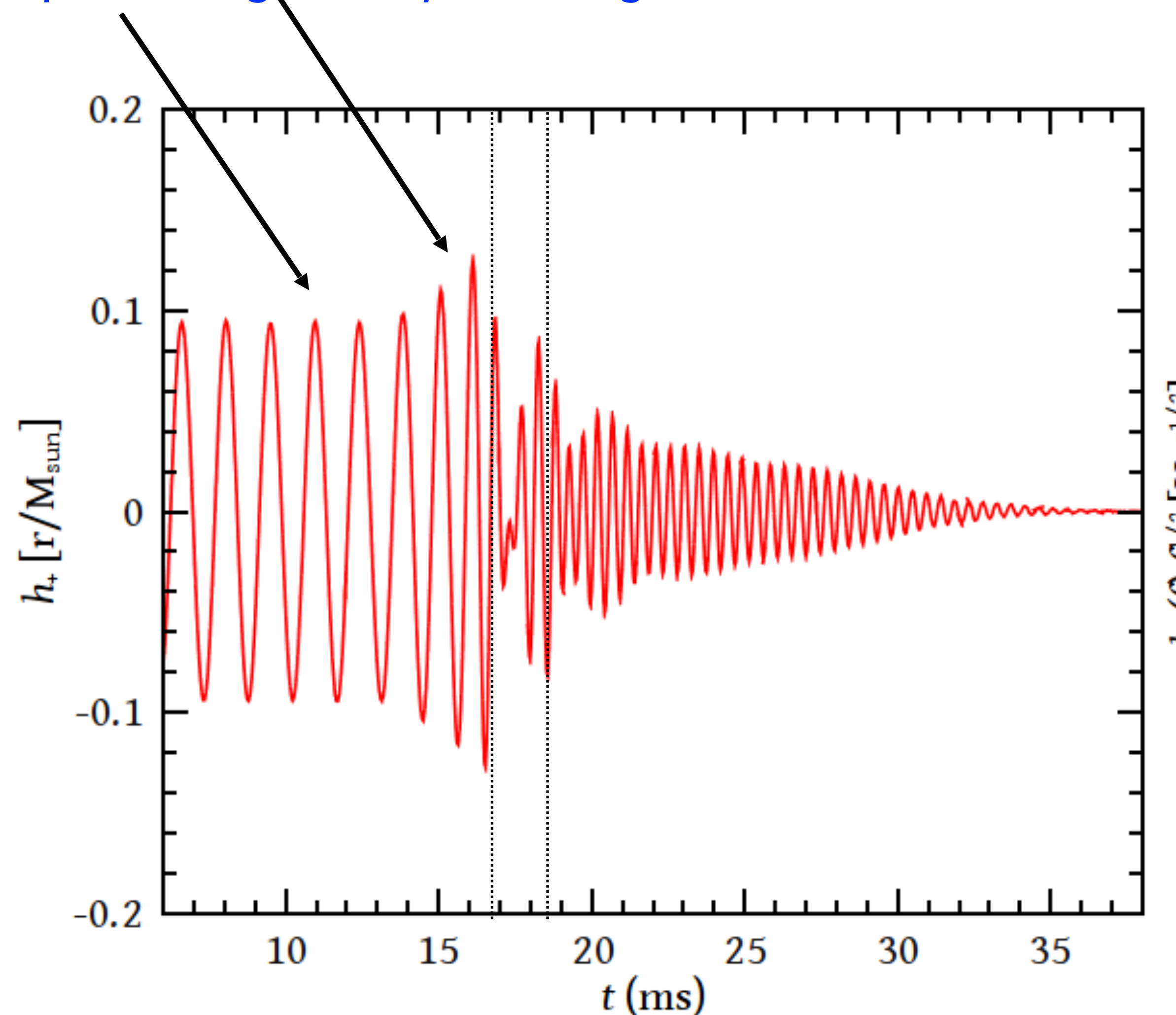


Stergioulas et al. (2011)

POST-MERGER PHASE IN BNS MERGERS

Time domain: three distinct phases of the GW signal:

inspiral, merger and *post-merger oscillations*.

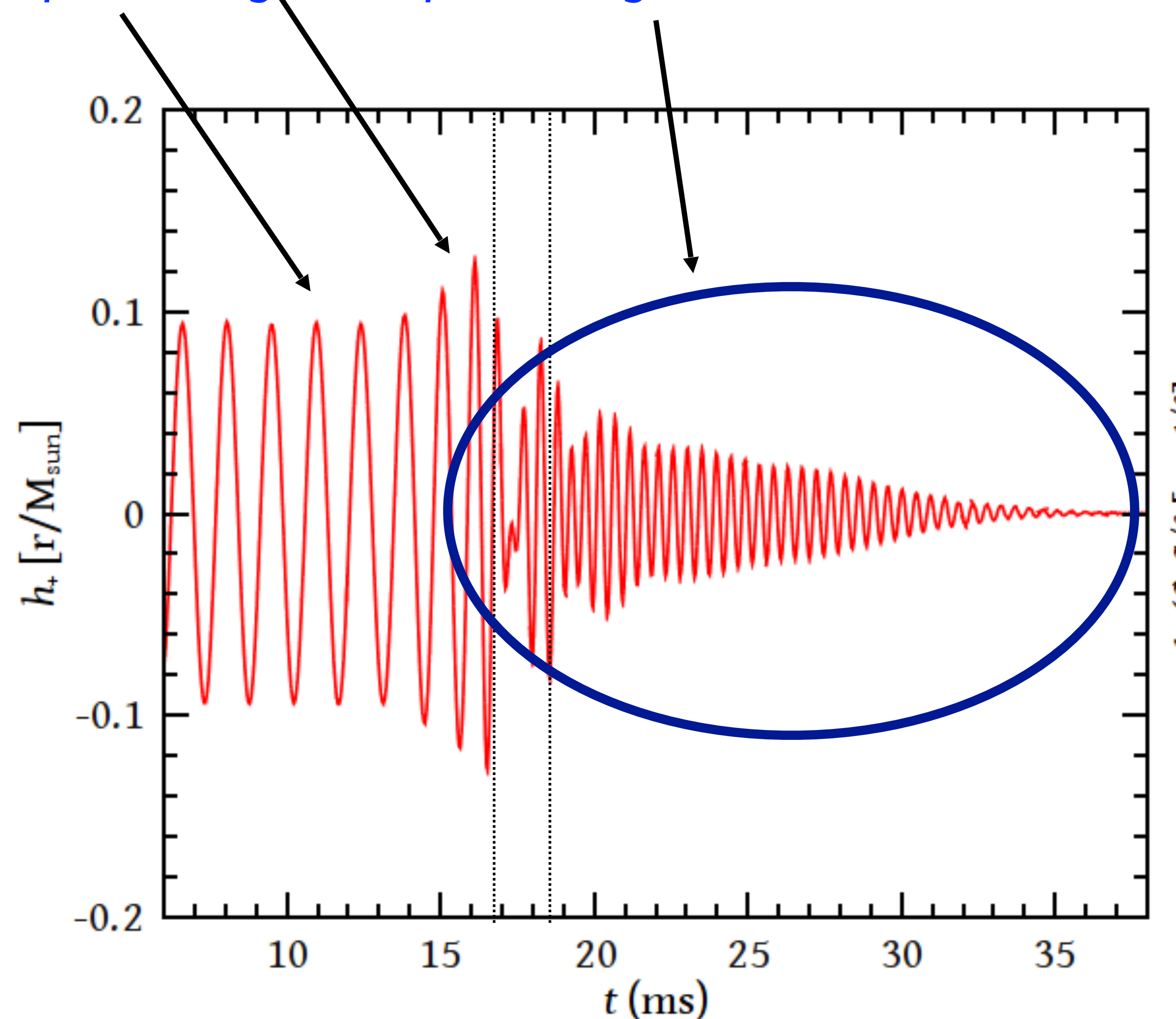


Stergioulas et al. (2011)

POST-MERGER PHASE IN BNS MERGERS

Time domain: three distinct phases of the GW signal:

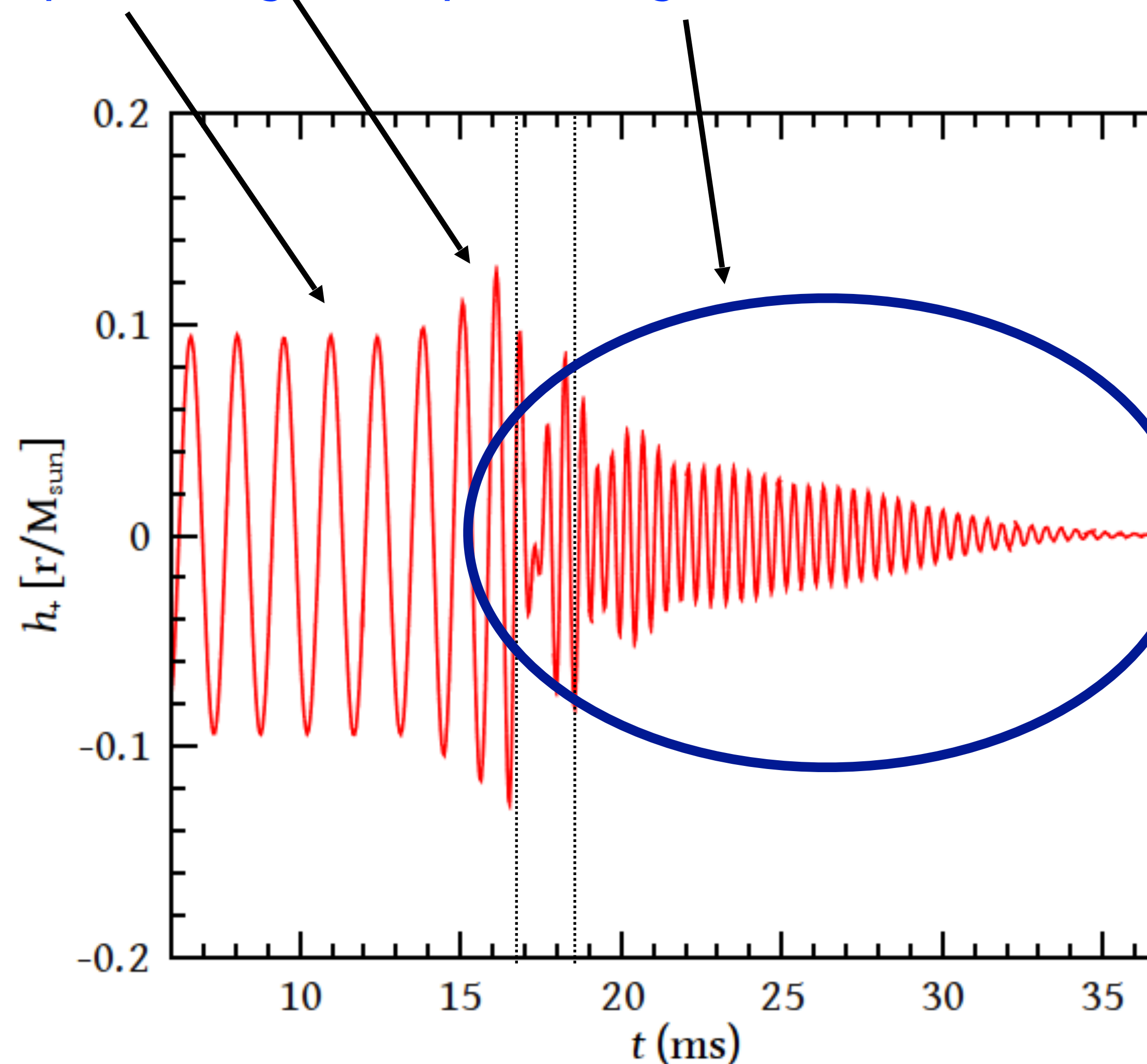
inspiral, merger and *post-merger oscillations*.



Stergioulas et al. (2011)

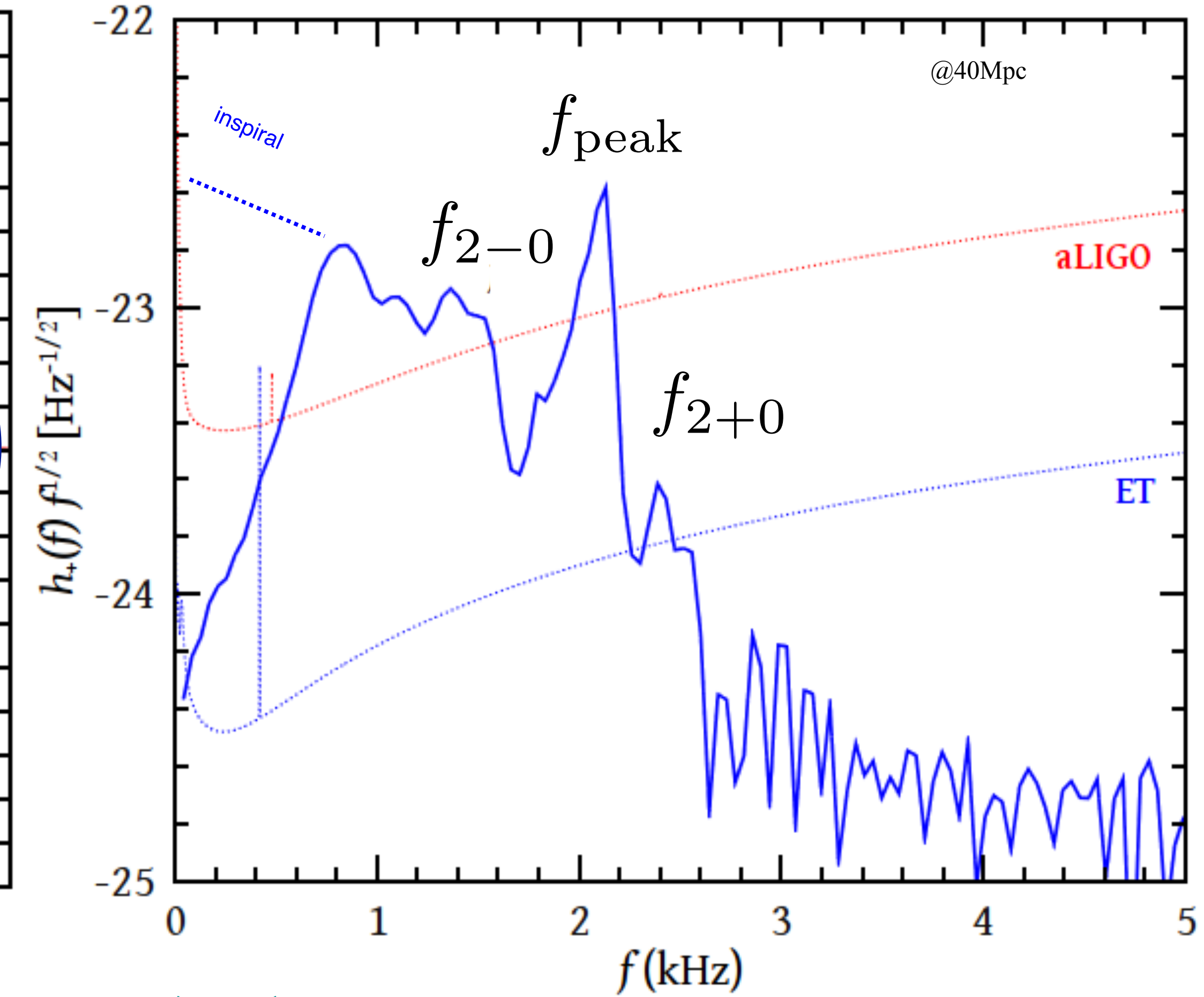
POST-MERGER PHASE IN BNS MERGERS

Time domain: three distinct phases of the GW signal:
inspiral, *merger* and *post-merger oscillations*.



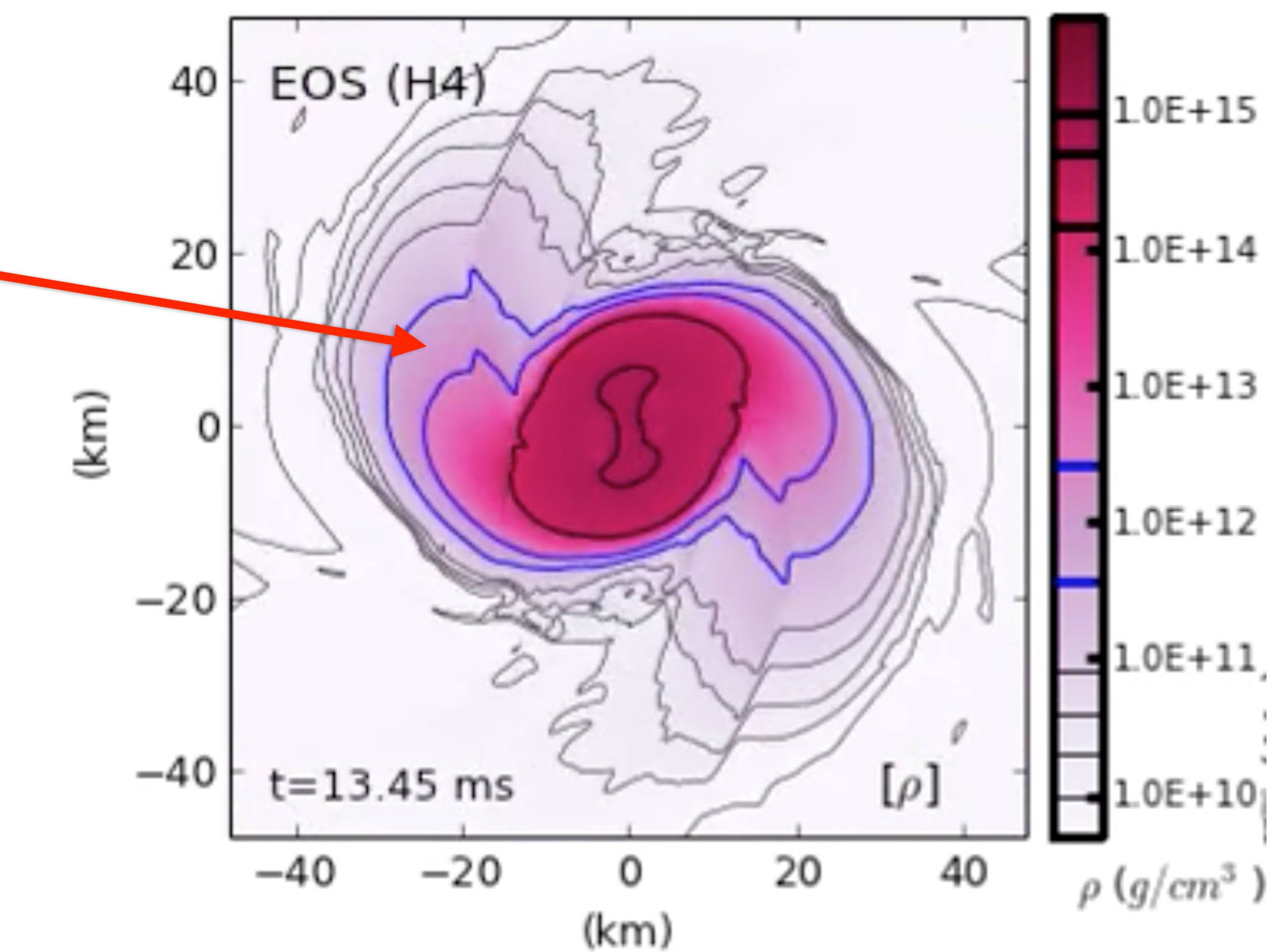
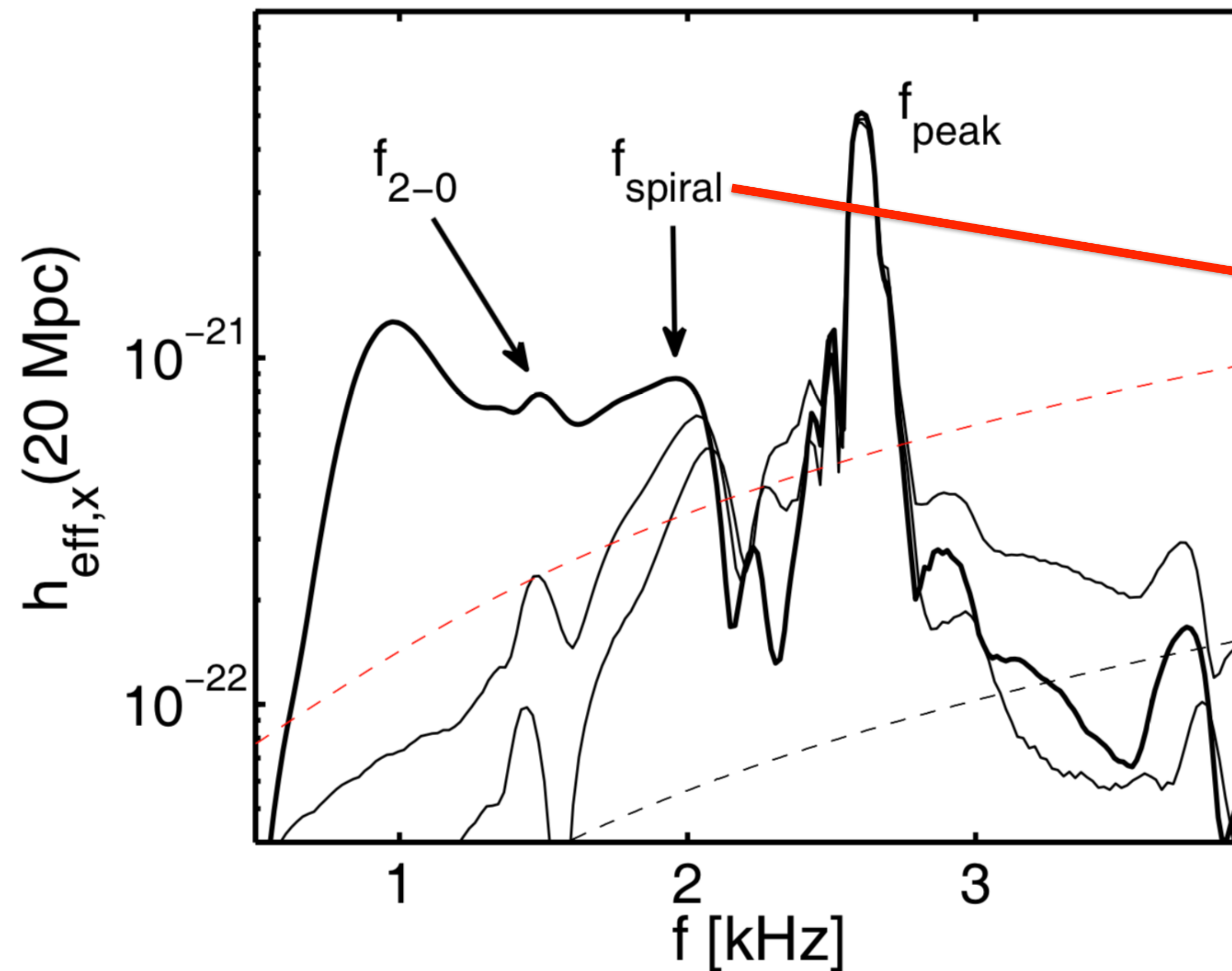
Frequency domain:
 f_{peak} : $l=m=2$ fundamental mode.

f_{2-0}, f_{2+0} : nonlinear combination tones

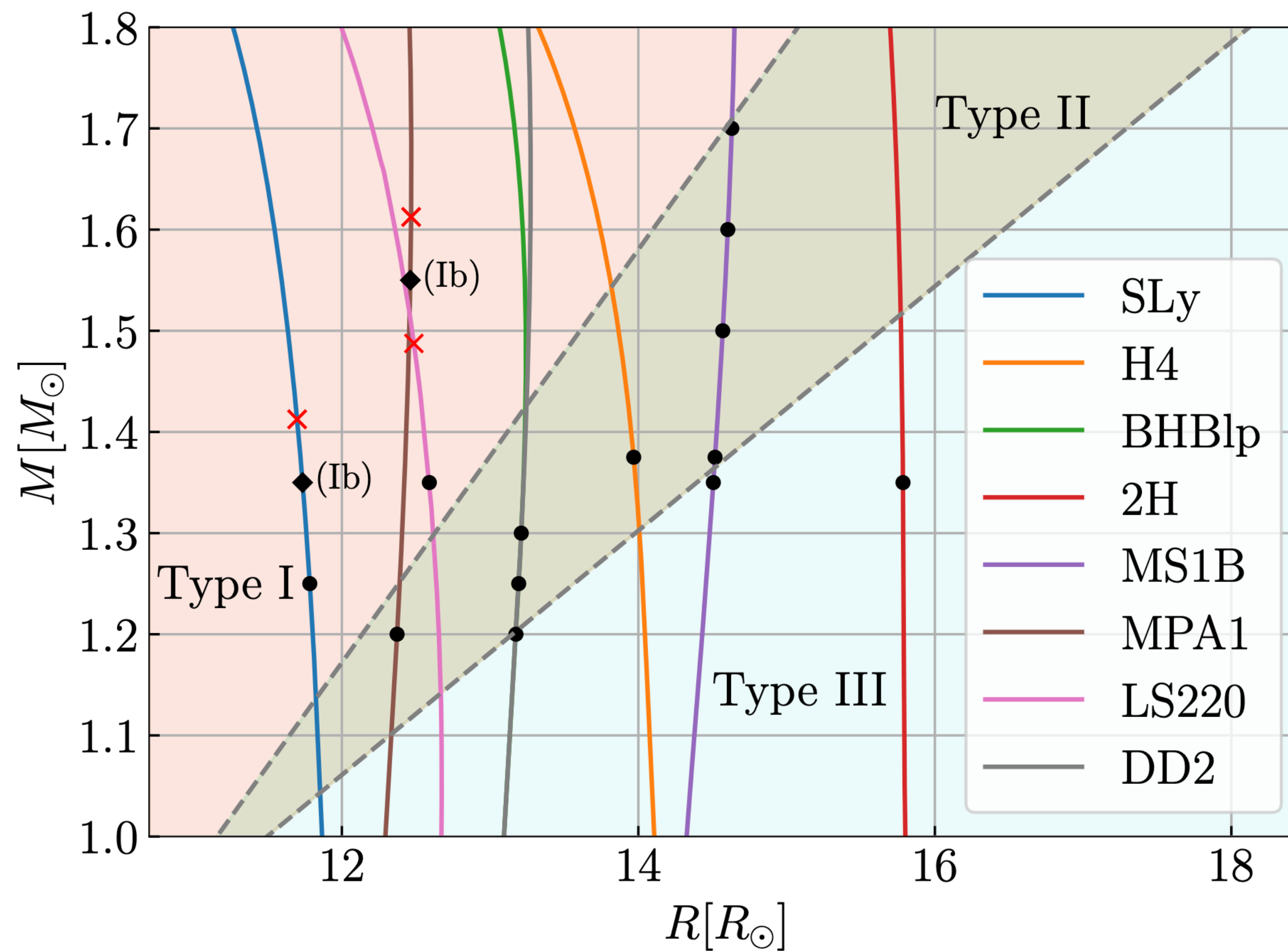


POST-MERGER PHASE IN BNS MERGERS

Orbiting spiral arms also lead to a distinct frequency f_{spiral}



CLASSIFICATION OF POST-MERGER WAVEFORMS



- Bauswein & Stergioulas (2015)
Vretinaris, Bauswein & Stergioulas (2020)
- Type I:**
 f_{2-0} stronger than f_{spiral}
- Type II:**
 f_{2-0} comparable to f_{spiral}
- Type III:**
 f_{spiral} stronger than f_{2-0}
- Type Ib:**
(close to M_{thres})

EMPIRICAL RELATIONS OF POST-MERGER FREQUENCIES

$$f_{\text{peak}} M_{\text{chirp}} = 1.392 - 0.108 M_{\text{chirp}} + 51.70 \tilde{\Lambda}^{-1/2}$$

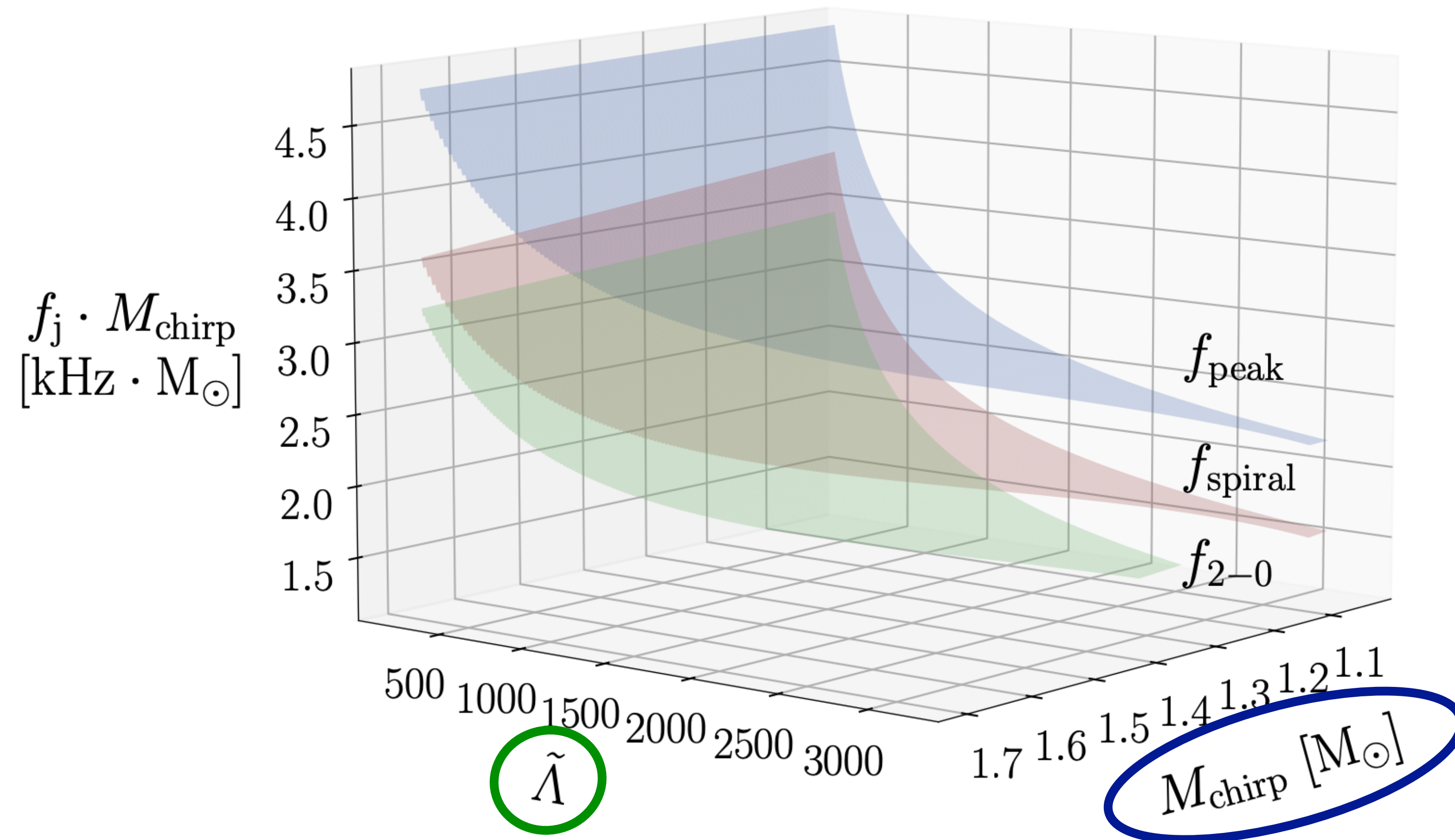
Vretinaris, Bauswein & Stergioulas (2020)

$$f_{2-0} M_{\text{chirp}} = 0.558 - 0.406 M_{\text{chirp}} + 48.696 \tilde{\Lambda}^{-1/2}$$

Vretinaris et al. (2025)

$$f_{\text{spiral}} M_{\text{chirp}} = 1.2 - 0.442 M_{\text{chirp}} + 45.819 \tilde{\Lambda}^{-1/2}$$

Vretinaris et al. (2025)



EMPIRICAL RELATIONS OF POST-MERGER FREQUENCIES

$$f_{\text{peak}} M_{\text{chirp}} = 1.392 - 0.108 M_{\text{chirp}} + 51.70 \tilde{\Lambda}^{-1/2}$$

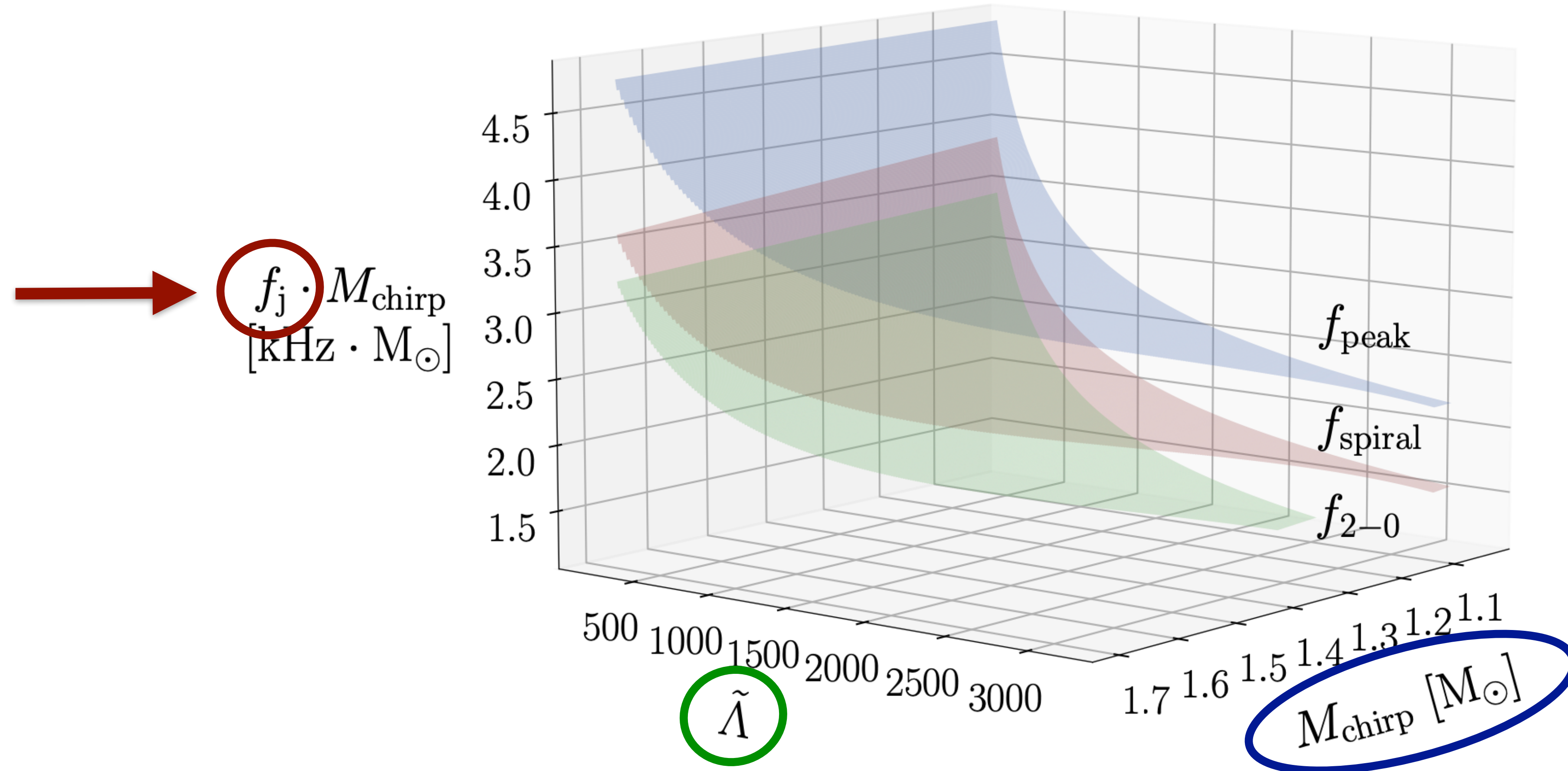
Vretinaris, Bauswein & Stergioulas (2020)

$$f_{2-0} M_{\text{chirp}} = 0.558 - 0.406 M_{\text{chirp}} + 48.696 \tilde{\Lambda}^{-1/2}$$

Vretinaris et al. (2025)

$$f_{\text{spiral}} M_{\text{chirp}} = 1.2 - 0.442 M_{\text{chirp}} + 45.819 \tilde{\Lambda}^{-1/2}$$

Vretinaris et al. (2025)



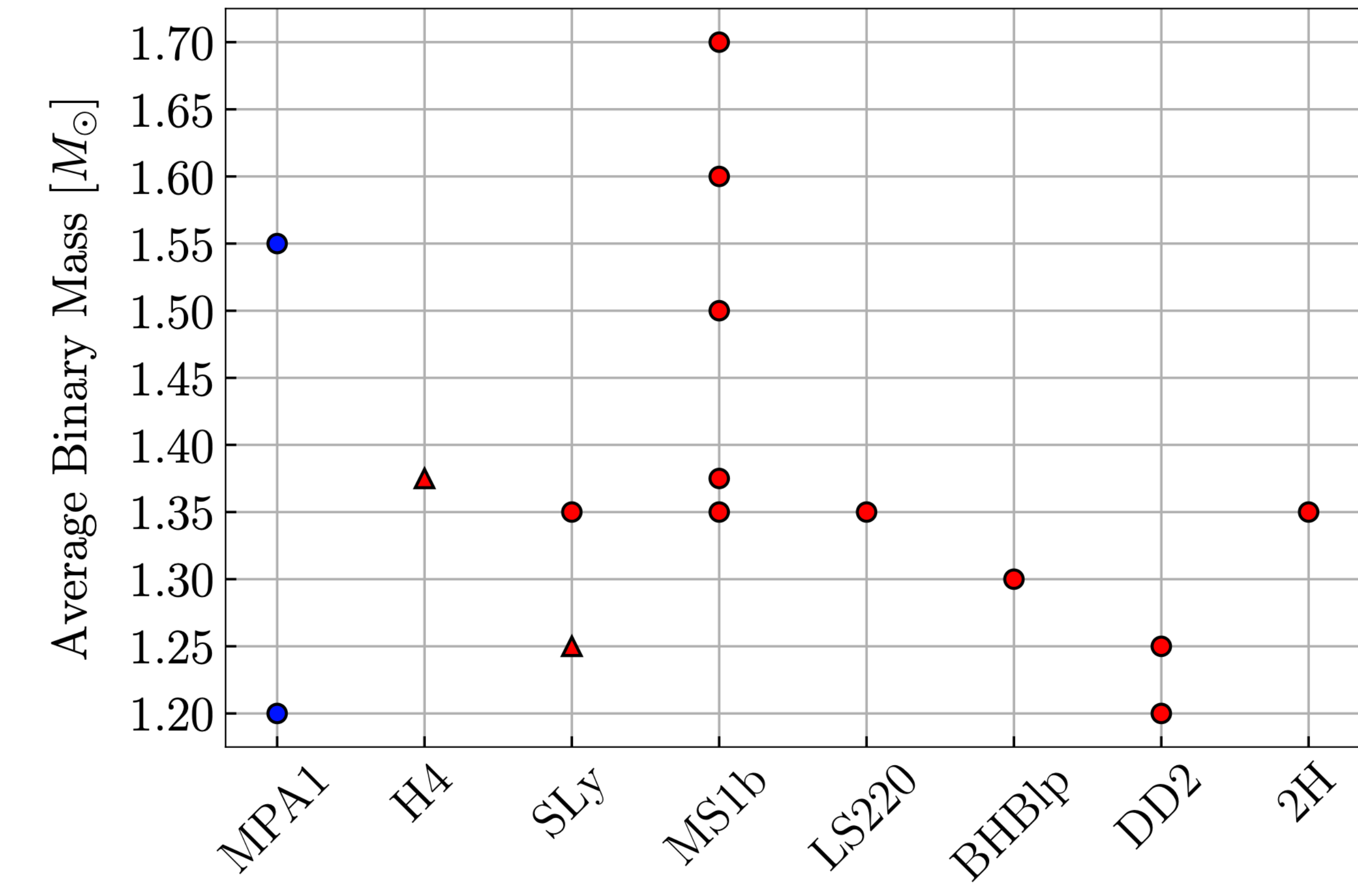
ACCELERATION OF POST-MERGER INFERENCE

13 numerical waveforms from the CoRe database (Gonzalez et al. 2022)

+2 numerical waveforms from Soultanis, Bauswein & Stergioulas (2022)

Label	EOS	q	(Average) Mass	References
THC:0036:R03	SLy	1.0	1.350	[47]
THC:0019:R05	LS220	1.0	1.350	[101, 102]
BAM:0088:R01	MS1b	1.0	1.500	[99, 100]
THC:0002:R01	BHBlp	1.0	1.300	[101, 102]
THC:0011:R01	DD2	1.0	1.250	[101, 102]
BAM:0070:R01	MS1b	1.0	1.375	[103]
BAM:0065:R03	MS1b	1.0	1.350	[104]
THC:0010:R01	DD2	1.0	1.200	[101, 102]
BAM:0002:R02	2H	1.0	1.350	[104]
BAM:0053:R01	H4	1.5	1.375	[105]
BAM:0124:R01	SLy	1.5	1.250	[103]
BAM:0090:R02	MS1b	1.0	1.600	[99, 100]
BAM:0092:R02	MS1b	1.0	1.700	[99, 100]
Soultanis et al.	MPA1	1.0	1.200	[67]
Soultanis et al.	MPA1	1.0	1.550	[67]

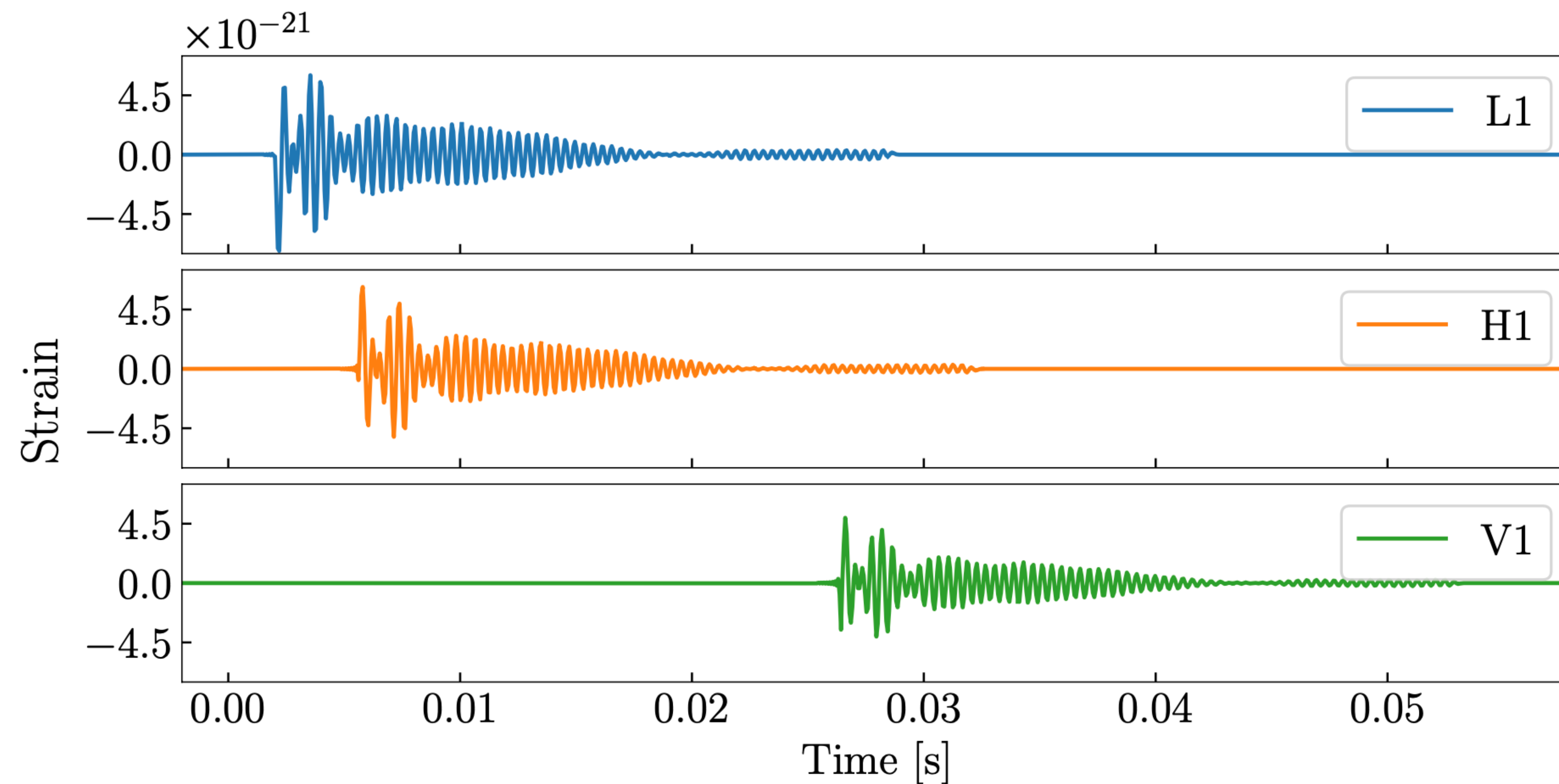
Extension of the set of 9 waveforms used in previous work by Easter et al. (2020)



INJECTIONS IN 3-DETECTOR NETWORK

Waveforms are injected in 3-detector HLV network at design sensitivity, using BILBY (Ashton et al. 2019)

We choose post-merger SNR of 8, 16 and 50, to simulate detection by 3G network (ET/CE) at distances as close as 200Mpc.



ANALYTIC BNS POST-MERGER WAVEFORM MODELS

Several analytic models exist in the time- and frequency-domains.

Here, we extend the analytic model of Easter et al. (2020) as follows:

$$\begin{aligned} h(\boldsymbol{\theta}, t) &= h_+(\boldsymbol{\theta}, t) - i h_{\times}(\boldsymbol{\theta}, t) \\ &= \sum_{j=1}^4 [h_{j,+}(\boldsymbol{\theta}, t) - i h_{j,\times}(\boldsymbol{\theta}, t)] \\ h_{j,+}(\boldsymbol{\theta}, t) &= A_j \exp \left[-\frac{t}{T_j} \right] \cos [2\pi f_j t (1 + a_j t) + \psi_j] \end{aligned}$$

ANALYTIC BNS POST-MERGER WAVEFORM MODELS

Several analytic models exist in the time- and frequency-domains.

Here, we extend the analytic model of Easter et al. (2020) as follows:

$$\begin{aligned} h(\boldsymbol{\theta}, t) &= h_+(\boldsymbol{\theta}, t) - i h_{\times}(\boldsymbol{\theta}, t) \\ &= \sum_{j=1}^4 [h_{j,+}(\boldsymbol{\theta}, t) - i h_{j,\times}(\boldsymbol{\theta}, t)] \\ h_{j,+}(\boldsymbol{\theta}, t) &= A_j \exp \left[-\frac{t}{T_j} \right] \cos [2\pi f_j t (1 + a_j t) + \psi_j] \end{aligned}$$

Intrinsic parameters $\boldsymbol{\theta} = \{A_j, T_j, f_j, a_j, \psi_j\}$ for $j \in [1, 4]$

$h_{j,\times}(\boldsymbol{\theta}, t)$ is obtained by applying a $\pi/2$ phase shift to $h_{j,+}(\boldsymbol{\theta}, t)$

- We have added a 4th oscillator at high frequencies $> f_{\text{peak}}$ (e.g. f_{2+0})
- Amplitudes A_j are free parameters

INFORMED PRIORS

In Easter et al. (2020) flat priors in a wide frequency range of 1-5 kHz for every oscillator were used.

- Here, we take advantage of the empirical relations to set Gaussian priors in a narrow frequency range around each expected frequency.
- In addition, the priors differ, according to the type of the post-merger waveform:
 - Type I: Gaussian priors, $\mathcal{N}(f_{2-0}, \sigma^2)$ for f_{2-0} and uniform priors $\mathcal{U}(1, 5)[\text{kHz}]$ for f_{spiral} .
 - Type II: Gaussian priors, $\mathcal{N}(f_{2-0}, \sigma^2)$ for f_{2-0} and $\mathcal{N}(f_{\text{spiral}}, \sigma^2)$ for f_{spiral} .
 - Type III: Gaussian priors, $\mathcal{N}(f_{\text{spiral}}, \sigma^2)$ for f_{spiral} and uniform priors $\mathcal{U}(1, 5)[\text{kHz}]$ for f_{2-0} .

where $\sigma = 3 \times \text{max error of empirical relations}$. For f_{peak} : Gaussian ; for f_4 : flat in $[f_{\text{peak}} + 0.3\text{kHz}, 5\text{kHz}]$.

priors for A_j : uniform in [-24, -19]

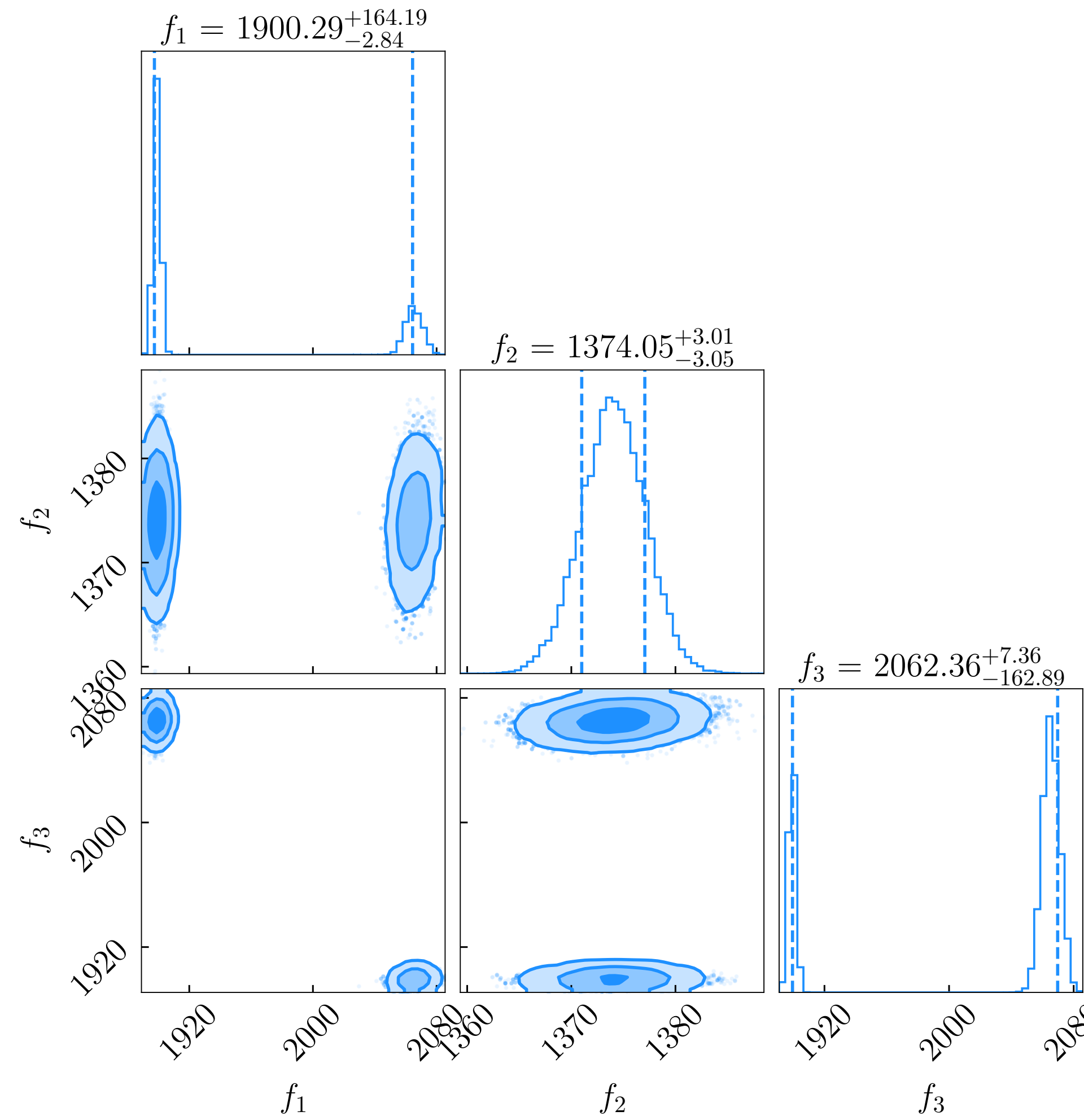
priors for a_j : uniform in [-6.4, 6.4]

priors for remaining parameters: as in Easter et al. (2020)

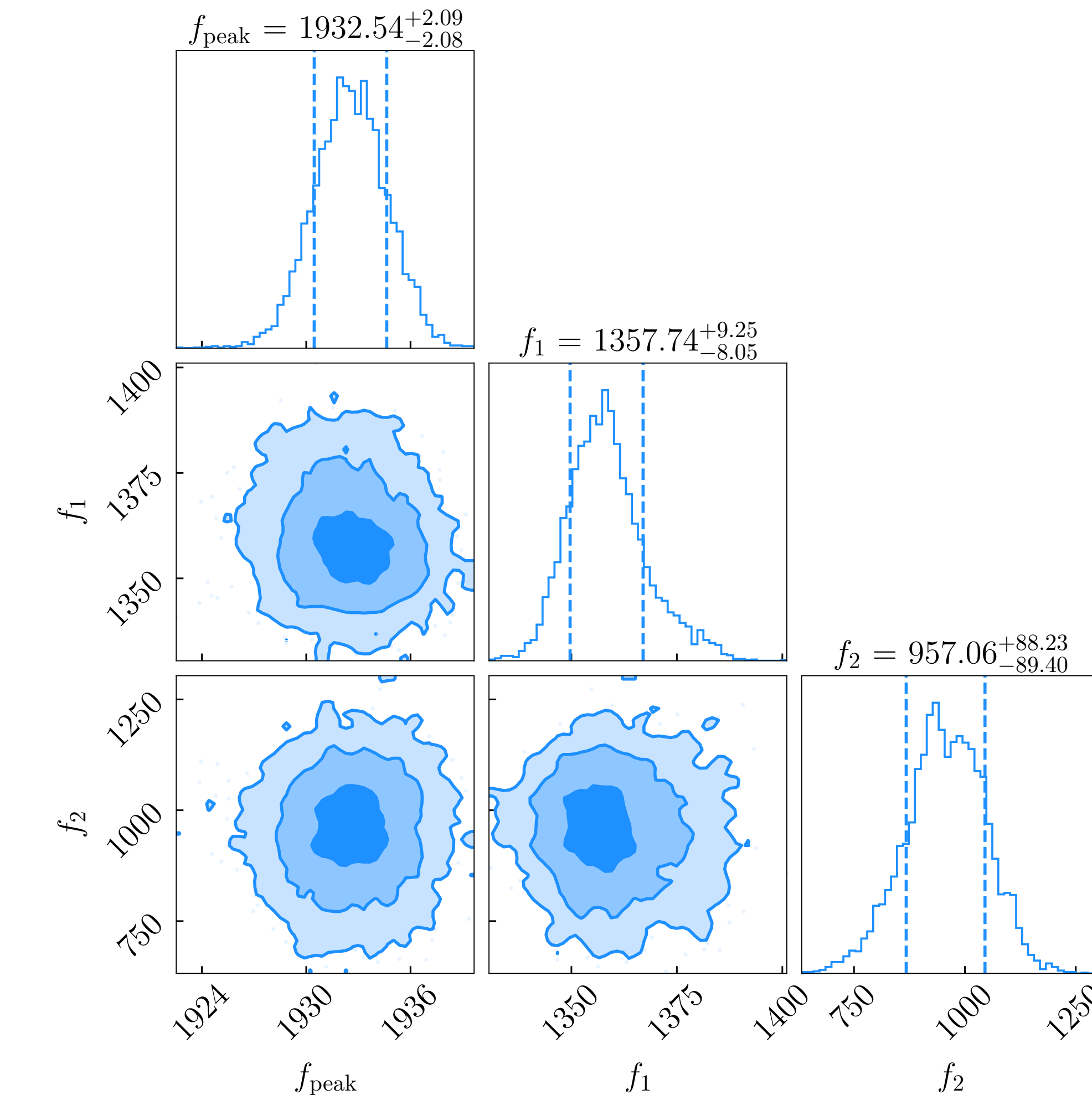
POSTERIOR DISTRIBUTIONS

EOS 2H 1.35+1.35, SNR = 50

using flat priors



using informed priors (through empirical relations)

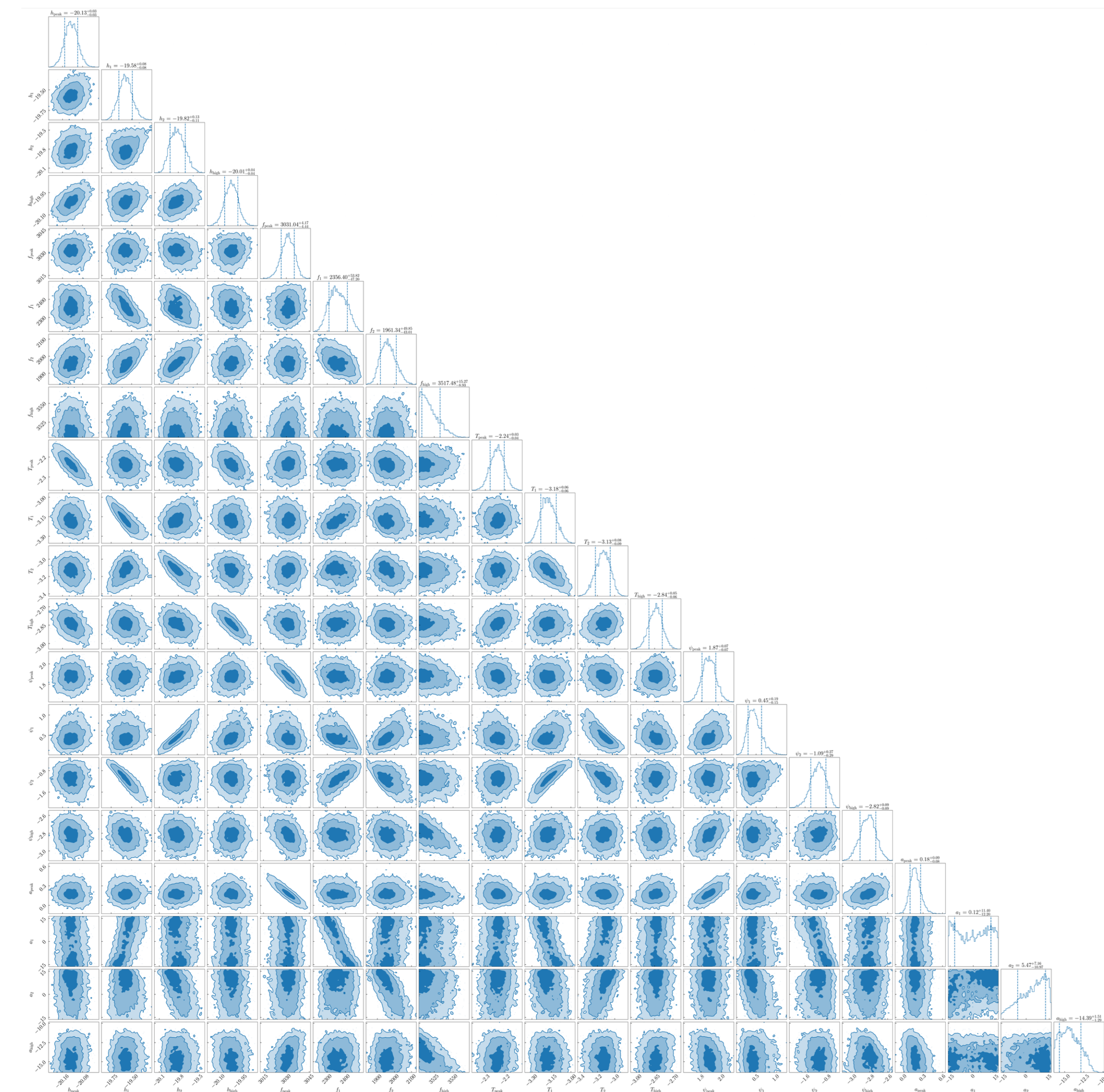


POSTERIOR DISTRIBUTIONS

EOS MPA 1.55+1.55, SNR = 50

using informed priors

all parameters



POCOMC: PRECONDITIONED MONTE CARLO SAMPLER

Preconditioned Monte Carlo Sampling (Karamanis et al. 2022)

PMC targets an **annealed version of the posterior**, with density given by

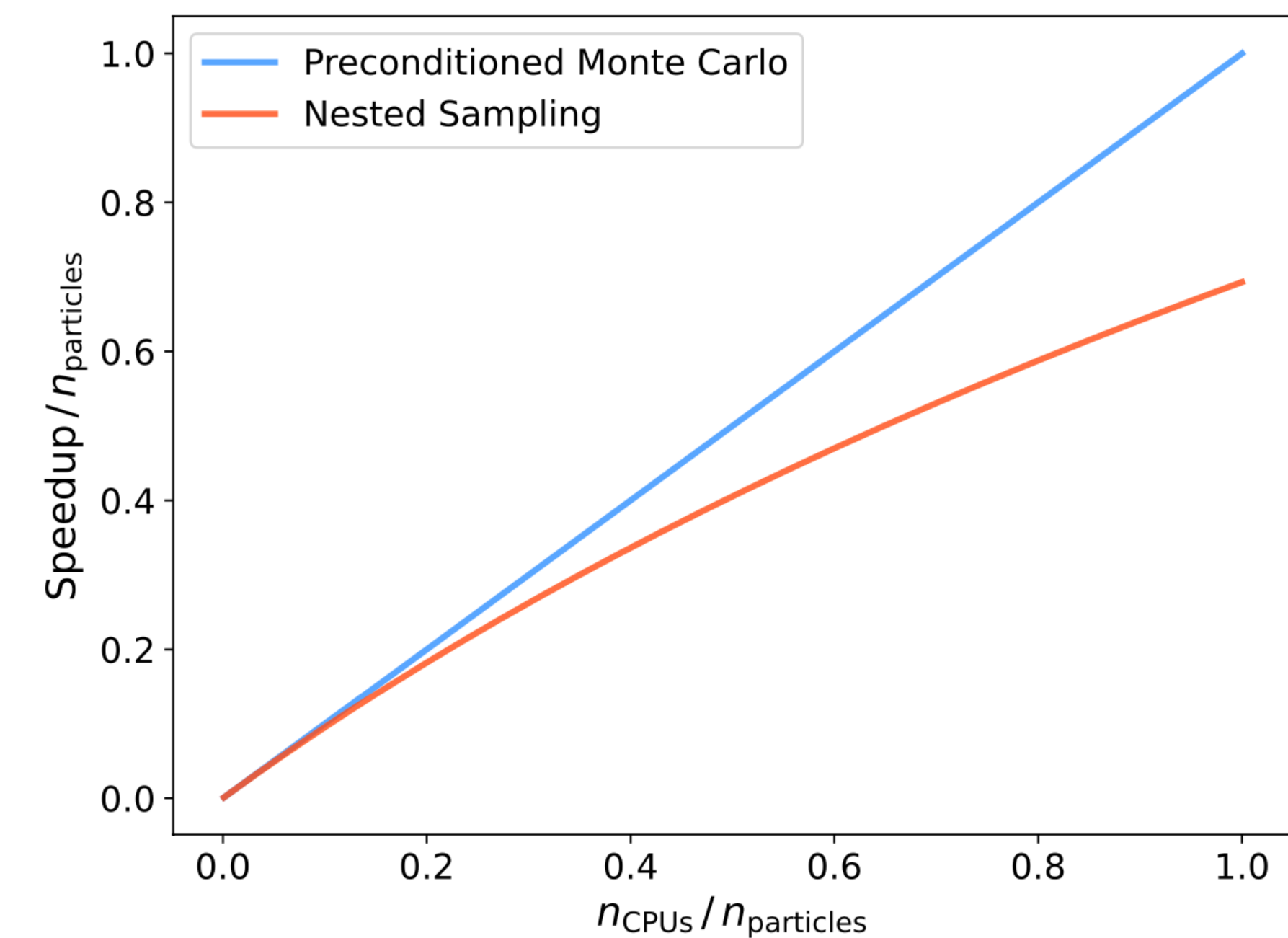
$$p_t(\boldsymbol{\theta} \mid d) \propto \mathcal{L}^{\beta_t}(\boldsymbol{\theta} \mid d)\pi(\boldsymbol{\theta})$$

where β_t a parameter (inverse temperature).

We use 2000 particles that transition from the prior ($\beta_0 = 0$) to the posterior distribution ($\beta_T = 1$), through a sequence of reweighting, resampling and mutation steps.



<https://github.com/minaskar/pocomc>



PocoMC is highly parallelizable

POCOMC: PRECONDITIONED MONTE CARLO SAMPLER

Preconditioned Monte Carlo Sampling (Karamanis et al. 2022)

PMC targets an **annealed version of the posterior**, with density given by

$$p_t(\boldsymbol{\theta} \mid d) \propto \mathcal{L}^{\beta_t}(\boldsymbol{\theta} \mid d)\pi(\boldsymbol{\theta})$$

where β_t a parameter (inverse temperature).

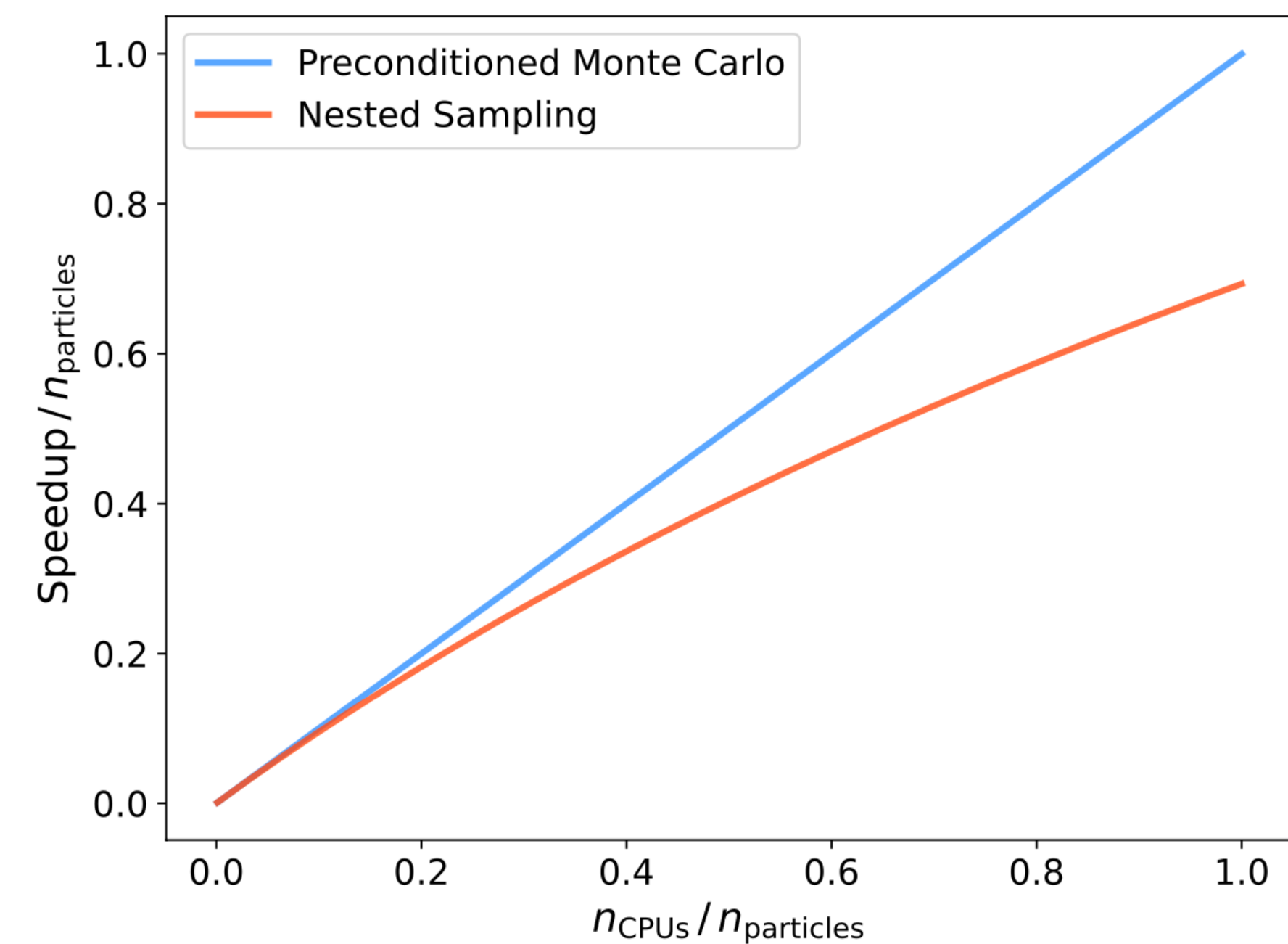
We use 2000 particles that transition from the prior ($\beta_0 = 0$) to the posterior distribution ($\beta_T = 1$), through a sequence of reweighing, resampling and mutation steps.

After each iteration, a **normalizing flow** transforms the distribution to a simpler one (almost Gaussian), decorrelating the parameters. This allows for a much faster sampling.

On same number of CPUs: pocoMC is **~10 times faster** than dynesty.

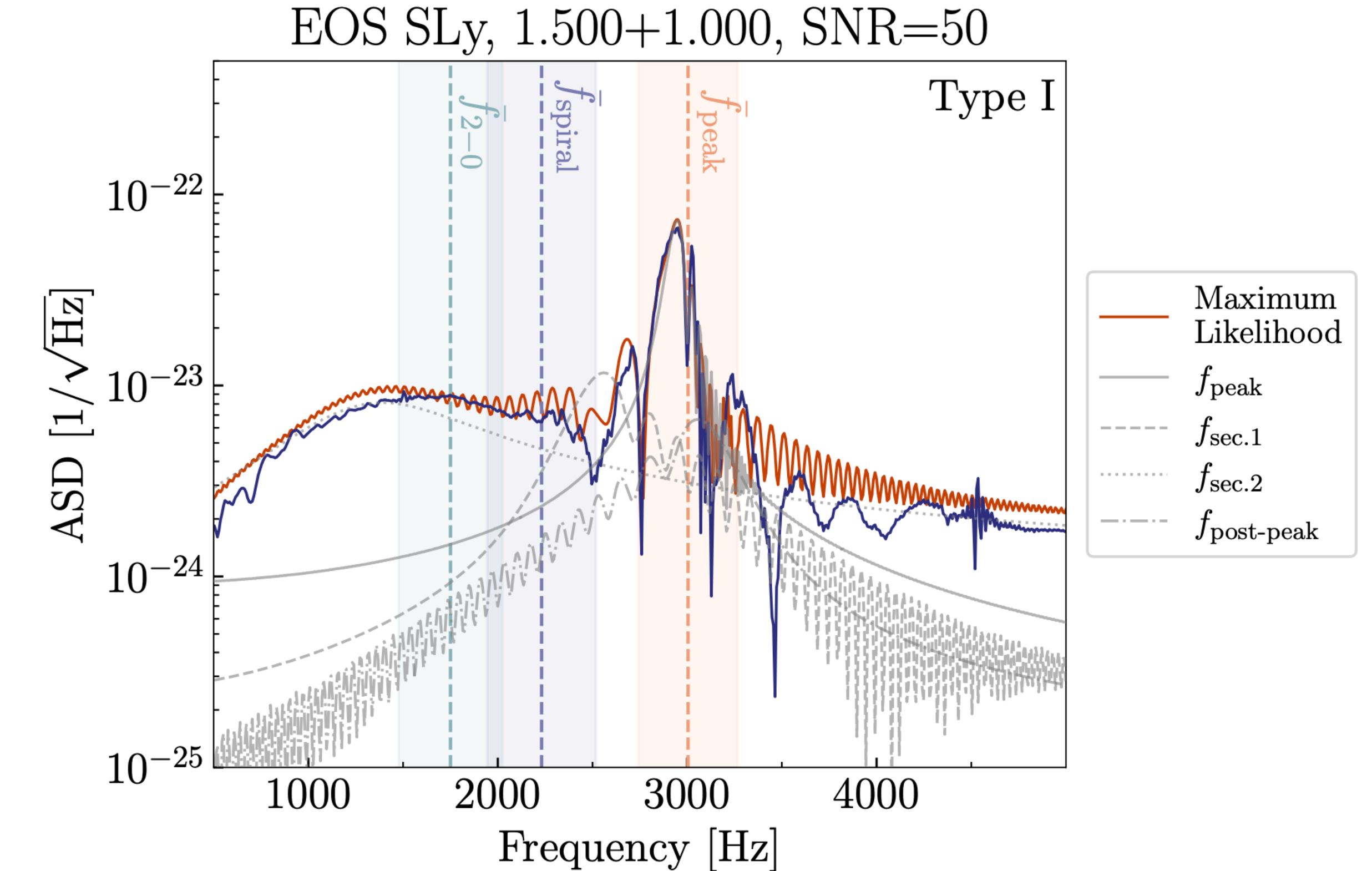
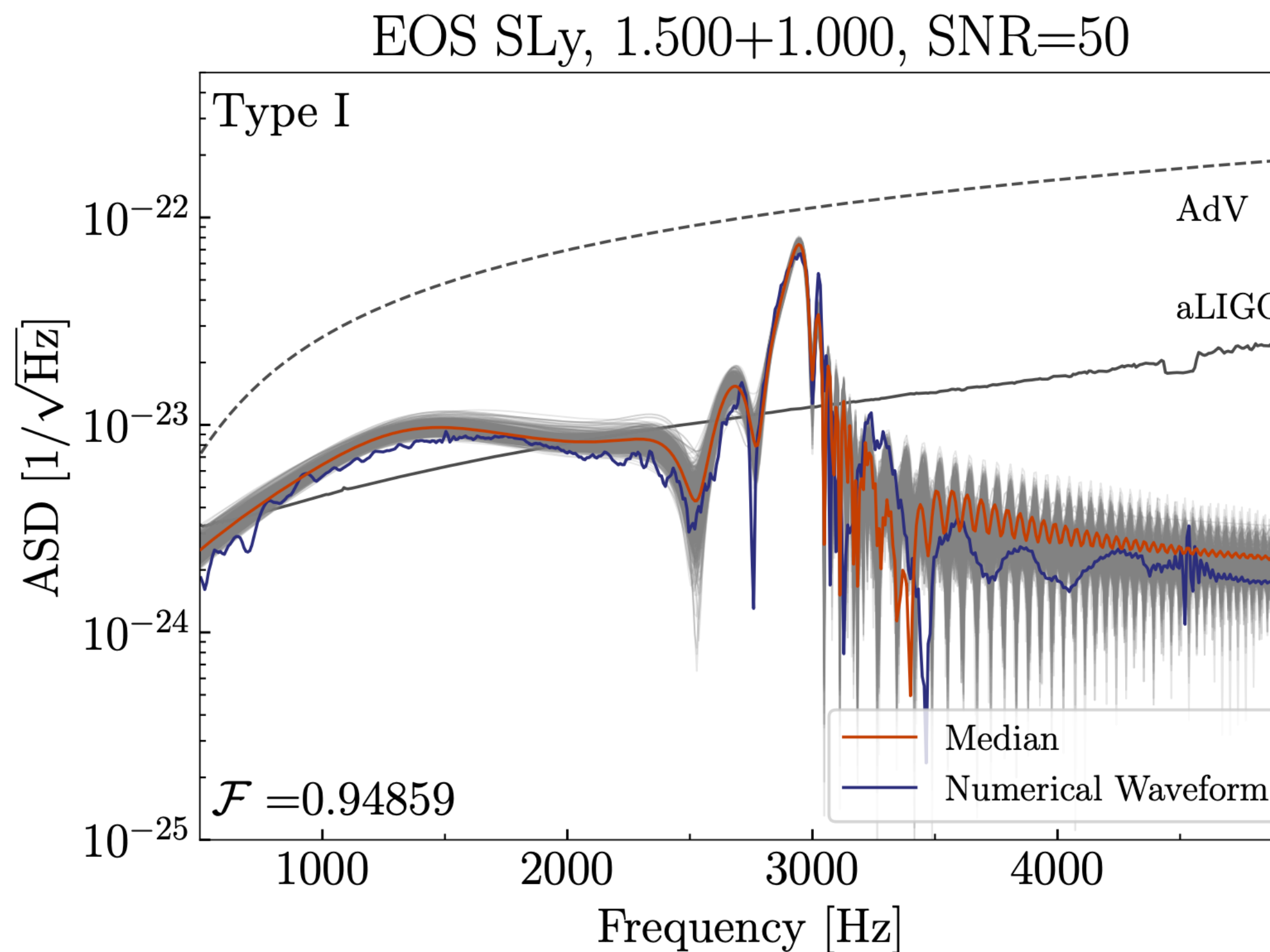


<https://github.com/minaskar/pocomc>



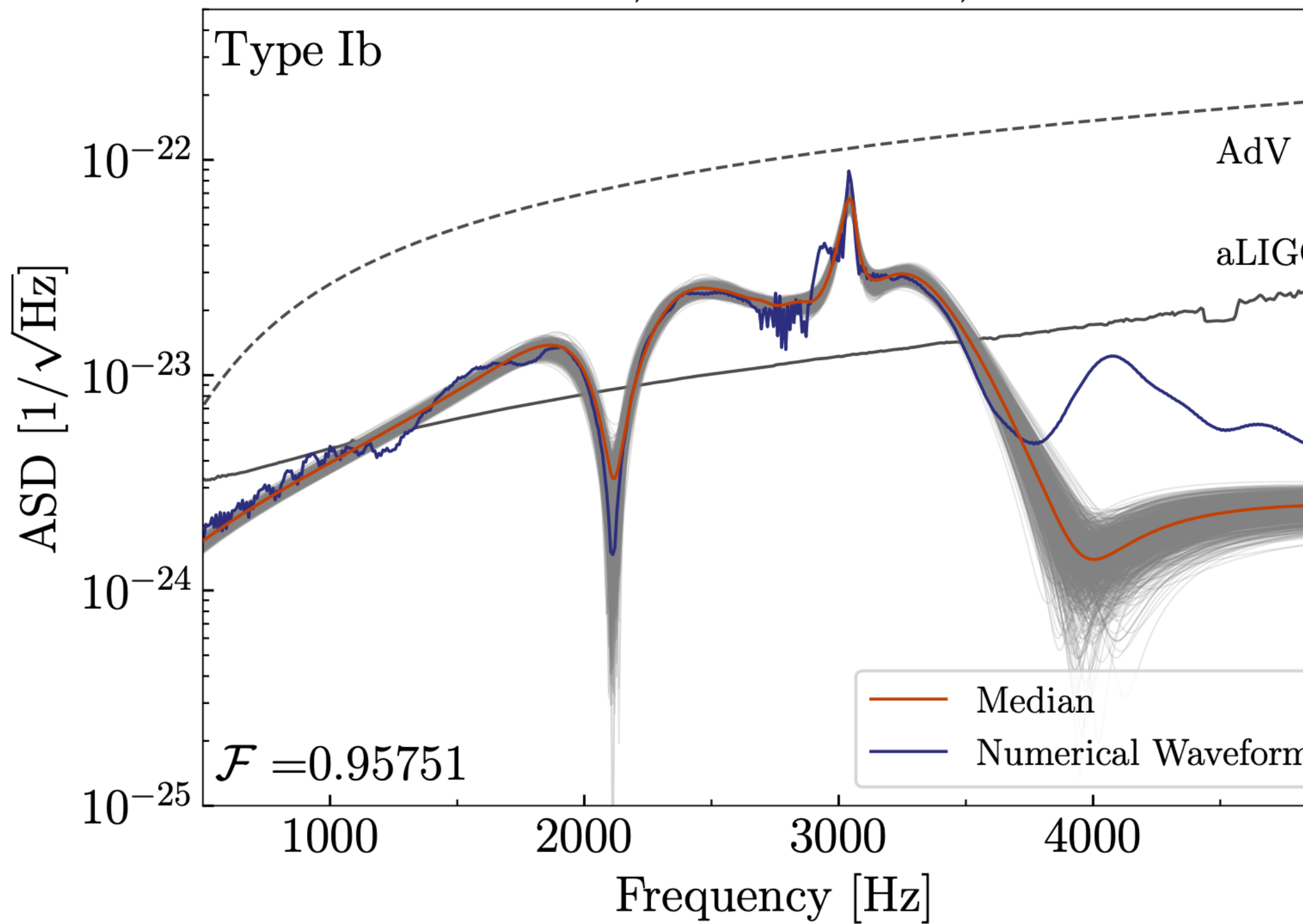
PocoMC is highly parallelizable

RECONSTRUCTION IN THE FREQUENCY DOMAIN

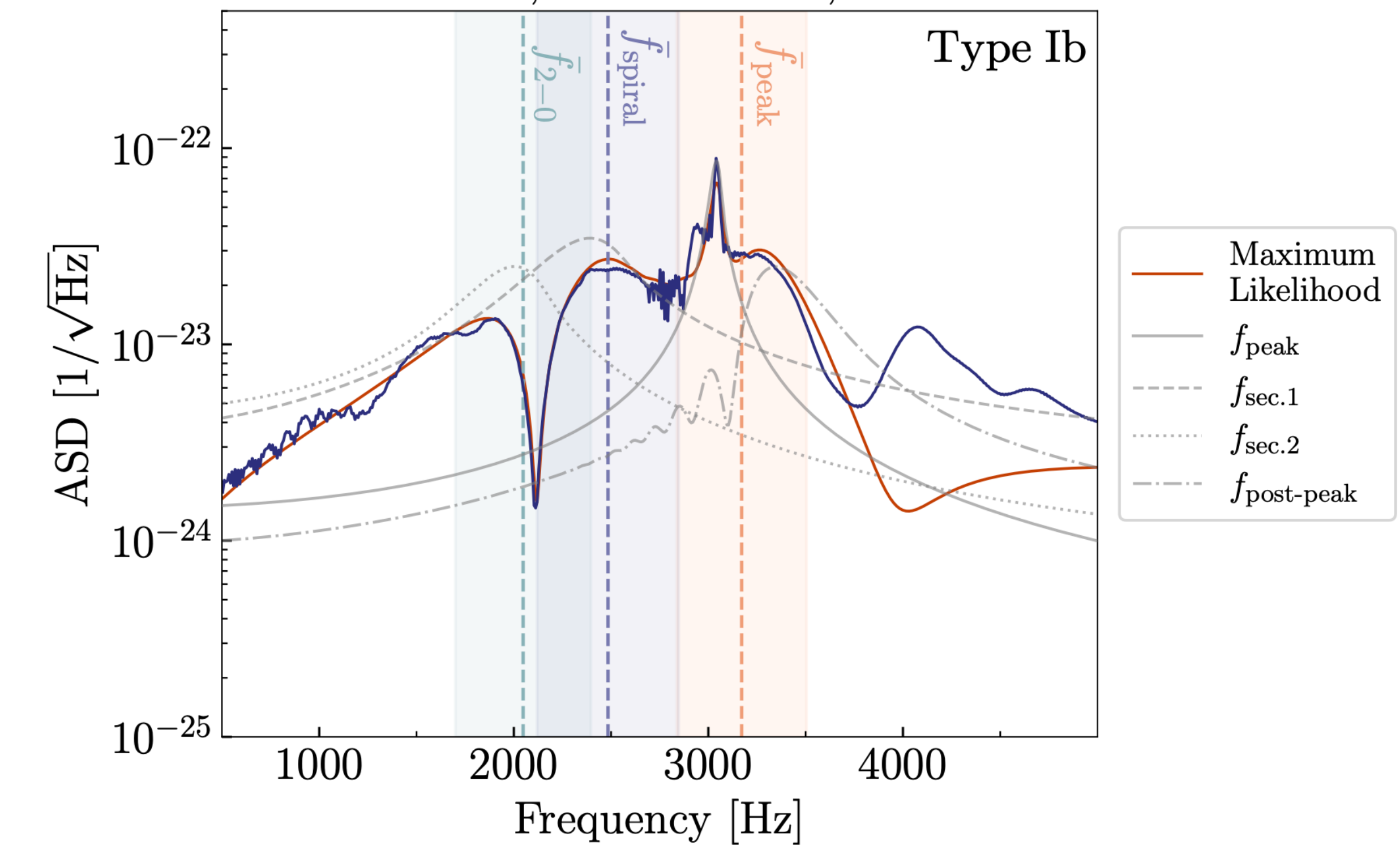


RECONSTRUCTION IN THE FREQUENCY DOMAIN

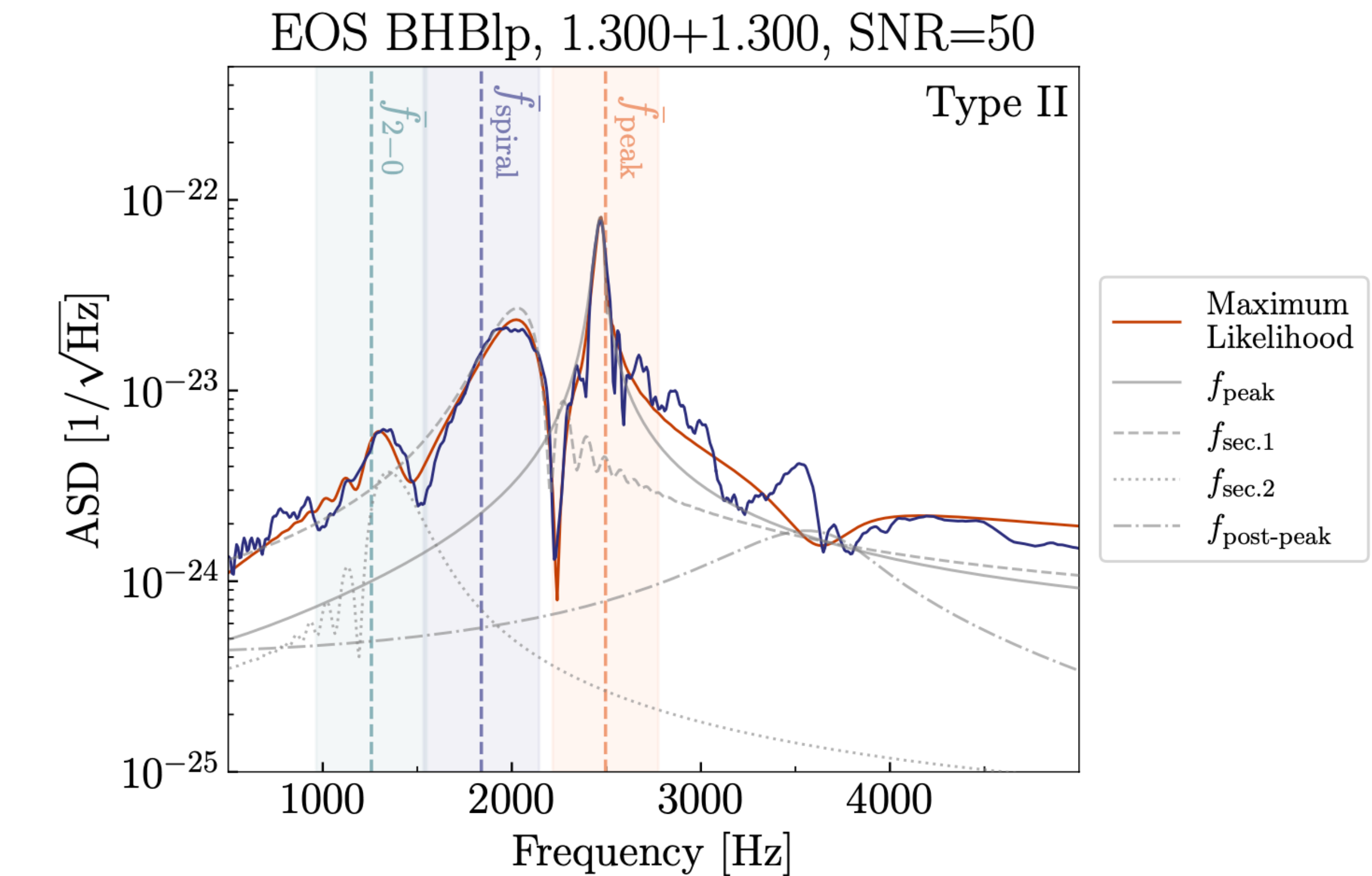
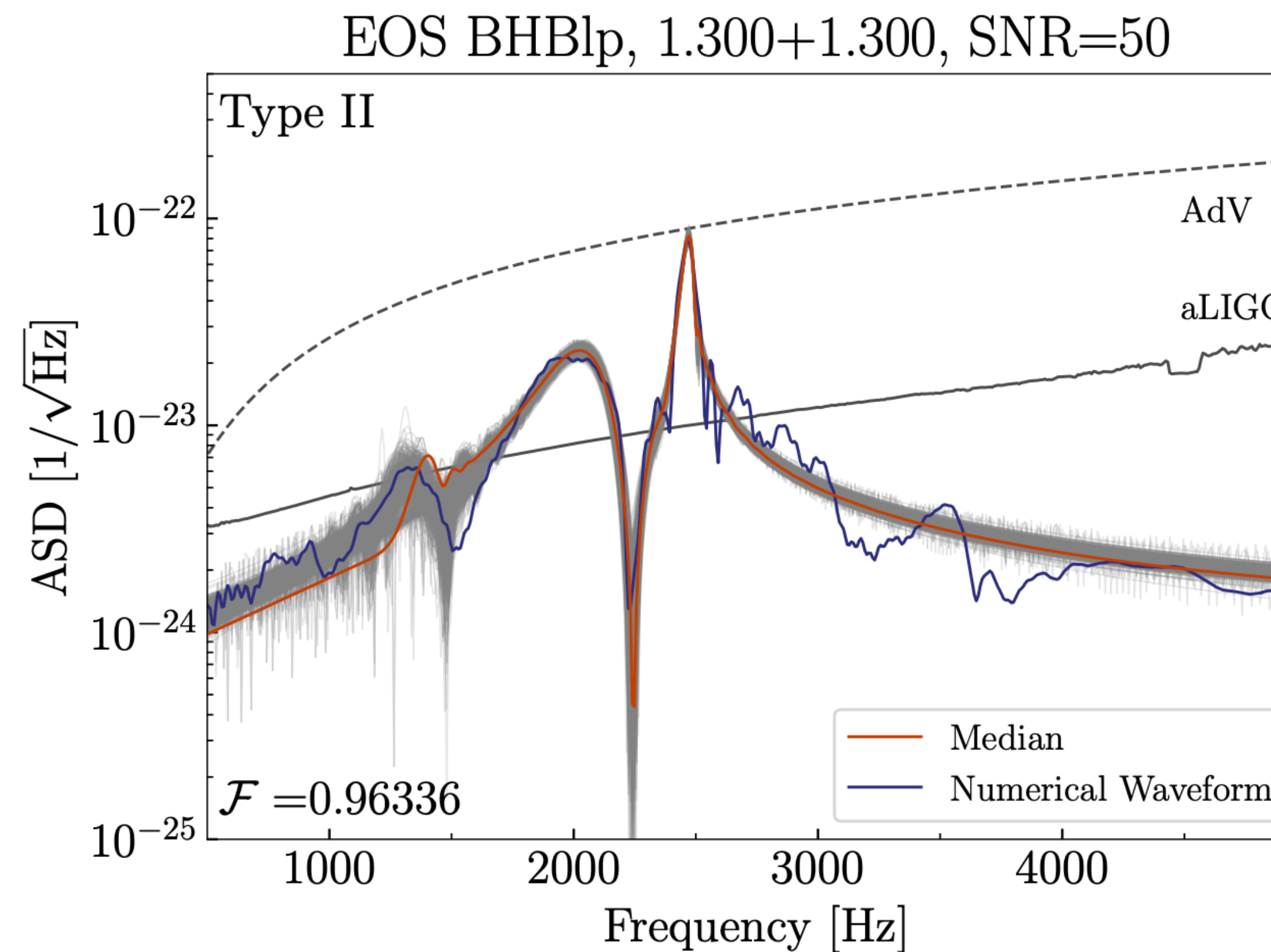
EOS MPA1, 1.550+1.550, SNR=50



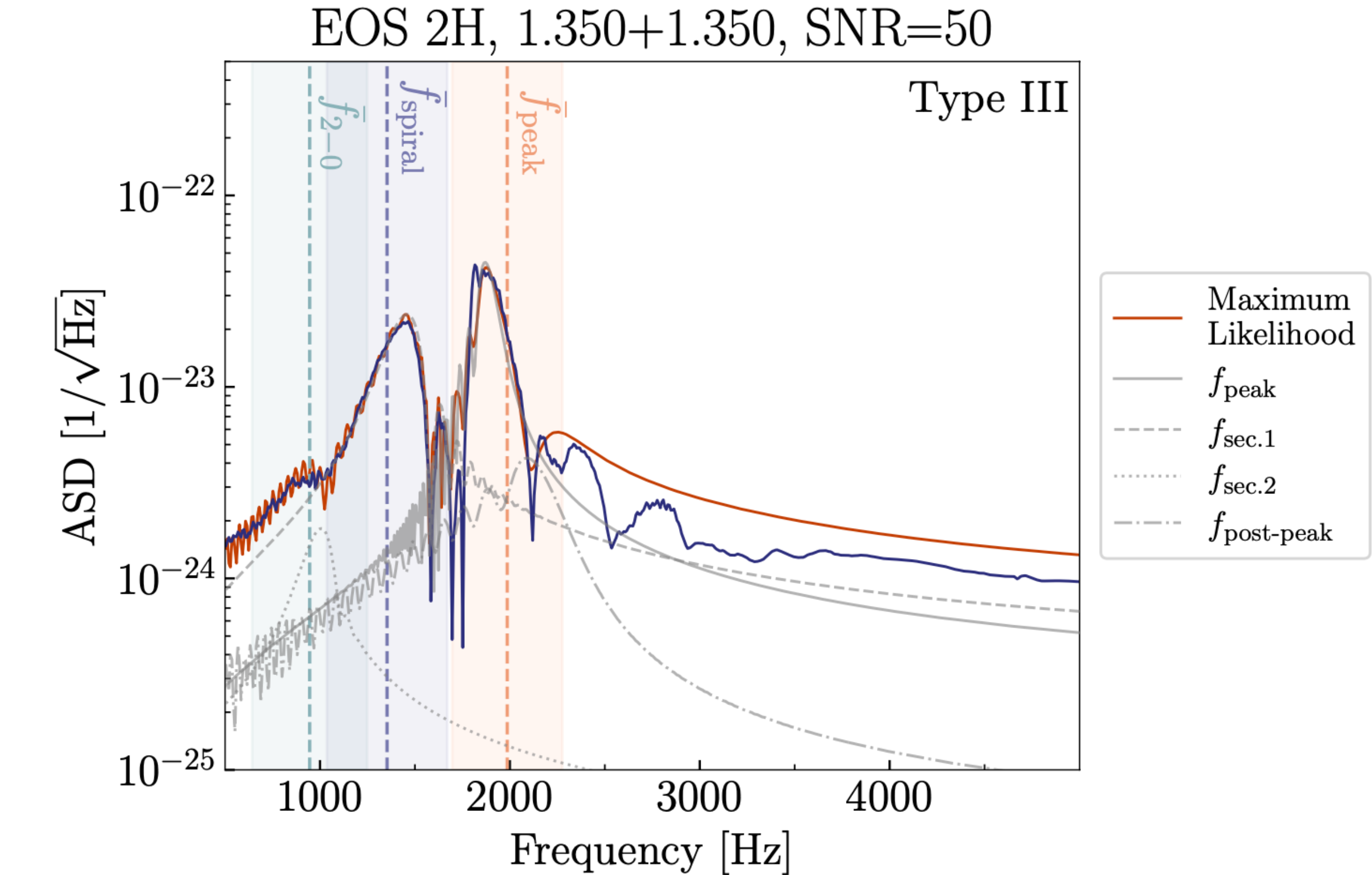
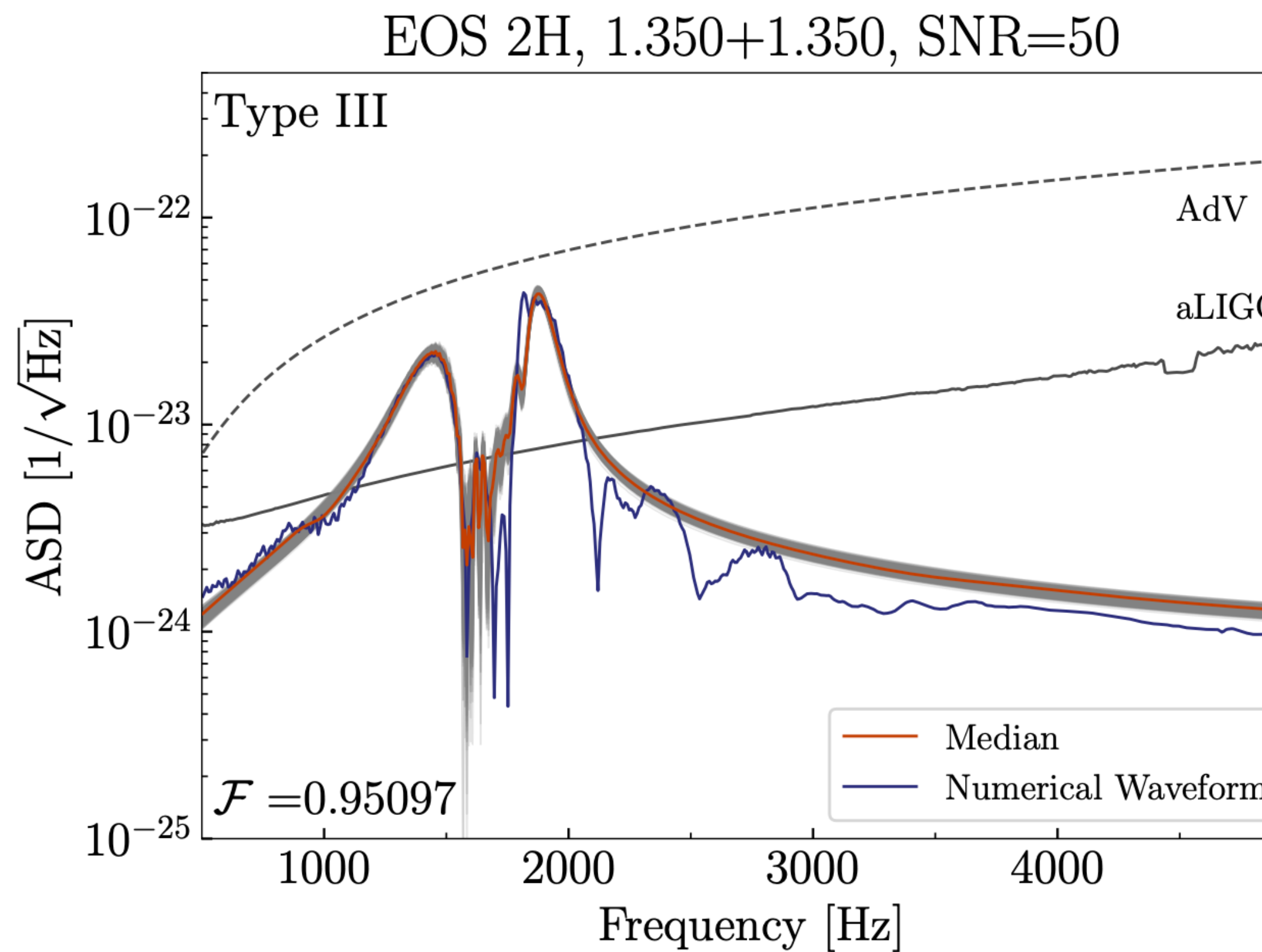
EOS MPA1, 1.550+1.550, SNR=50



RECONSTRUCTION IN THE FREQUENCY DOMAIN



RECONSTRUCTION IN THE FREQUENCY DOMAIN

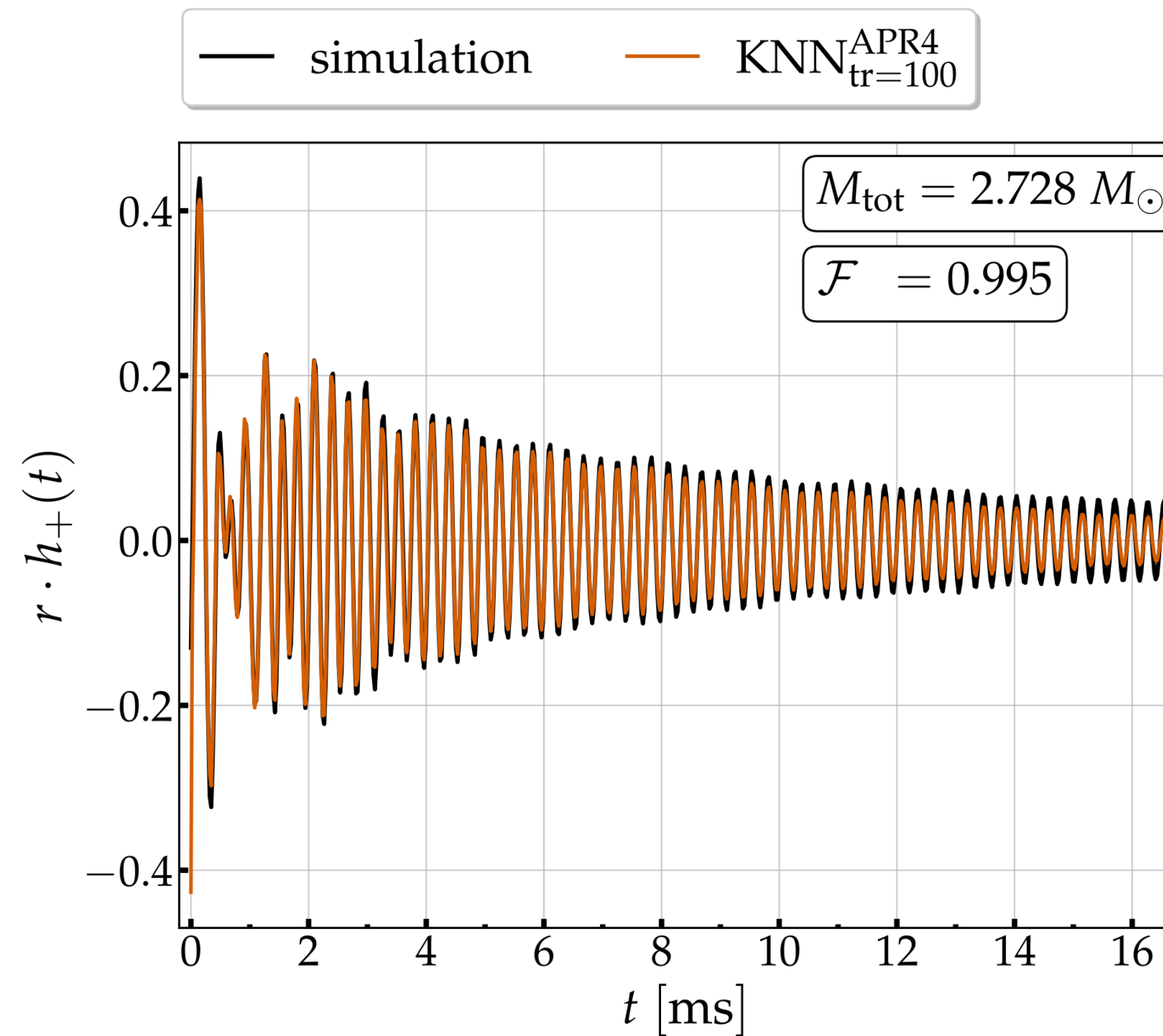


APPLICATION OF MACHINE LEARNING TO THE POST-MERGER PHASE

Problem: Only $O(200)$ substantially different numerical BNS simulations are currently available.

Solution: Construct surrogate model of post-merger GWs as function of e.g. M , q , $\text{EOS}(\Lambda)$

Time domain surrogate model using
K-Nearest Neighbor (KNN) regression:

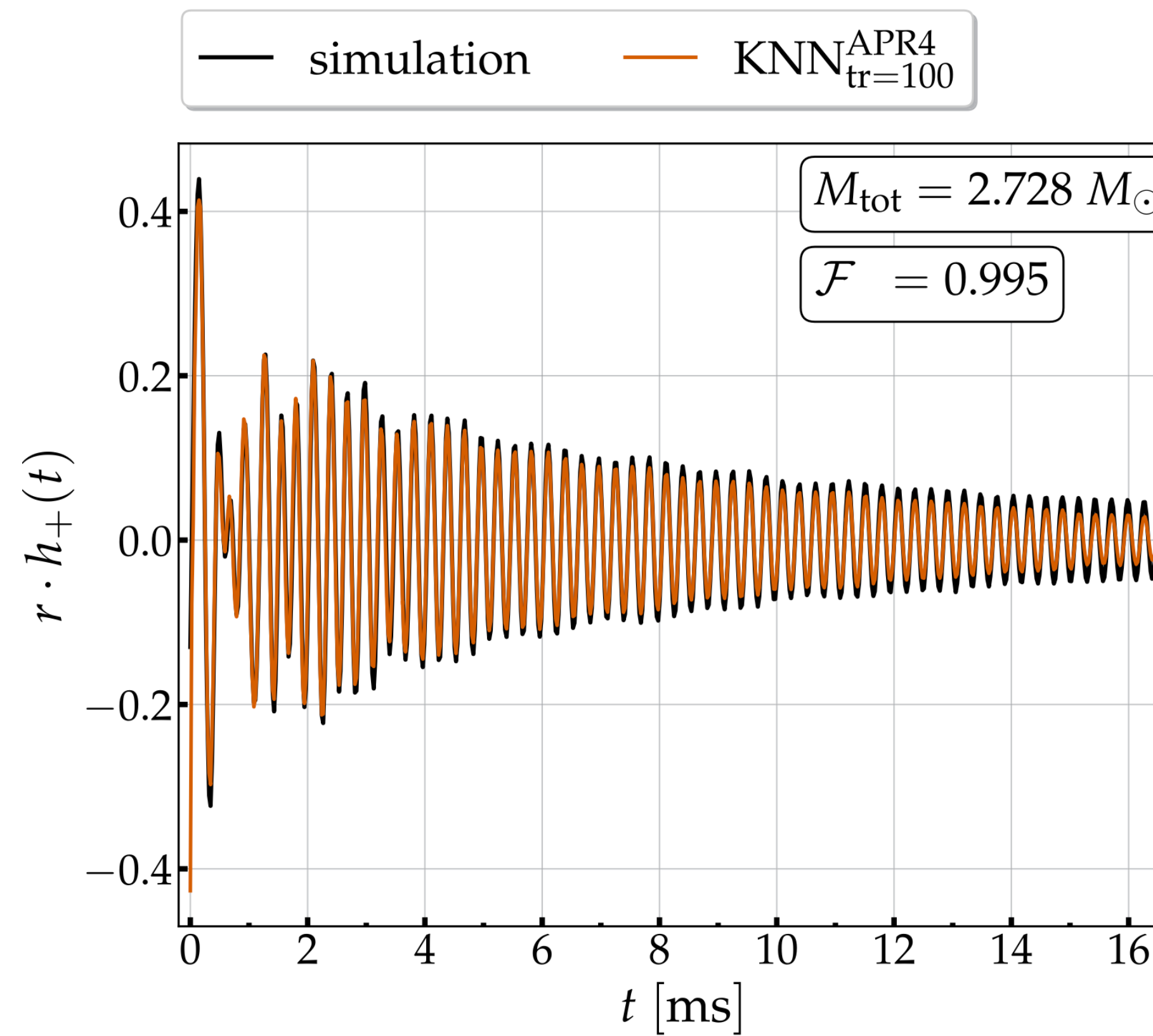


APPLICATION OF MACHINE LEARNING TO THE POST-MERGER PHASE

Problem: Only $O(200)$ substantially different numerical BNS simulations are currently available.

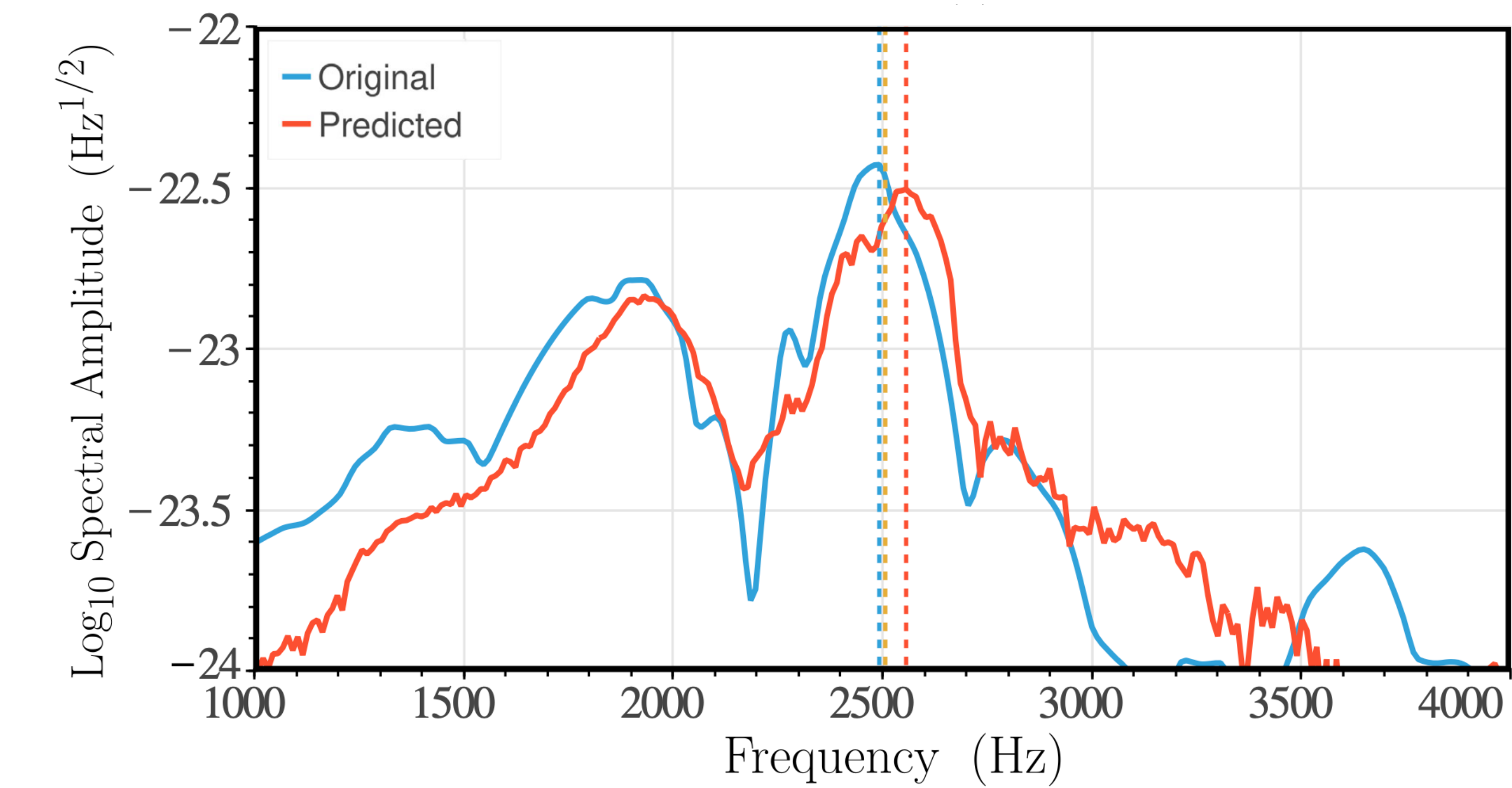
Solution: Construct surrogate model of post-merger GWs as function of e.g. M , q , $\text{EOS}(\Lambda)$

Time domain surrogate model using
K-Nearest Neighbor (KNN) regression:



Soultanis et al. (2025)

Frequency domain surrogate model using
Artificial Neural Networks (ANN) regression:



Pesios et al. (2024)

K-NEAREST NEIGHBOR REGRESSION IN THE TIME DOMAIN

Training set: 20-100 different M_{tot} ($q=1$) between 2.4 and 2.8 M_{sun} .

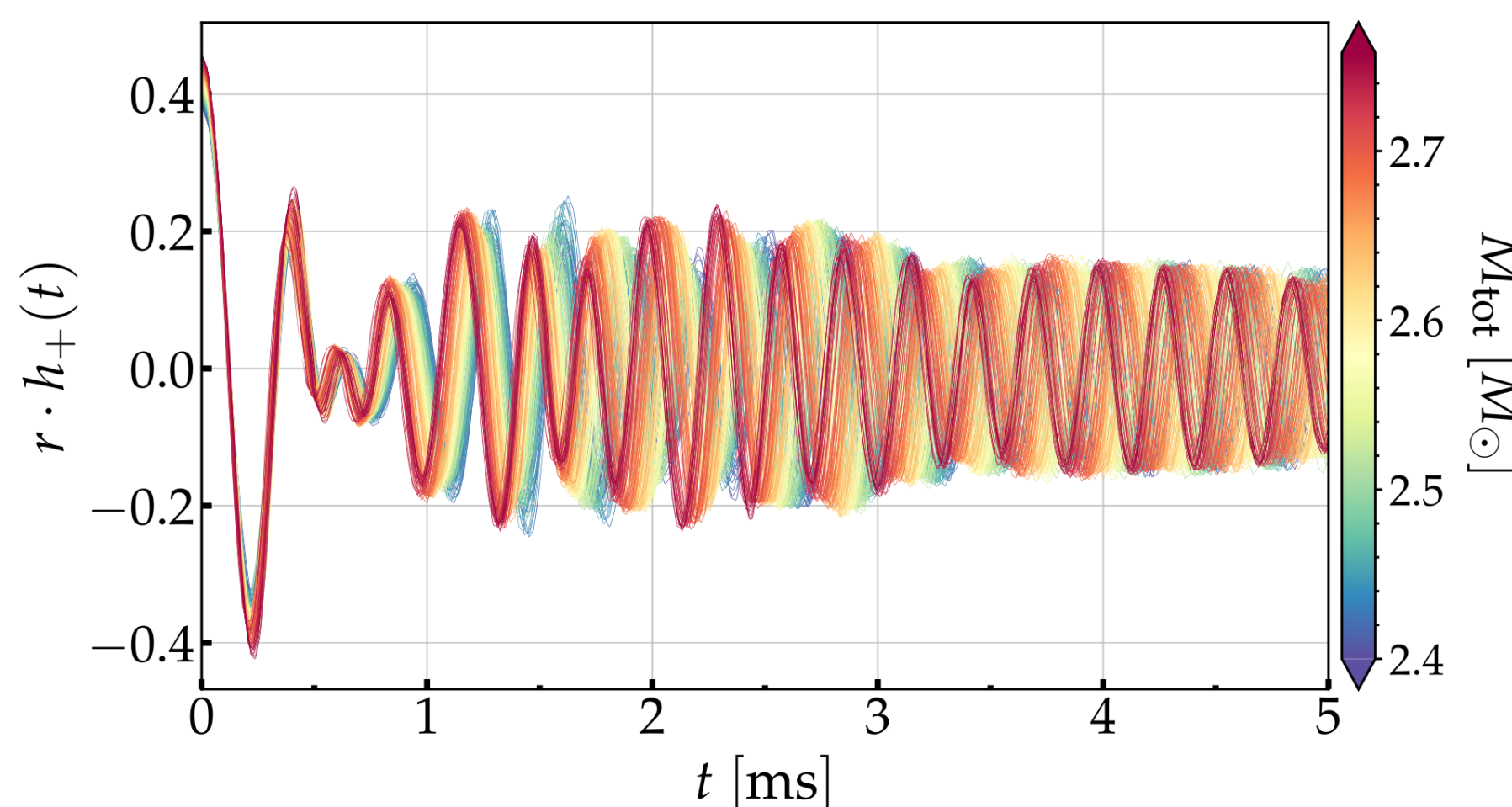
Choose specific EOS (APR4; SFHX).

Complex GW strain:

$$h(t) = h_+(t) + i h_\times(t)$$

$$= |h(t)| \cdot e^{+i\phi(t)},$$

Signals are aligned at merger time:



K-NEAREST NEIGHBOR REGRESSION IN THE TIME DOMAIN

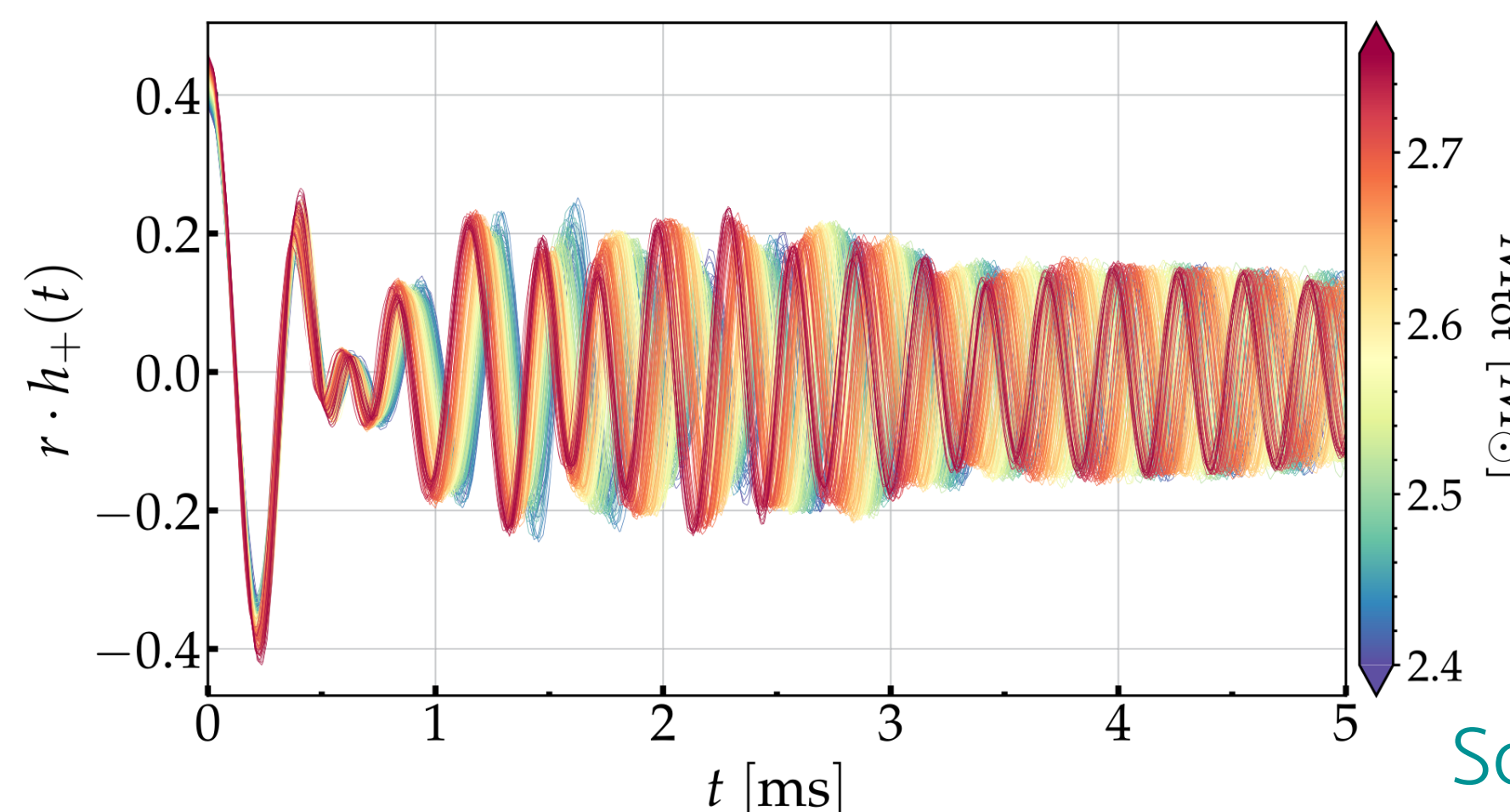
Training set: 20-100 different M_{tot} ($q=1$) between 2.4 and 2.8 M_{sun} .

Choose specific EOS (APR4; SFHX).

Complex GW strain:

$$\begin{aligned} h(t) &= h_+(t) + i h_\times(t) \\ &= |h(t)| \cdot e^{+i\phi(t)}, \end{aligned}$$

Signals are aligned at merger time:



Input features:

$$\vec{X}_i = \{M_{\text{tot}}, t_j\}$$

Predictions:

$$\vec{Y}_i = \text{strain data}$$

KNN algorithm:

For given input \vec{X}_0 , find set N_0 of K nearest neighbors

The prediction is a weighted average

$$\vec{Y}_0 = \frac{1}{K} \sum_{\vec{X}_i \in N_0} \frac{w_i \cdot \vec{Y}_i}{W}, \quad \text{where } W = \sum_{\vec{X}_i \in N_0} w_i$$

and $w_i = 1/d_i$ where d_i is the distance between \vec{X}_0

and \vec{X}_i .

Hyperparameters: K and w_i

(tuned to optimal choices using a validation set)

K-NEAREST NEIGHBOR REGRESSION IN THE TIME DOMAIN

Noise-weighted inner product for two signals:

$$\langle h_1(t), h_2(t) \rangle \equiv 4 \operatorname{Re} \int_0^\infty df \frac{\tilde{h}_1(f) \cdot \tilde{h}_2^*(f)}{S_h(f)}$$

Overlap:

$$\mathcal{O} \equiv \frac{\langle h_1(t), h_2(t) \rangle}{\sqrt{\langle h_1(t), h_1(t) \rangle \langle h_2(t), h_2(t) \rangle}}$$

Faithfulness (maximized overlap)

$$\mathcal{F} \equiv \max_{\phi_0, t_0} \frac{\langle h_1(t), h_2(t) \rangle}{\sqrt{\langle h_1(t), h_1(t) \rangle \langle h_2(t), h_2(t) \rangle}}$$

K-NEAREST NEIGHBOR REGRESSION IN THE TIME DOMAIN

Noise-weighted inner product for two signals:

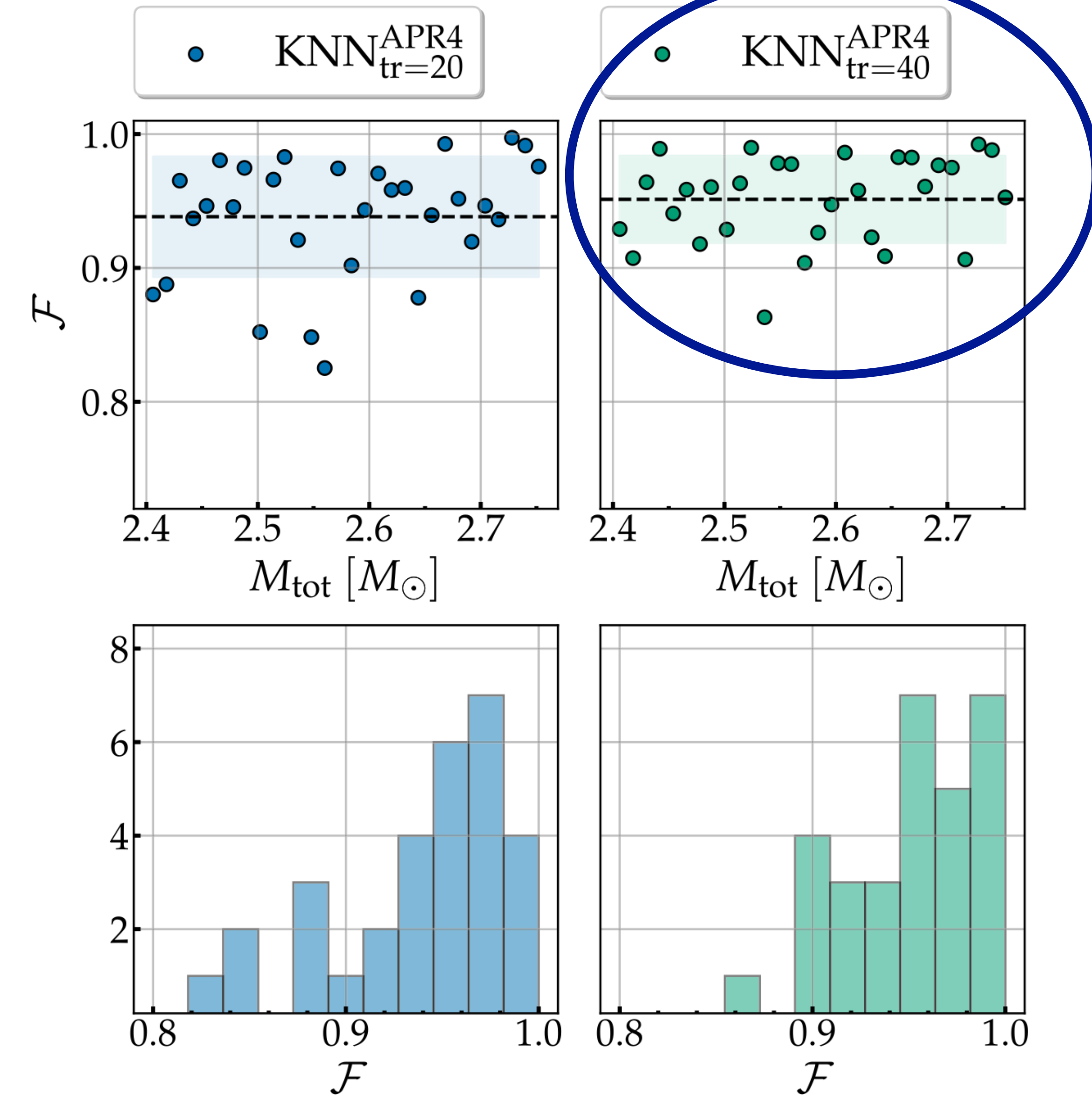
$$\langle h_1(t), h_2(t) \rangle \equiv 4 \operatorname{Re} \int_0^\infty df \frac{\tilde{h}_1(f) \cdot \tilde{h}_2^*(f)}{S_h(f)}$$

Overlap:

$$\mathcal{O} \equiv \frac{\langle h_1(t), h_2(t) \rangle}{\sqrt{\langle h_1(t), h_1(t) \rangle \langle h_2(t), h_2(t) \rangle}}$$

Faithfulness (maximized overlap)

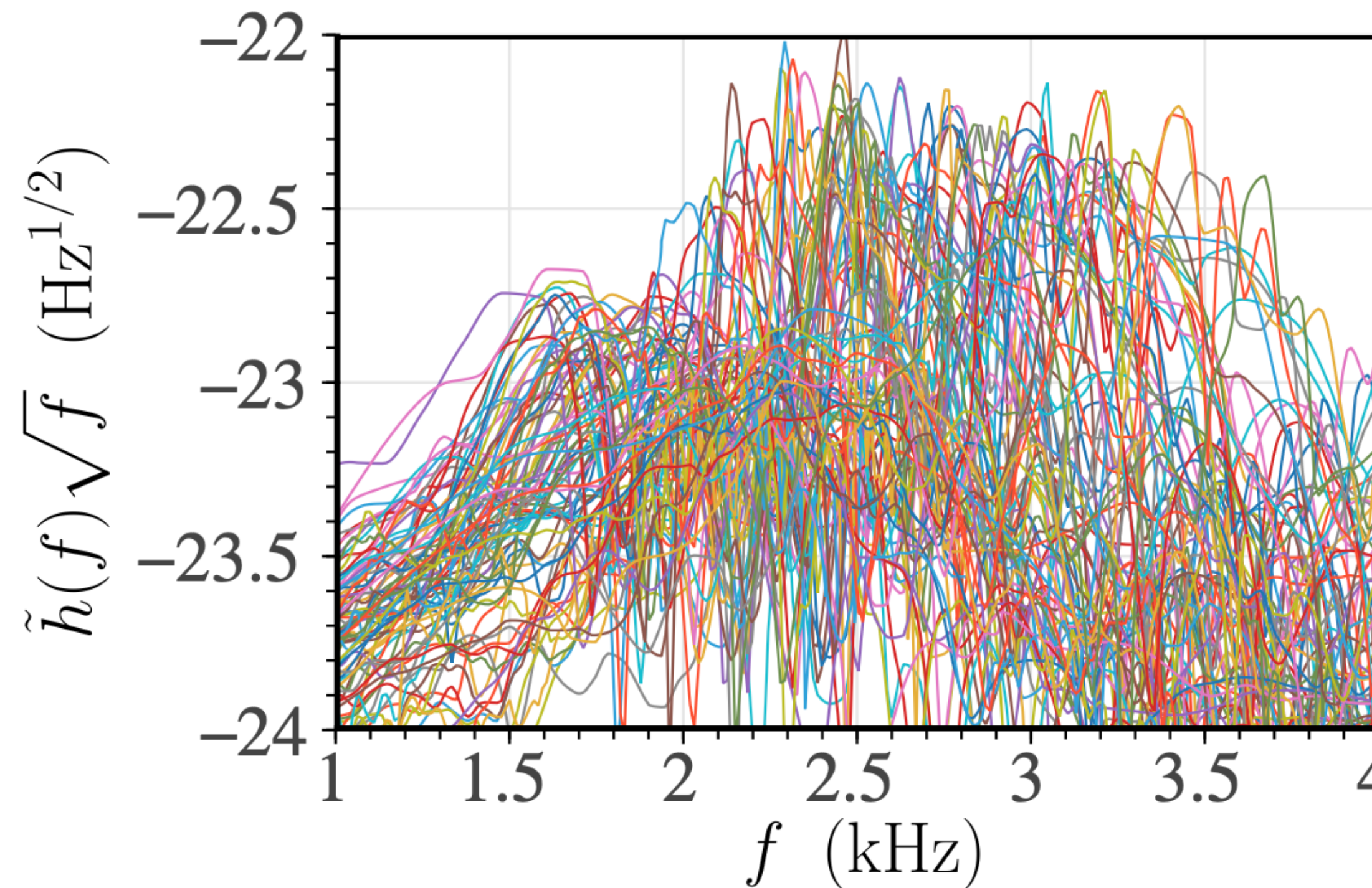
$$\mathcal{F} \equiv \max_{\phi_0, t_0} \frac{\langle h_1(t), h_2(t) \rangle}{\sqrt{\langle h_1(t), h_1(t) \rangle \langle h_2(t), h_2(t) \rangle}}$$



ANN REGRESSION IN THE FREQUENCY DOMAIN

Expanded training set: 87 equal-mass models using 14 different EOS

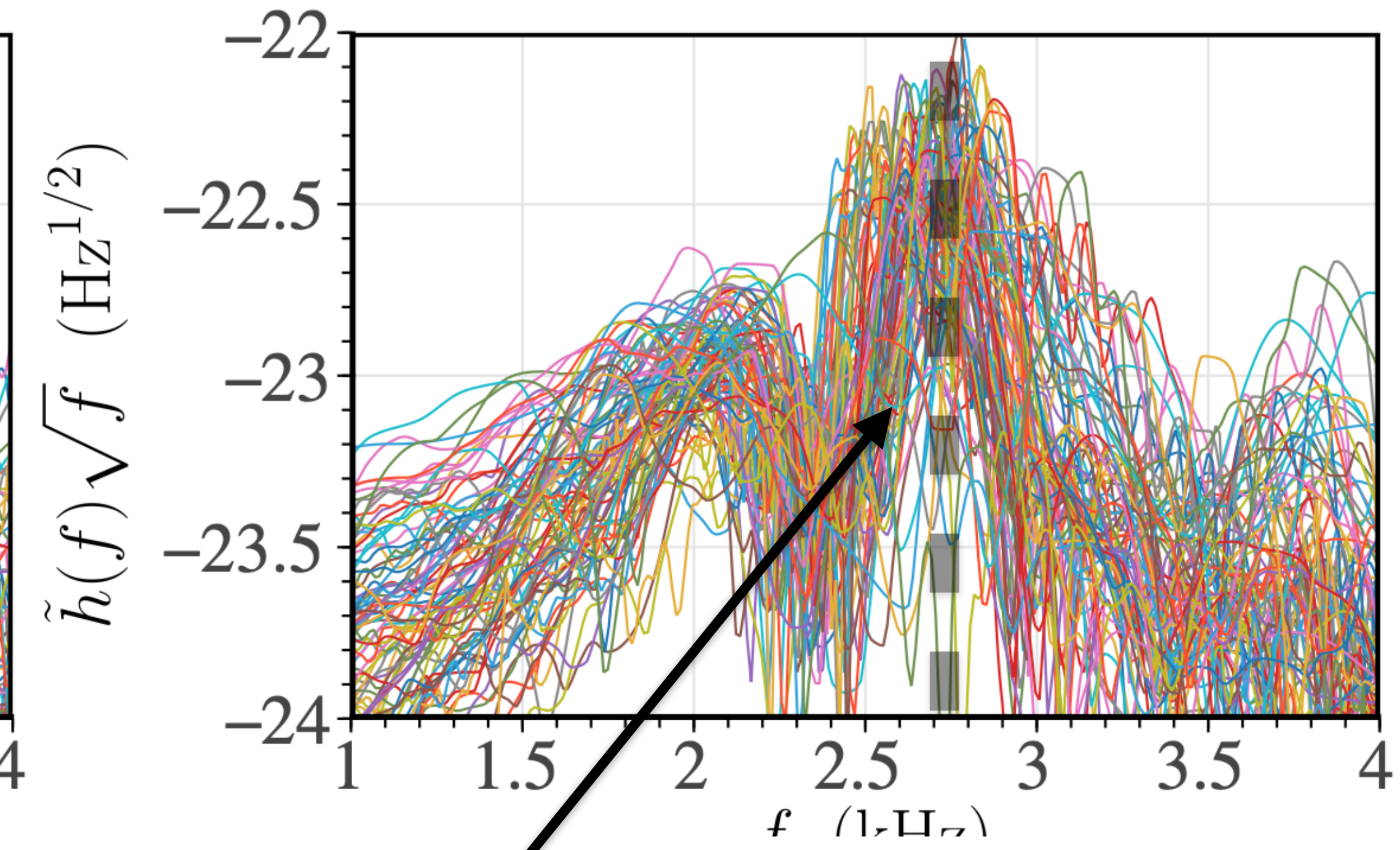
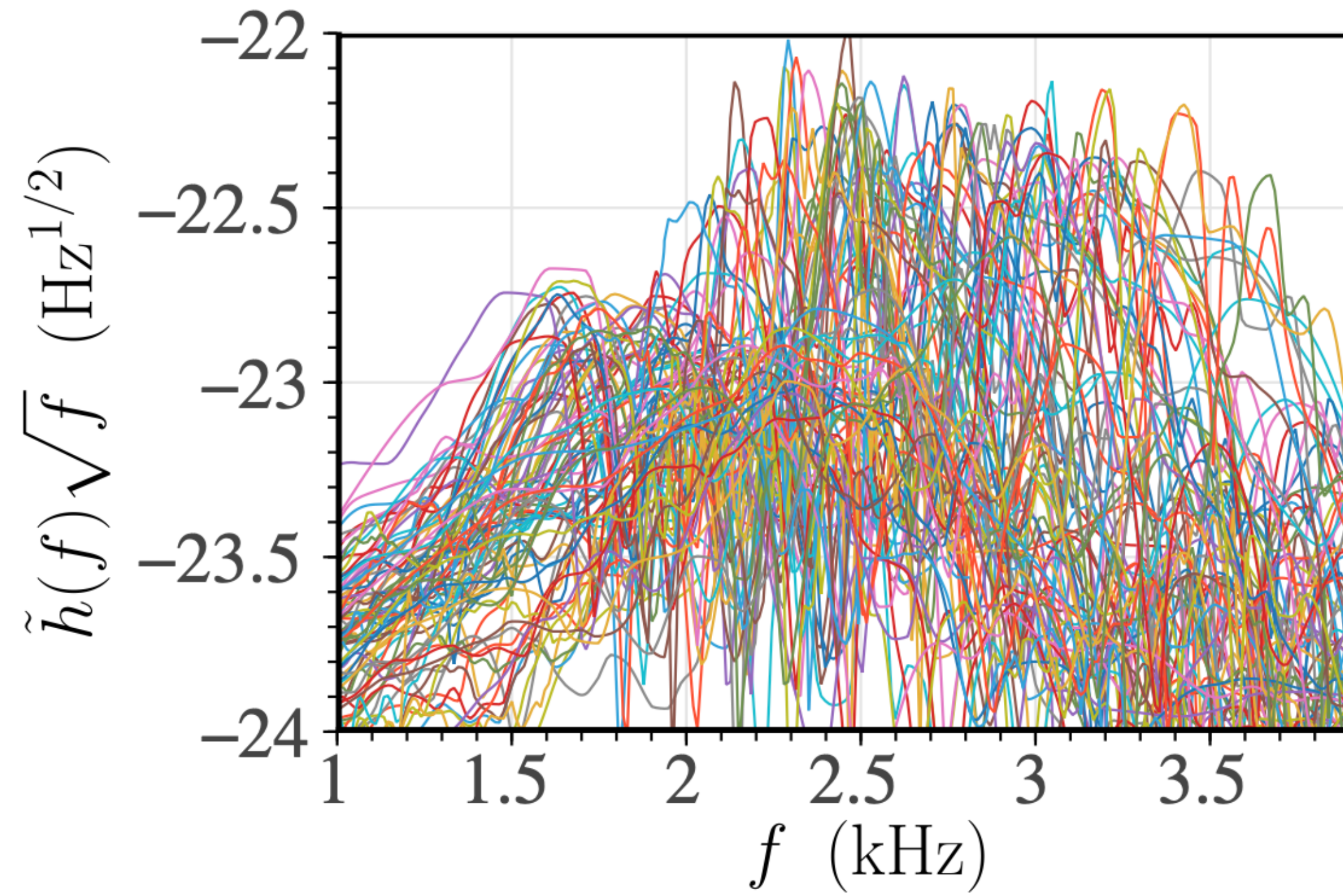
Surrogate model now depends on both mass and tidal deformability.



ANN REGRESSION IN THE FREQUENCY DOMAIN

Expanded training set: 87 equal-mass models using 14 different EOS

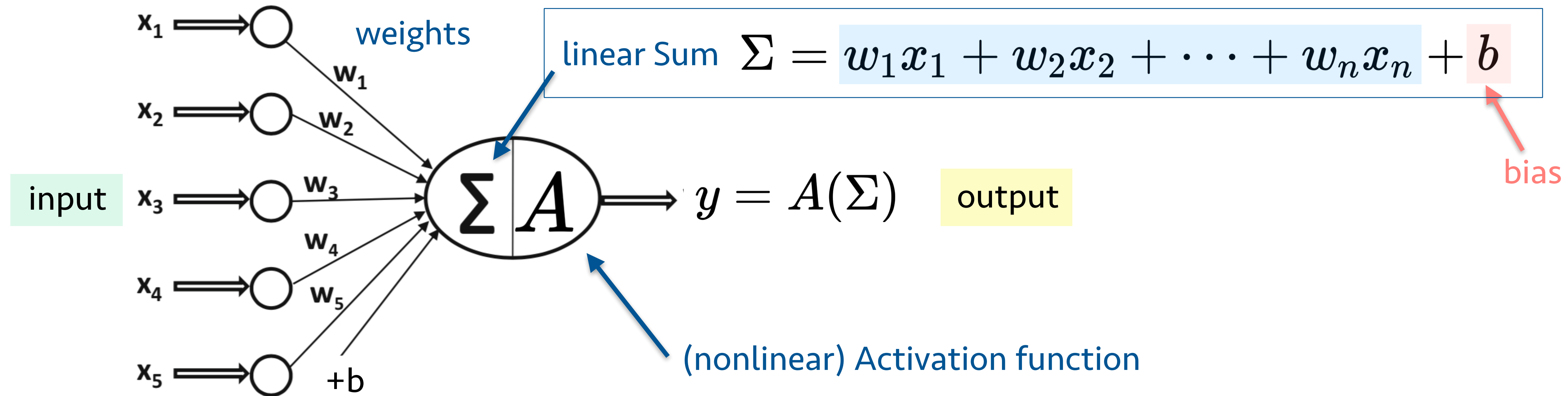
Surrogate model now depends on both mass and tidal deformability.



Partial alignment of spectra using empirical relation:
$$f_{\text{peak}}(\kappa_2^\tau, M) = 4 \frac{\beta_1}{M} \ln \left(\frac{\beta_0}{8\kappa_2^\tau} \right)$$

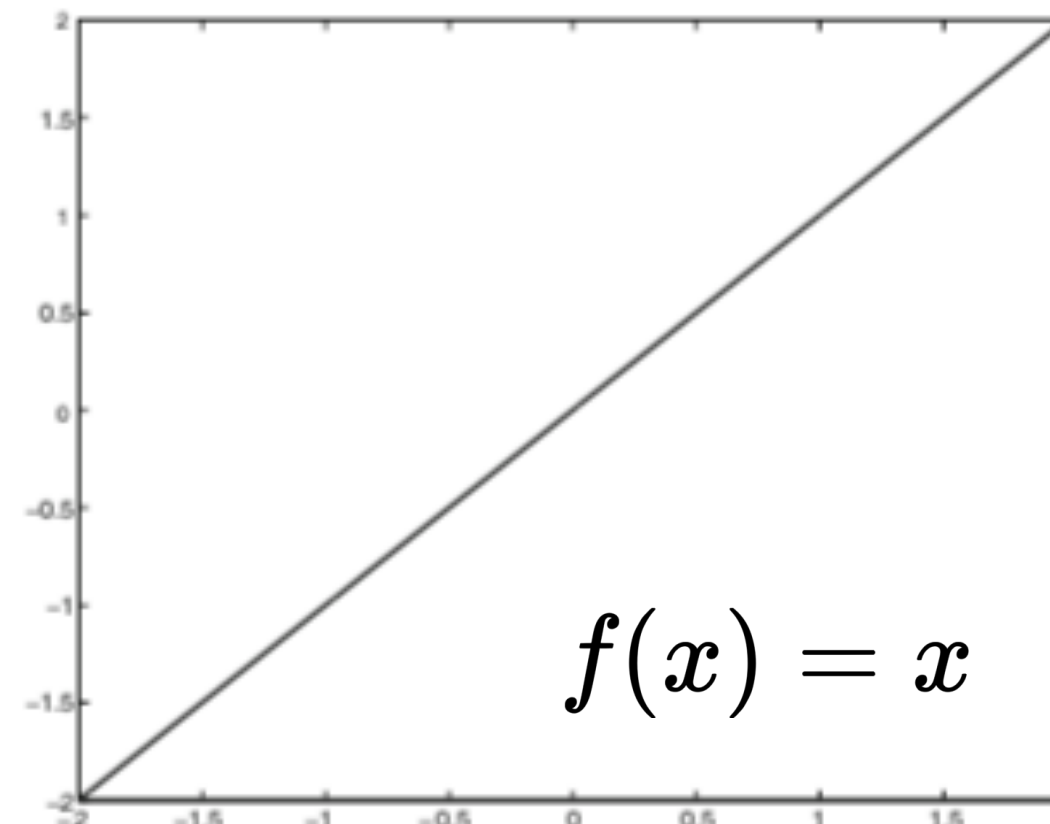
ARTIFICIAL NEURON

- Each neuron in the network maps several **input values** x_1, \dots, x_n to an **output value** y

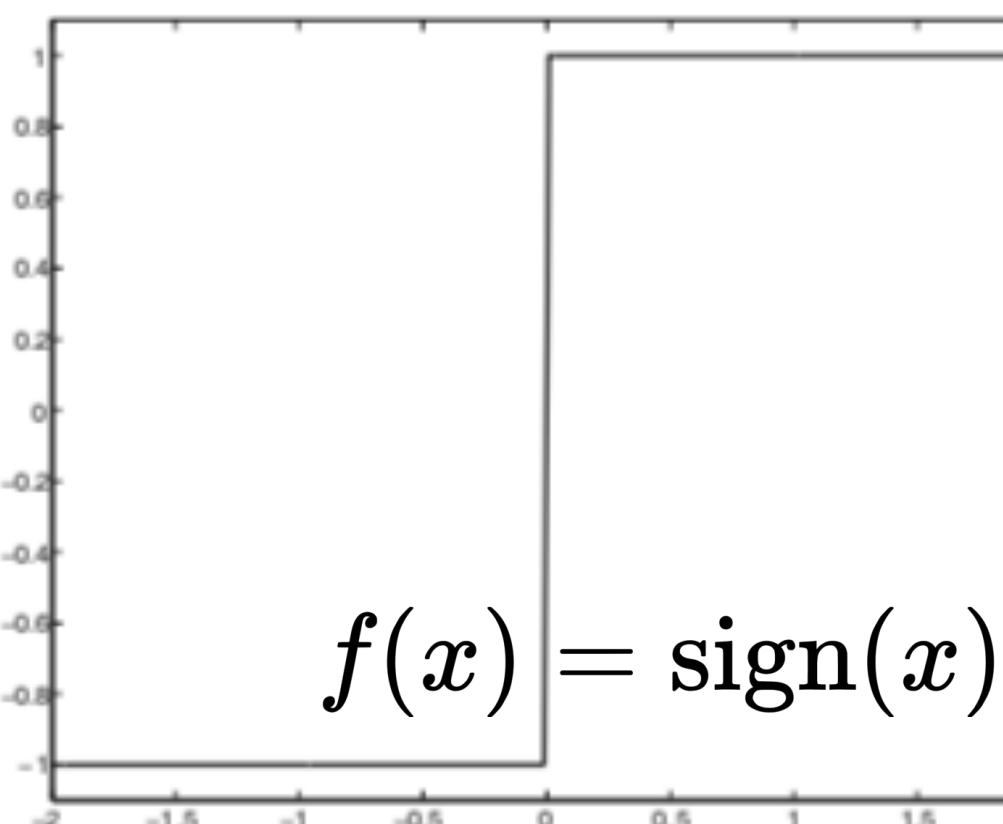


ACTIVATION FUNCTIONS

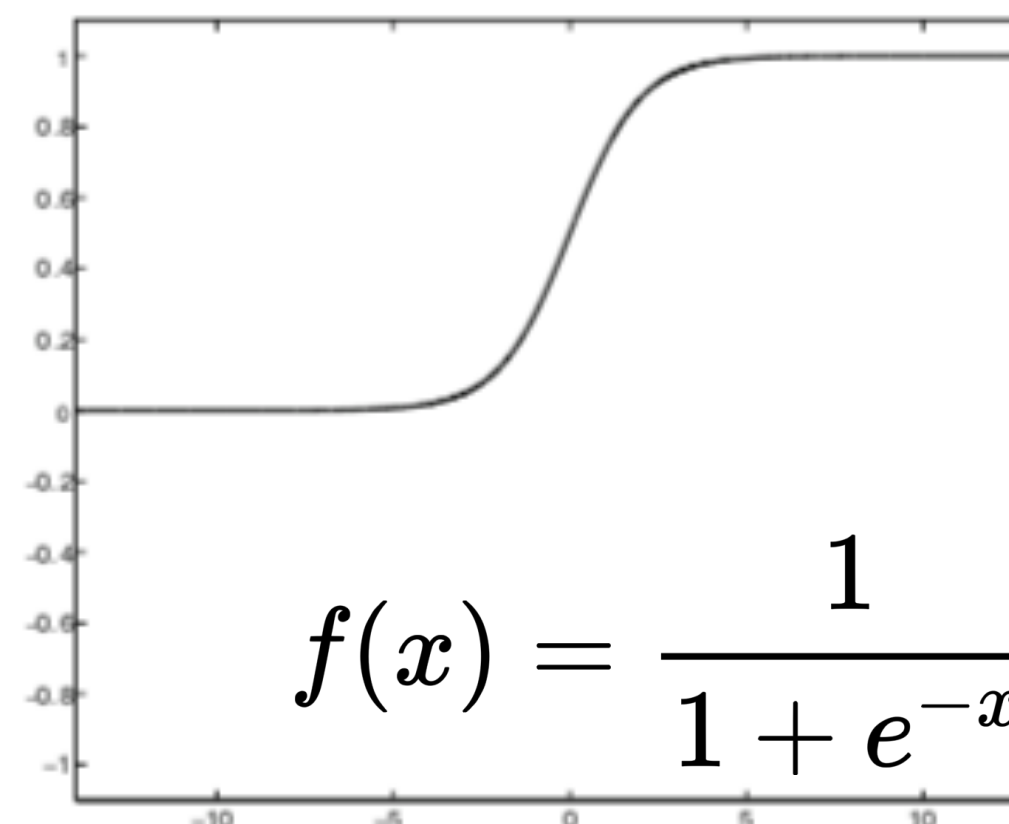
- Different common activation functions:



(a) Identity

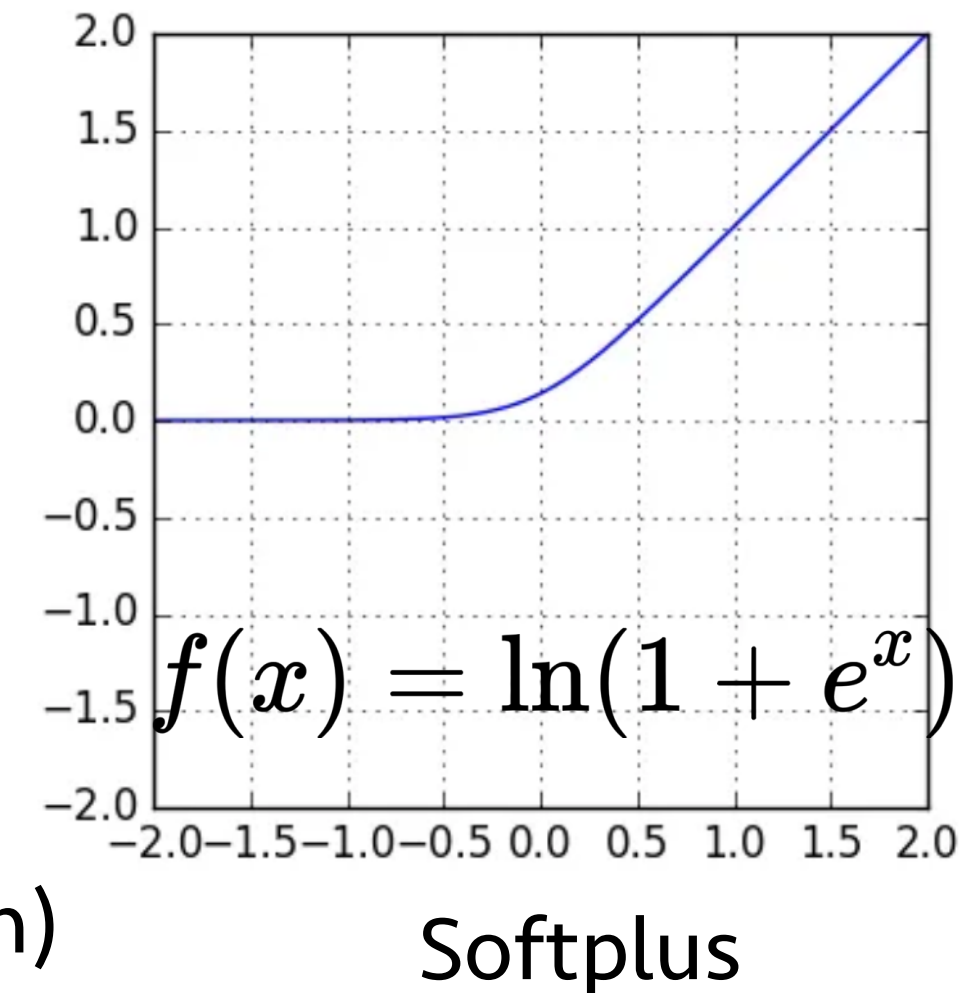


(b) Sign

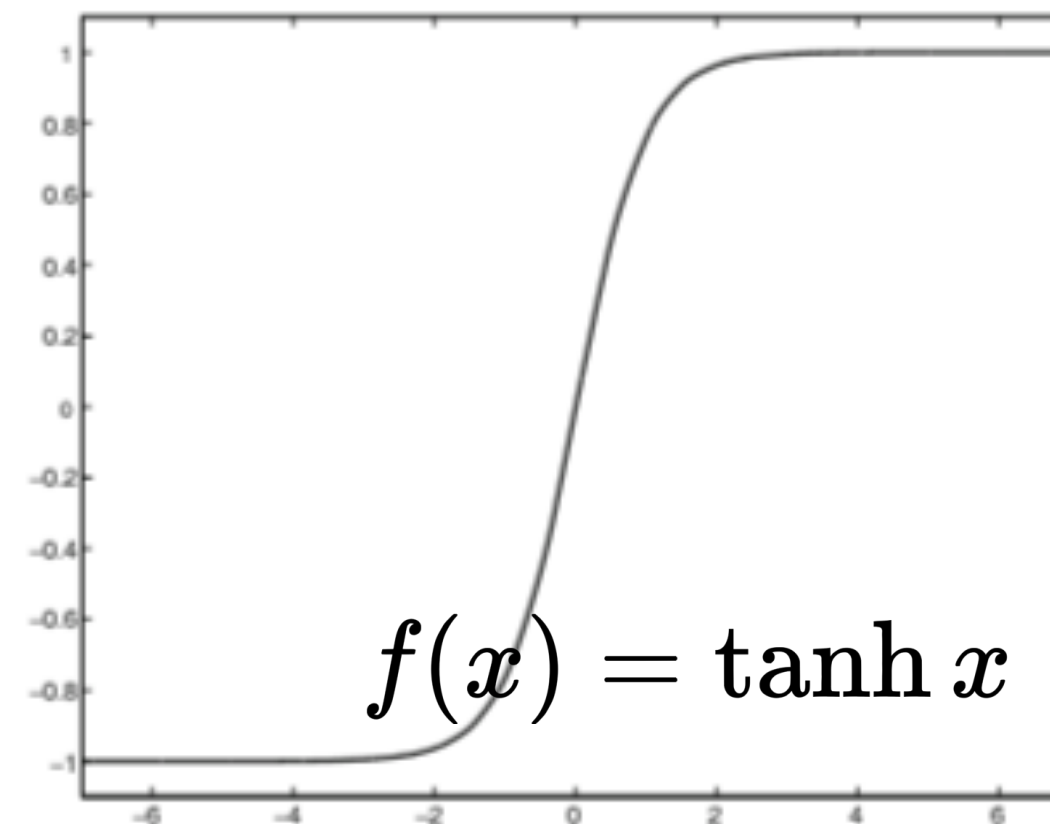


$$f(x) = \frac{1}{1 + e^{-x}}$$

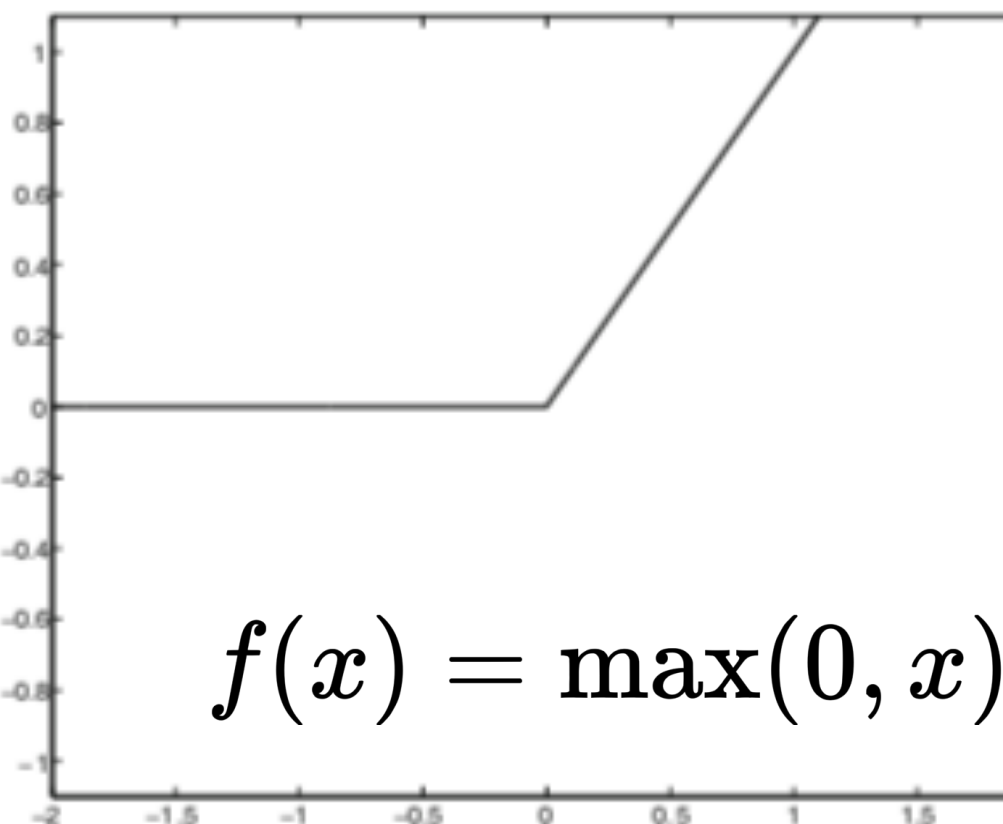
(c) Sigmoid (logistic function)



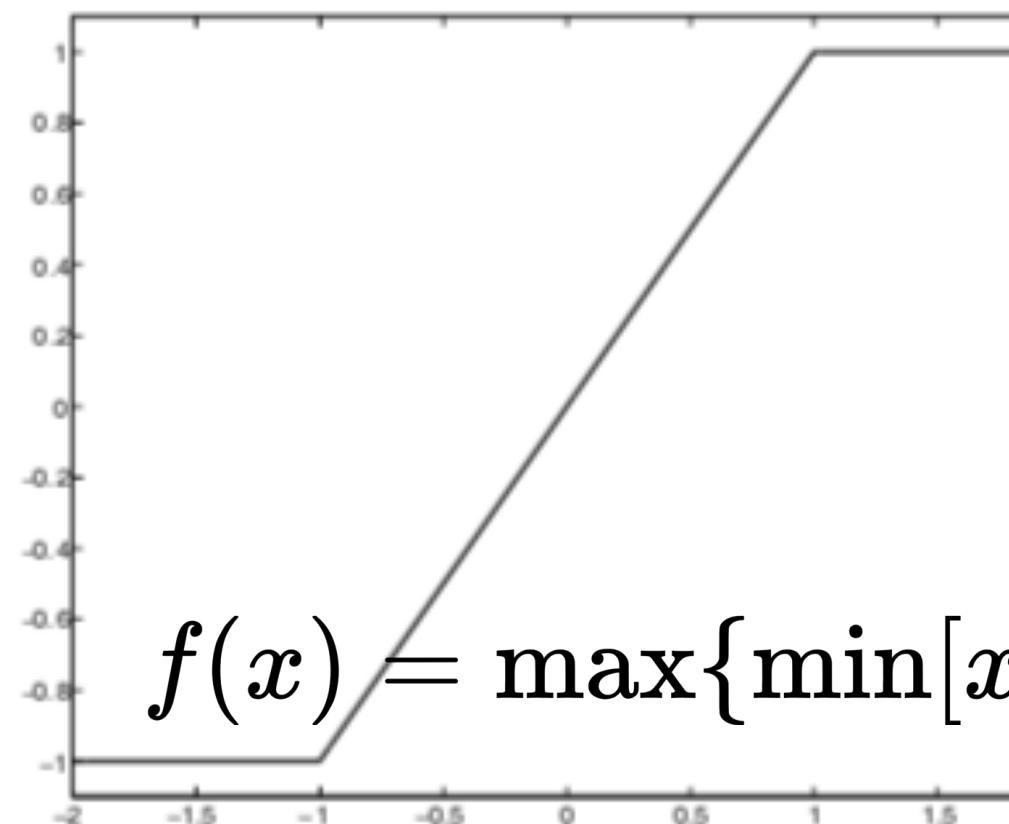
Softplus



(d) Tanh



(e) ReLU



(f) Hard Tanh

(Rectified Linear Unit)

ANN SURROGATE IN THE FREQUENCY DOMAIN

Input features:

- 1) Mass, 2) tidal coupling constant, 3) dR/dM

Prediction:

Magnitude of GW spectrum (1-4 kHz).

ANN SURROGATE IN THE FREQUENCY DOMAIN

Input features:

- 1) Mass, 2) tidal coupling constant, 3) dR/dM

Prediction:

Magnitude of GW spectrum (1-4 kHz).

4-layer feed-forward ANN

Added Gaussian noise and dropout layers

Adam optimizer

Layer	Type	Shape	Activation	Params
1	Gaussian noise (0.1)	(None, 3)	...	0
2	Dense	(None, 200)	Linear	800
3	Gaussian noise (0.05)	(None, 200)	...	0
4	Dropout (0.15)	(None, 200)	...	0
5	Dense	(None, 400)	Sigmoid	80400
6	Gaussian noise (0.1)	(None, 400)	...	0
7	Dropout (0.15)	(None, 400)	...	0
8	Dense	(None, 400)	Sigmoid	160400
9	Gaussian noise (0.1)	(None, 400)	...	0
10	Dropout (0.05)	(None, 400)	...	0
11	Dense	(None, 370)	Linear	148370

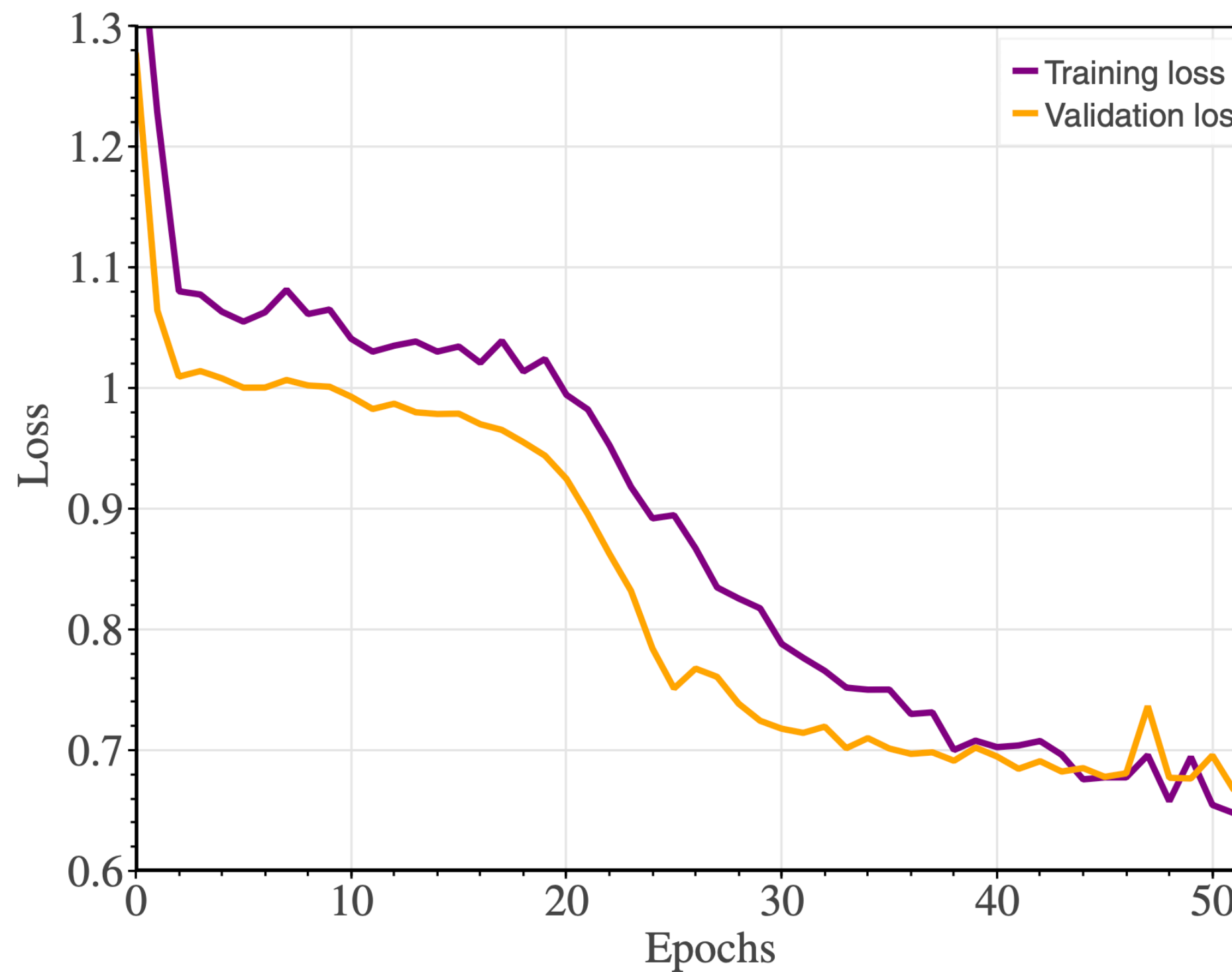
ANN SURROGATE IN THE FREQUENCY DOMAIN

Input features:

- 1) Mass, 2) tidal coupling constant, 3) dR/dM

Prediction:

Magnitude of GW spectrum (1-4 kHz).



4-layer feed-forward ANN

Added Gaussian noise and dropout layers

Adam optimizer

Layer	Type	Shape	Activation	Params
1	Gaussian noise (0.1)	(None, 3)	...	0
2	Dense	(None, 200)	Linear	800
3	Gaussian noise (0.05)	(None, 200)	...	0
4	Dropout (0.15)	(None, 200)	...	0
5	Dense	(None, 400)	Sigmoid	80400
6	Gaussian noise (0.1)	(None, 400)	...	0
7	Dropout (0.15)	(None, 400)	...	0
8	Dense	(None, 400)	Sigmoid	160400
9	Gaussian noise (0.1)	(None, 400)	...	0
10	Dropout (0.05)	(None, 400)	...	0
11	Dense	(None, 370)	Linear	148370

ANN SURROGATE IN THE FREQUENCY DOMAIN

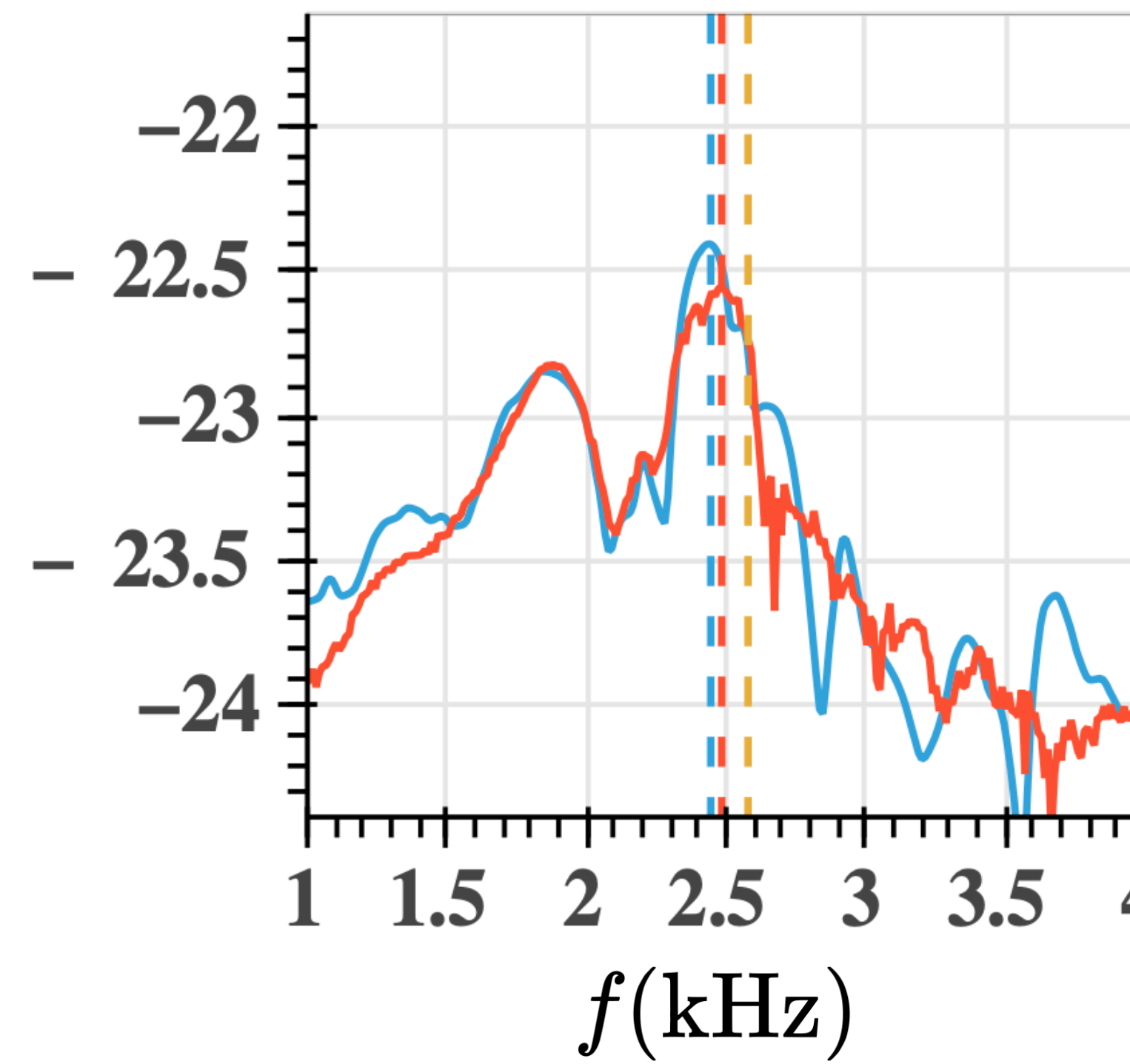
Typical examples of predicted magnitudes of GW spectra

FF = O = overlap

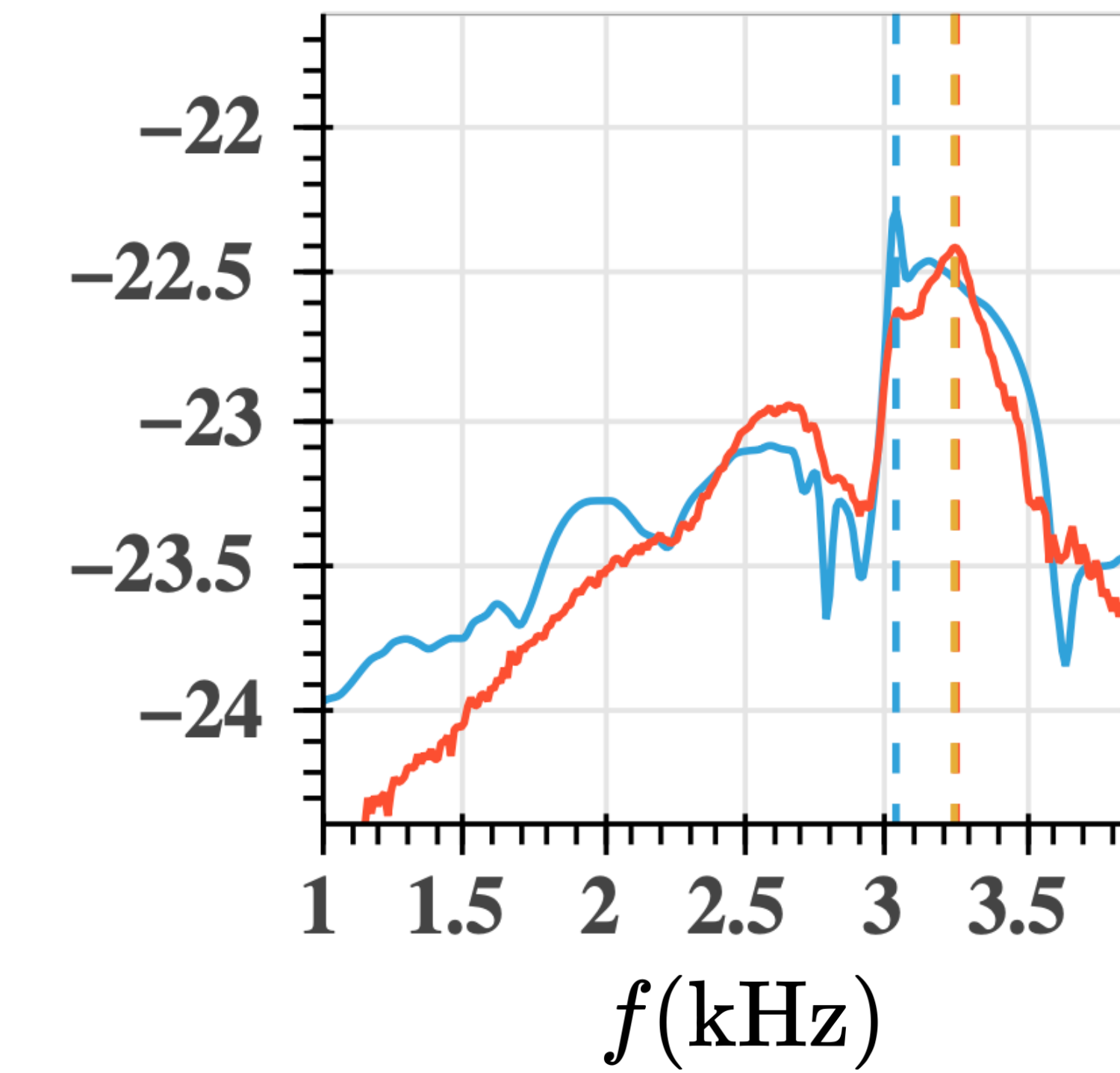
Impact of uncertainty in empirical relation offset by re-calibration of spectra.

ANN outperforms multivariate linear regression.

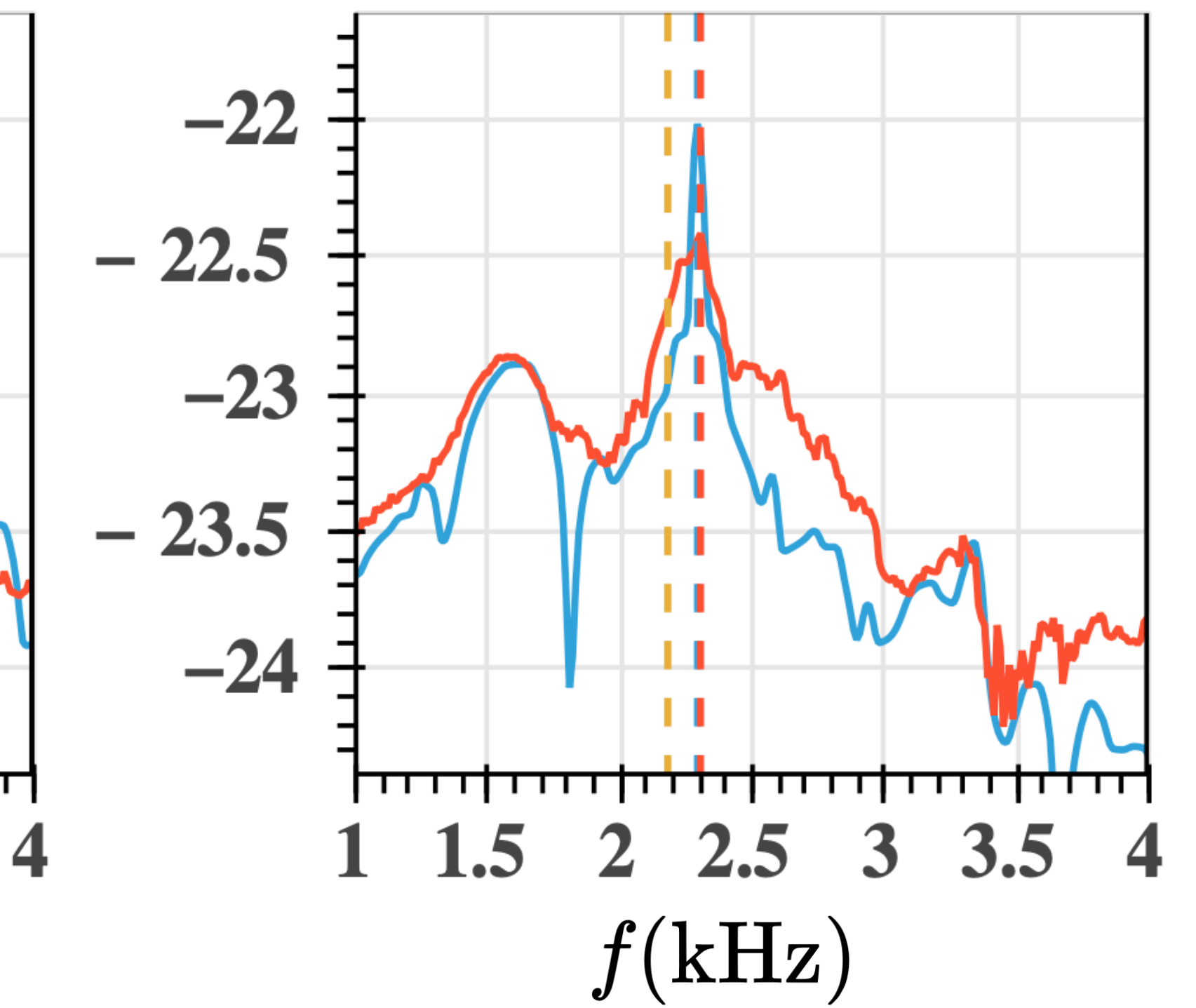
ALF2, M12500, FF: 0.971



APR4, M12500, FF: 0.94

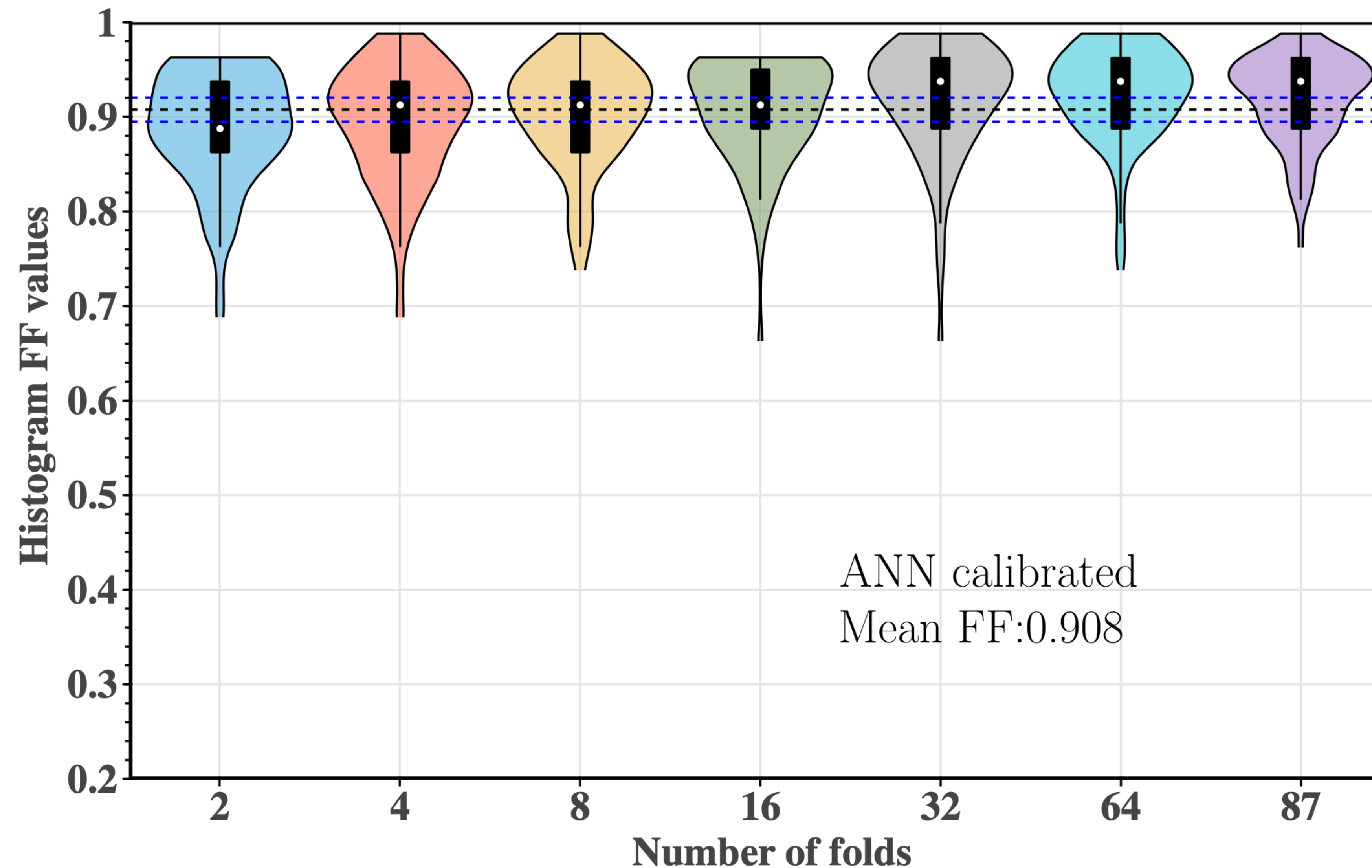


GNH3, M12500, FF: 0.862



ANN SURROGATE IN THE FREQUENCY DOMAIN

Cross-validation study of fitting factors distribution:

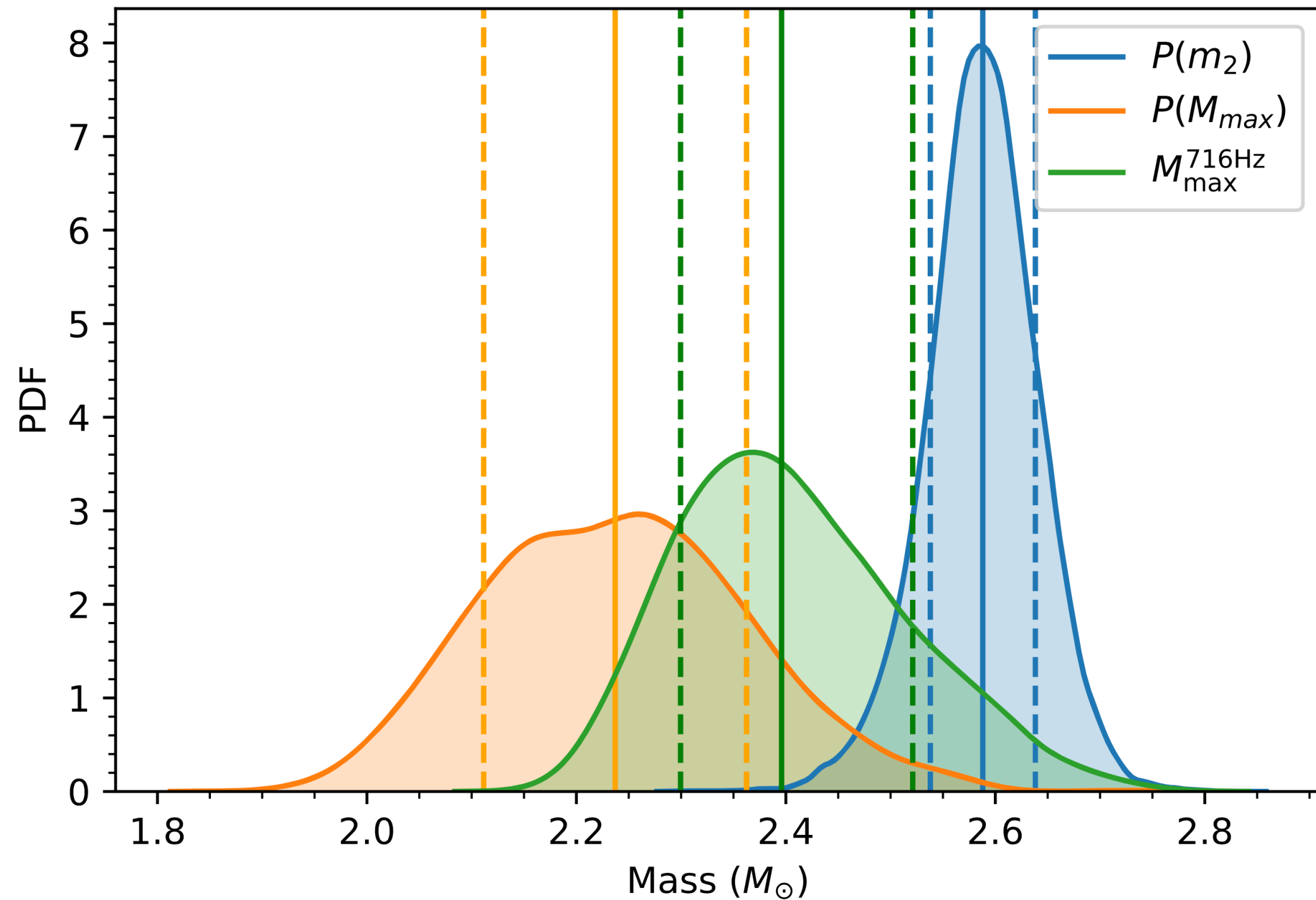


PART C.

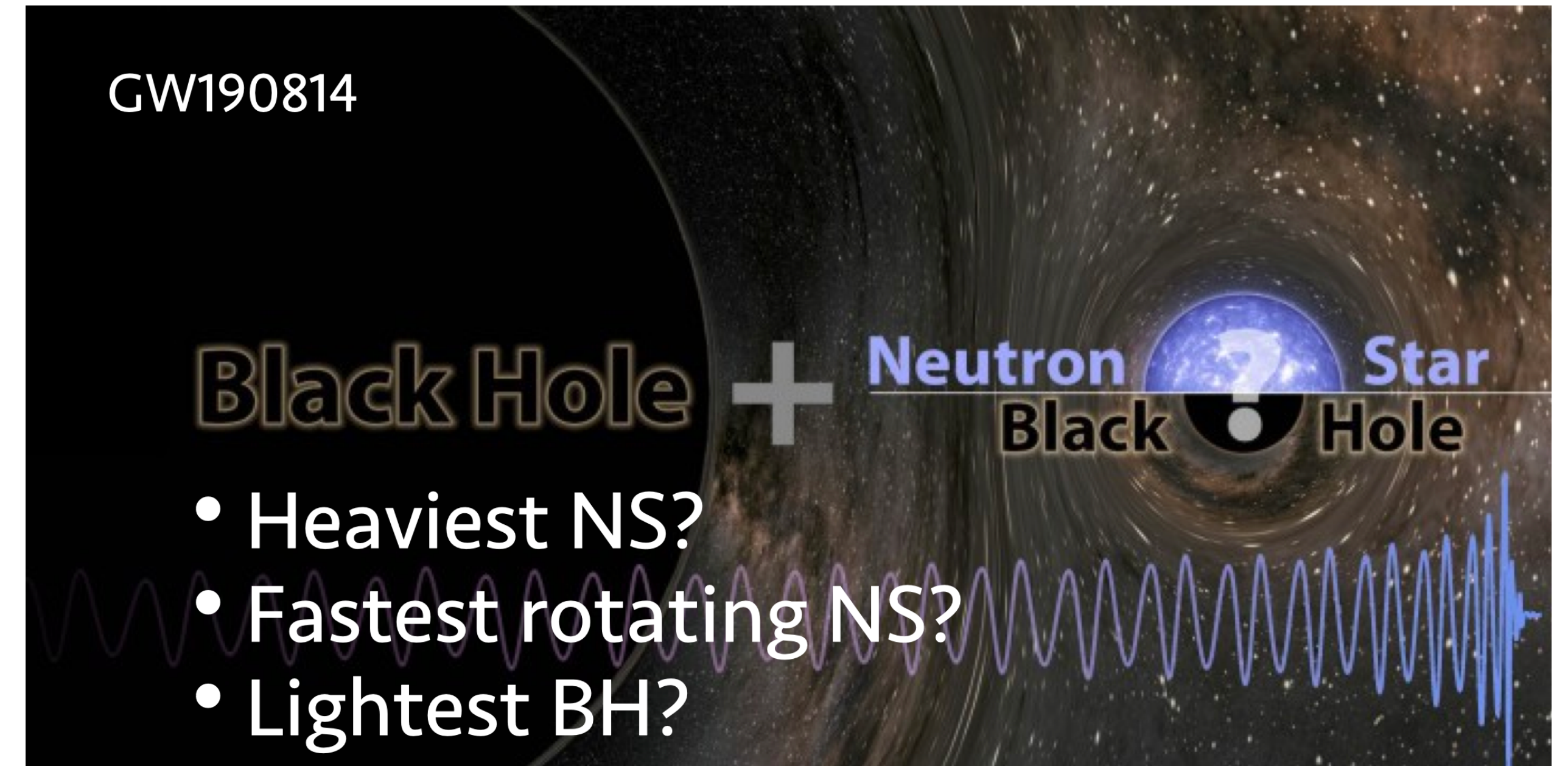
**NEUTRON STAR MODELS IN ALTERNATIVE
THEORIES OF GRAVITY**

HIGH MASS NEUTRON STARS?

What was the nature of the lighter component in GW190814?

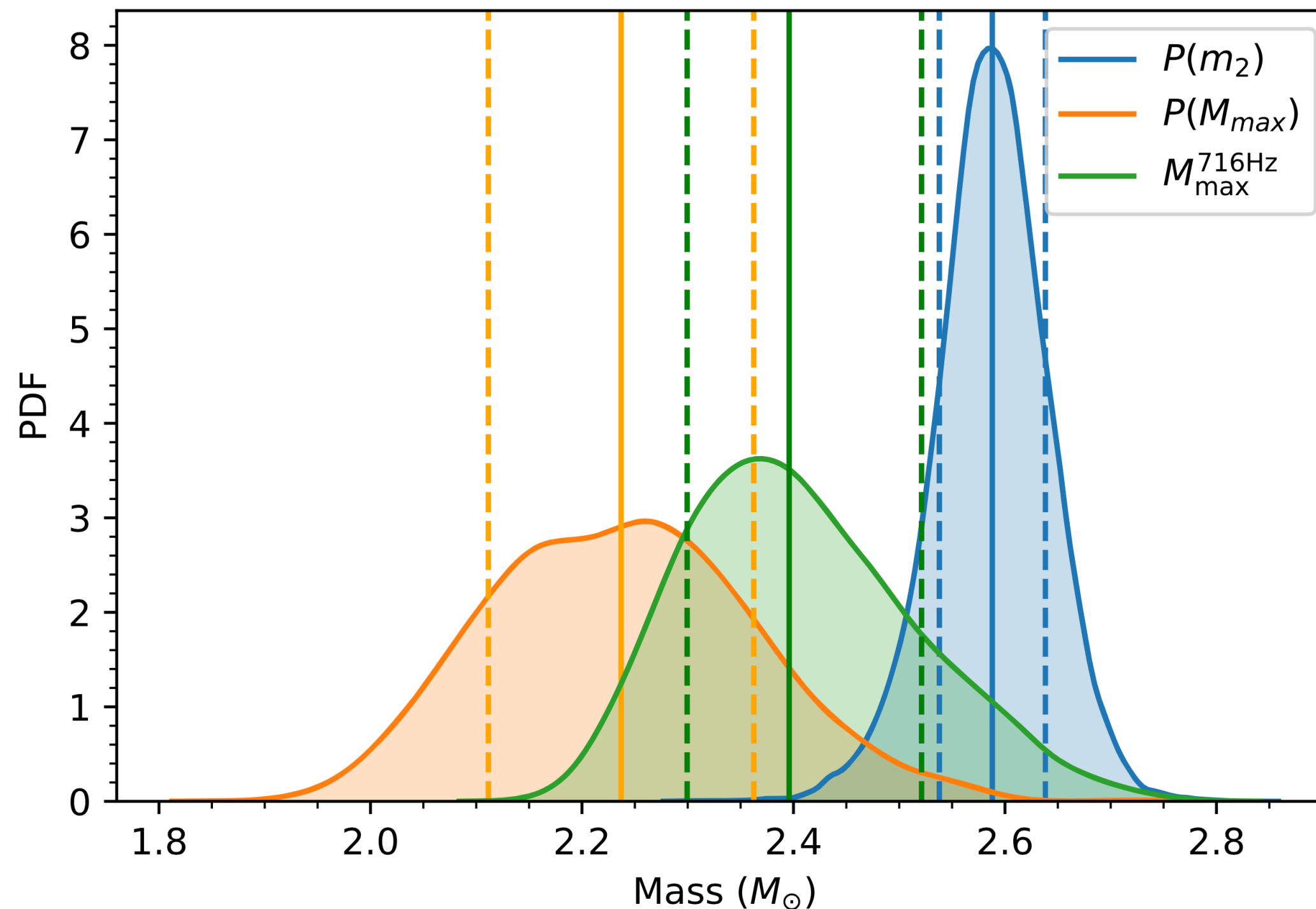


Biswas, Nandi, Char, Bose, Stergioulas (2021)

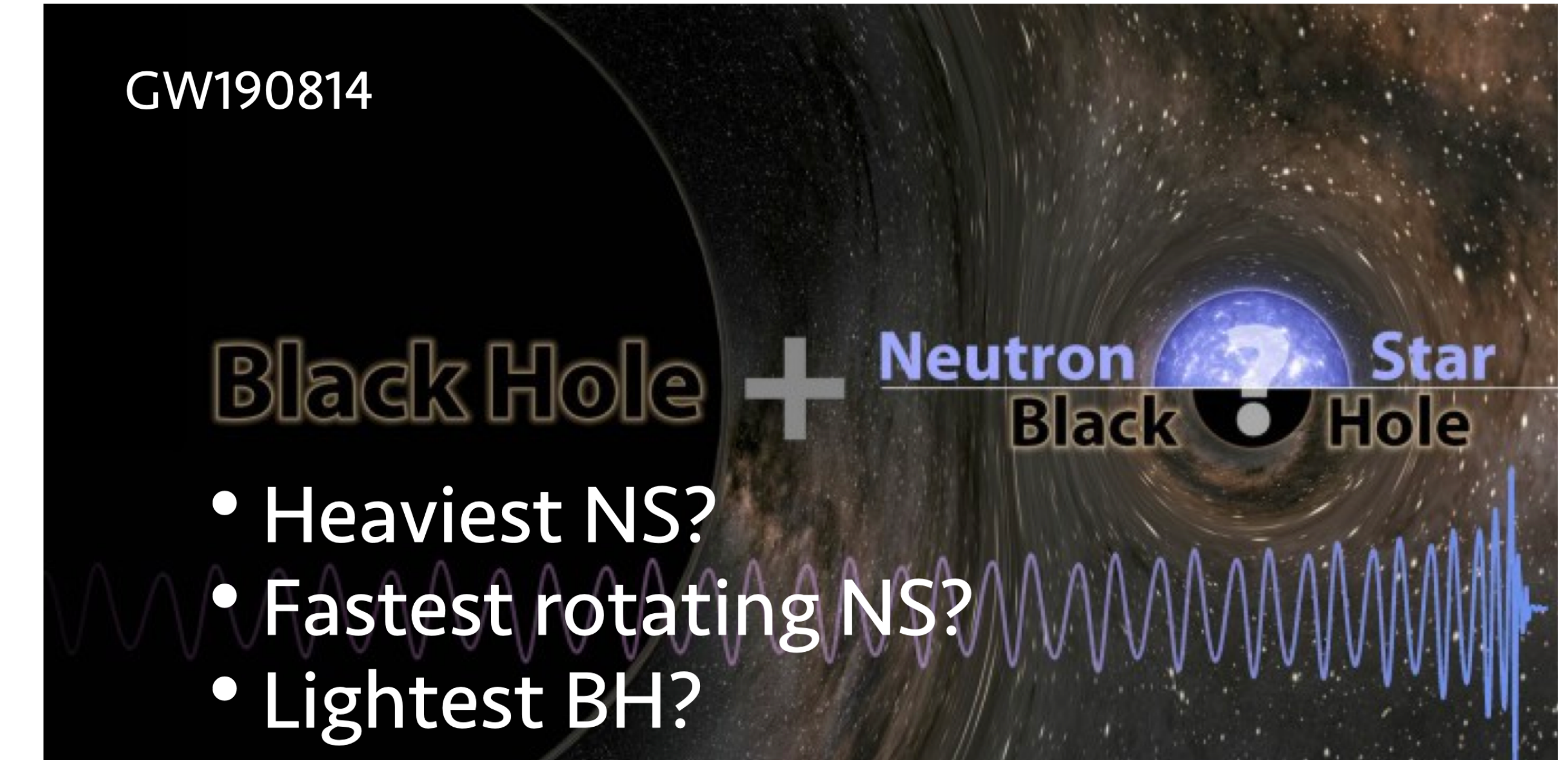


HIGH MASS NEUTRON STARS?

What was the nature of the lighter component in GW190814?



Biswas, Nandi, Char, Bose, Stergioulas (2021)



Another possibility: if the correct theory of gravity is not GR, then heavier NS might exist!

How can this degeneracy be resolved?

NS IN 4D EINSTEIN-GAUSS-BONNET GRAVITY

We consider the action

$$S = \frac{1}{2\kappa} \int d^4x \sqrt{-g} \{ R + \alpha [\phi \mathcal{G} + 4G_{\mu\nu} \nabla^\mu \phi \nabla^\nu \phi - 4(\nabla \phi)^2 \square \phi + 2(\nabla \phi)^4] \} + S_m$$

where $\kappa = 8\pi G/c^4$, $\mathcal{G} = R^2 - 4R_{\mu\nu}R^{\mu\nu} + R_{\mu\nu\rho\sigma}R^{\mu\nu\rho\sigma}$ is the Gauss-Bonnet scalar and S_m is the matter Lagrangian.

This theory possesses an exact vacuum solution describing nonrotating, static black holes with line element

$$ds^2 = -h(r)dt^2 + \frac{dr^2}{f(r)} + r^2 d\Omega^2$$

where

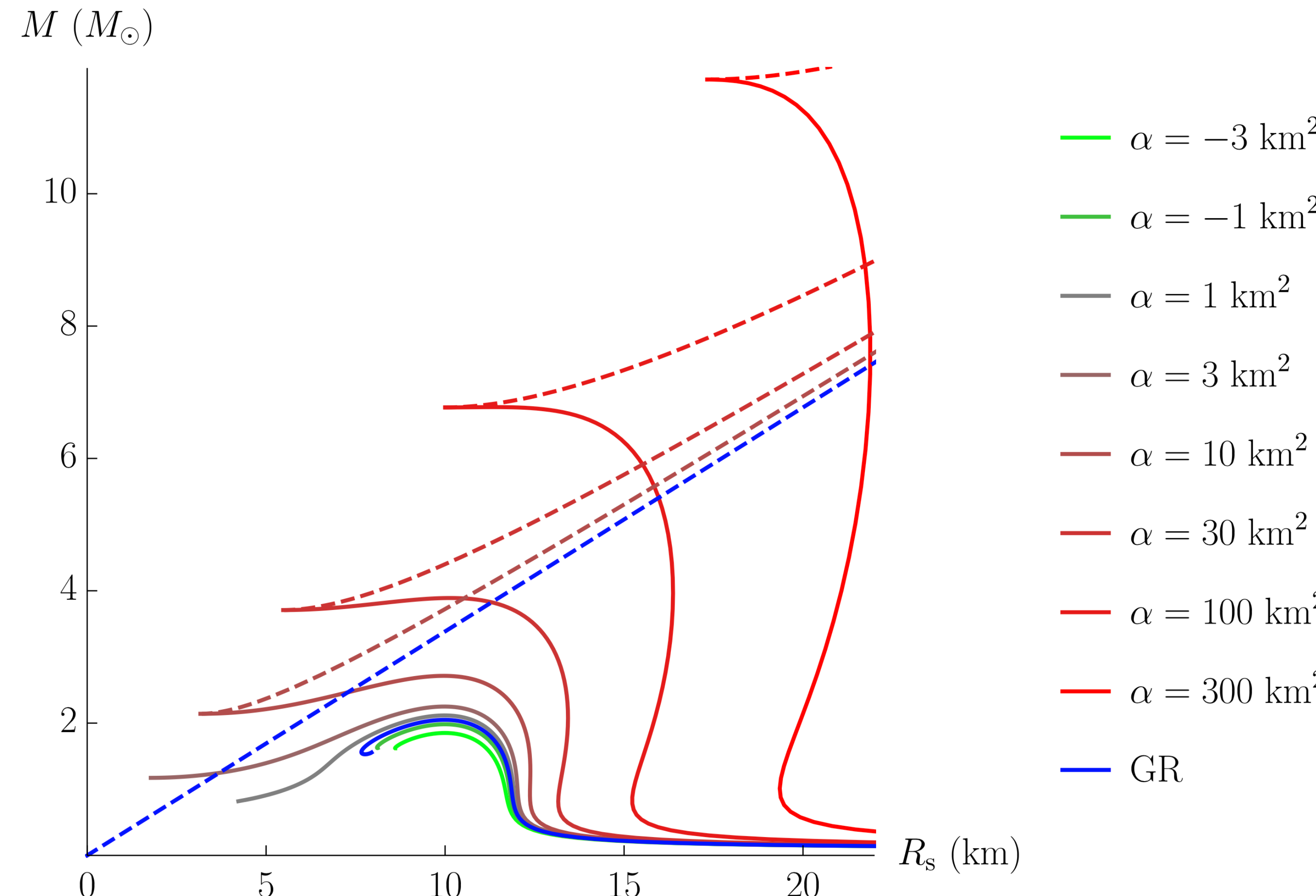
$$h(r) = f(r) = 1 + \frac{r^2}{2\alpha} \left(1 - \sqrt{1 + \frac{8\alpha M}{r^3}} \right) \quad (M \rightarrow \text{ADM mass})$$

and the shift-symmetric scalar field is

$$\phi(r) = \int dr \frac{\sqrt{f-1}}{r\sqrt{f}}$$

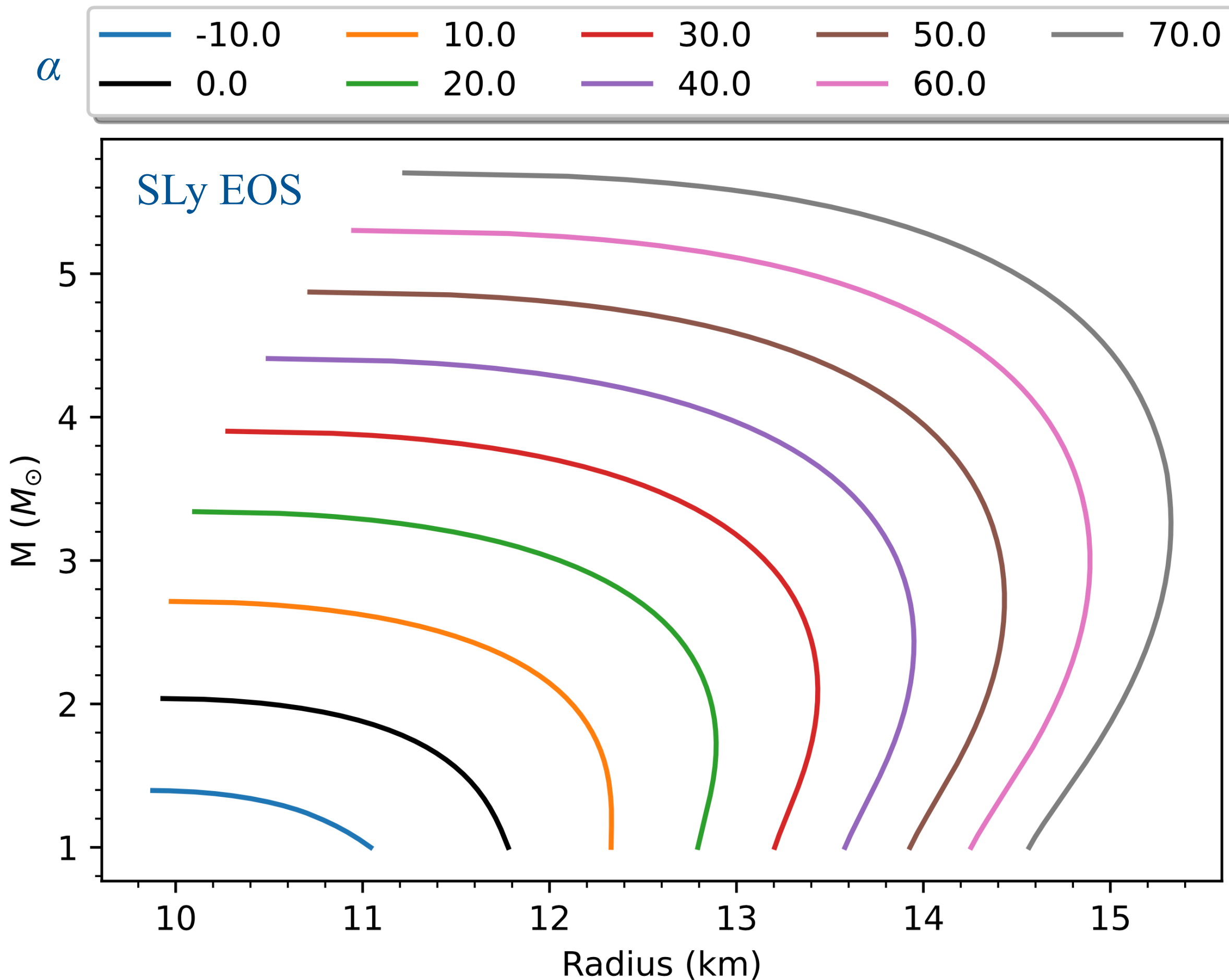
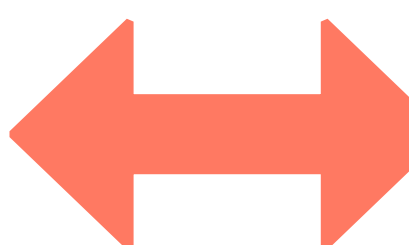
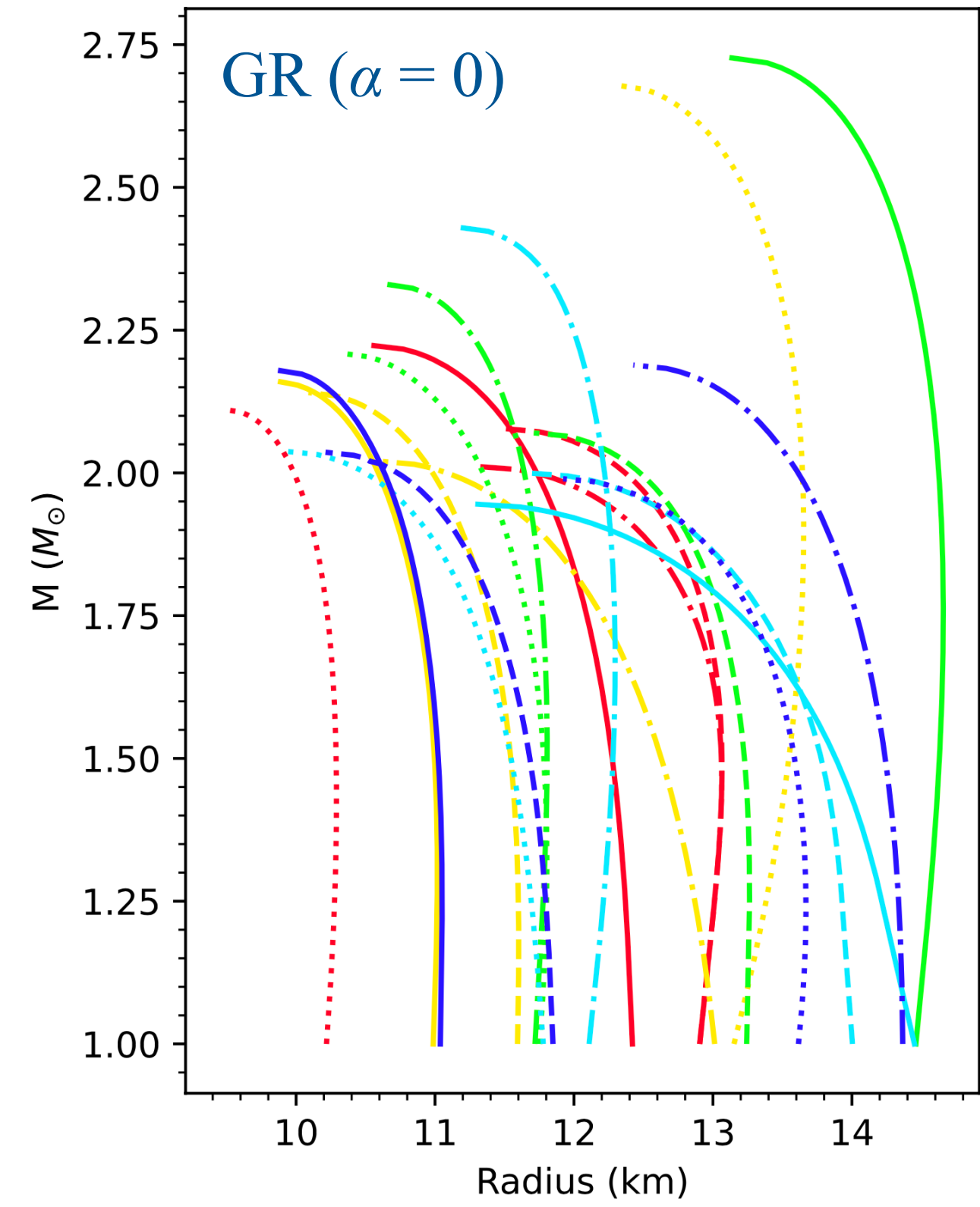
SEQUENCES OF EQUILIBRIUM MODELS

For the **SLy EOS**, we show representative cases of sequences of NS equilibrium models (solid lines) and BHs (dashed lines). For $\alpha > 0$, the NS solutions merge with the minimum mass BH solution.



EOS-GRAVITY DEGENERACY

In this theory, constructing equilibrium sequences for the same EOS, but different α , mimics the effect of using different EOS in GR.



Need to use a large number of observations to break the degeneracy!

ANN SURROGATE MODELS FOR NUMERICAL SOLUTIONS

EOS collection

Name	Number #
APR	1
BHBLP	2
DD2	3
eosAU	4
eosUU	5
BSk20	6
LS220	7
LS375	8
GS1	9
GS2	10
APR3 (PP)	11
ENG (PP)	12
GNH3 (PP)	13
H4 (PP)	14
MPA1 (PP)	15
SLy4 (PP)	16
WFF2 (PP)	17
SFHo	18
TM1	19
TMA	20

Surrogate models

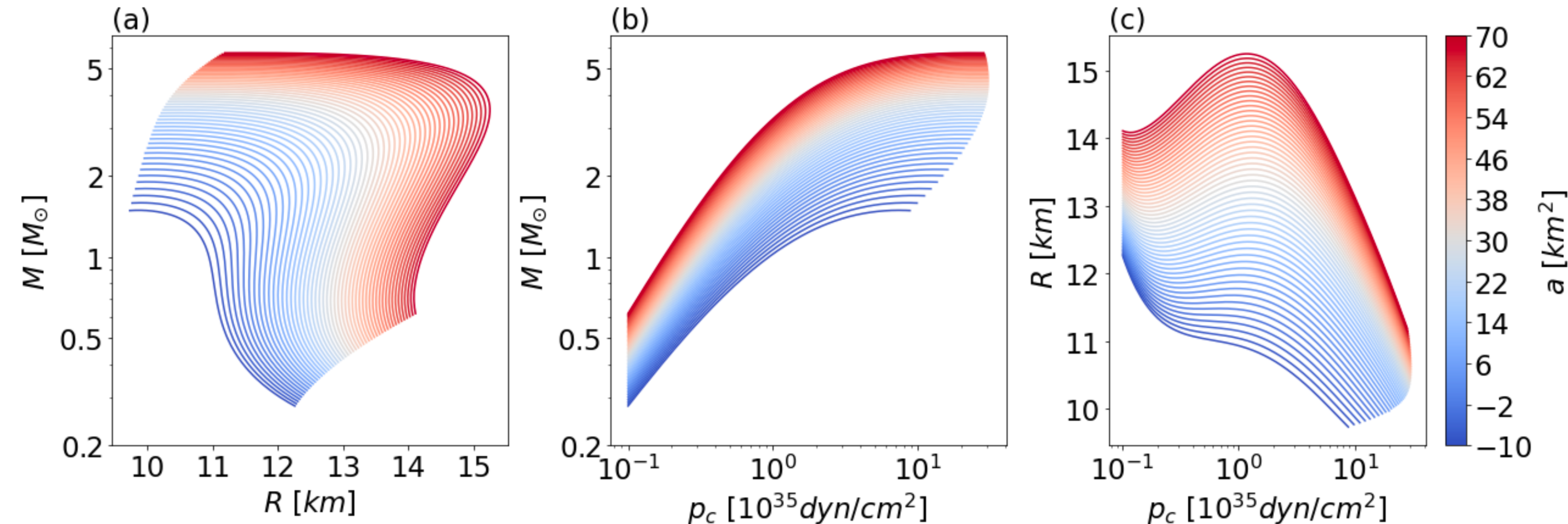
$$f_1(\text{EoS}; \alpha, p_c) \rightarrow (M, R)$$

$$f_2(\text{EoS}; \alpha, M) \rightarrow R$$

Network architecture for each EOS

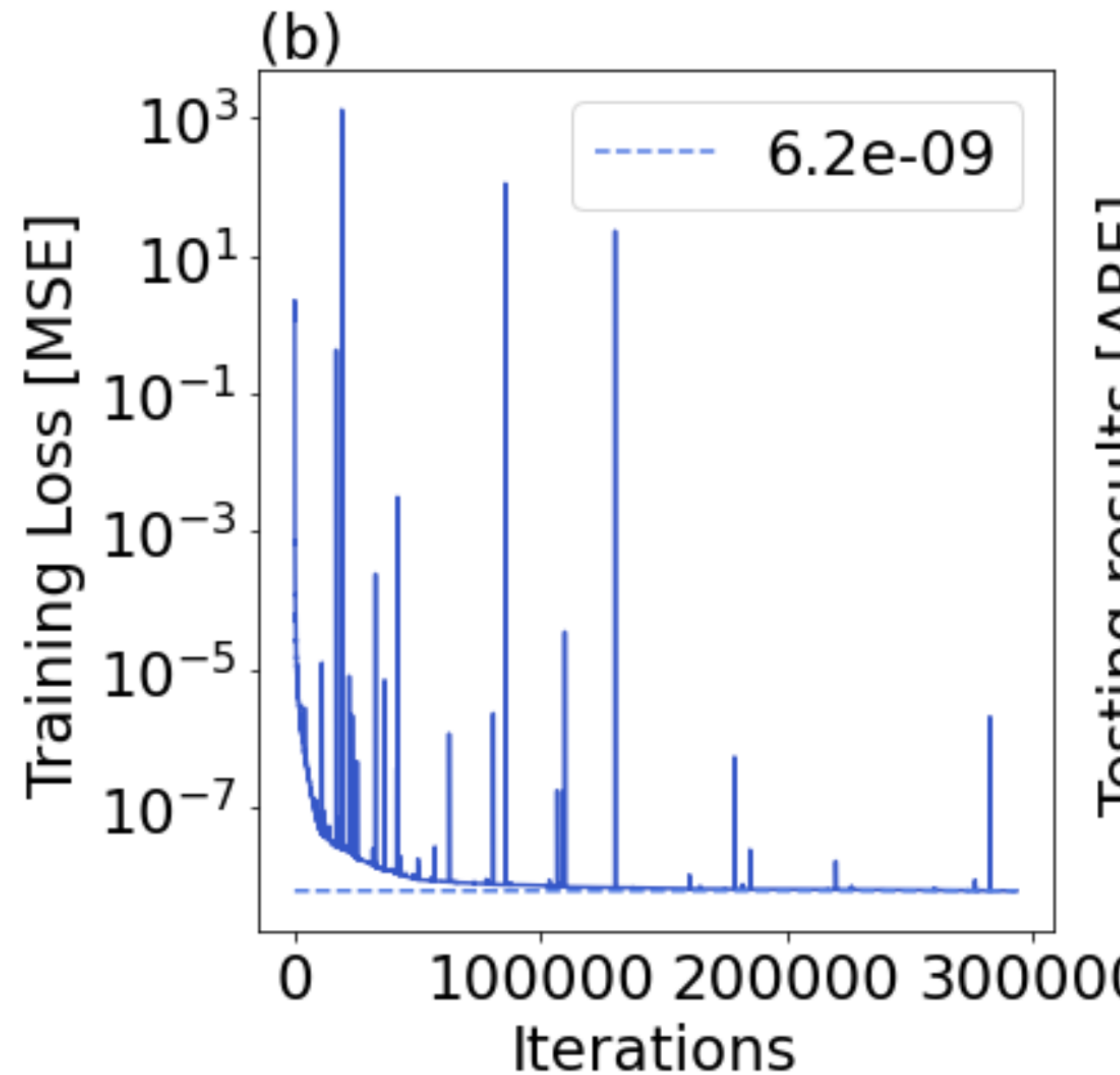
Layer	Type f_1	Type f_2
Input layer	(α, p_c)	(α, M)
Hidden layer 1	25-tanh	25-tanh
Hidden layer 2	35-relu	35-relu
Hidden layer 3	25-tanh	25-tanh
Output layer	(M, R)	R

Training set for each EOS: $200 (p_c) \times 51 (\alpha) = 10200$ equilibrium models

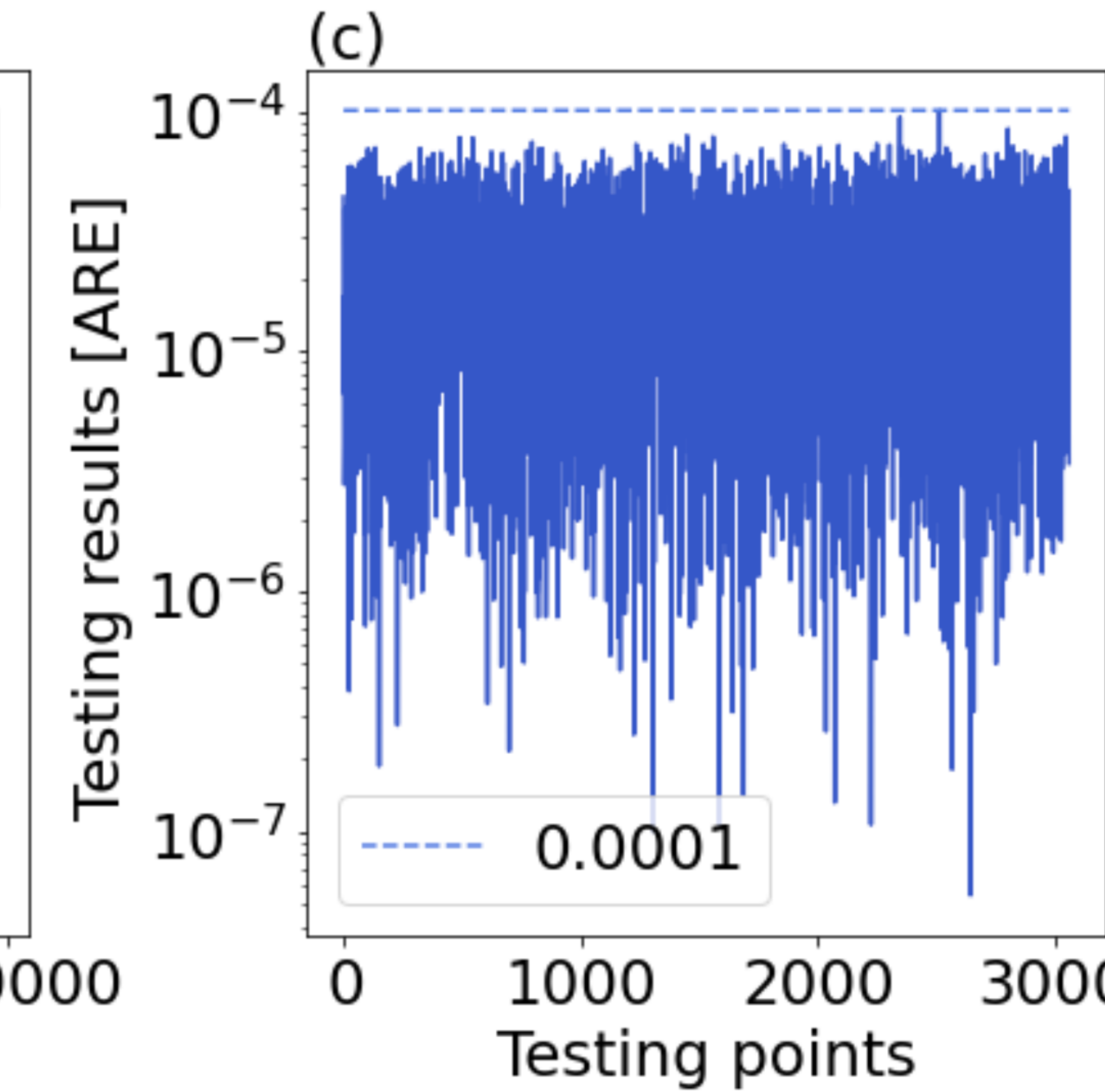


ACCURACY OF f_1 ANN SURROGATE MODEL FOR EOS BSk20

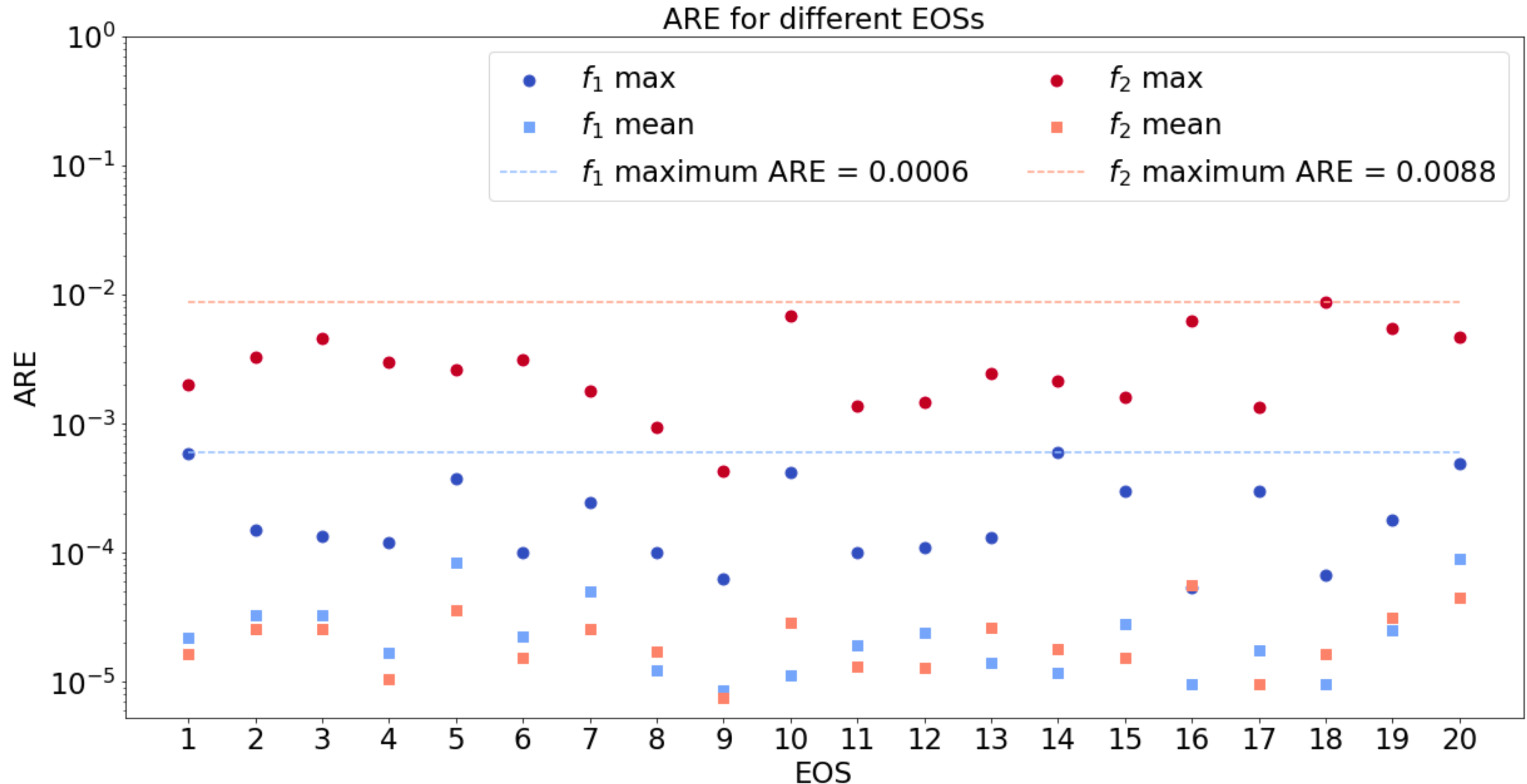
Loss function:
Mean Square Error (MSE)



Accuracy test:
Absolute Relative Error

$$\text{ARE}_i = \frac{1}{m} \sum_{j=1}^m \left| \frac{Y_i^j - Y_{i,\text{true}}^j}{Y_{i,\text{true}}^j} \right|$$


ACCURACY OF ANN SURROGATE MODELS FOR ALL EOS



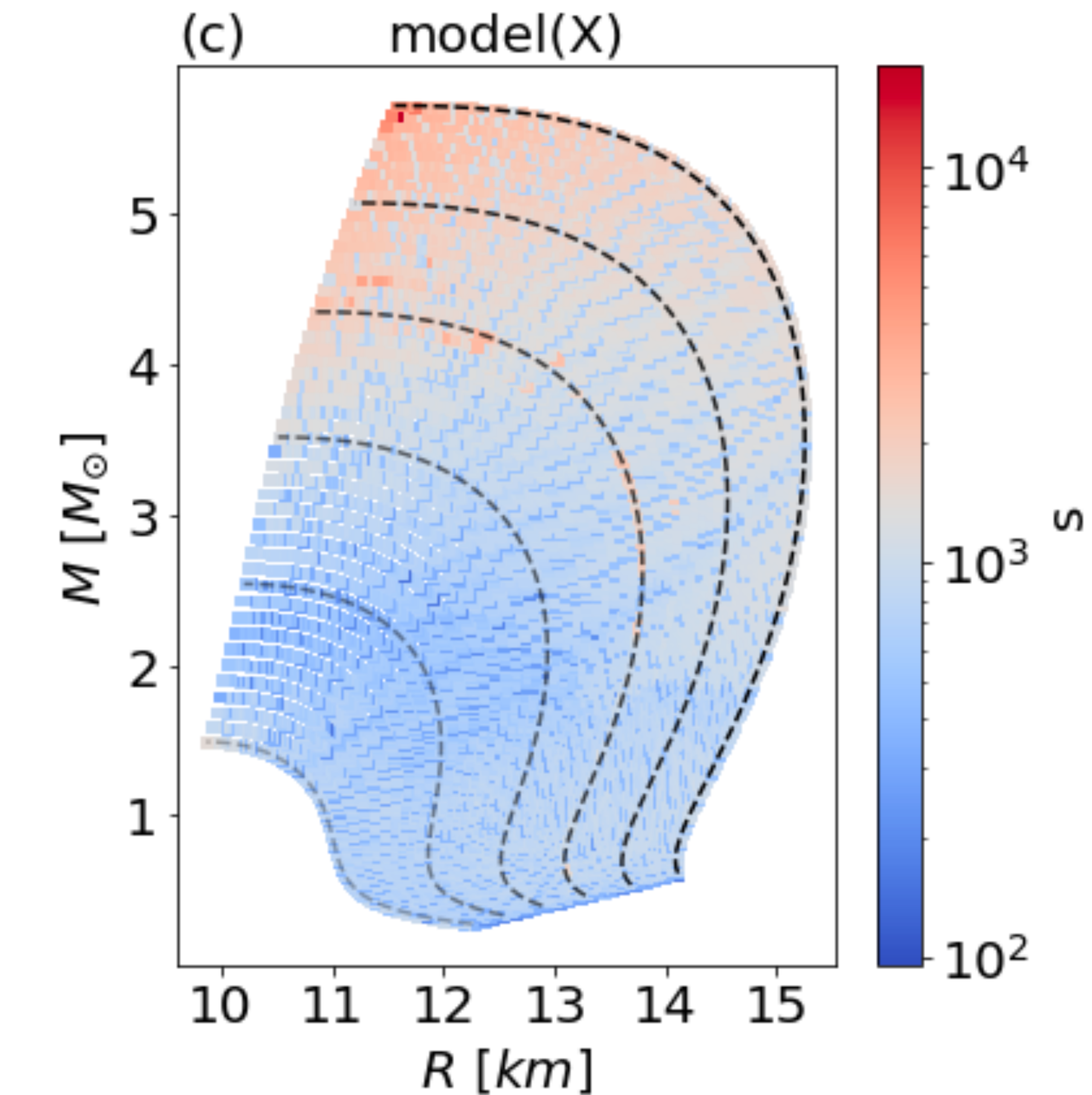
SPEED-UP ACHIEVED WITH THE ANN SURROGATE MODELS

Speed-up of ANN surrogate model compared to original numerical code

$$s = \frac{\Delta t_{\text{ANN}}}{\Delta t_{\text{num}}}$$

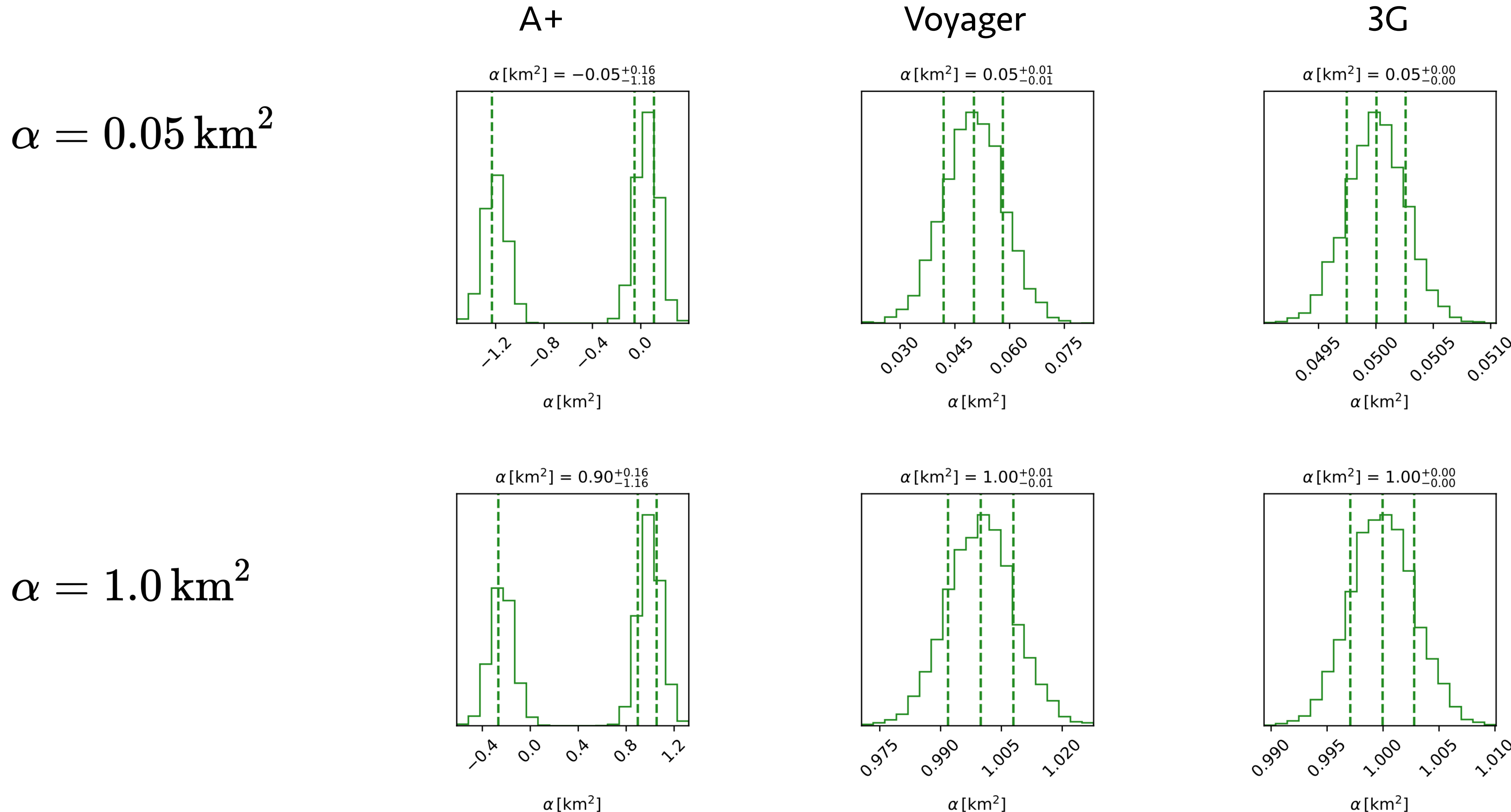
Numerical code run time:	(Mean)	(Min)	(Max)
	1003.5 ms	147.96 ms	18122.4 ms
Output method	Speed Up (Mean)	Speed Up (Minimum)	Speed Up (Maximum)
model.predict(X)	25.12	0.97	464.56
model(X)	921.9	95.6	18102.1
model.predict(\mathbf{X})	31295.5	4614.5	565157.2

The achieved speed-up allows for millions of MCMC calls in a Bayesian inference computation with minimal overhead.

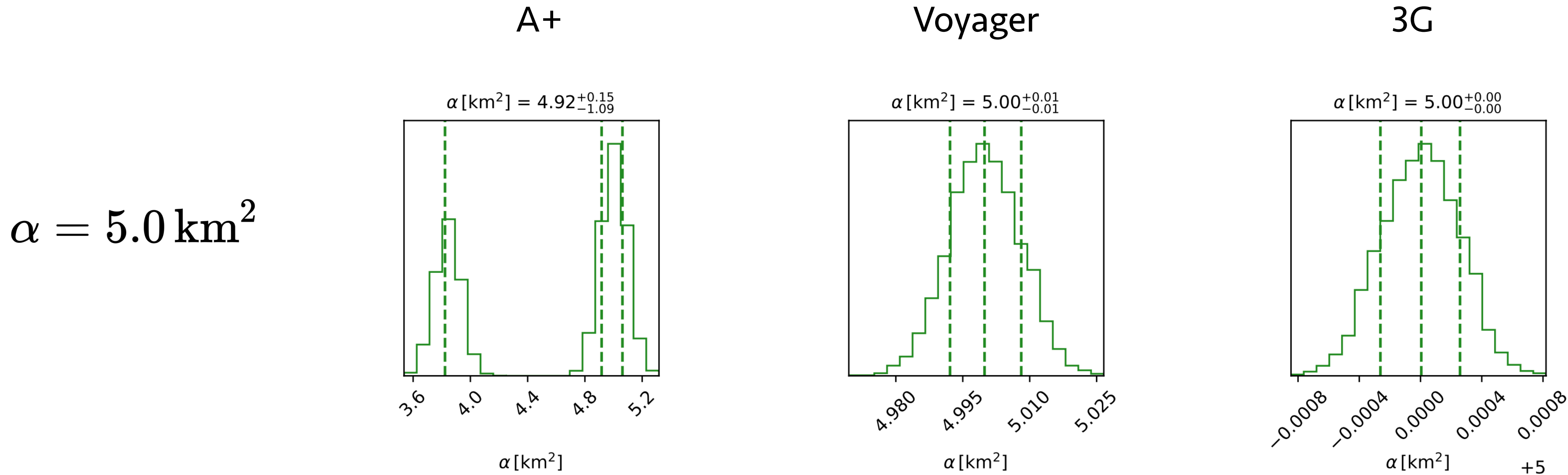


RECOVERY OF INJECTED α VALUES

Hierarchical Bayesian Inference using astrophysical constraints for a set of 20 EOS:



RECOVERY OF INJECTED α VALUES



A+ : for an injection of $\alpha = 5 \text{ km}^2$, the GR value of $\alpha = 0$ is excluded at the 3σ level.

Voyager/3G : even departures from GR at the $\alpha = 0.05 \text{ km}^2$ level are accurately recovered.

THANK YOU FOR YOUR ATTENTION

SEARCH IN O3 DATA WITH ARESGW

Total number of BBH events previously found by GWTC+OGC+IAS+pycbc_KDE inside training range = **43**

We also find **8 new candidate events** $p_{\text{astro}} > 0.5$.

AresGW detects **42 out of the total of 51** events
(*most sensitive pipeline in this mass range*)

TABLE III: Performance of AresGW in comparison to the GWTC, OGC, IAS and pycbc_KDE [15] algorithms on all 51 candidate events (43 previously published plus 8 new events detected by AresGW) that are within the effective training range.

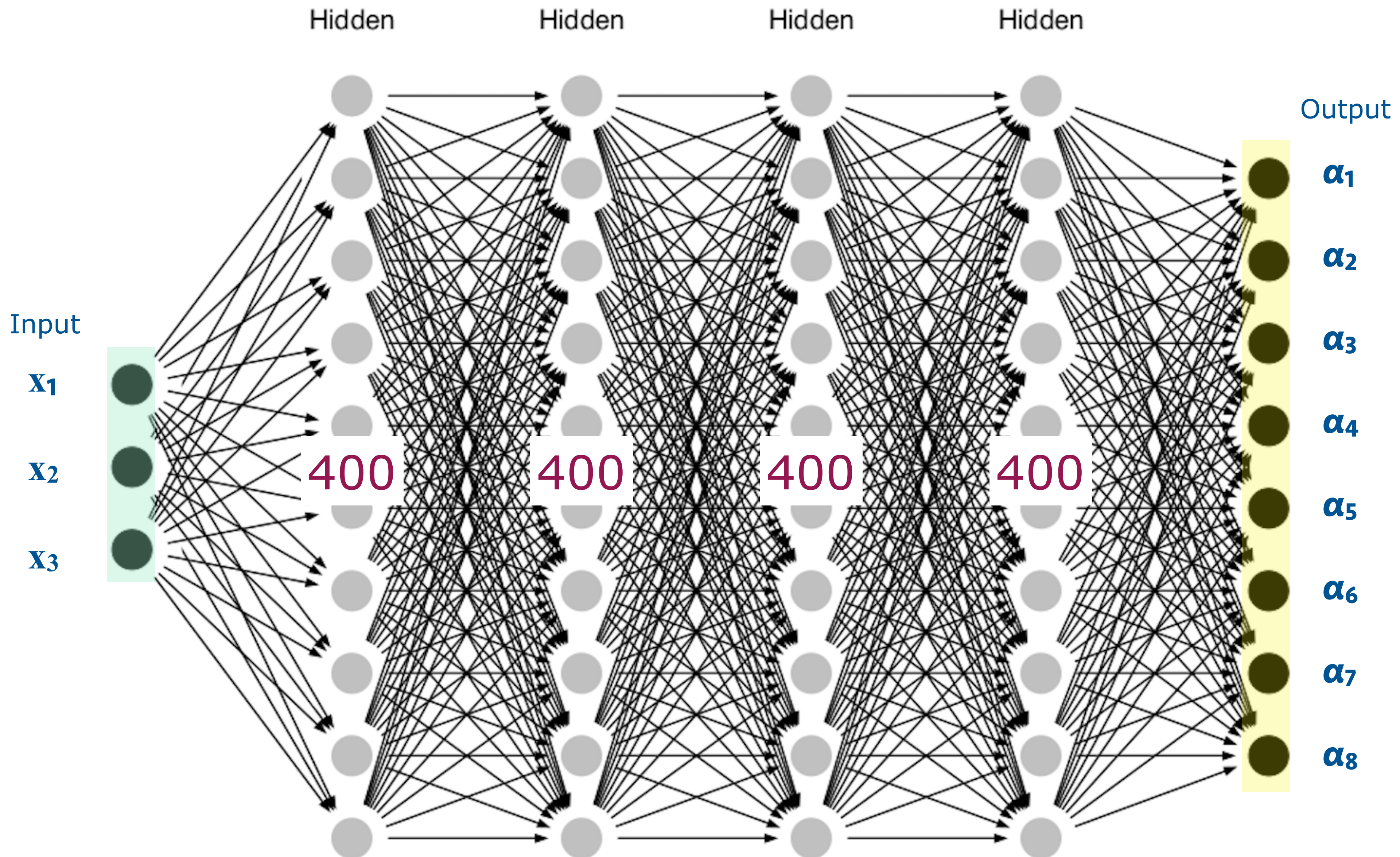
cwb	pycbc_broad	mbta	gstlal	pycbc_KDE	pycbc_bbh	IAS_a	IAS_b	OGC	AresGW
7	20	27	27	29	31	34	36	37	42

PARAMETERS OF NEW GW DETECTIONS WITH AresGW

TABLE VIII: Parameter estimation for the new AresGW candidate events.

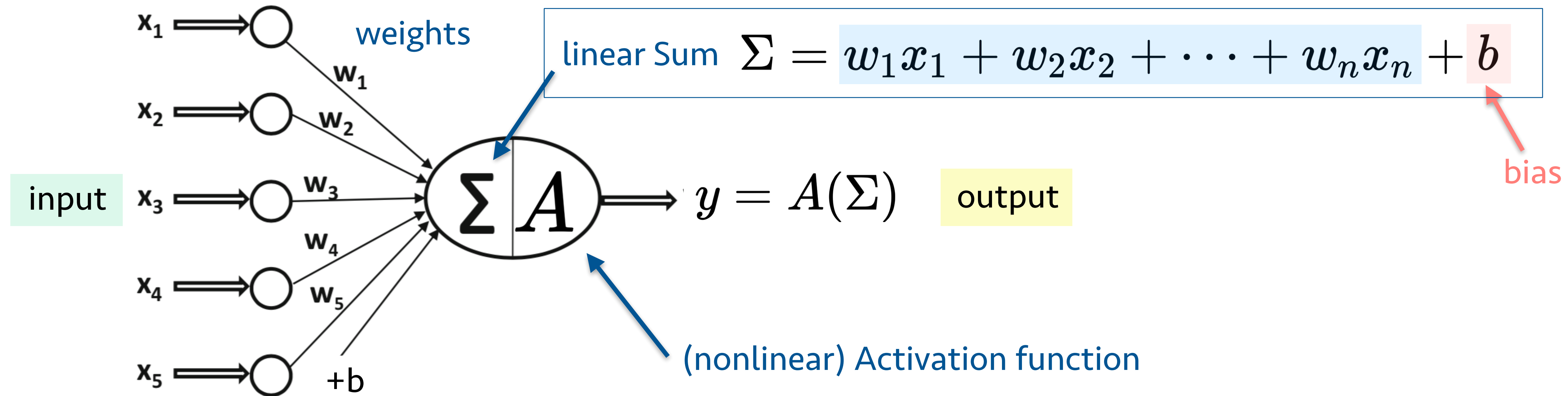
#	Event Name	\mathcal{M} (M_{\odot})	q	m_1 (M_{\odot})	m_2 (M_{\odot})	D_L (Mpc)	χ_{eff}	SNR (H1)	SNR (L1)	SNR $\hat{\rho}$ (network)
1	GW190511-125545	$28.95^{+9.45}_{-6.86}$	$0.72^{+0.25}_{-0.36}$	$40.7^{+16.2}_{-10.5}$	$28.2^{+11.6}_{-11.2}$	3707^{+3471}_{-2173}	$0.23^{+0.25}_{-0.29}$	2.29	7.34	7.29
2	GW190614-134749	$25.97^{+16.59}_{-6.20}$	$0.70^{+0.27}_{-0.36}$	$37.0^{+31.8}_{-10.7}$	$25.2^{+15.2}_{-9.7}$	6551^{+9562}_{-3558}	$0.05^{+0.34}_{-0.34}$	3.51	6.08	7.02
3	GW190607-083827	$30.48^{+7.21}_{-4.68}$	$0.78^{+0.19}_{-0.29}$	$40.5^{+12.0}_{-7.6}$	$31.0^{+9.1}_{-8.2}$	4928^{+2725}_{-2435}	$0.01^{+0.26}_{-0.30}$	4.04	7.29	8.33
4	GW190904-104631	$21.24^{+5.76}_{-4.40}$	$0.64^{+0.31}_{-0.33}$	$31.3^{+14.5}_{-8.5}$	$19.7^{+7.1}_{-7.2}$	5614^{+4441}_{-2864}	$0.05^{+0.30}_{-0.37}$	4.50	4.88	6.64
5	GW190523-085933	$23.82^{+10.24}_{-7.95}$	$0.49^{+0.45}_{-0.32}$	$41.7^{+19.3}_{-15.5}$	$19.4^{+14.6}_{-10.5}$	6091^{+6613}_{-3702}	$0.42^{+0.31}_{-0.45}$	3.48	5.14	6.02
6	GW200208-211609	$18.83^{+4.68}_{-3.18}$	$0.69^{+0.28}_{-0.40}$	$26.9^{+14.6}_{-6.3}$	$18.0^{+6.4}_{-6.9}$	3669^{+3413}_{-1985}	$0.01^{+0.37}_{-0.37}$	4.75	6.22	7.83
7	GW190705-164632	$27.21^{+7.34}_{-5.24}$	$0.52^{+0.41}_{-0.32}$	$44.7^{+24.8}_{-12.8}$	$23.0^{+11.7}_{-9.8}$	5692^{+4030}_{-2863}	$0.29^{+0.26}_{-0.34}$	4.42	6.88	8.11
8	GW190426-082124	$17.93^{+4.12}_{-3.42}$	$0.45^{+0.45}_{-0.28}$	$31.5^{+22.5}_{-11.3}$	$13.8^{+6.9}_{-5.2}$	3213^{+4555}_{-1573}	$-0.01^{+0.39}_{-0.50}$	5.15	4.46	6.41

ARTIFICIAL NEURAL NETWORKS



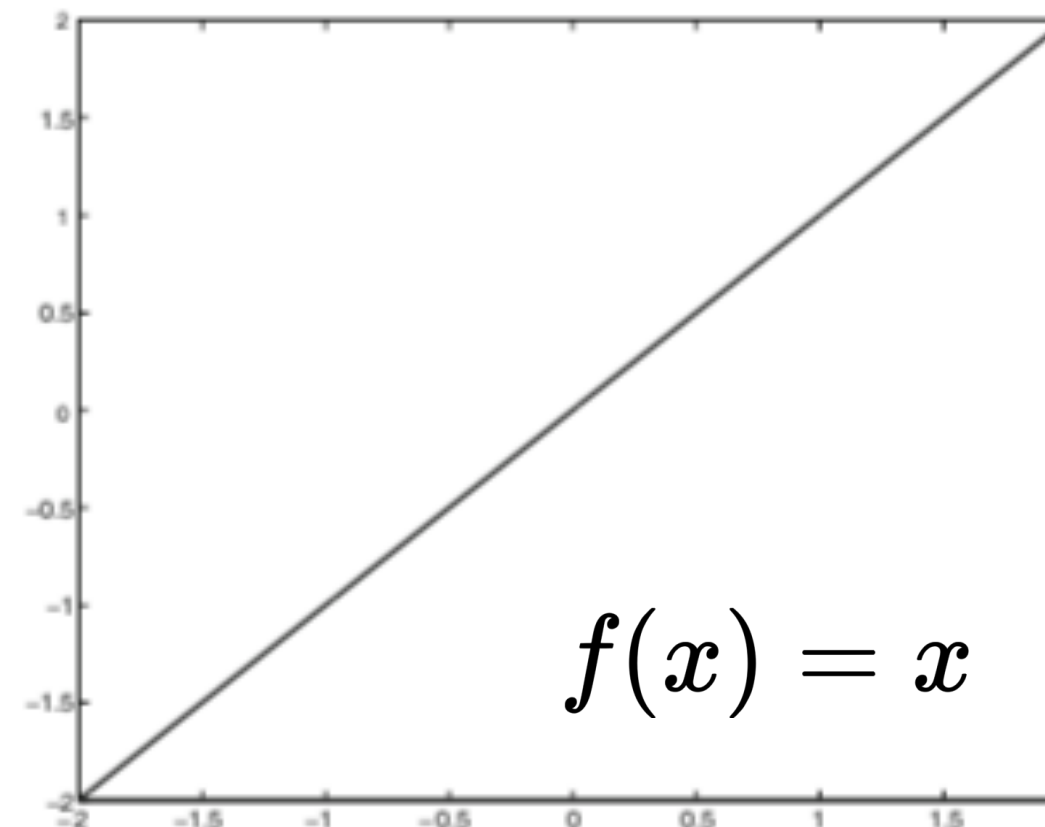
ARTIFICIAL NEURON

- Each neuron in the network maps several **input values** x_1, \dots, x_n to an **output value** y

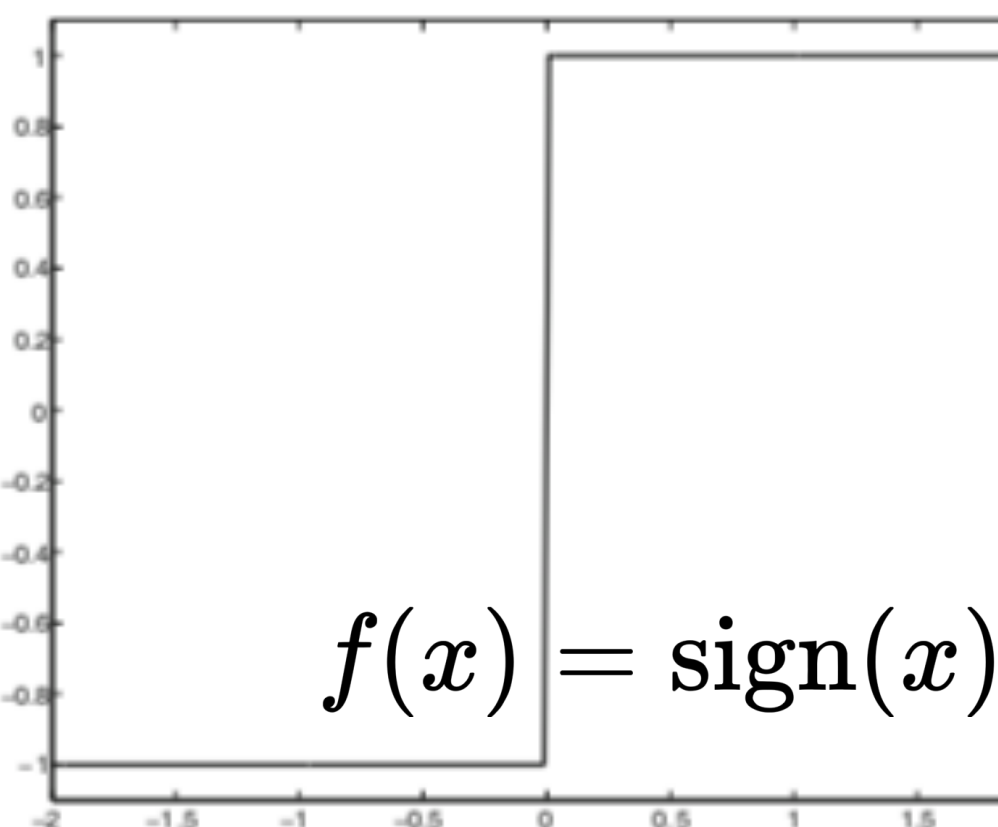


ACTIVATION FUNCTIONS

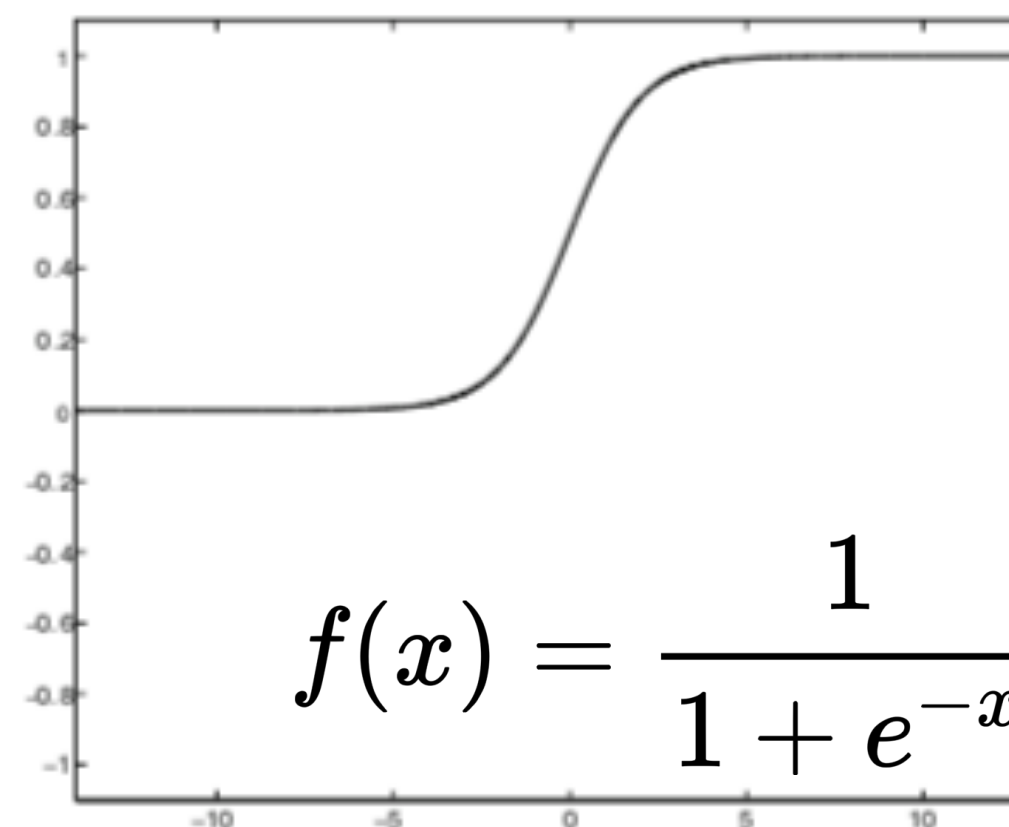
- Different common activation functions:



(a) Identity

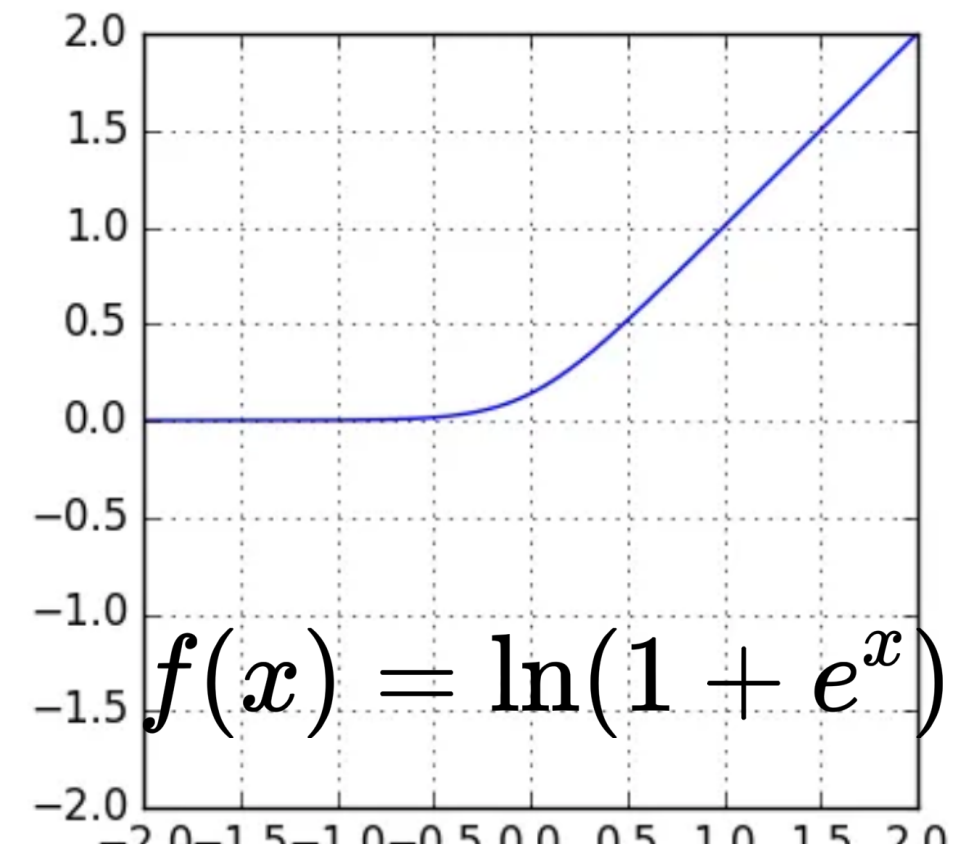


(b) Sign

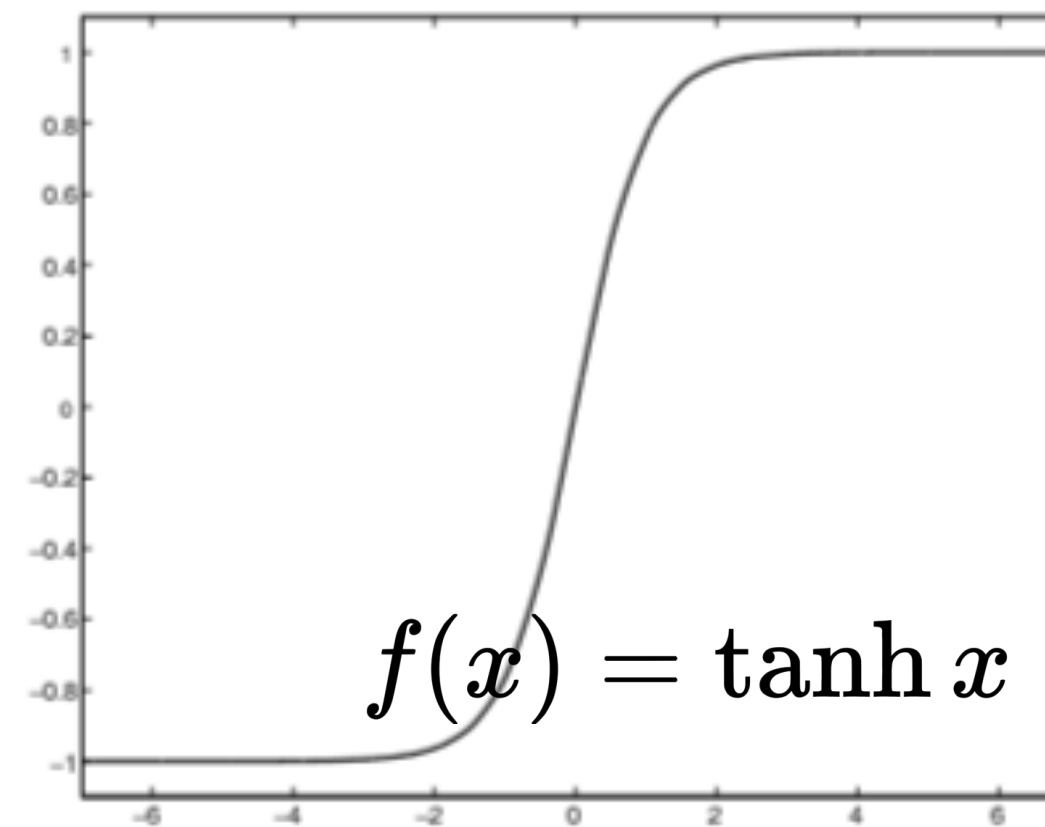


$$f(x) = \frac{1}{1 + e^{-x}}$$

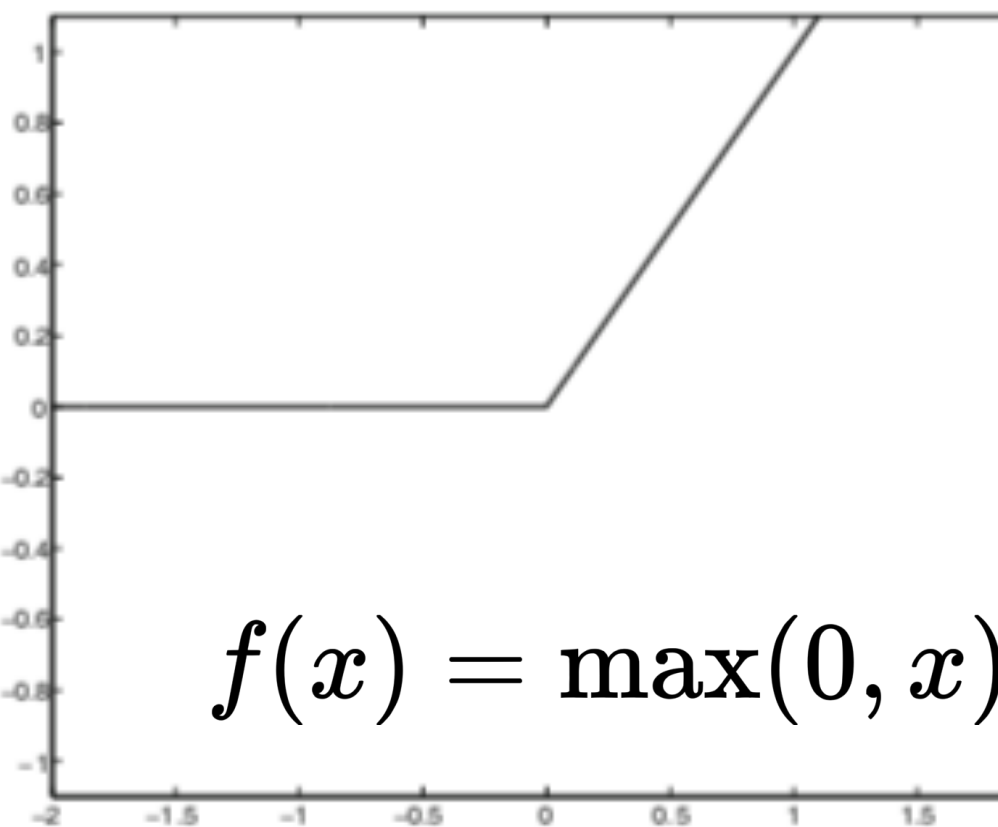
(c) Sigmoid (logistic function)



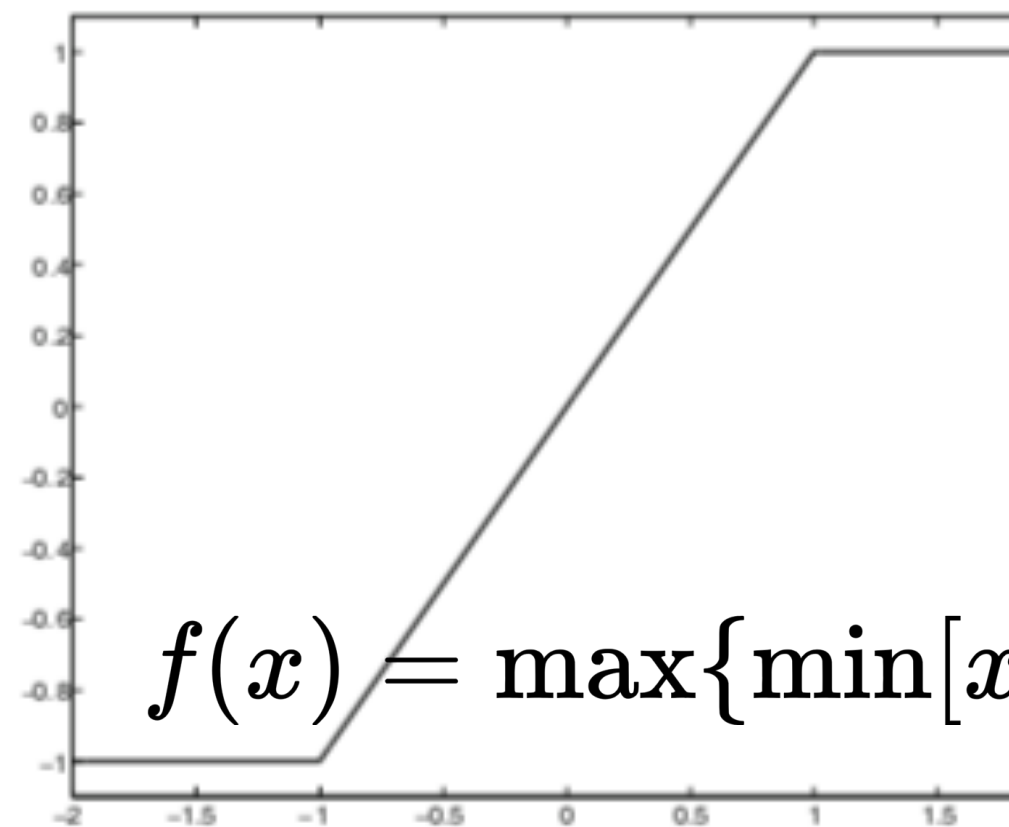
Softplus



(d) Tanh



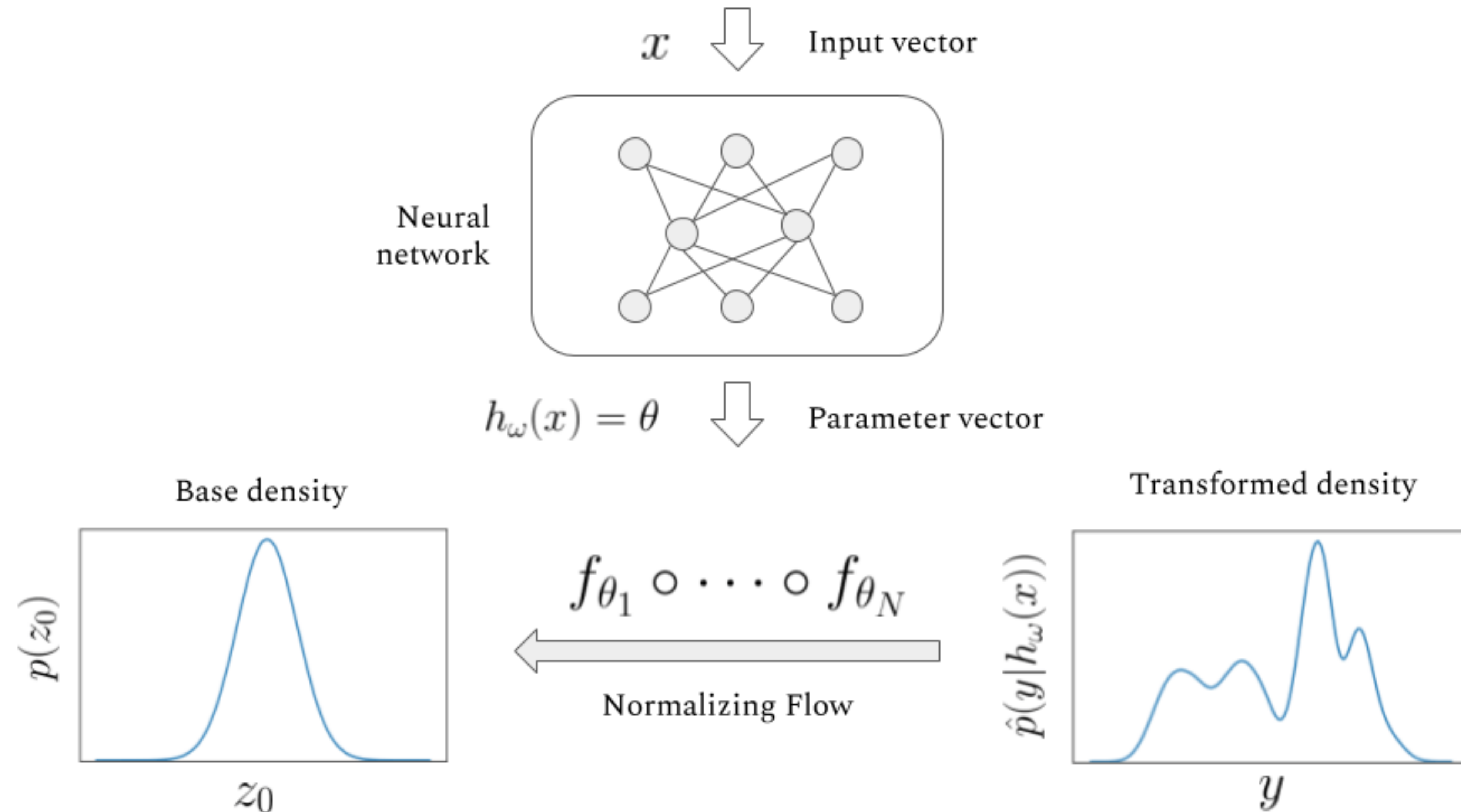
(e) ReLU



(f) Hard Tanh

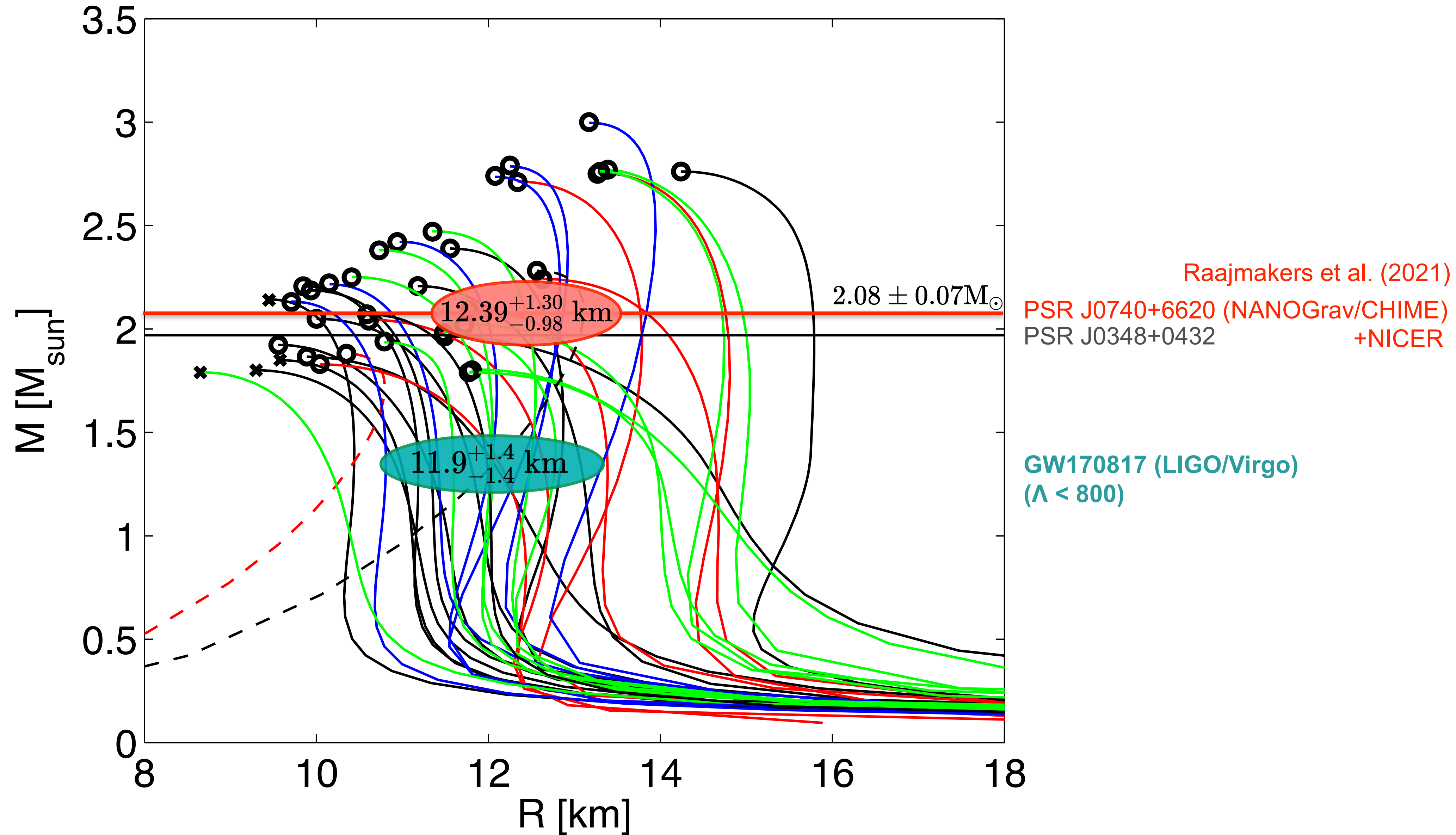
(Rectified Linear Unit)

NORMALIZING FLOWS



BACKUP SLIDES

CURRENT CONSTRAINTS ON MASS-RADIUS RELATION



ANN REGRESSION IN FREQUENCY DOMAIN

EOS	Waveforms	References	Component masses (in M_{\odot})
ALF2	10	Rezzolla and Takami [45] and CoRe v2 [27]	1.2, 1.225, 1.25, 1.275, 1.3, 1.325, 1.35, 1.3505, 1.375, 1.3755
APR4	7	Rezzolla and Takami [45]	1.2, 1.225, 1.25, 1.275, 1.3, 1.325, 1.35
BHBlp	4	CoRe v2 [27]	1.25, 1.3, 1.35, 1.4
BLh	4	CoRe v2 [27]	1.3, 1.3325, 1.364, 1.4
DD2	7	CoRe v2 [27]	1.2, 1.25, 1.3, 1.35, 1.364, 1.4, 1.5
ENG	1	CoRe v2 [27]	1.3495
GNH3	7	Rezzolla and Takami [45]	1.2, 1.225, 1.25, 1.275, 1.3, 1.325, 1.35
H4	13	Rezzolla and Takami [45] and CoRe v2 [27]	1.2, 1.225, 1.25, 1.275, 1.3, 1.325, 1.3495, 1.35, 1.3505, 1.3715, 1.3725, 1.3735, 1.3795
LS220	4	CoRe v2 [27]	1.2, 1.35, 1.364, 1.4
MPA1	8	Soultanis <i>et al.</i> [97]	1.2, 1.25, 1.3, 1.35, 1.4, 1.45, 1.5, 1.55
MS1	2	CoRe v2 [27]	1.3495, 1.351
MS1b	8	CoRe v2 [27]	1.35, 1.3505, 1.375, 1.3805, 1.381, 1.5, 1.6, 1.7
SFHo	2	CoRe v2 [27]	1.35, 1.364
SLy	10	Rezzolla and Takami [45] and CoRe v2 [27]	1.2, 1.225, 1.25, 1.275, 1.3, 1.325, 1.35, 1.351, 1.3575, 1.364

BAYESIAN PARAMETER ESTIMATION

Injected waveform

$$d(t) = h(t) + n(t)$$

Gaussian likelihood function

$$\mathcal{L}(d \mid \boldsymbol{\theta}) \propto \exp[-\langle d(t) - h(\boldsymbol{\theta}, t), d(t) - h(\boldsymbol{\theta}, t) \rangle]$$

where the inner product is

$$\langle h, g \rangle = 4\Re e \int_0^\infty \frac{\tilde{h}(f)\tilde{g}^*(f)}{S(f)} df$$

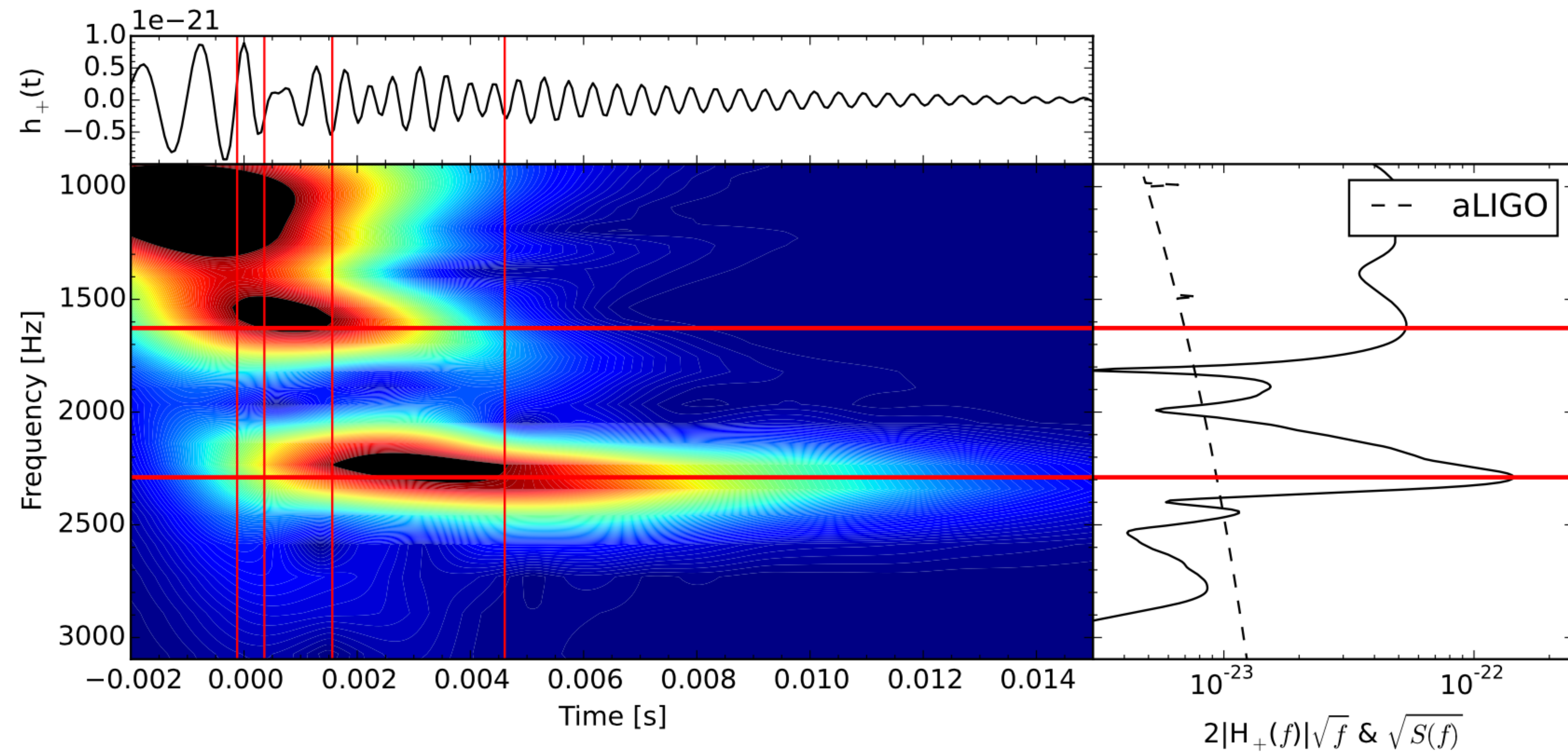
Fitting factor

$$\mathcal{F}(d(t), h(\boldsymbol{\theta}, t)) \equiv \frac{\langle d(t) \mid h(\boldsymbol{\theta}, t) \rangle}{\sqrt{\langle d(t) \mid d(t) \rangle \langle h(\boldsymbol{\theta}, t) \mid h(\boldsymbol{\theta}, t) \rangle}}$$

Optimal SNR

$$\rho_{\text{opt},i} = \langle h, h \rangle^{1/2} \quad \rho_{\text{opt}} = \left(\sum_{i \in \text{HLV}} \rho_{\text{opt},i}^2 \right)^{1/2}$$

POST-MERGER SPECTROGRAMS

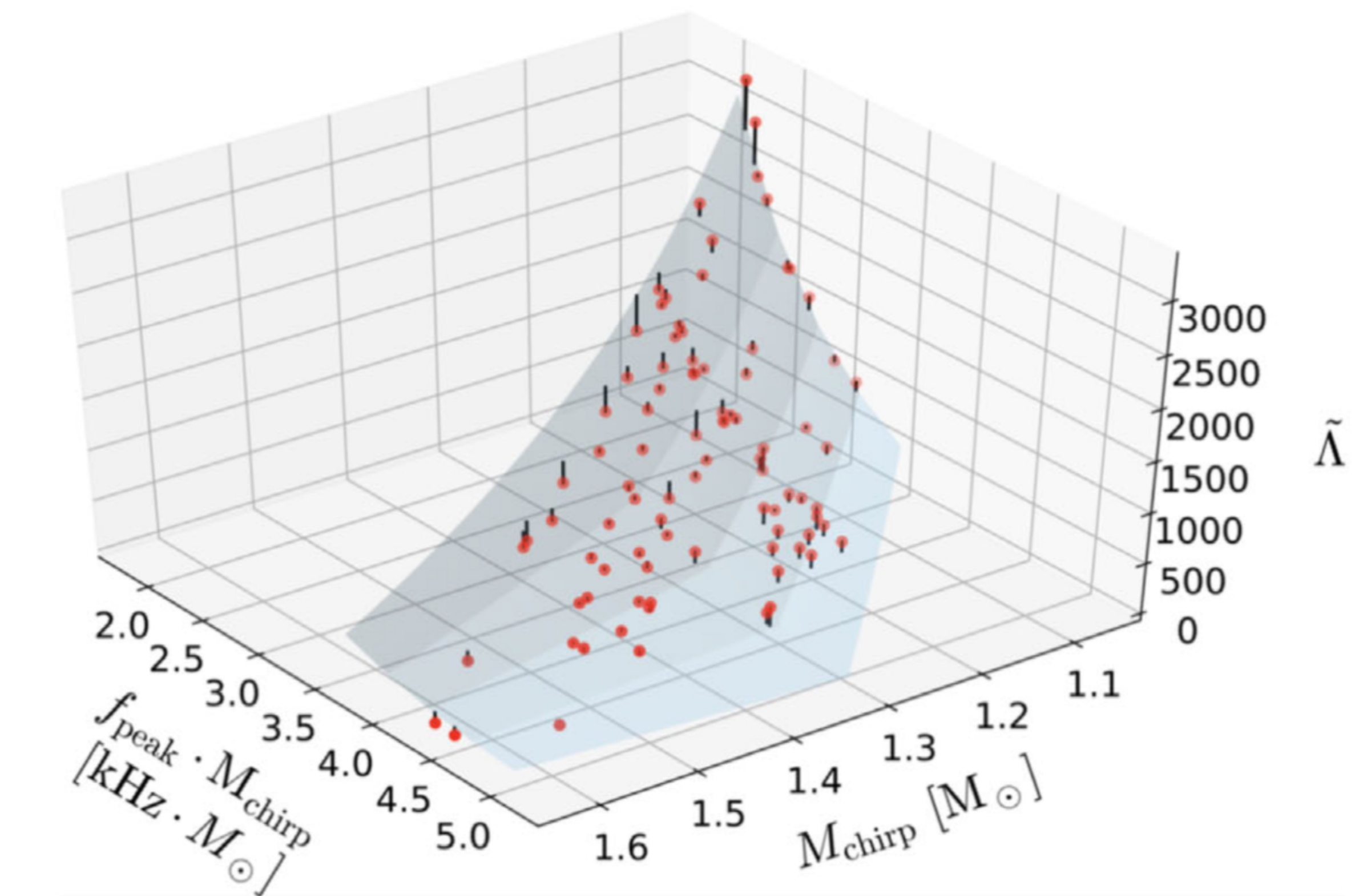
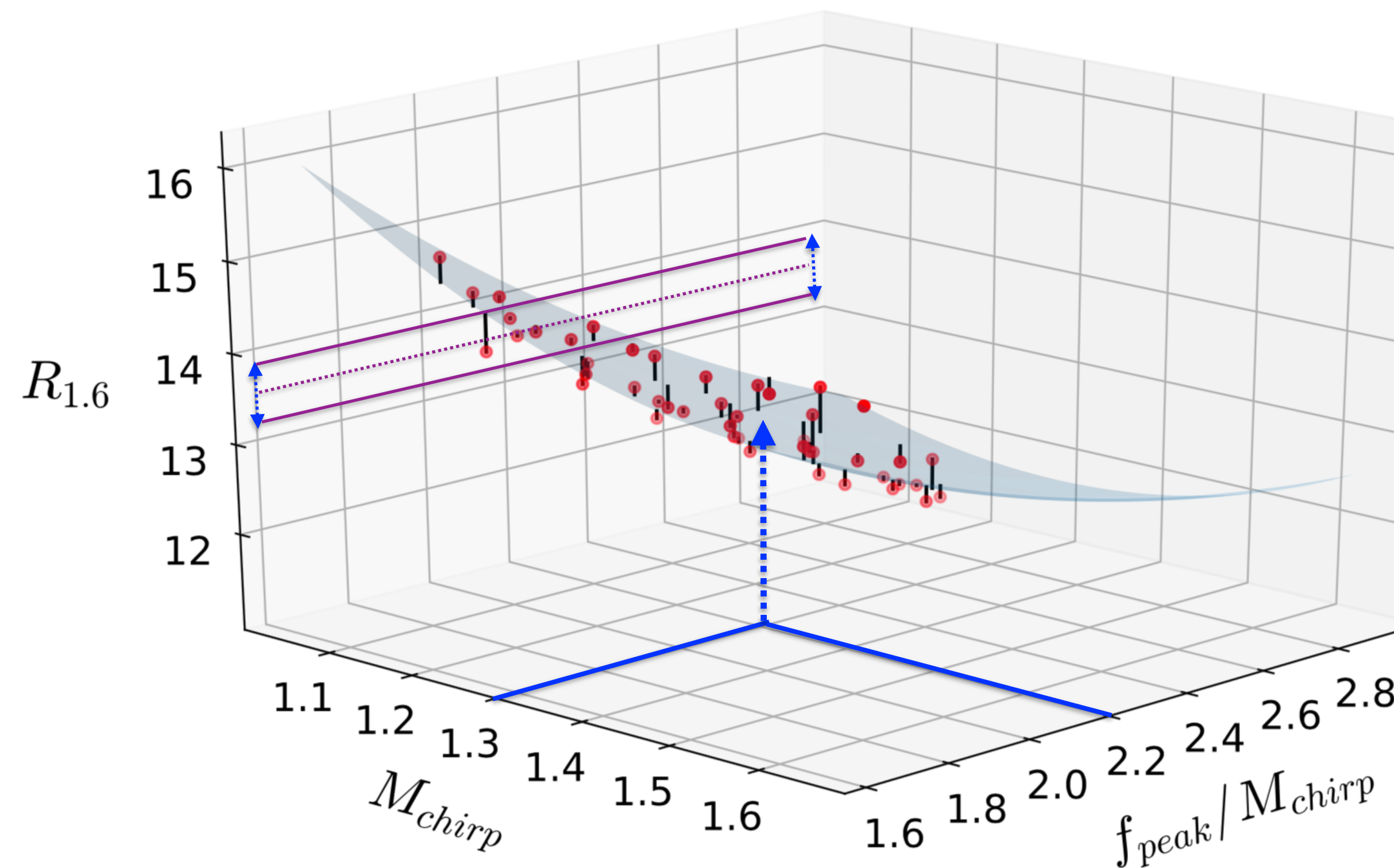


Clark, Bauswein, Stergioulas, Shoemaker (2016)

EMPIRICAL RELATIONS FOR GW ASTEROSEISMOLOGY OF BNS MERGERS

$$R_{1.6} = 43.796 - 19.984M_{\text{chirp}} - 12.921f_{\text{peak}}/M_{\text{chirp}} + 4.674M_{\text{chirp}}^2 + 3.371f_{\text{peak}} + 1.26(f_{\text{peak}}/M_{\text{chirp}})^2$$

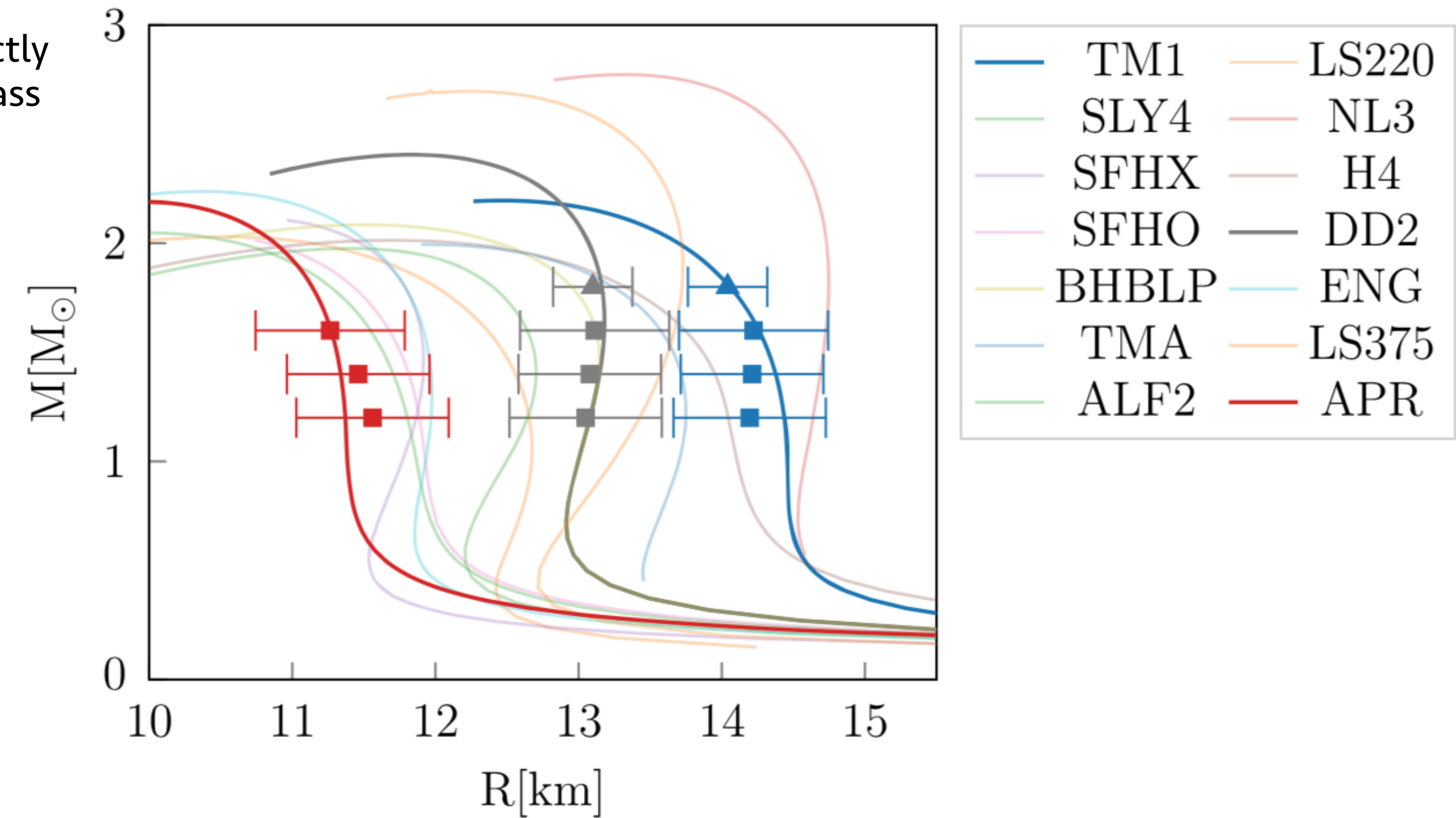
$$\tilde{\Lambda} = -1344 + 108.9M_{\text{chirp}}f_{\text{peak}} + 17208f_{\text{peak}}^{-2}$$



Vretinaris, Stergioulas & Bauswein (2020)

EOS CONSTRAINTS THROUGH POST-MERGER REMNANTS

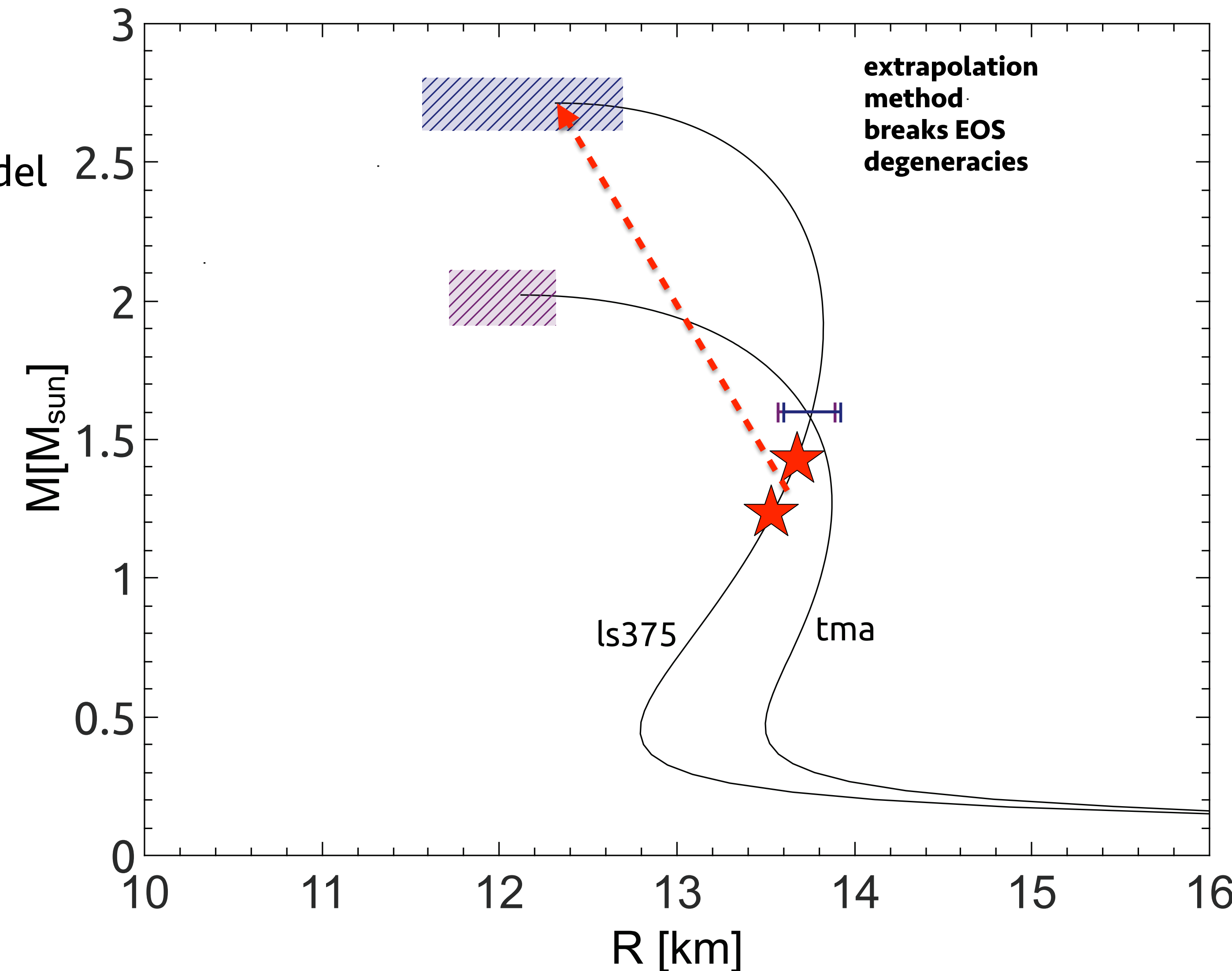
It will be possible to directly extract the radius in a mass range $1.2 - 1.8 M_{\odot}$



Vretinaris, Stergioulas & Bauswein (2020)

EXTRAPOLATION METHOD

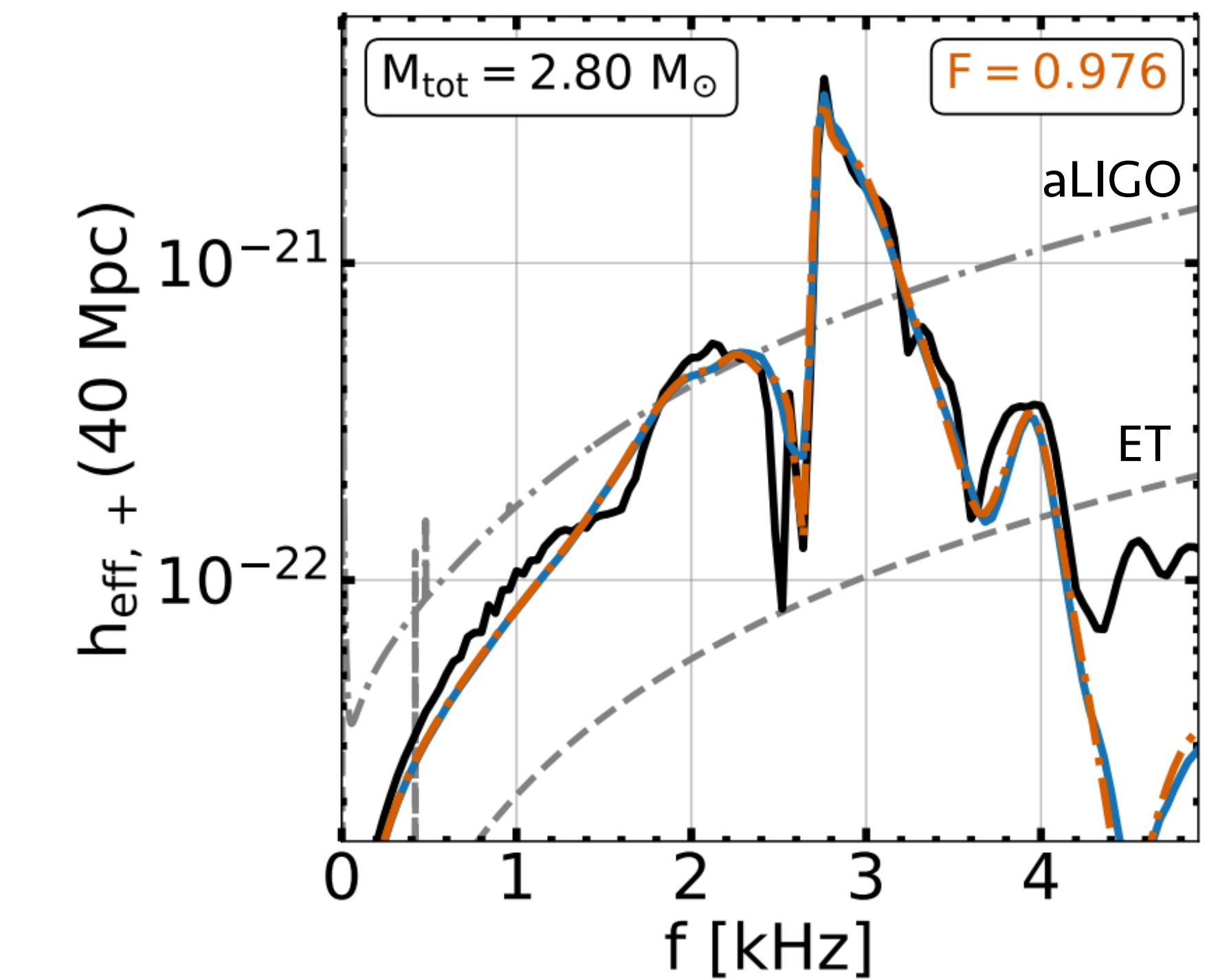
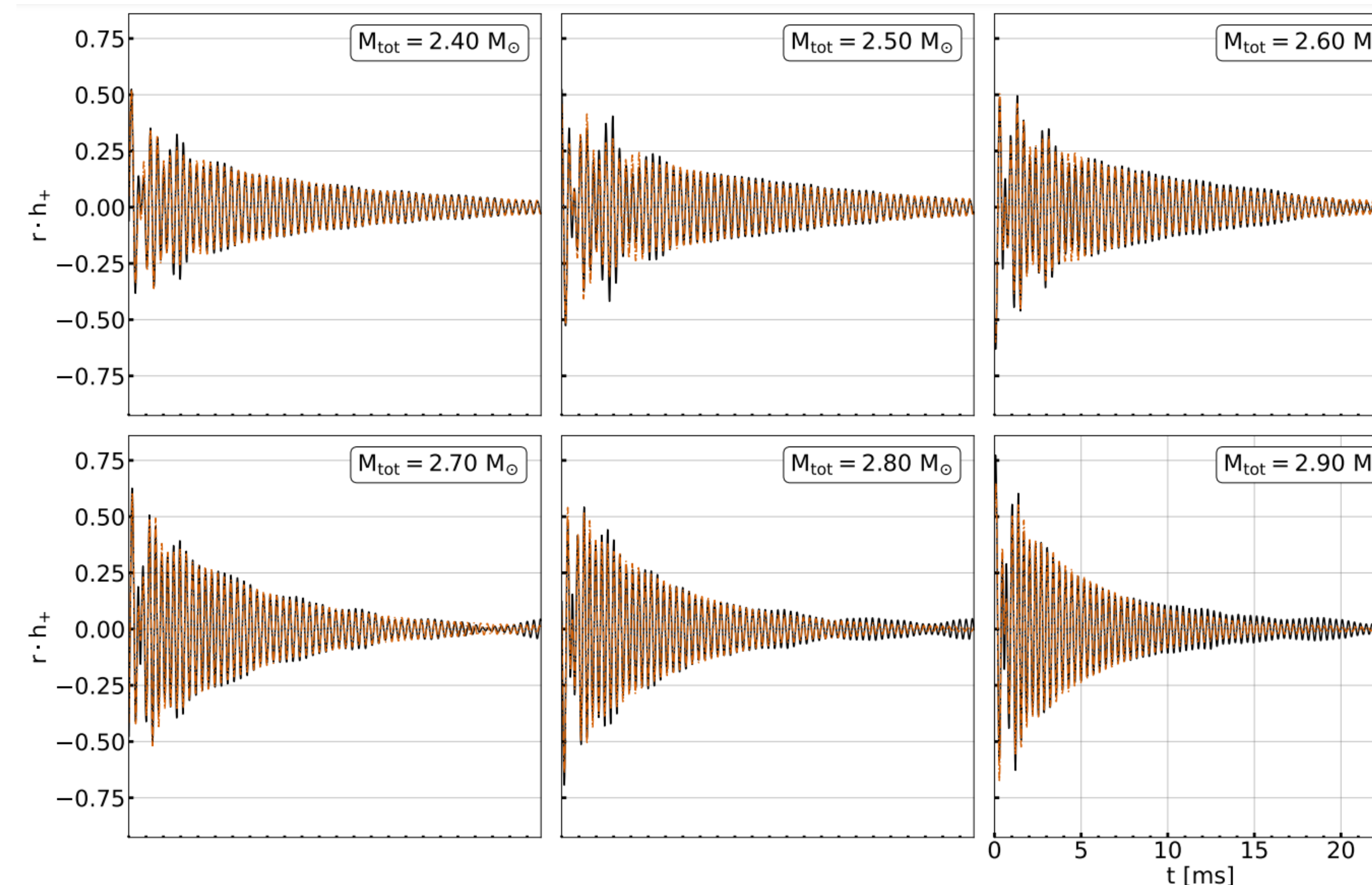
Extrapolation method allows for constraints on maximum mass model using only low-mass detections.



Bauswein, Stergioulas (2015)

NEW ANALYTIC WAVEFORM TEMPLATE

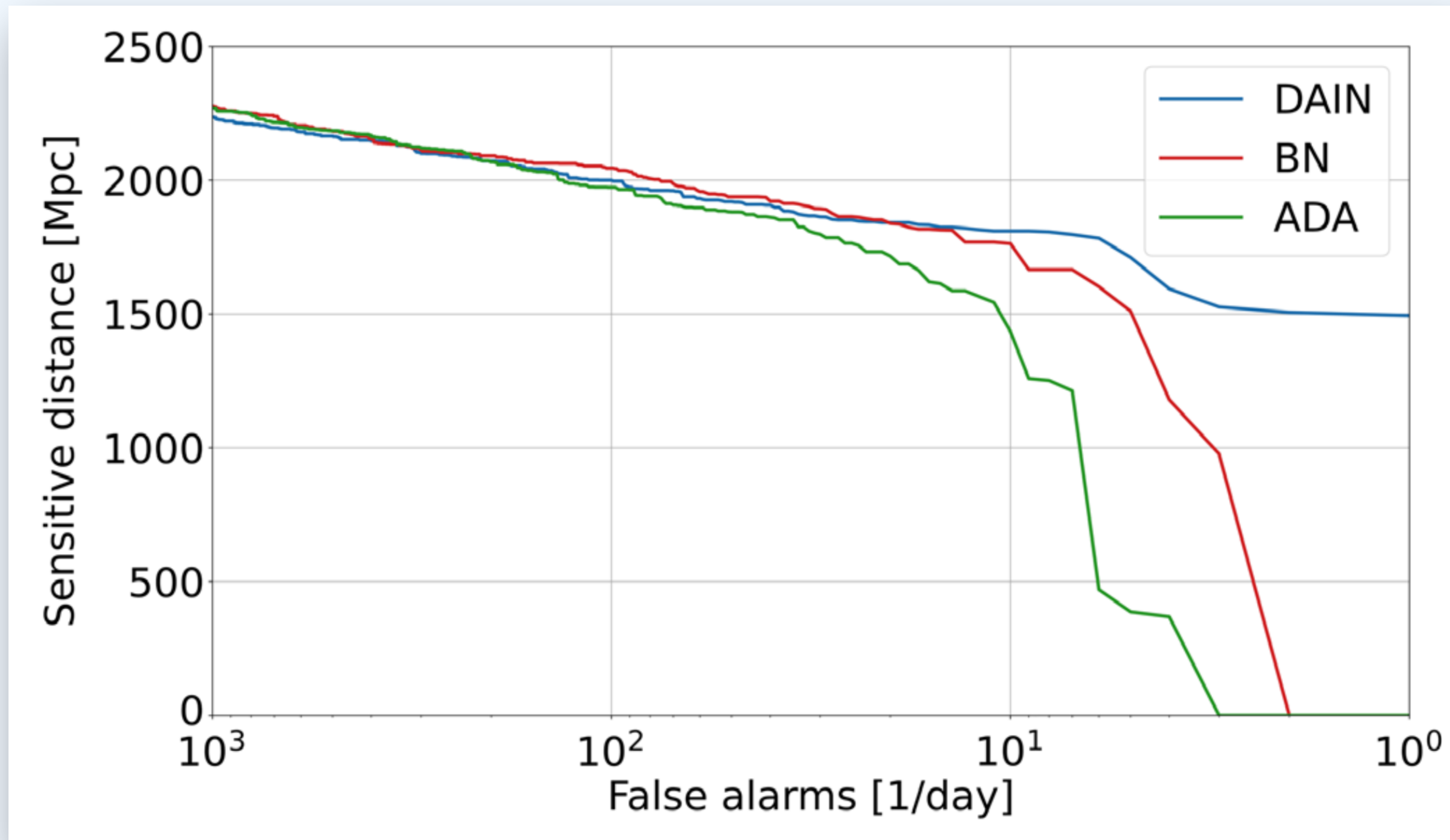
Relies only on physical parameters



Soultanis, Bauswein, Stergioulas (2022)

ADAPTIVE INPUT NORMALIZATION

Significant Improvement in Sensitive Distance using DAIN

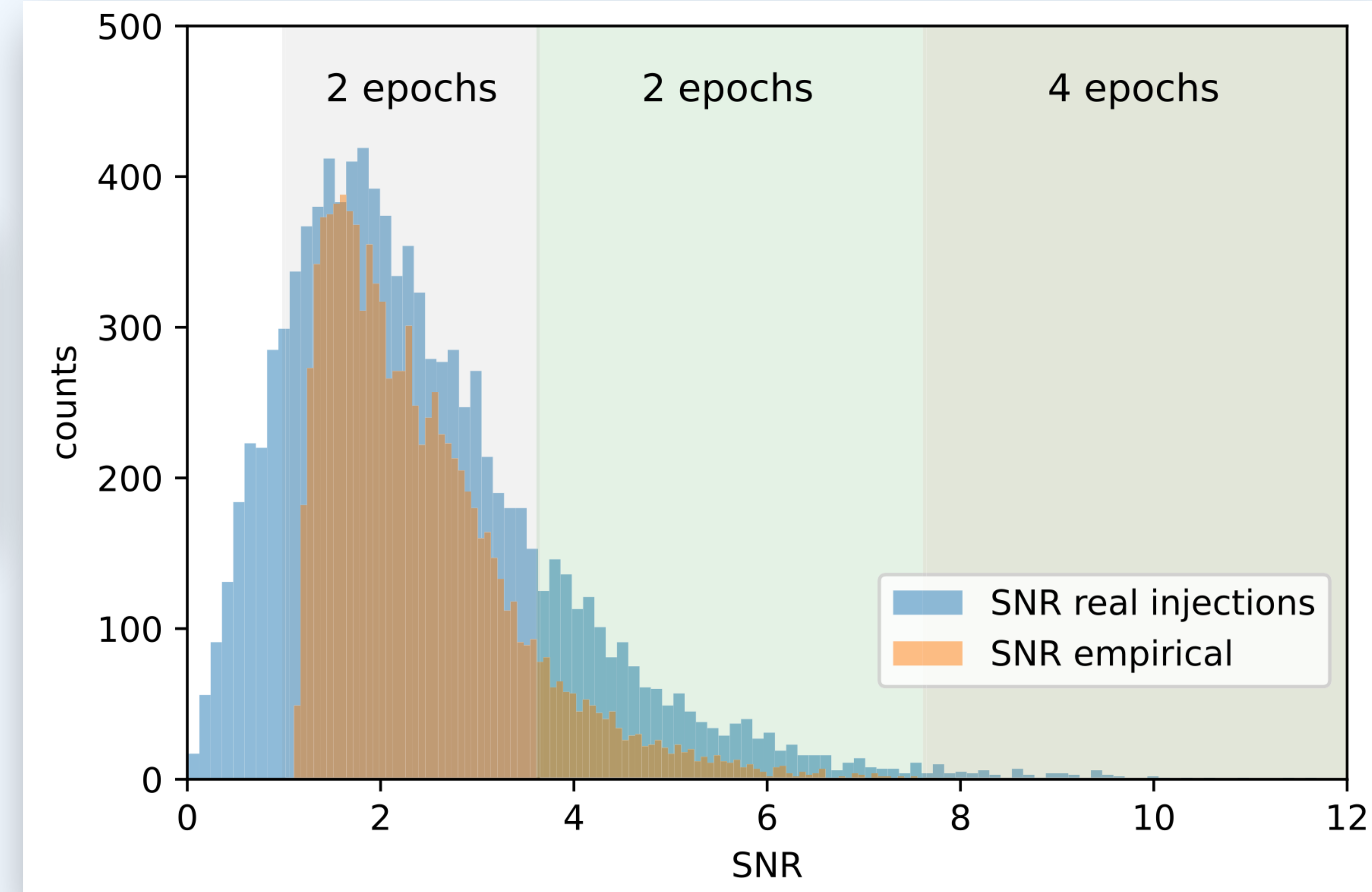


CURRICULUM LEARNING

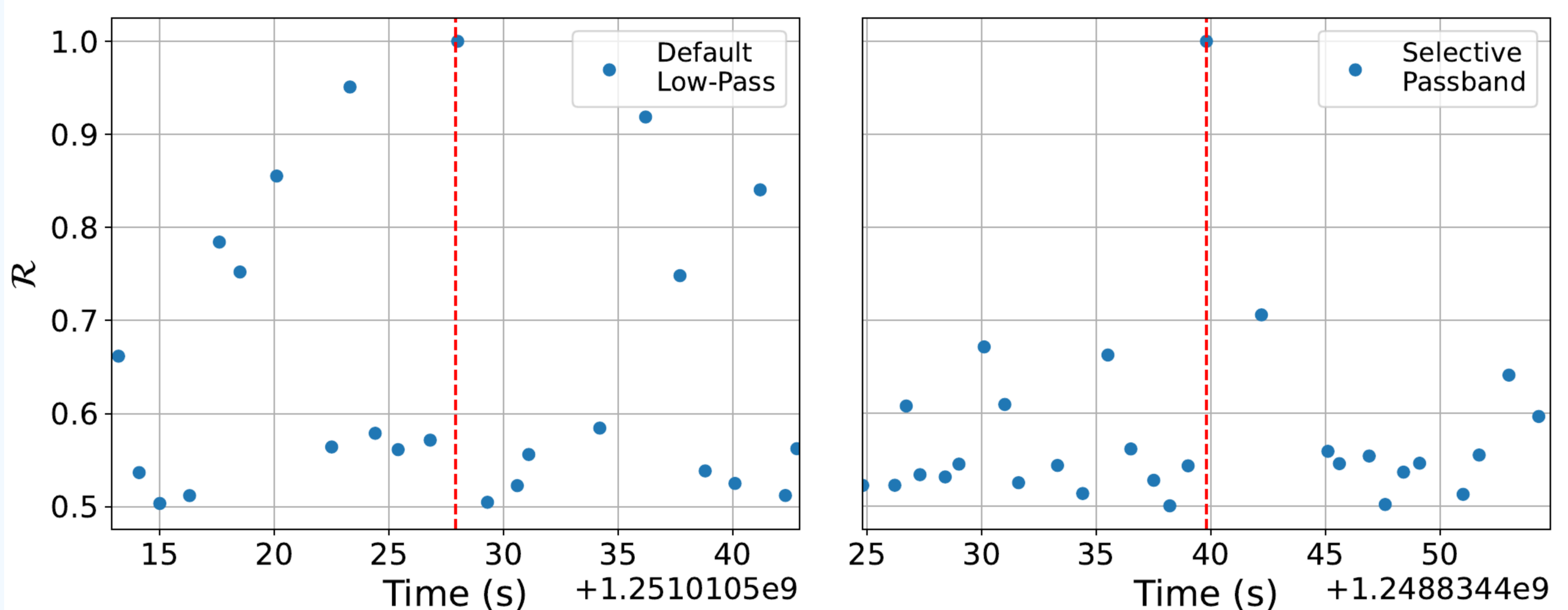
Curriculum learning based
on signal-to-noise ratio (**SNR**)

Epochs	Min(SNR)	Max(SNR)
4	7.63	100
2	3.63	100
2	1	3.63
2	1	7.63
Remaining	0	∞

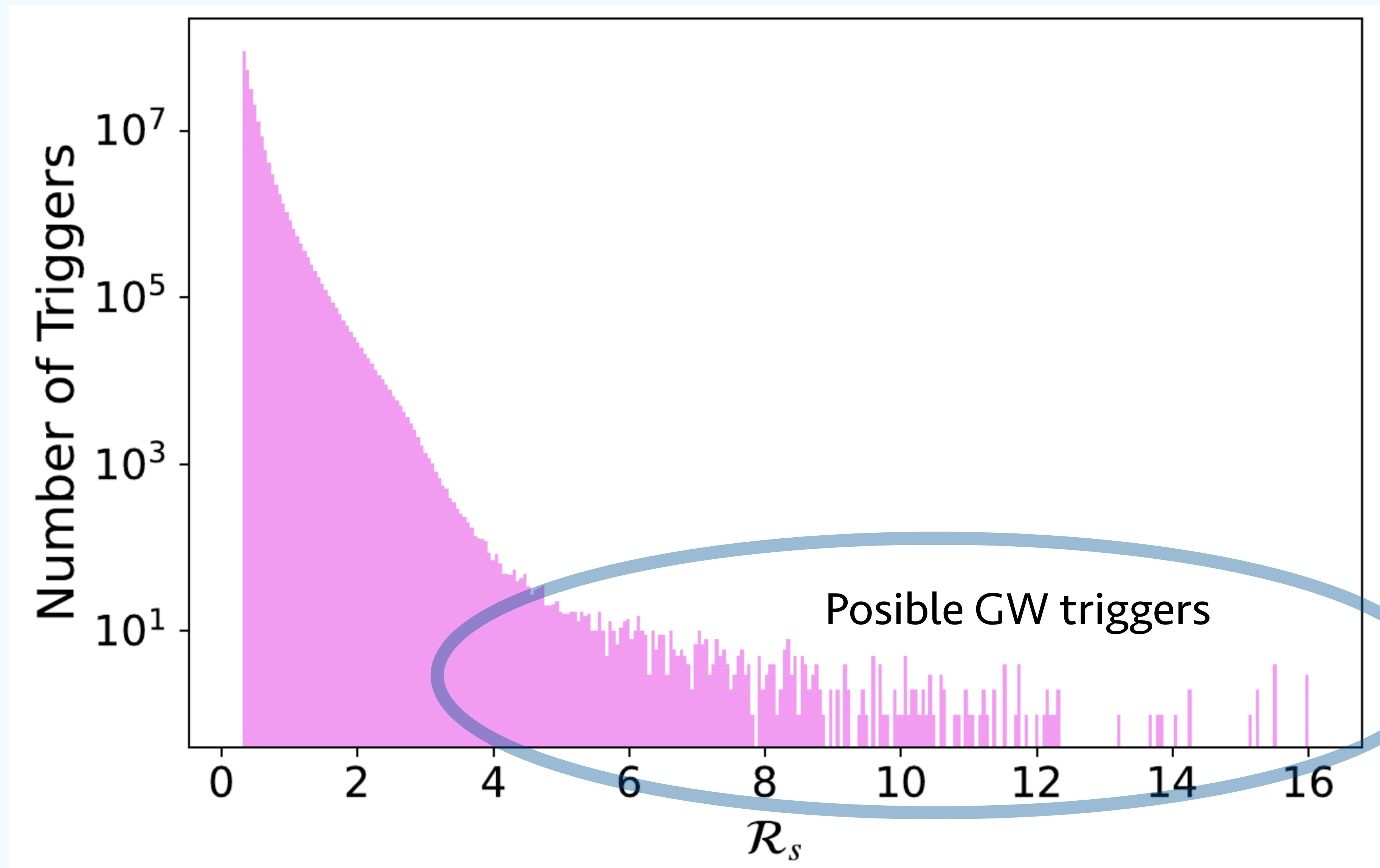
The networks learns the louder
signals first and then refines its
weights to accommodate
weaker signals



HIERARCHICAL TRIGGER CLASSIFICATION SCHEME

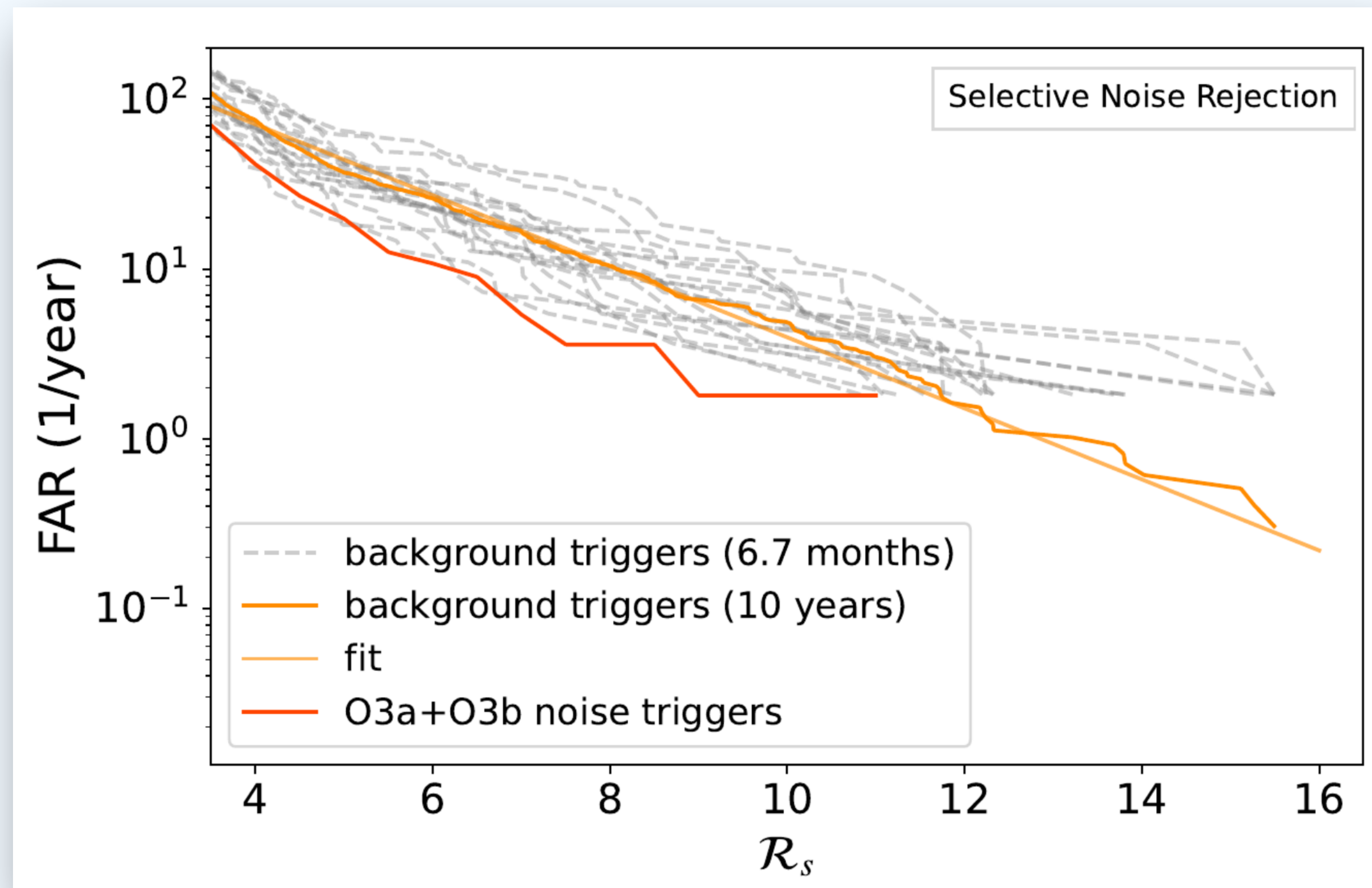


RANKING STATISTIC DISTRIBUTION



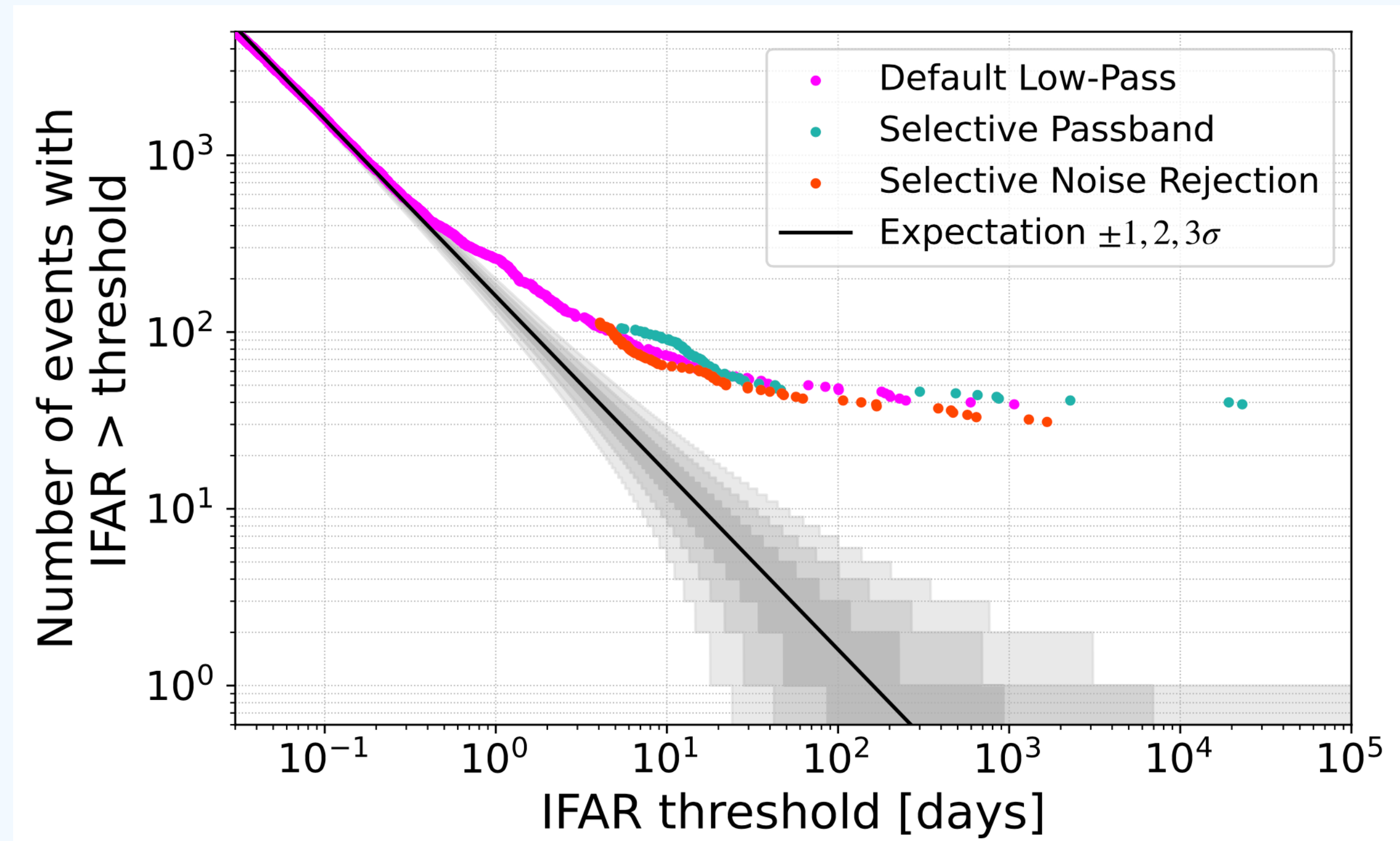
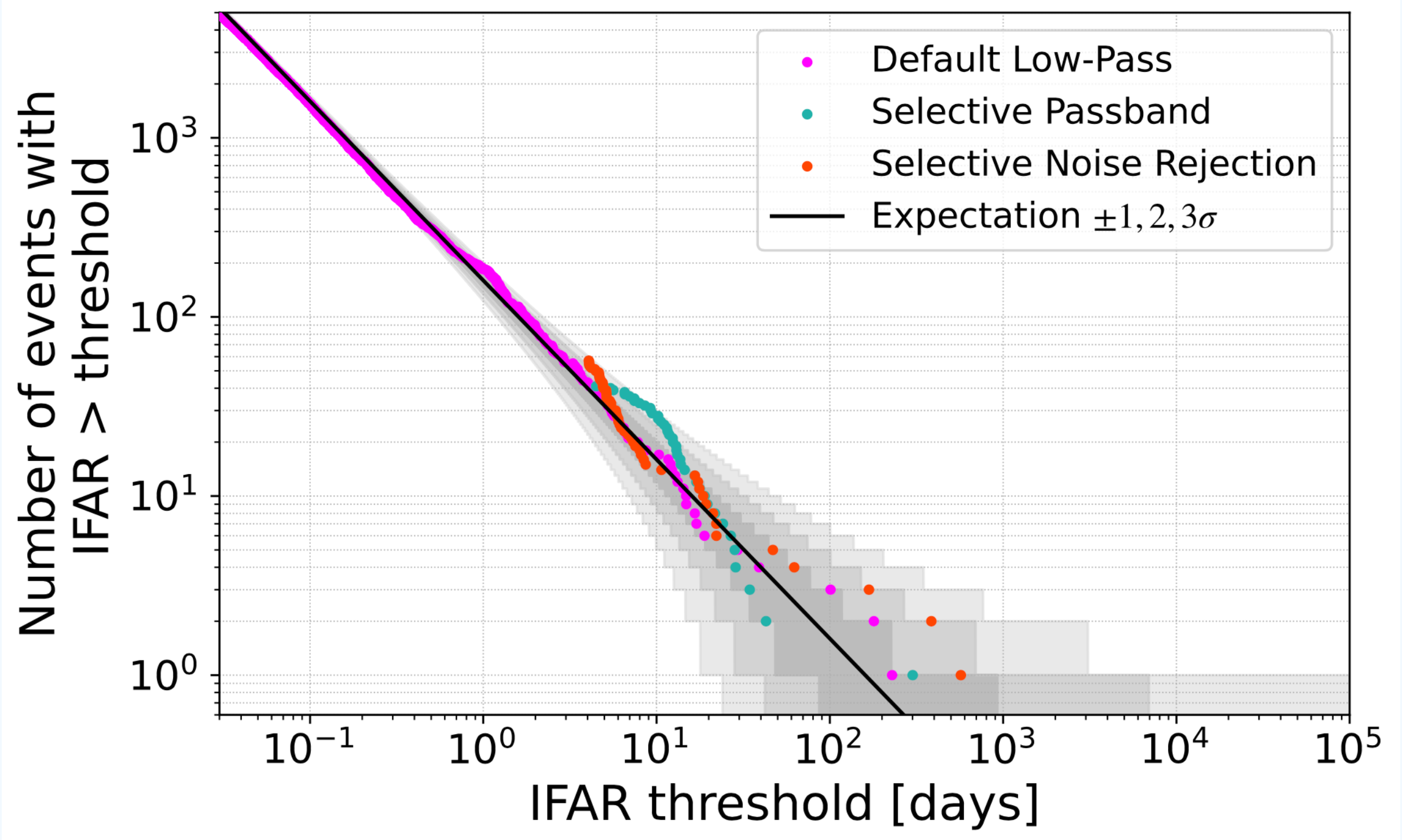
FALSE-ALARM RATE

FAR: We construct a 10-year background using time-slides of O3 noise

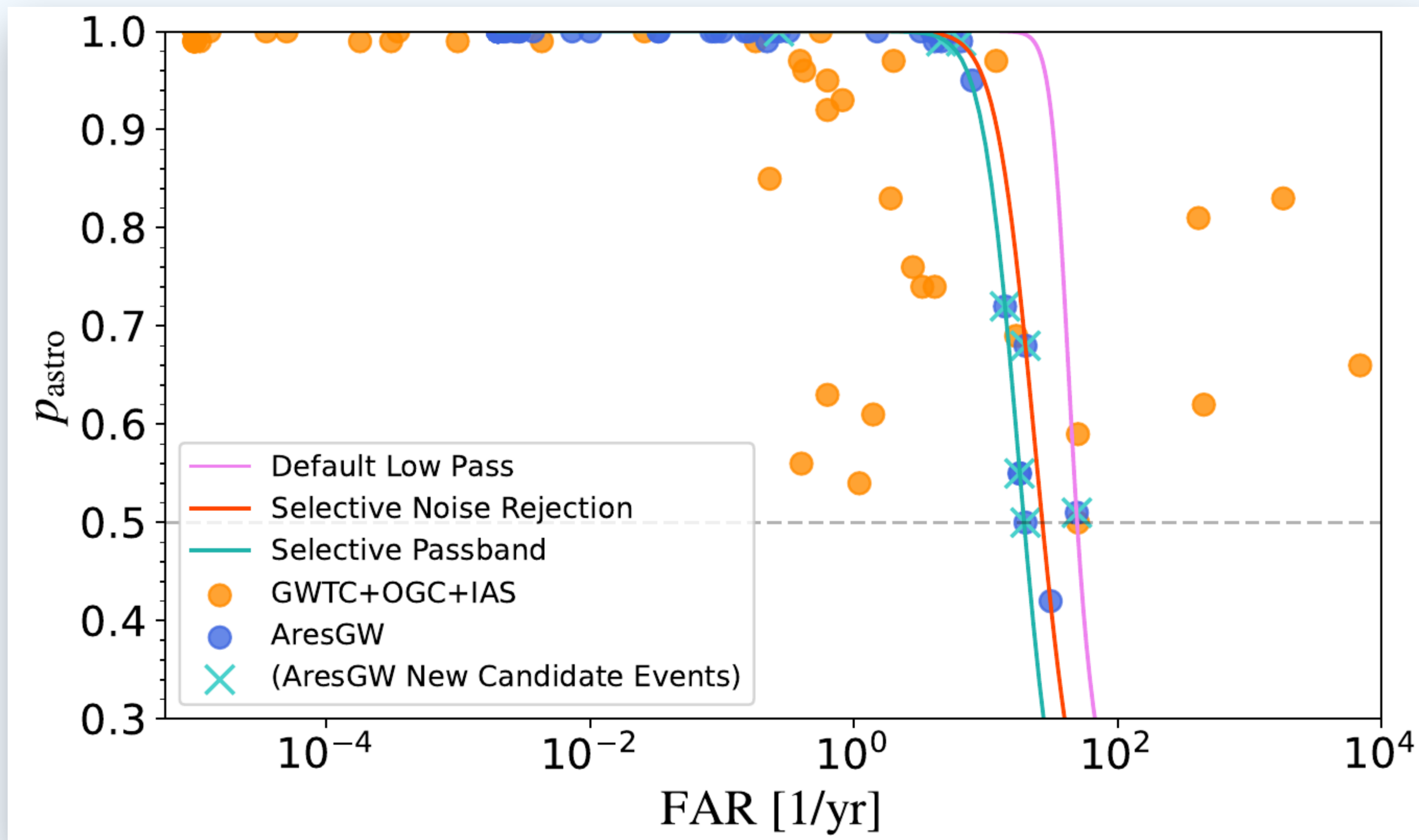


O3 STATISTICS

AresGW performance on O3 data



ASTROPHYSICAL PROBABILITY



PARAMETERS OF NEW GW DETECTIONS WITH AresGW

TABLE VIII: Parameter estimation for the new AresGW candidate events.

#	Event Name	\mathcal{M} (M_{\odot})	q	m_1 (M_{\odot})	m_2 (M_{\odot})	D_L (Mpc)	χ_{eff}	SNR (H1)	SNR (L1)	SNR $\hat{\rho}$ (network)
1	GW190511-125545	$28.95^{+9.45}_{-6.86}$	$0.72^{+0.25}_{-0.36}$	$40.7^{+16.2}_{-10.5}$	$28.2^{+11.6}_{-11.2}$	3707^{+3471}_{-2173}	$0.23^{+0.25}_{-0.29}$	2.29	7.34	7.29
2	GW190614-134749	$25.97^{+16.59}_{-6.20}$	$0.70^{+0.27}_{-0.36}$	$37.0^{+31.8}_{-10.7}$	$25.2^{+15.2}_{-9.7}$	6551^{+9562}_{-3558}	$0.05^{+0.34}_{-0.34}$	3.51	6.08	7.02
3	GW190607-083827	$30.48^{+7.21}_{-4.68}$	$0.78^{+0.19}_{-0.29}$	$40.5^{+12.0}_{-7.6}$	$31.0^{+9.1}_{-8.2}$	4928^{+2725}_{-2435}	$0.01^{+0.26}_{-0.30}$	4.04	7.29	8.33
4	GW190904-104631	$21.24^{+5.76}_{-4.40}$	$0.64^{+0.31}_{-0.33}$	$31.3^{+14.5}_{-8.5}$	$19.7^{+7.1}_{-7.2}$	5614^{+4441}_{-2864}	$0.05^{+0.30}_{-0.37}$	4.50	4.88	6.64
5	GW190523-085933	$23.82^{+10.24}_{-7.95}$	$0.49^{+0.45}_{-0.32}$	$41.7^{+19.3}_{-15.5}$	$19.4^{+14.6}_{-10.5}$	6091^{+6613}_{-3702}	$0.42^{+0.31}_{-0.45}$	3.48	5.14	6.02
6	GW200208-211609	$18.83^{+4.68}_{-3.18}$	$0.69^{+0.28}_{-0.40}$	$26.9^{+14.6}_{-6.3}$	$18.0^{+6.4}_{-6.9}$	3669^{+3413}_{-1985}	$0.01^{+0.37}_{-0.37}$	4.75	6.22	7.83
7	GW190705-164632	$27.21^{+7.34}_{-5.24}$	$0.52^{+0.41}_{-0.32}$	$44.7^{+24.8}_{-12.8}$	$23.0^{+11.7}_{-9.8}$	5692^{+4030}_{-2863}	$0.29^{+0.26}_{-0.34}$	4.42	6.88	8.11
8	GW190426-082124	$17.93^{+4.12}_{-3.42}$	$0.45^{+0.45}_{-0.28}$	$31.5^{+22.5}_{-11.3}$	$13.8^{+6.9}_{-5.2}$	3213^{+4555}_{-1573}	$-0.01^{+0.39}_{-0.50}$	5.15	4.46	6.41

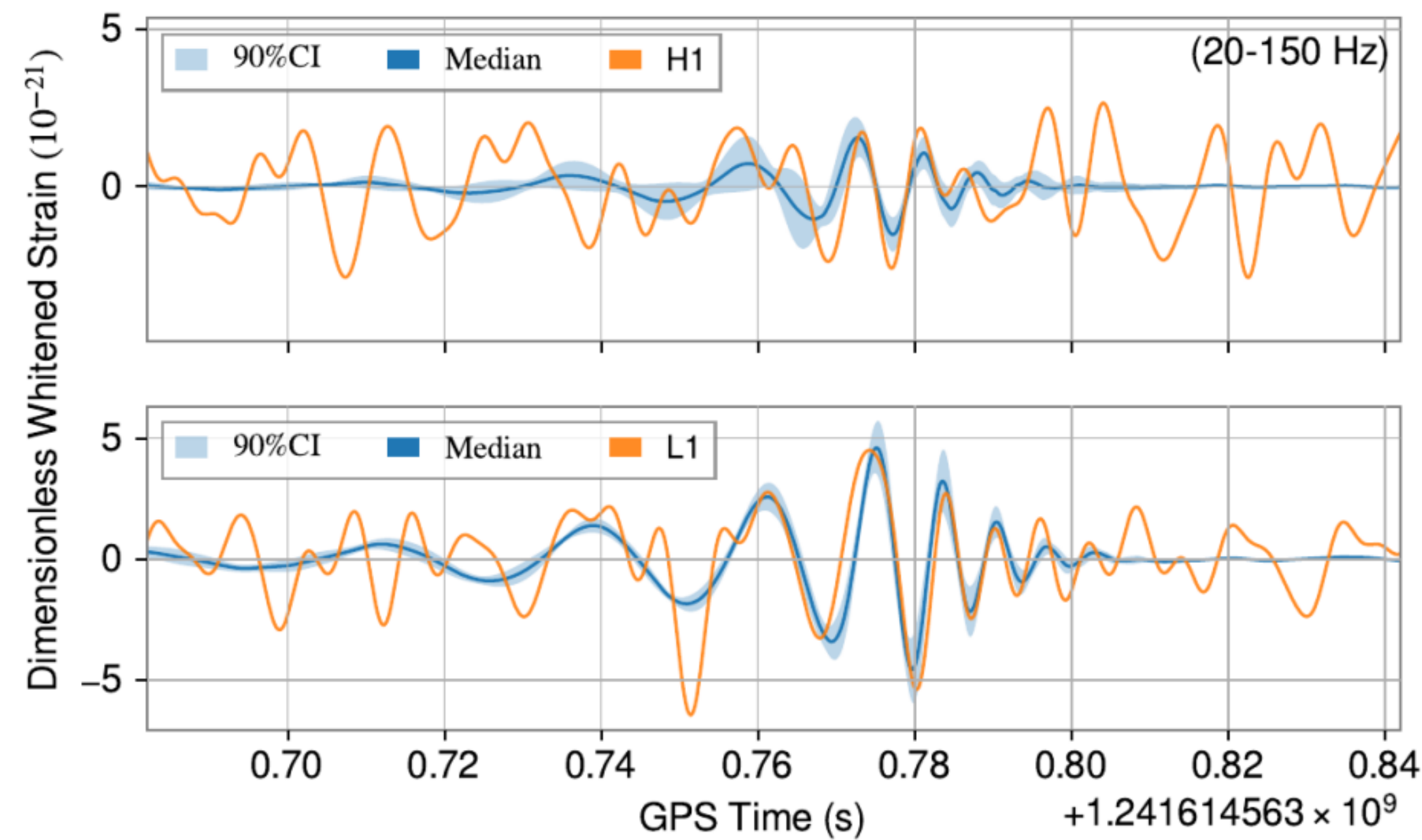


FIG. 35: Whitened, bandpassed strain data and reconstructed waveform for the new event GW190511_125545 identified by AresGW.

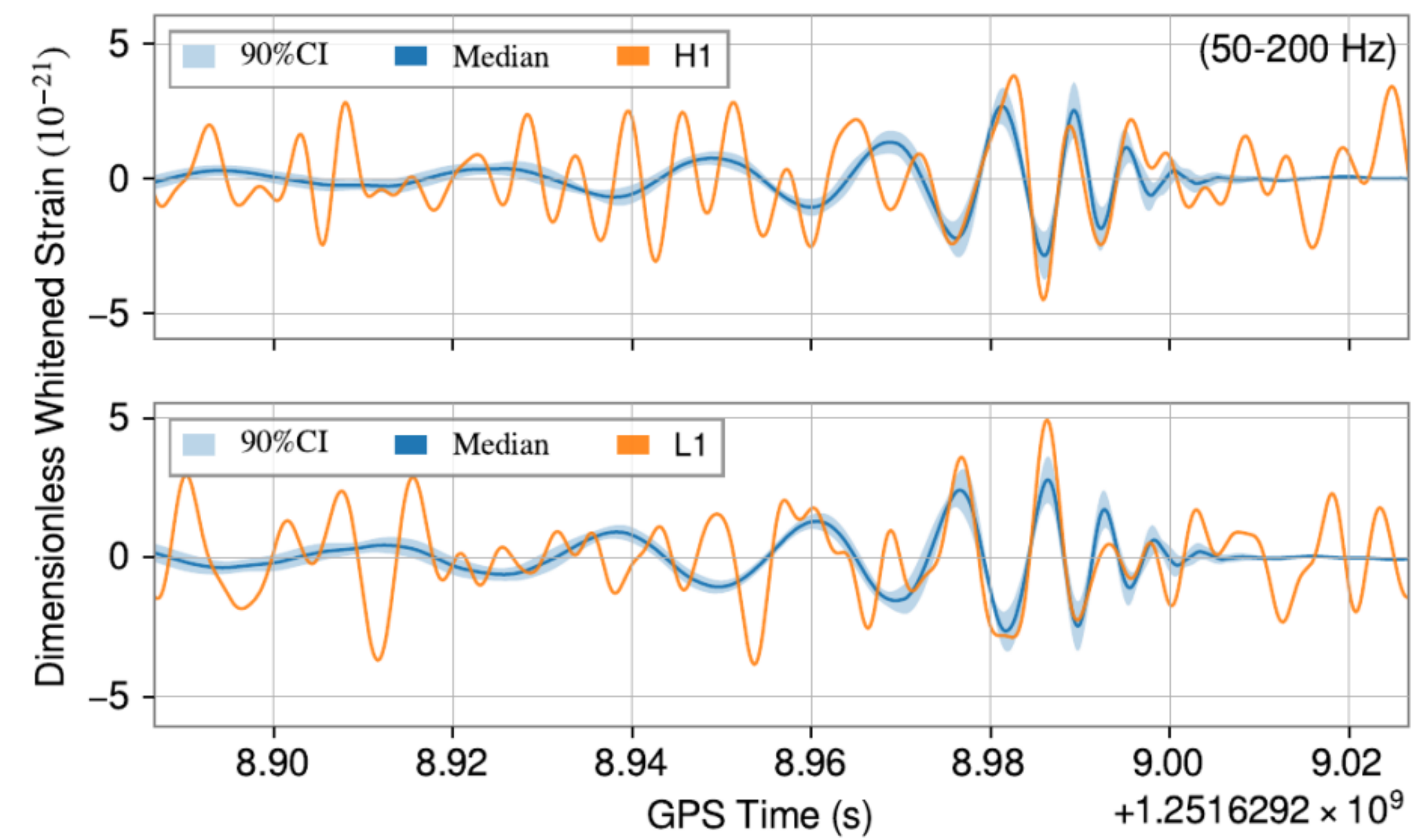


FIG. 38: Same as Fig. 35, but for the new event GW190904_104631.

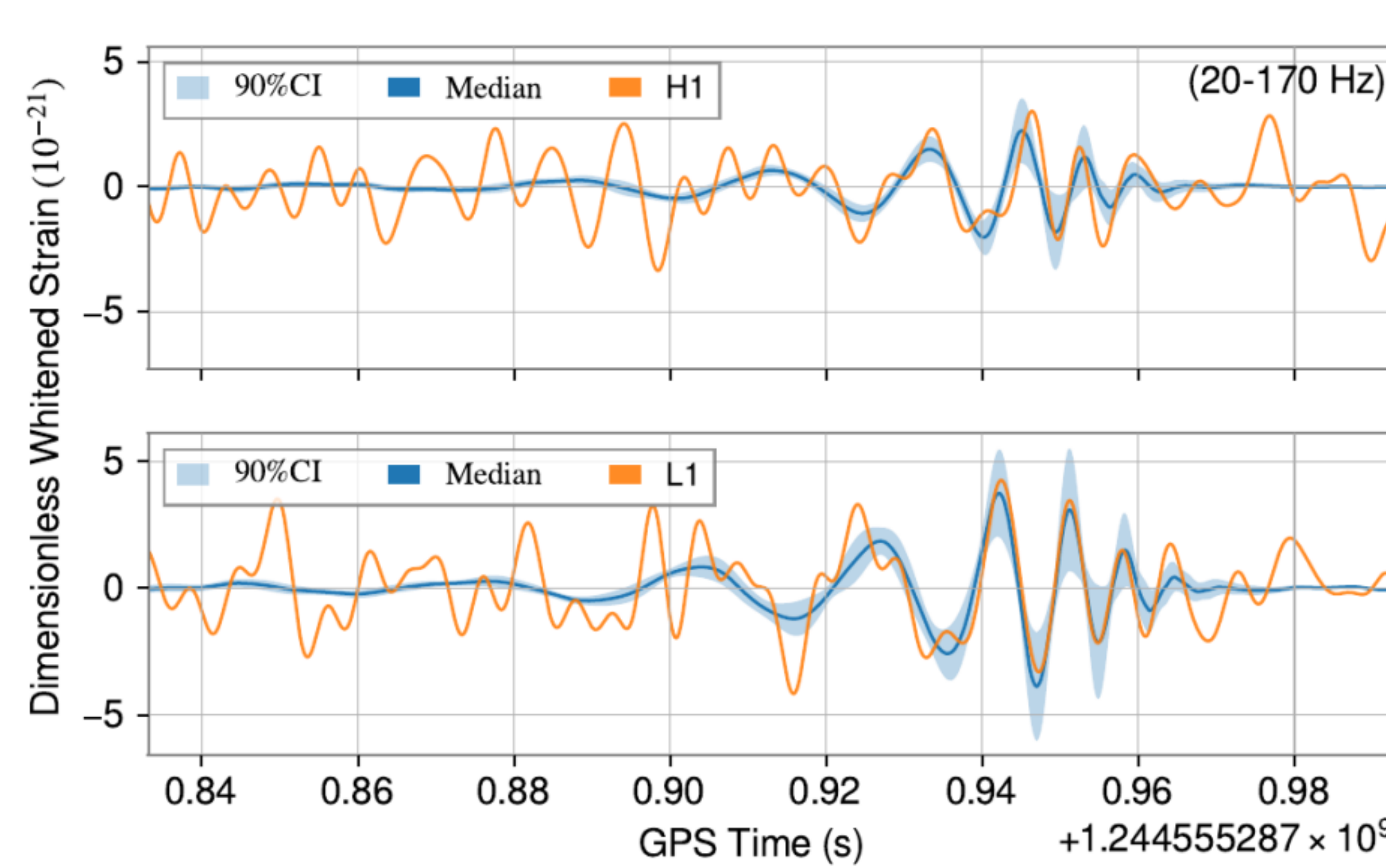


FIG. 36: Same as Fig. 35, but for the new event
GW190614_134749.

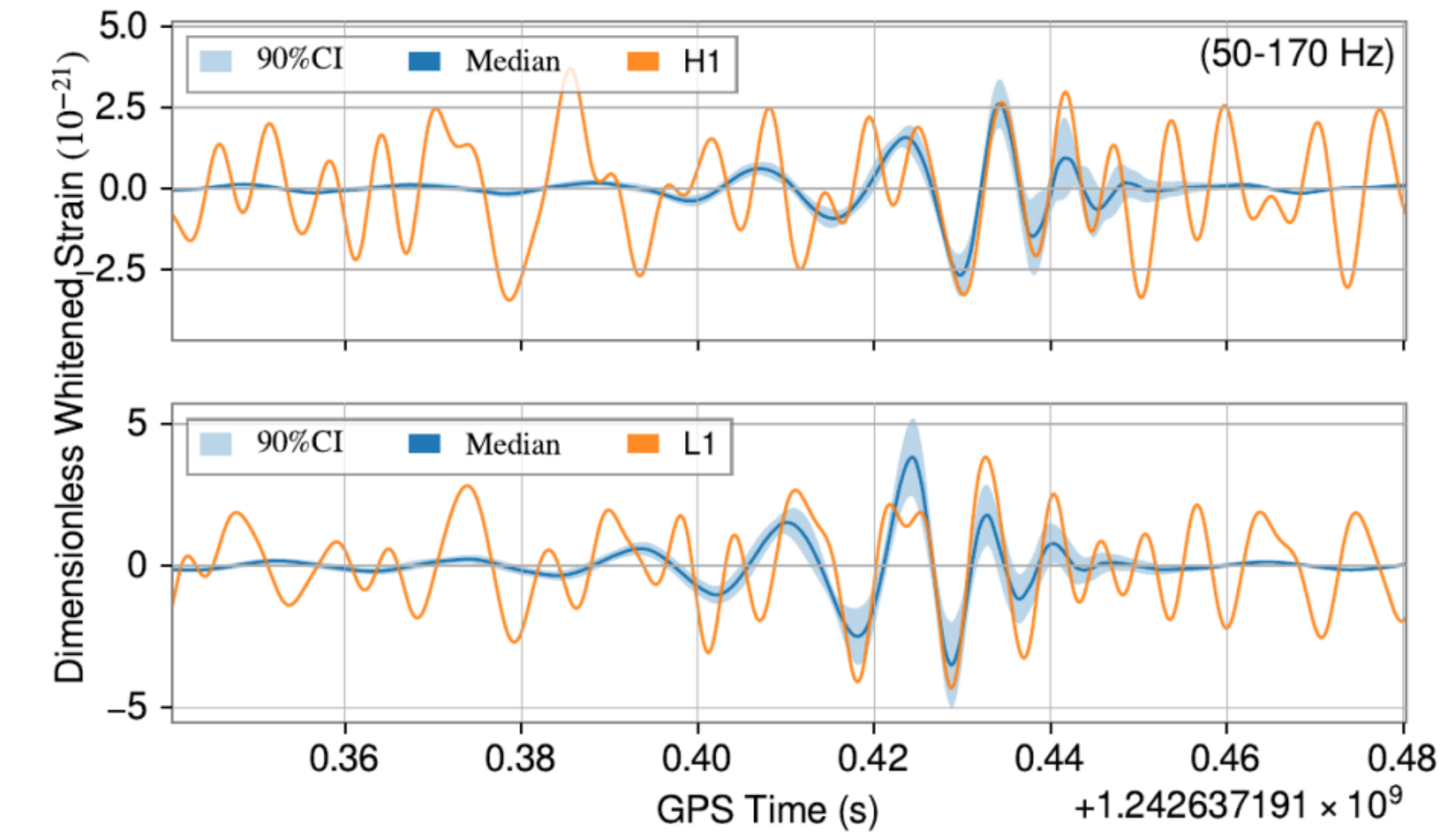


FIG. 39: Same as Fig. 35, but for the new event
GW190523_085933.

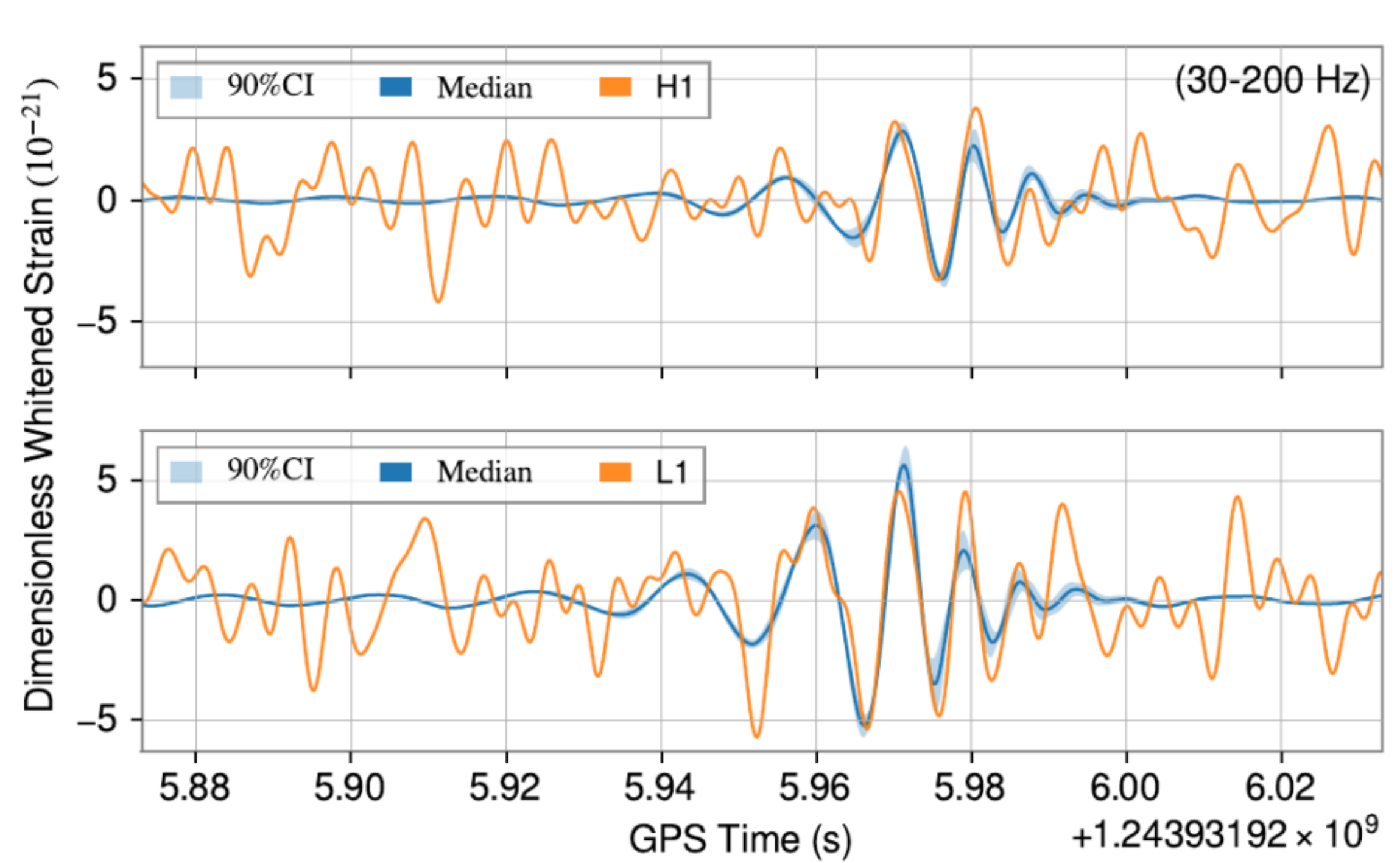


FIG. 37: Same as Fig. 35, but for the new event
GW190607_083827.

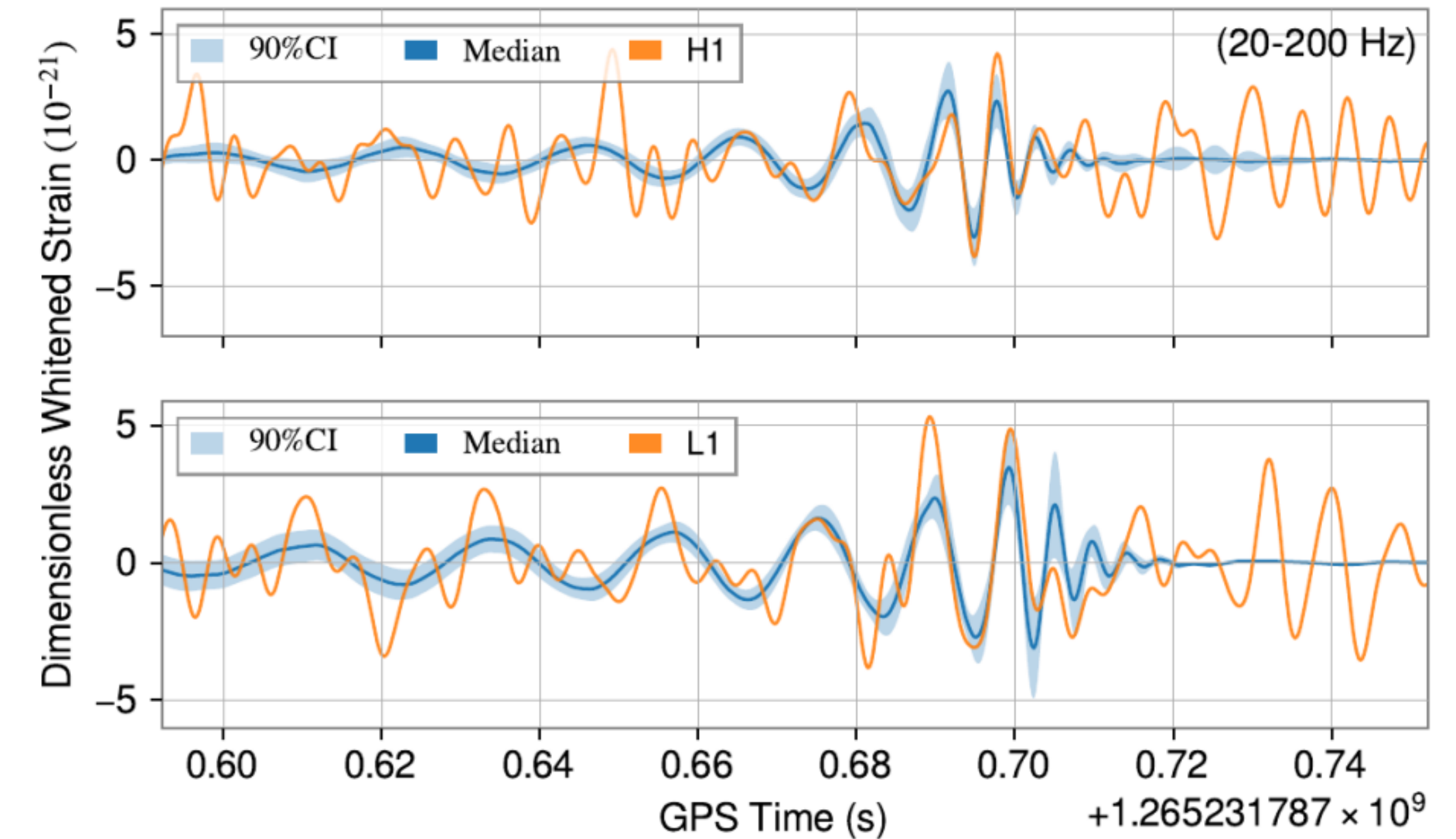


FIG. 40: Same as Fig. 35, but for the new event
GW200208_211609.

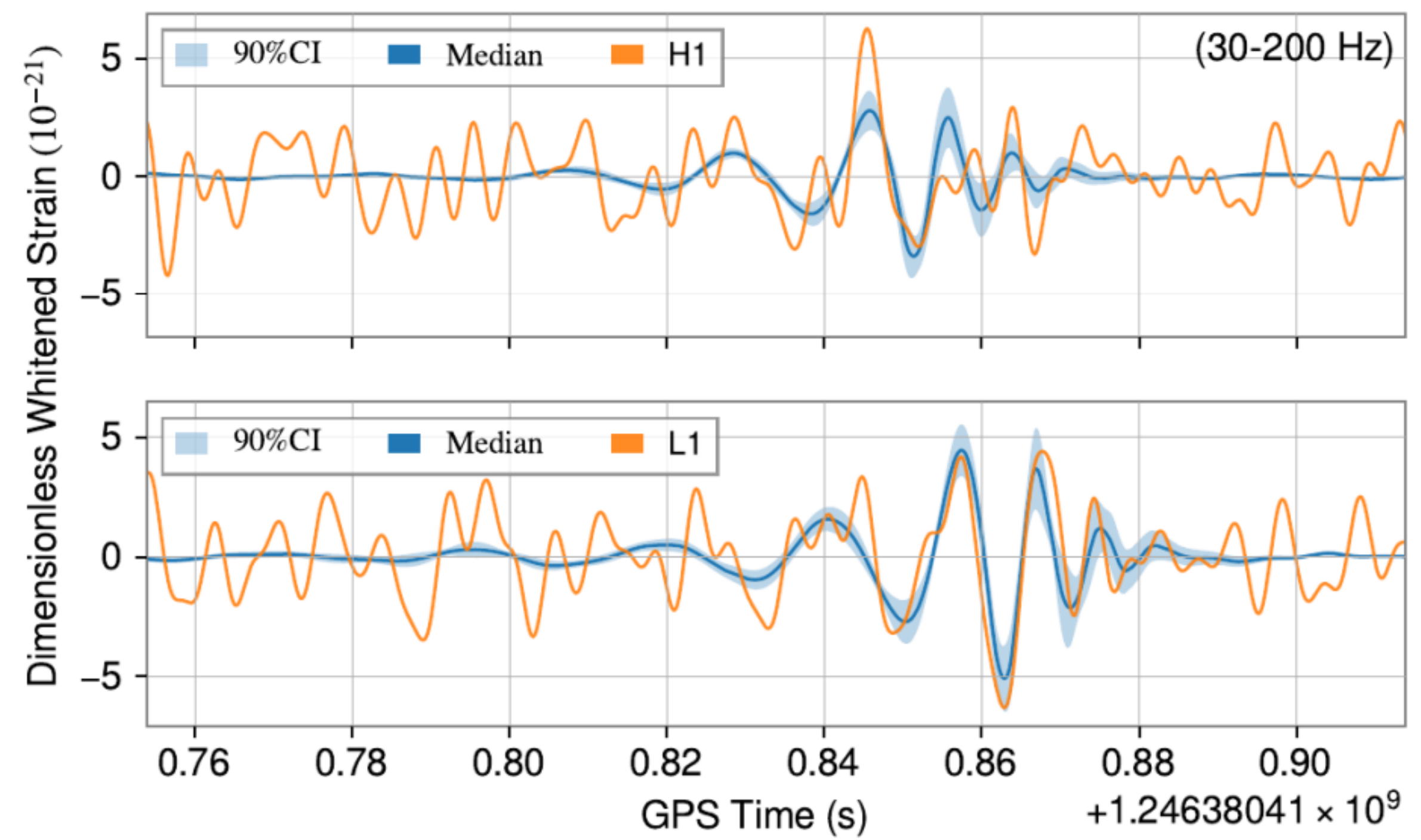


FIG. 41: Same as Fig. 35, but for the new event
GW190705_164632.

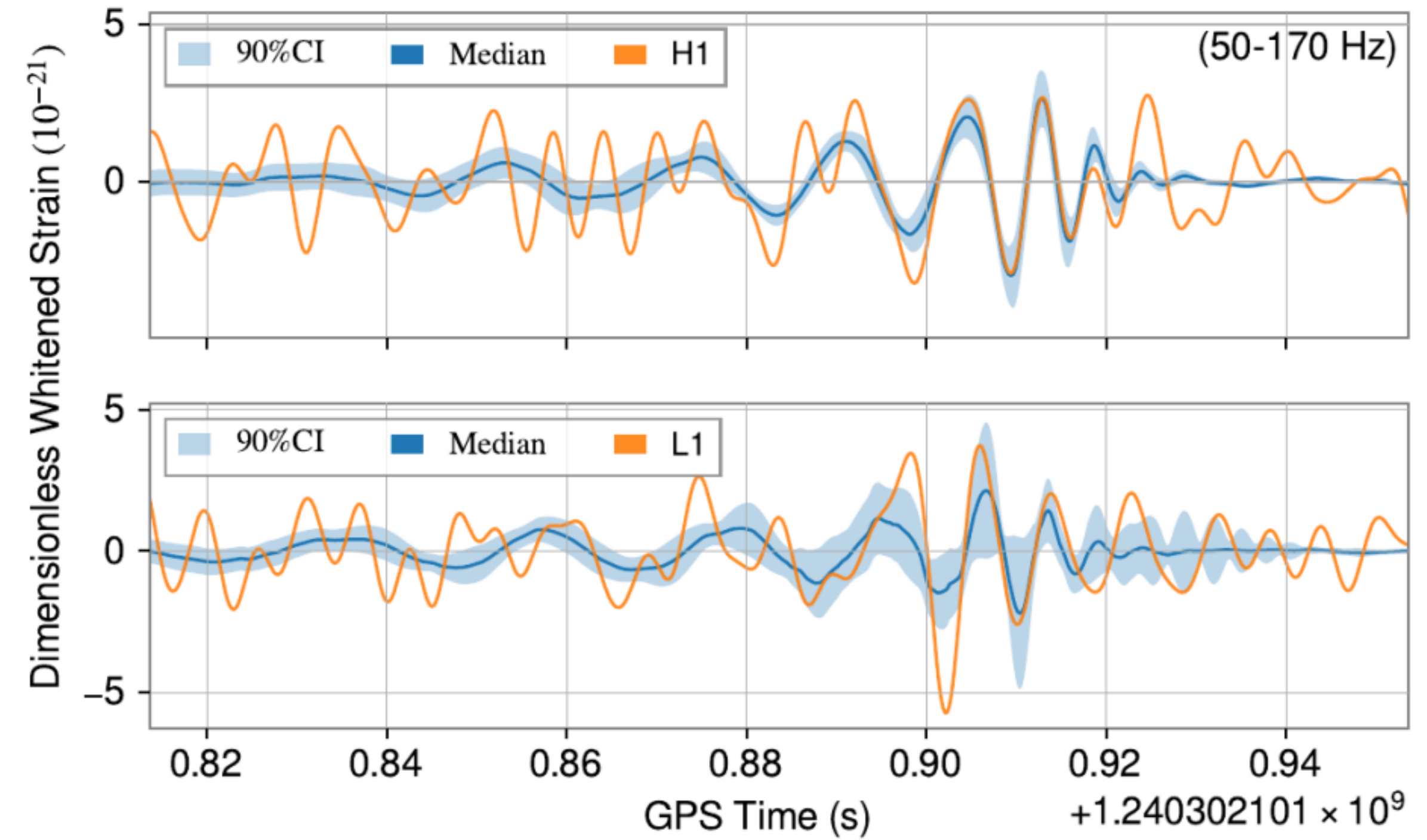
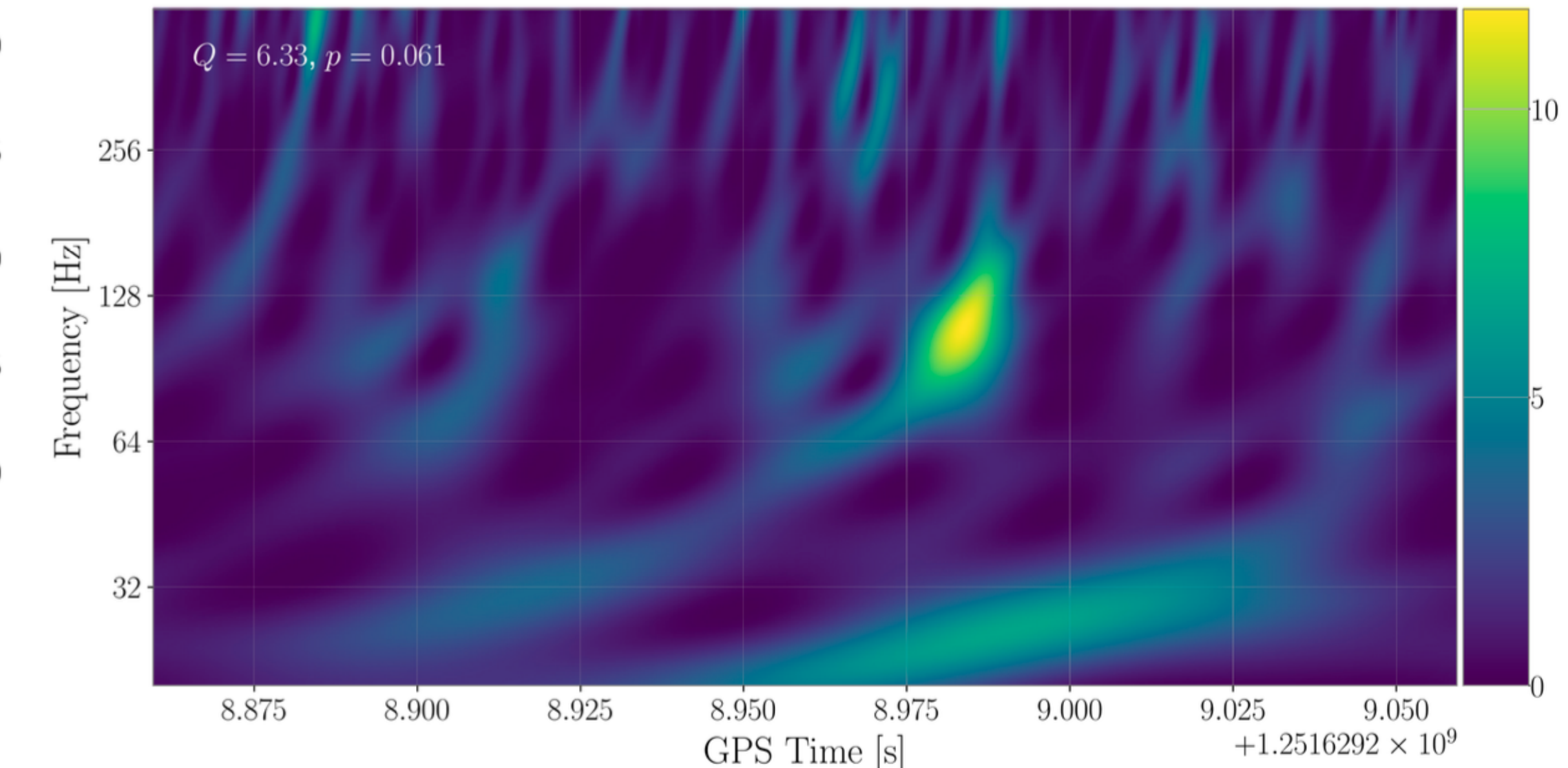
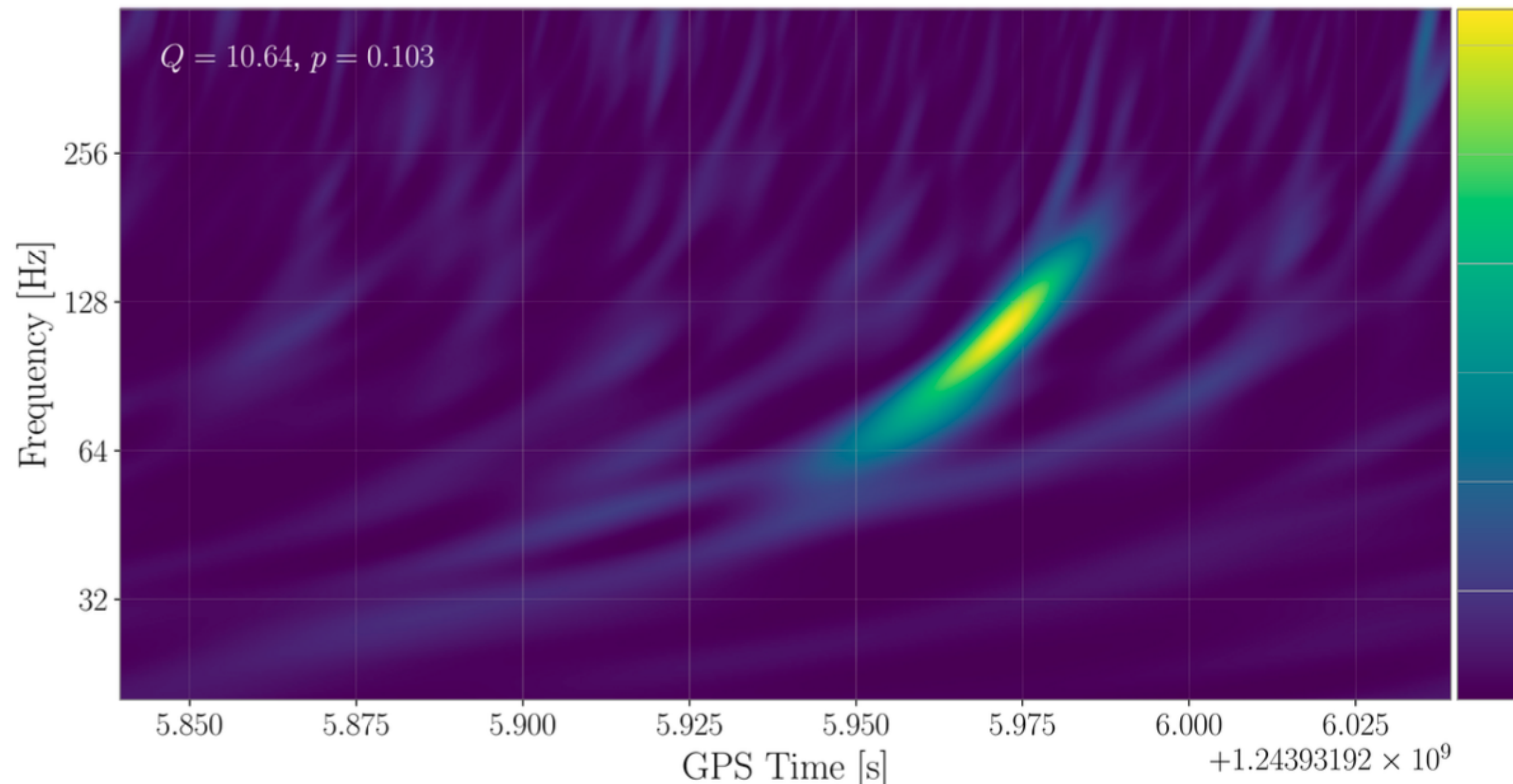
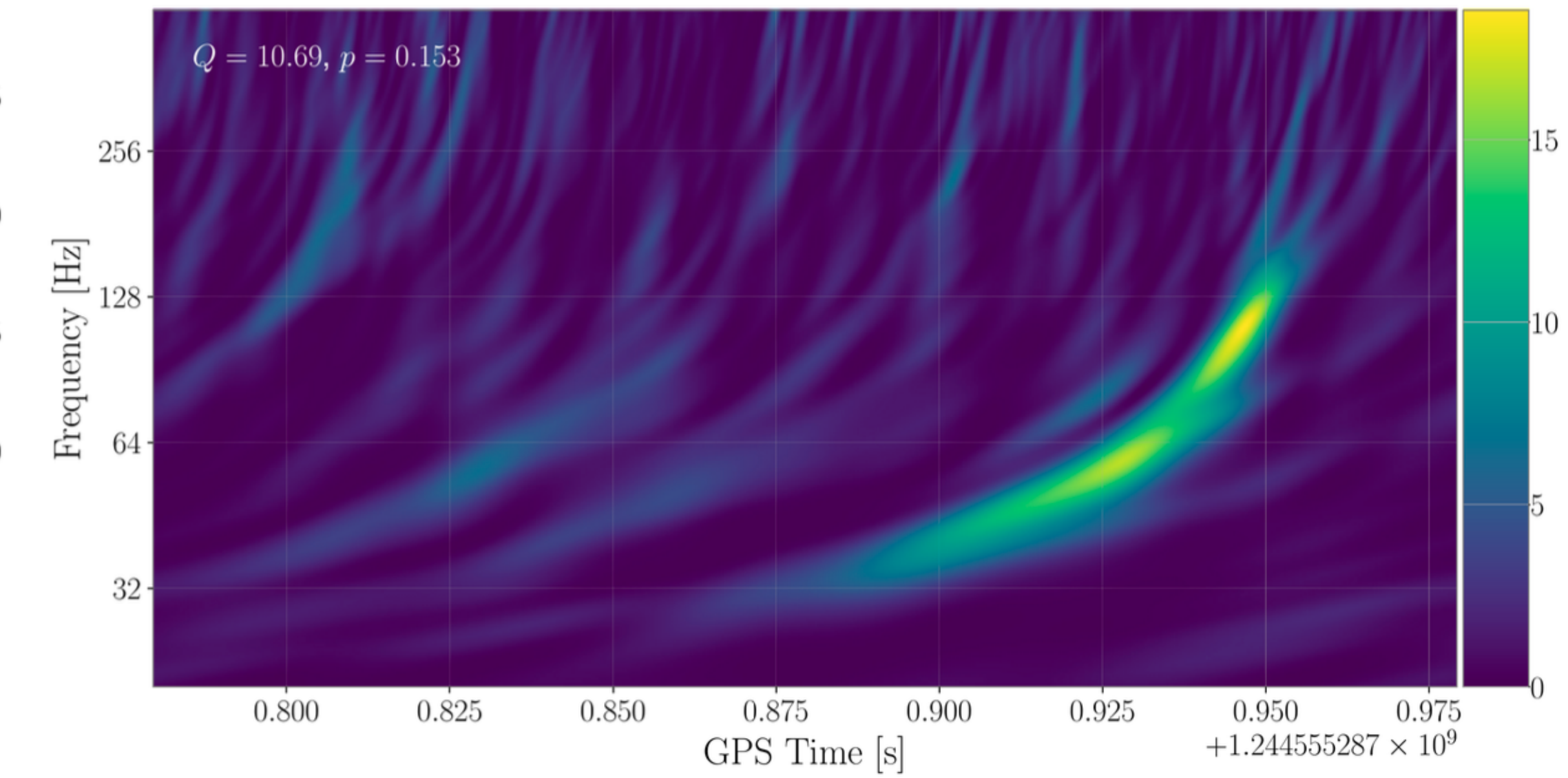
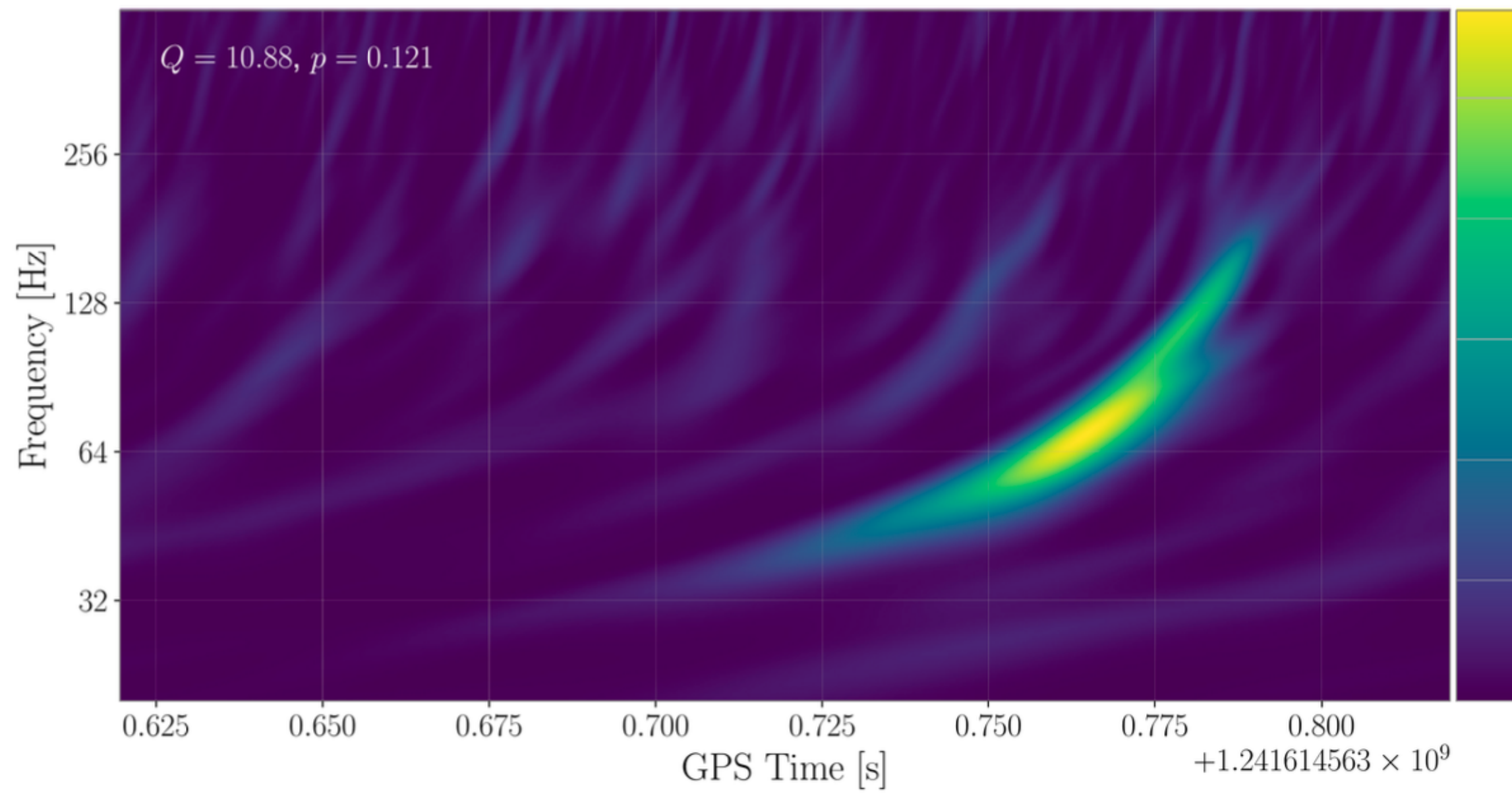
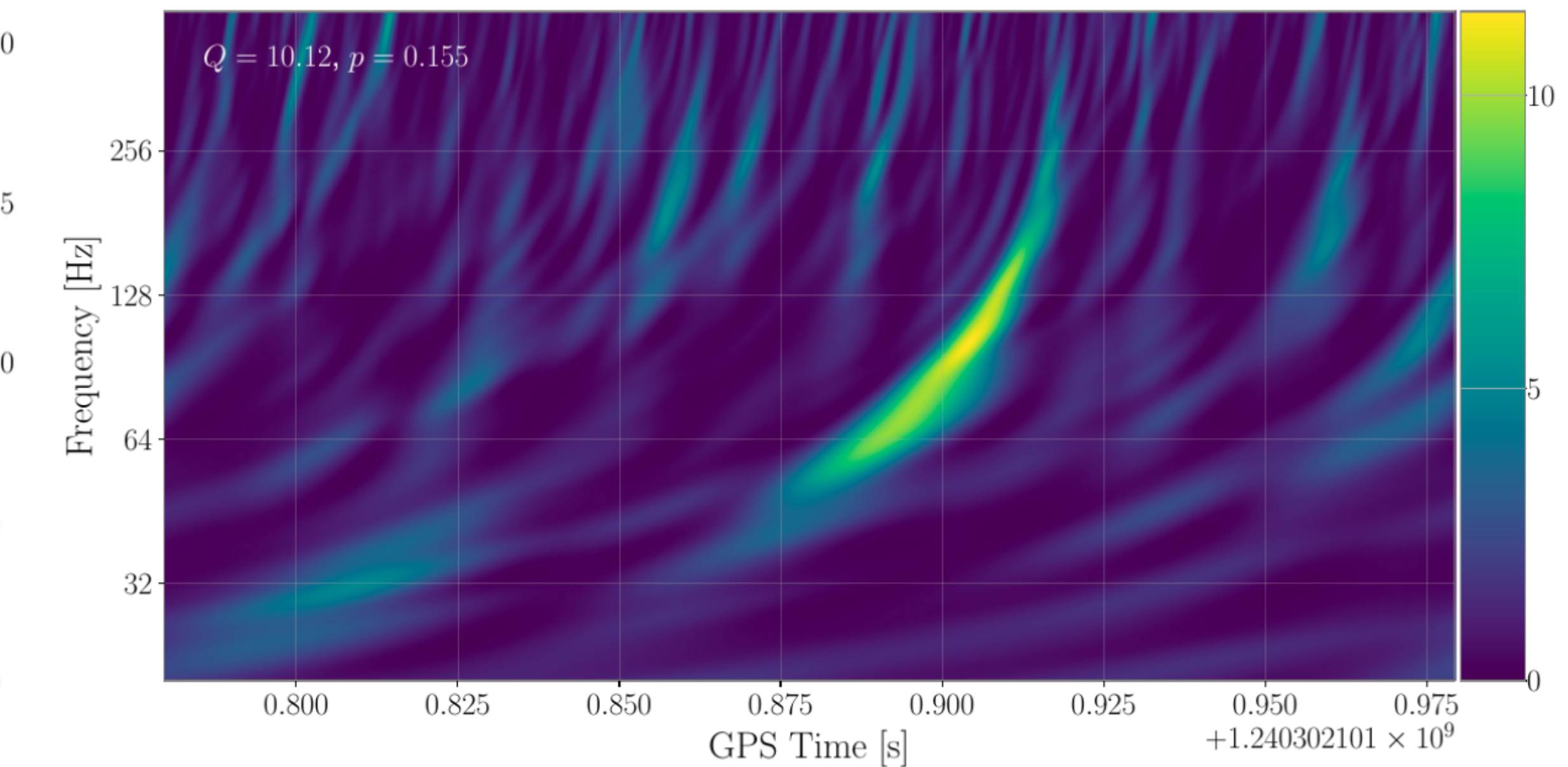
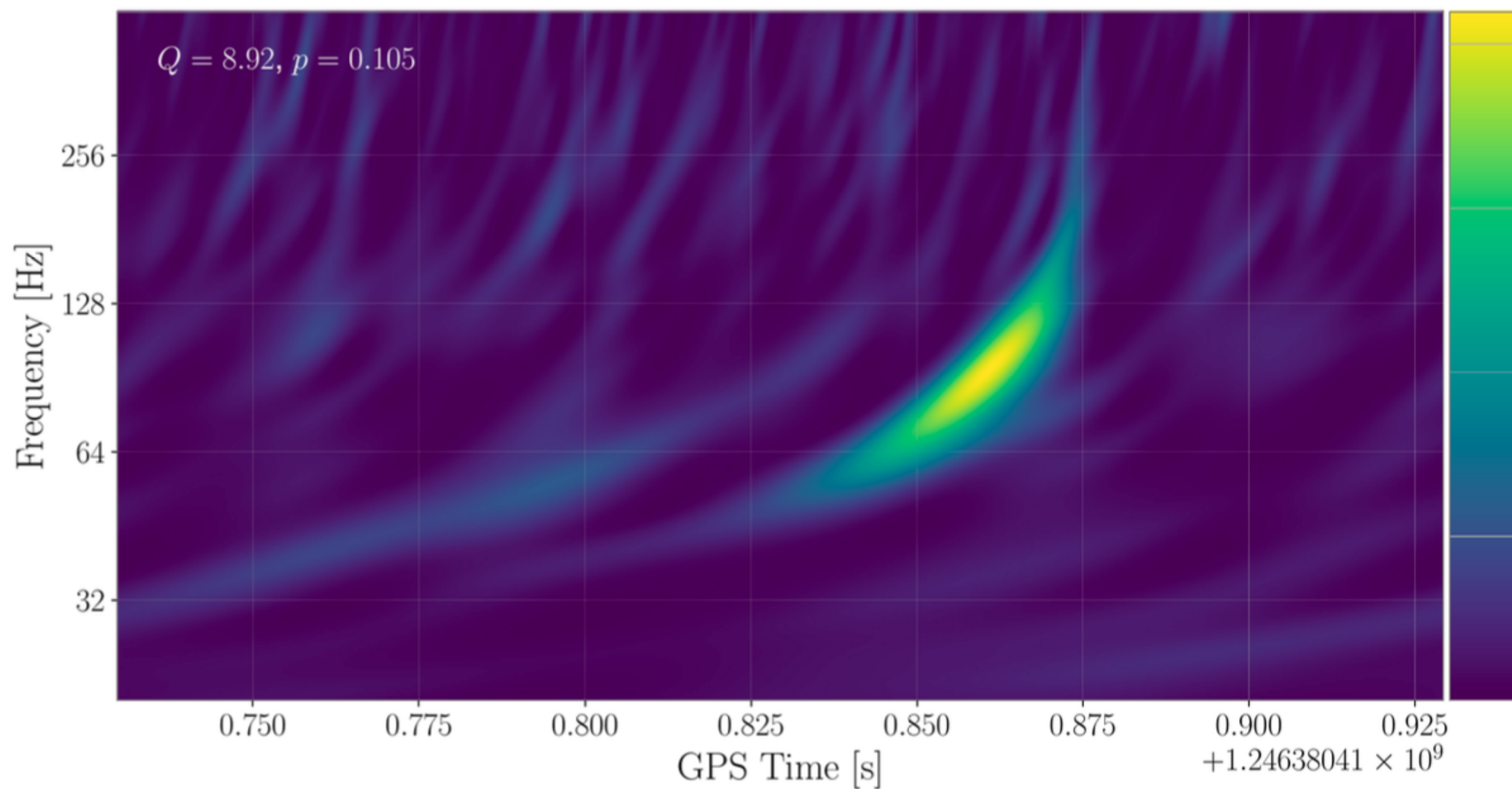
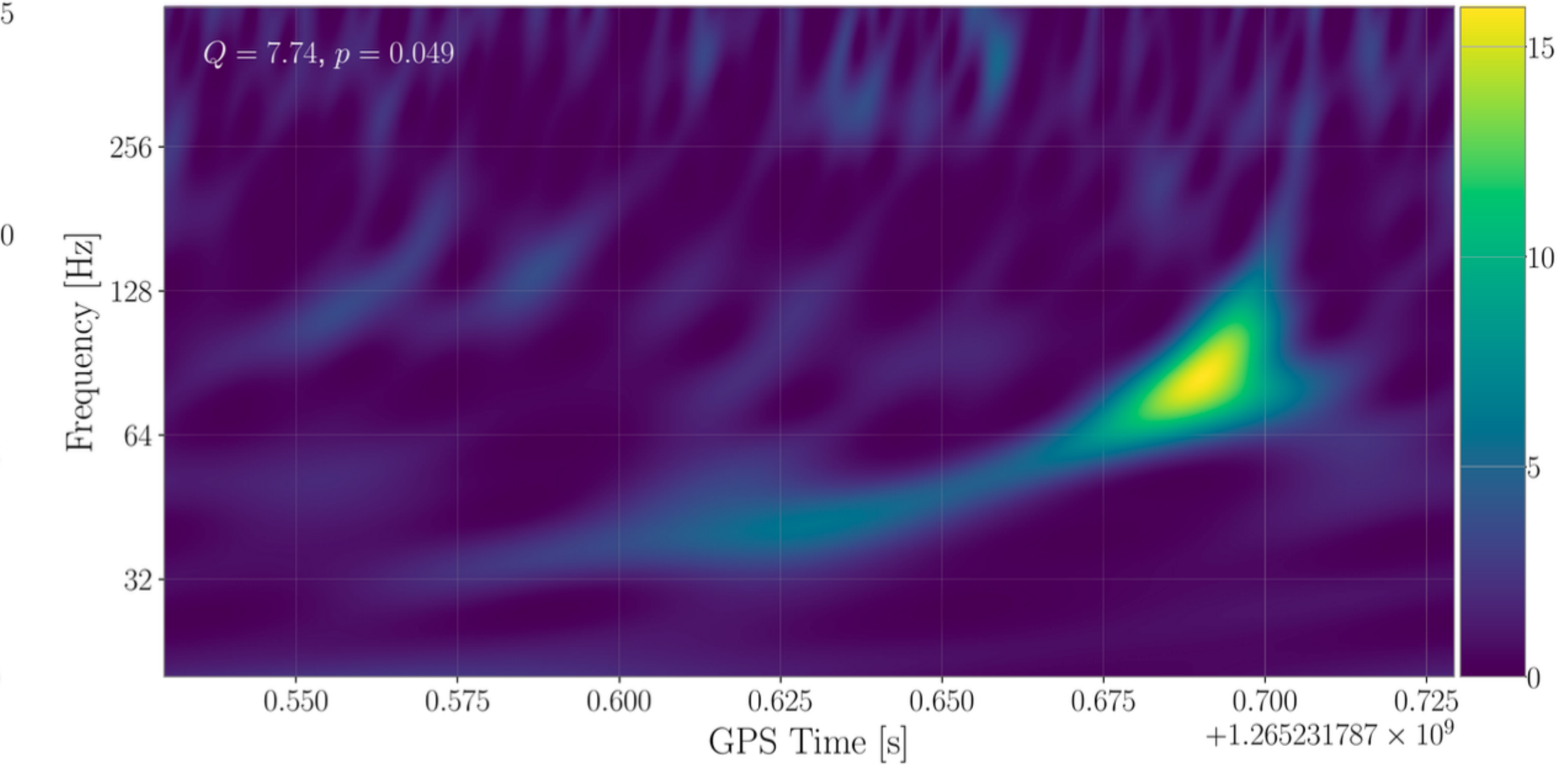
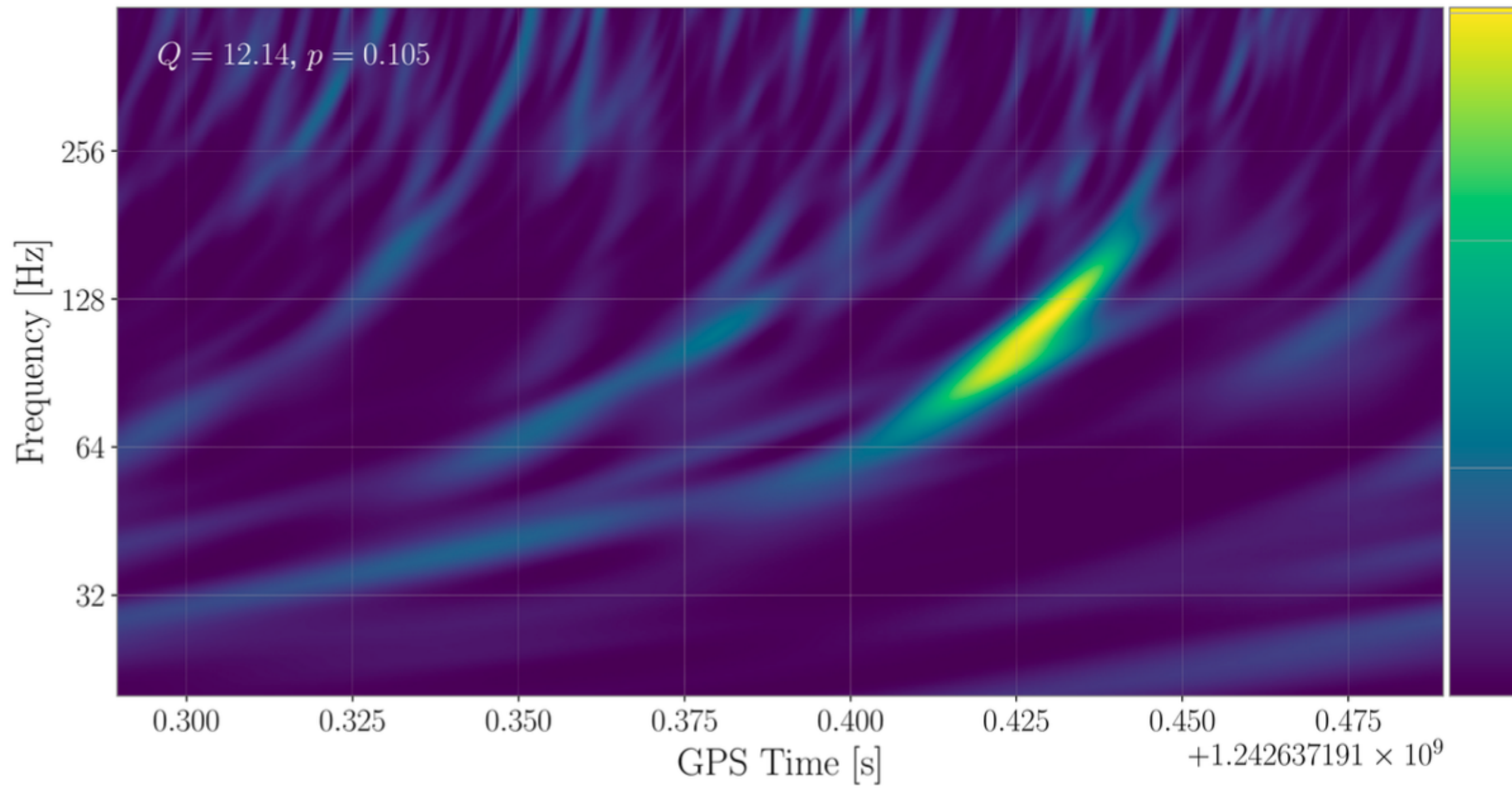


FIG. 42: Same as Fig. 35, but for the new event
GW190426_082124.

ARESGW NEW CANDIDATE EVENTS



ARESGW NEW CANDIDATE EVENTS



DATASETS AND PARAMETER SPACE

Dataset 1

- Purely Gaussian noise (with aLIGOZeroDetHighPower PSD)
- no spin, no higher-order modes
- 10-50 Msun component masses (uniformly)

Dataset 2

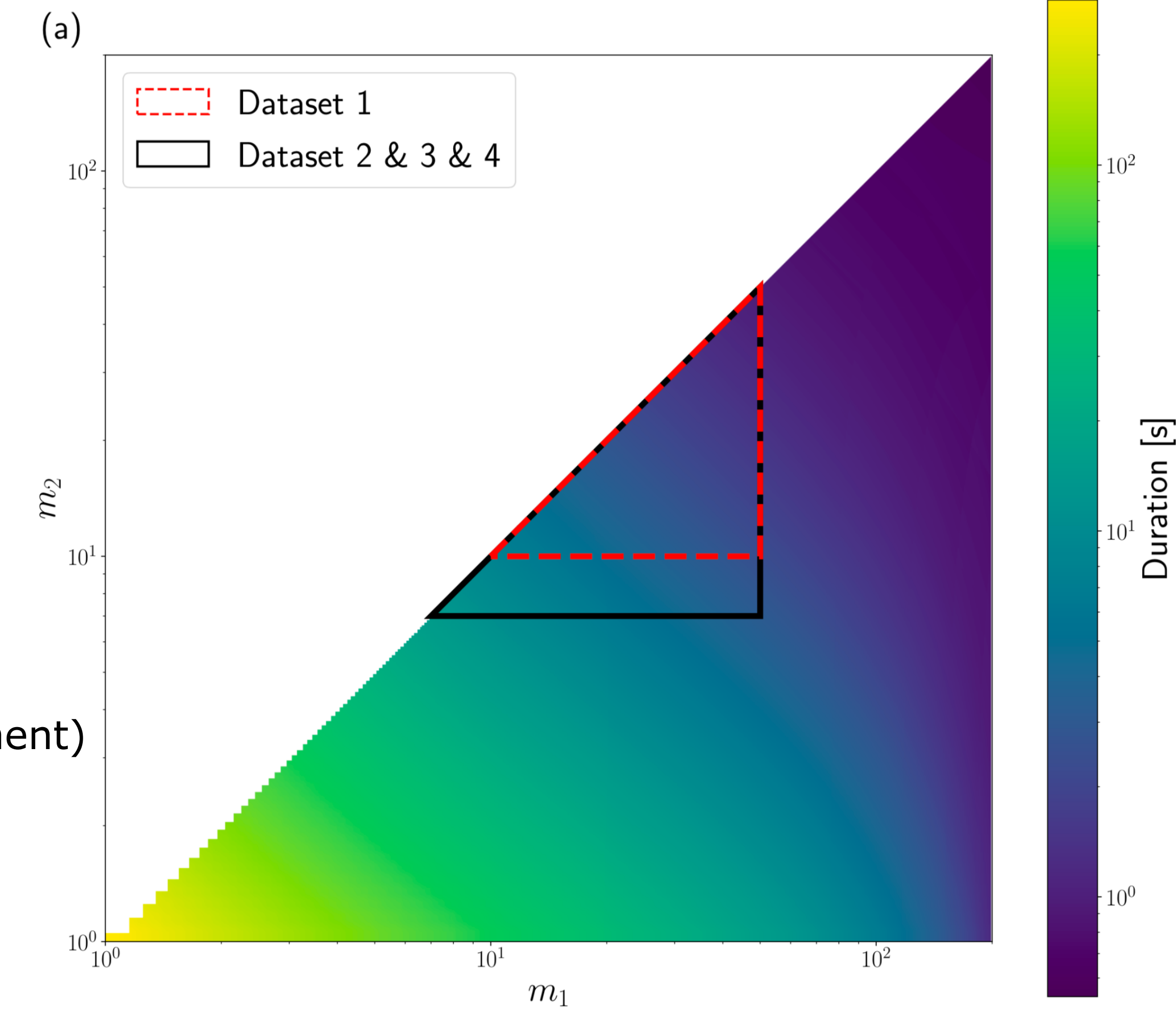
- Gaussian noise (but with O3a PSD)
- aligned spin (-0.99,0.99), no higher-order modes
- 7-50 Msun (uniformly)

Dataset 3

- Gaussian noise (but with O3a PSD, random for each 2h segment)
- non-aligned spin (with isotropic distribution in magnitude)
- higher-order modes up to (4,-4) as in IMRPhenomXPHM
- 7-50 Msun (uniformly)

Dataset 4

- as dataset 3, but with real noise sampled from O3a parts (excl. any GWTC-2 detections)



Evaluation

Evaluation:

1. Each algorithm is evaluated on the background dataset and returns a ranking statistic for each (false) positive event.
2. FAR at given ranking statistic $R = (\# \text{ of background events with ranking statistic} > R) / \text{duration } T$

$$\text{FAR}(\mathcal{R}) = \frac{N_{\text{FP},\mathcal{R}}}{T}$$

1. For uniform (*in volume*) injections up to a distance d_{\max} , the sensitive volume is approximately

$$V(\text{FAR}) \approx V(d_{\max}) \frac{N_{I,\text{FAR}}}{N_I}$$

where $N_{I,\text{FAR}}$ = found injections at given FAR and N_I = total # of found injections (within $\pm \Delta t$ each).

However, the injections are not uniform in volume, but are sampled over the *chirp distance*, instead:

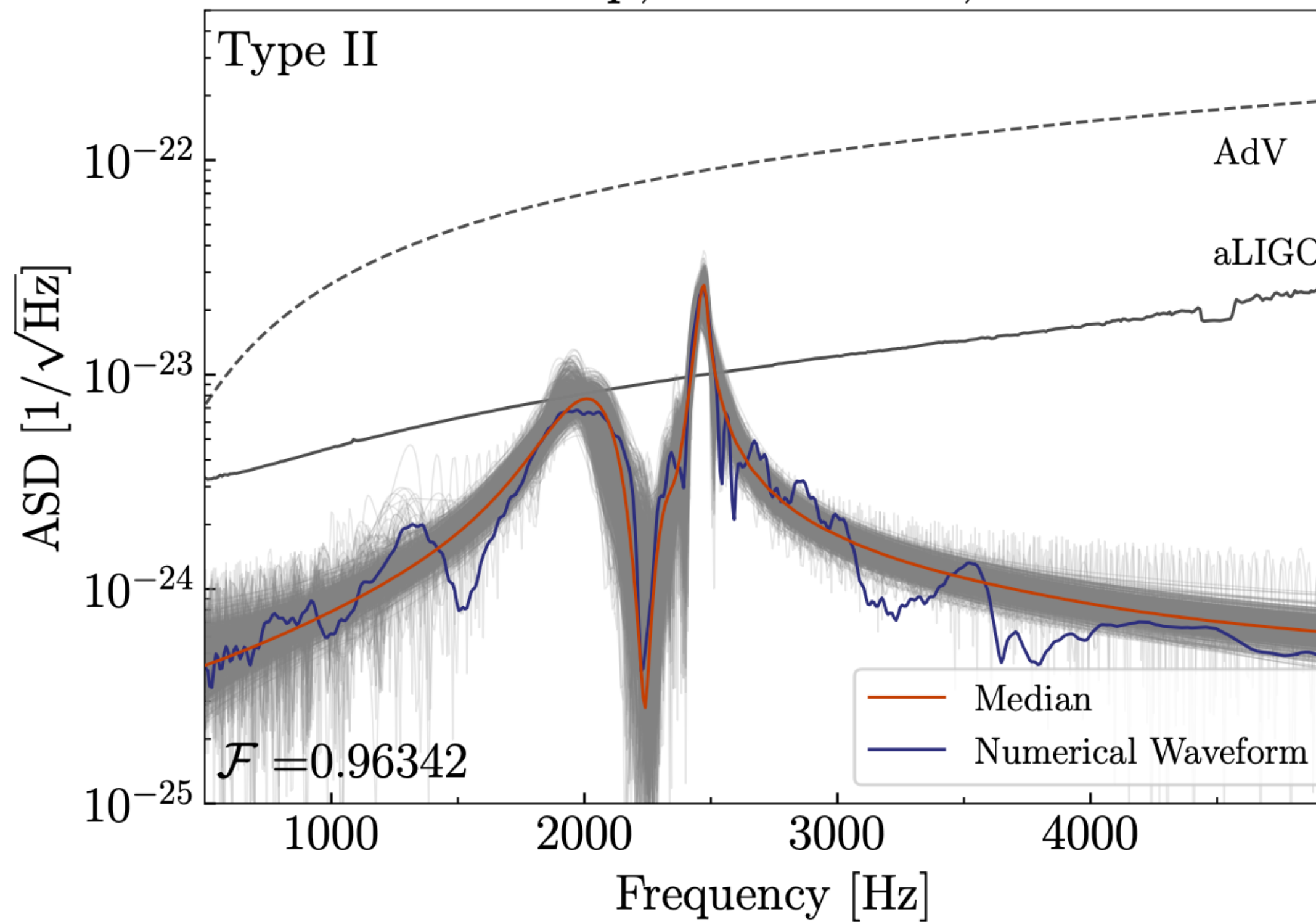
$$d_c = d \left(\frac{\mathcal{M}_{c,0}}{\mathcal{M}_c} \right)^{5/6}$$

with $\mathcal{M}_{c,0} = 1.4/2^{1/5} M_\odot$. To account for that:

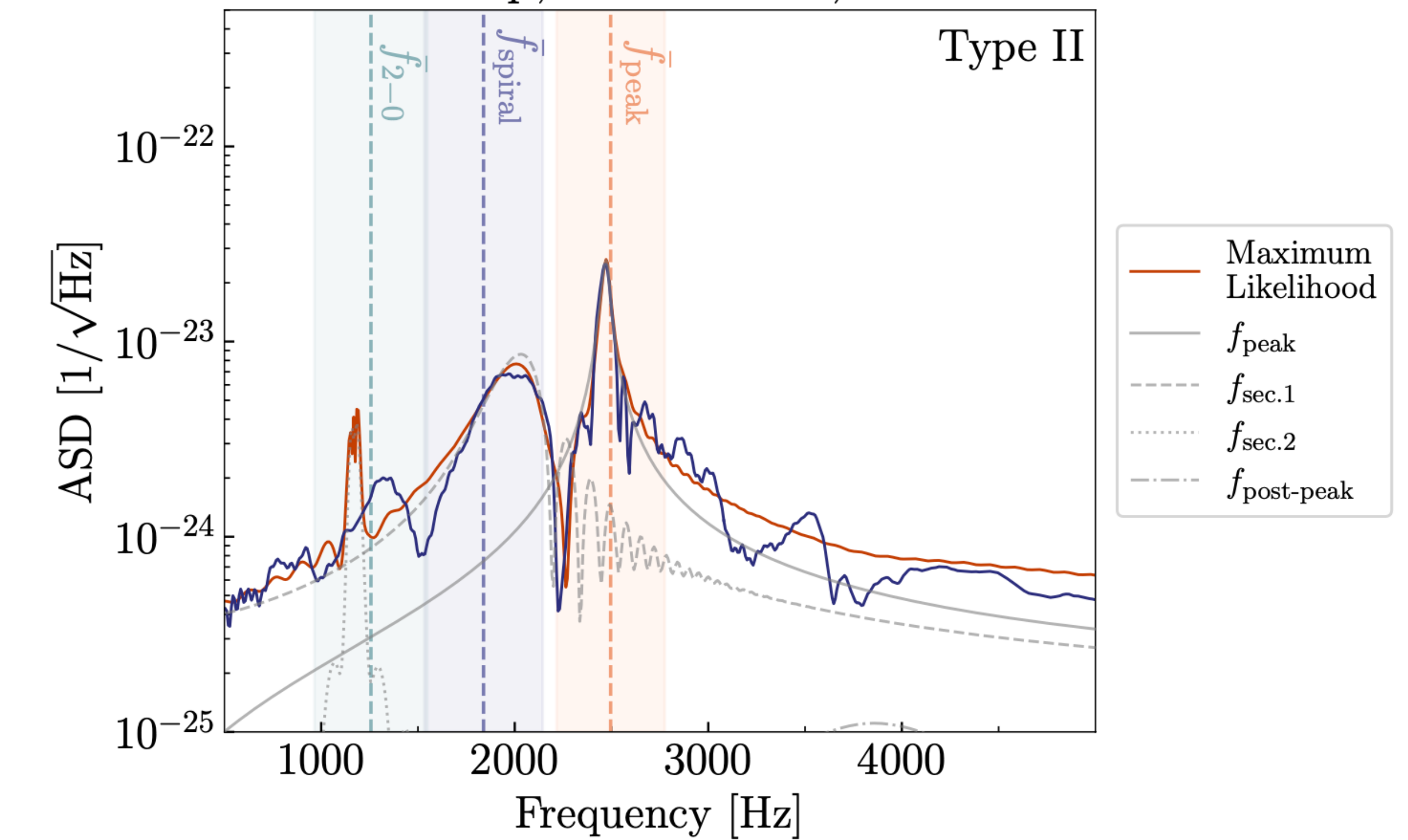
$$V(\text{FAR}) \approx \frac{V(d_{\max})}{N_I} \sum_{i=1}^{N_{I,\text{FAR}}} \left(\frac{\mathcal{M}_{c,i}}{\mathcal{M}_{c,\max}} \right)^{5/2}$$

RECONSTRUCTION IN THE FREQUENCY DOMAIN

EOS BHBlp, 1.300+1.300, SNR=16

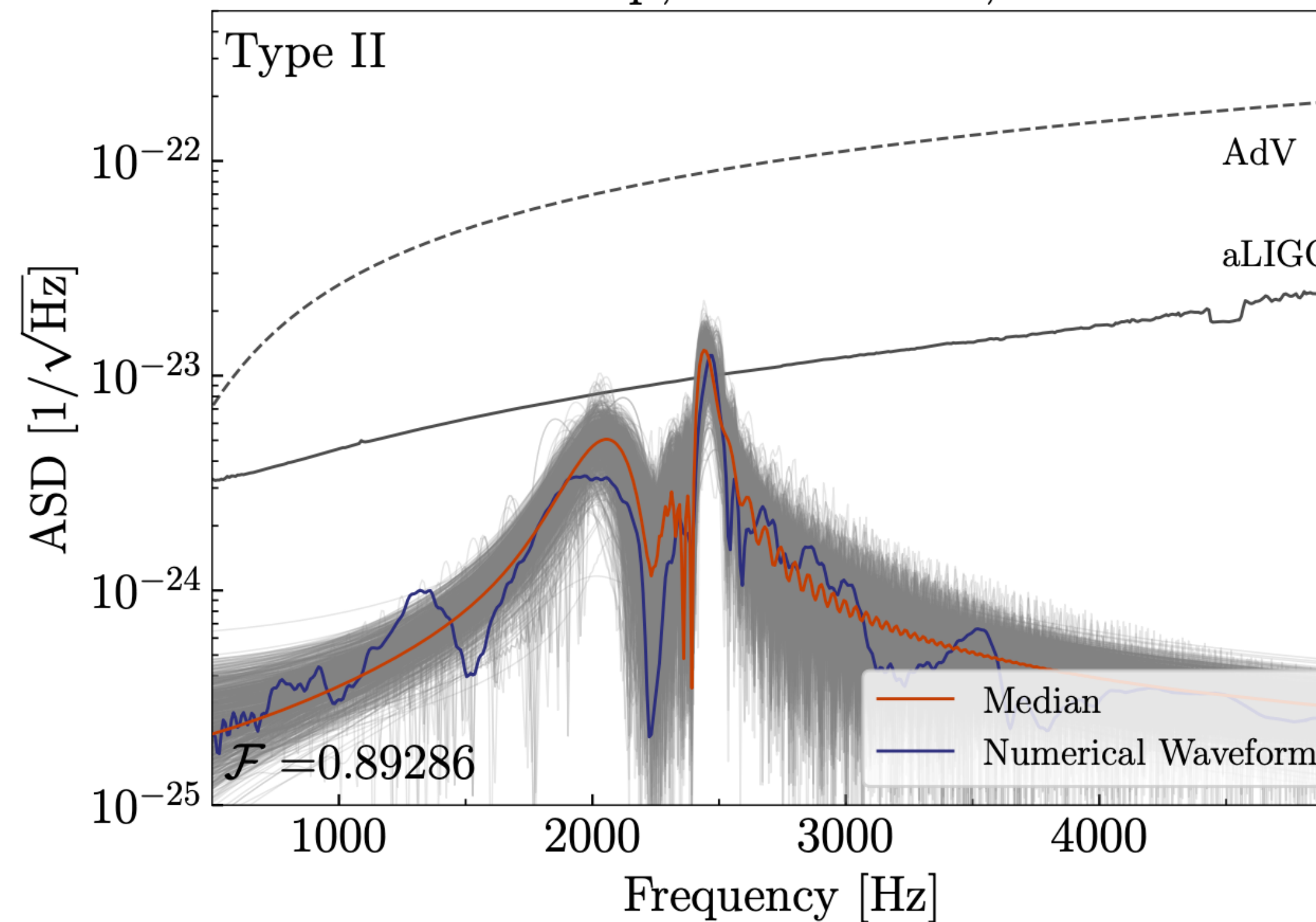


EOS BHBlp, 1.300+1.300, SNR=16

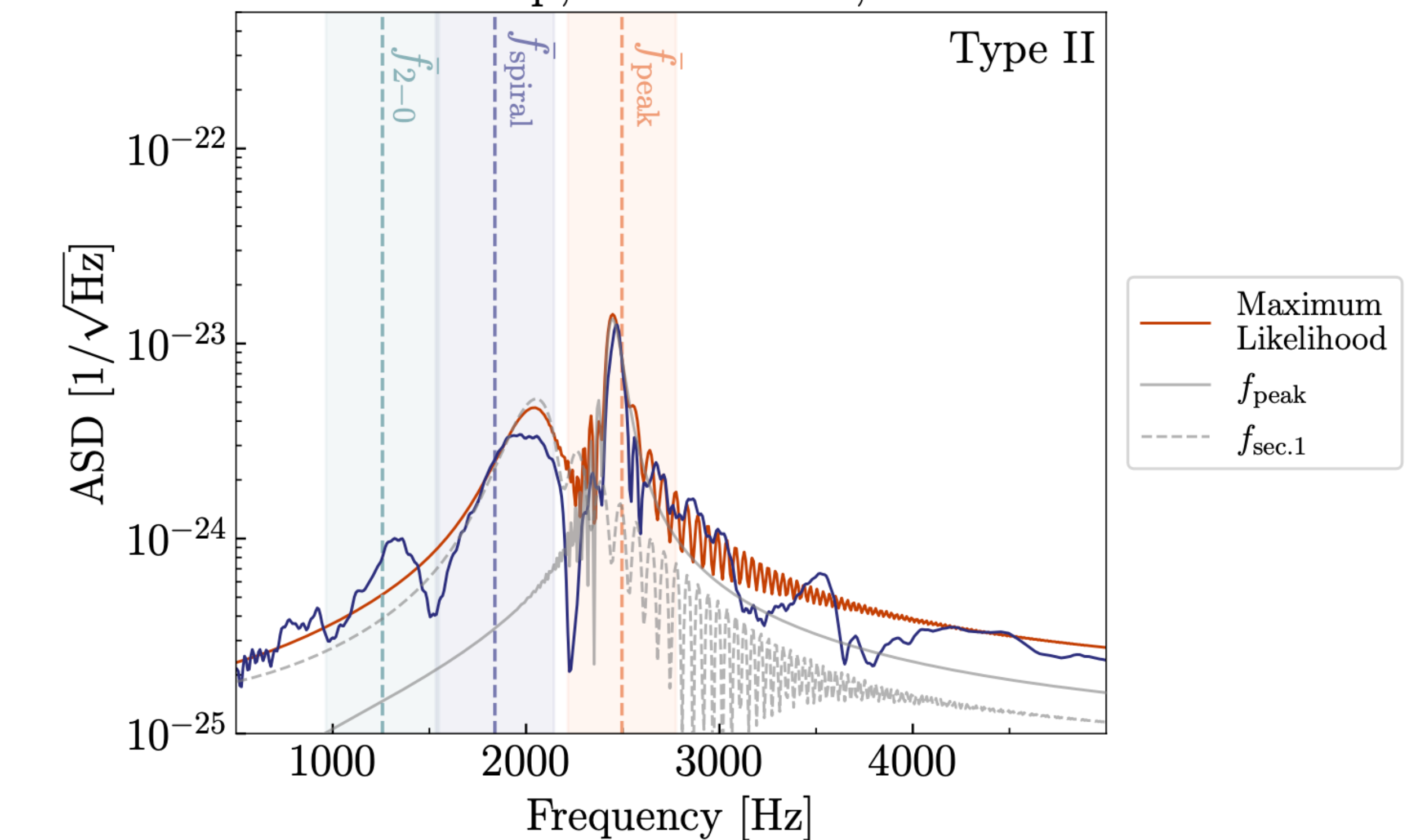


RECONSTRUCTION IN THE FREQUENCY DOMAIN

EOS BHBlp, 1.300+1.300, SNR=8



EOS BHBlp, 1.300+1.300, SNR=8



FITTING FACTORS FOR SNR=50

The fitting factors achieved are consistent with those in Easter et al. (2020) for a smaller set of EOS.

